STUDIES OF PICTURE SIGNAL BANDWIDTH COMPRESSION

A Thesis submitted for the
degree of Doctor of Philosophy.

by

Birendra Prasada.

Electrical Engineering Department
Imperial College
London.

May, 1960.

ABSTRACT

The thesis is concerned with the bandwidth compression of television signals. A survey of existing bandwidth reduction schemes has been made. These schemes fall into two categories: those which exploit the "perceptual redundancy" or limitations of human vision and those which exploit the statistical structure of the signal.

Detailed investigations have been made to assess the practical realizibility of a statistical scheme for television bandwidth compression proposed by Cherry and Gouriet[1]. In this system a picture is scanned with variable-velocity, the velocity of scan being controlled by the amount of "detail" in the picture. A flying-spot variable-velocity scanning system has been designed and built. The problems in the design of wide-band electro-magnetic deflection systems have been studied. The transmitter is essentially a non-linear feedback encoder and has led to some interesting problems related to stability of the system and to the signal to noise ratio. The effect of source noise on the system performance has been emphasized. Certain limitations due to the photomultiplier tube, and the phosphor characteristics and their effects on the system have been pointed out.

The "run-lengths" or the intervals between the significant transitions in the picture have been defined. The run-length statistics of test card 'C' have been obtained. The potential bandwidth compression of the picture has been calculated. An apparatus has been constructed to measure the "run-length" statistics of various pictures.

An open-loop system of bandwidth compression has been discussed which uses variable rate sampling. Using the statistics obtained from test card 'C', the storage requirement of the open loop system has been computed.

The weakness of the deterministic detail detectors has been pointed out and the need for statistical detail detectors, capable of combating noise, has been stressed.

ACKNOWLEDGEMENTS

The author wishes to express his gratitude to Professor Colin Cherry for his understanding help and encouragement throughout this project.

Many colleagues in the laboratory have been helpful in several ways. Particular thanks are due to Mr. T.C.Sidhan who provided many valuable suggestions during the design of the equipment, especially in connection with the design of the Ratchet Time Base, and for endless discussions. The interest shown in the work by Dr. M.P. Beddoes and Mr. H.B.Voelcker Jr. is acknowledged with thanks.

The author appreciates the assistance given by Mr. A.W. White and the workshop staff in the construction of the apparatus.

The author is indebted to Dr. A.J.Barlow for the help provided in photographic work.

A Flying-Spot Scanner was provided by Marconi W.T.Co.Ltd., whose general interest in the work is appreciated.

The project was supported by British Telecommunication Research Ltd., to which the author is also grateful for the provision of a maintainance grant. The continued interest of Mr. D.G.Holloway of B.T.R.Ltd., and Mr. W.G . Rann of the National Research and Development Corporation is greatly appreciated.

CONTENTS

Section		Page
1.	INTRODUCTION	9
1.1.	Philosophy of Present day Television	10
1.1.1.	Capability of the Systen	13
1.2.	Statistical Coding of Signal	14
1.3.	N on-Statistical Coding of Signal	15
1.4.	Some Properties of Human Vision	16
1.5.	The Scanned Information Source	18
1.6.	The Efficient Coding of T.V.Signals	19
1.6.1.	The Variable Velocity Scanner	21
1.6.2.	Schroter's Systen	28
1.6.3.	Linear Prediction	29
1.6.4.	Shannon-Fano Code	30
1.6.5.	Run-Length Coding	31
1.6.6.	Tapered Quantization of T.V.Signals	34
1.6.7.	Predictive Quantization	36
1.6.8.	"Synthetic Highs"	41
1.6.9.	Contour Interpolation	44
1.6.10.	Some Other Proposals	46
1.7.	Discussion	47
1.7.1.	Storage Requirements	48
1.7.2.	Schemes in Tandem	50
1.7.3.	Graham's and Schreiber's Coders	51
1.8.	Errors	57
1.8.1.	Channel Noise	58
1.8.2.	Source Noise	58

Section		Page
1.8.3.	Quantization Noise	58
1.9.	Specialised Uses	60
1.10.	Summary	60
2.	THE VARIABLE-VELOCITY SCANNING SYSTEM	61
2.1.	Earlier Work	61
2.2.	Some Limitations	66
2.3.	A New Slide Scanner	67
2.3.1.	The Marconi Flying-Spot Scanner	68
2.4.	The Variable-Velocity Flying-Spot Scanning Systen	70
2.5.	Components of the Systen	75
2.5.1.	C.R.T. for the Scanner	75
2.5.2.	The Optical Systen	77
2.5.3.	The Photomultiplier Tube	77
2.5.4.	The Head Amplifier	78
2.5.5.	The Differentiator	78
2.5.6.	The Full-Wave Rectifier	84
2.5.7.	The High Gain Amplifier	84
2.5.8.	The Variable-Velocity Time Base	87
2.5.9.	The Deflection Amplifier	92
2.5.10.	Scanner Tube Supplies	106
2.6.	Design of the Receiver	106
2.6.1.	Video Amplifier	106
2.6.2.	Line Deflection Amplifier	106
2.6.3.	Ratchet Time Base	110

Section		Page
3	STUDY OF THE SYSTEM	116
3.1.	Method of Evaluation of Bandwidth Reduction	116
3.2.	Experimental Results	119
3.2.1.	An Experiment to Investigate Phosphor Loading and System Stability	121
3.2.2.	An Experiment with Special Signal	123
3.2.3.	The "Beat"Effect - Re-entrant Spot	129
3.3.	The Bandwidth of the Feedback Loop	132
3.4.	Some Spectral Measurements	134
3.4.1.	Experimental Set-up	134
3.4.2.	Some Results	137
3.4.3.	Measurements after differentiation and Full-wave Rectification	141
3.4.4.	Theoretical Analysis	141
3.5.	Discussion	154
4	COMPRESSIBILITY OF PICTURES	157
4.1.	Turning Points and Significant Intervals	157
4.2.	Potential Bandwidth Compression by Variable-Velocity Scanning	158
4.3.	Measurements on Test Card 'C'	160
4.4.	Accuracy and Limitations	169
4.5.	The Statistics Measuring Apparatus	170
4.6.	Design and Testing of the Apparatus	171

Section		Page
5.	THE OPEN LOOP SYSTEM	175
5.1.	Variable Rate Sampling	175
5.2.	A New System	177
5.3.	Some Computations	181
5.4.	Storage Requirements	185
6.	THE POSITION CHANNEL	188
7.	PICTURE DETAIL DETECTION	191
7.1.	Statistical Approach	191
7.2.	Short-Term Bandwidth	192
7.3.	Effect of Visual Properties	194
7.4.	Discussion	194
8.	SUMMARY OF CONCLUSIONS	196
9.	APPENDICES	199
10.	REFERENCES	223

1. INTRODUCTION.

The enormous bandwidth requirement of the standard television service is undesirable for many reasons. Firstly, this precludes picture transmission in the long range radio bands, through ocean cables or by any other means except co-axial cables, waveguides and line-of-sight radio frequency links; secondly there are some applications of television e.g. recording and storage which are made considerably more difficult and expensive due to the large bandwidth requirement. Finally, there is a growing demand for spectrum space by colour television and other civil and military sources.

There are two aspects of this problem: broadcast service where the simplicity of the receiver is the main consideration; and television relay where the complexity of the equipment is relatively unimportant[2]. In broadcast television, the cost of the receiver, which has to be produced in large numbers is the primary consideration and spectrum utilisation takes a secondary place. Hence, for this purpose, only those systems will be of interest which reduce the bandwidth without increasing the receiver complexity. On the other hand, when television signals have to be relayed over long distances, either by cables or by radio-frequency links, the bandwidth has substantial influence on the economics of the system in terms of cable cost, repeater spacing, repeater amplifier design etc. In such cases, if some complicated terminal equipment, at each end, could reduce the channel bandwidth, this would be well worth having.

Information theory has given great impetus to this subject and a number of suggestions have been made which aim at reducing bandwidth of television signals. One of the few suggestions, which seems to have possibilities in the broadcast as well as relay field, achieves reduction of bandwidth by variable - velocity scanning.[1] Preliminary work on

variable - velocity scanning has already been done by other workers[3,4] which will be discussed later in this thesis.

This investigation was started with the following aims in view:

(1) To design and develop a variable - velocity scanner with an equivalent video bandwidth of 3 Mc/s.

(2) To assess potential bandwidth compressibility of typical pictures by this or similar means by measuring a relevant picture statistic .

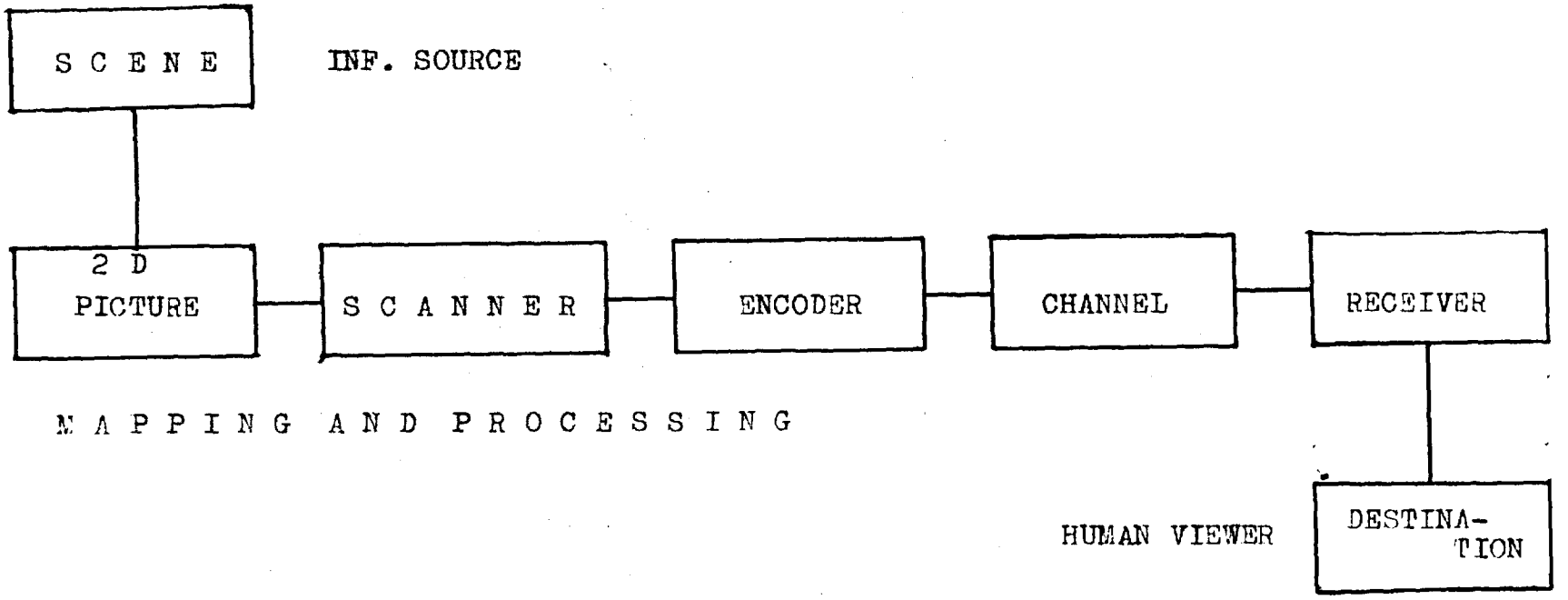
(3) To make a survey of the field and to suggest improvements on the present system of coding and consider the possibilities for the future.

The justification and relevance of these aims will become apparent after the basis of the present day television transmission and some of the more important developments the field have been studied.

1.1. Philosophy of Present day Television.

The primary function of a television system (Fig.1) is to produce on the screen of the receiver a visual pattern which best represents to the viewer the subject before the camera. A scene, for its complete specifications, needs three spatial dimensions and one of time if it is changing. When a scene, by its projection on a plane, is transformed into a picture, the brightness becomes a continuous function of the vertical and horizontal position (x,y) within the picture area, and of time t[5]. It is not possible to express the brightness distribution as the function of a single variable, viz. time. Therefore, the information contained in a picture cannot be transmitted in its entirety over a channel of finite bandwidth and in finite time and to describe the picture, quantisation becomes a logical necessity.[6].

A picture can be approximated by an array of dots - the



F I G. 1.

A T E L E V I S I O N S Y S T E M

smaller the dot, the higher the resolution. It is well known that the resolving power of the human eye is limited, so that decreasing the dot size, and increasing the number beyond a certain limit does not produce a better visual image. Thus, only a finite amount of data is needed to reconstruct a stationary picture which the viewer cannot distinguish from the original. Another property of the human eye, persistence of vision, is utilised in cinematography and picture transmission to create the illusion of smooth motion by superimposing in rapid succession a series of stationary pictures.

It is obvious, now, that to reproduce a moving picture, transmission of only finite amount of information is necessary.

The problem of coding the picture information, which has two spatial dimensions and one of time, for transmission through an one-dimensional (time) channel, is solved by the scanning process which was first suggested by M. Senlacq and successfully used by Nipkow[7]. The picture, in the British system, is broken into 405 horizontal lines and the intensity of each picture point in the line is specified. To create the illusion of continuous motion, the picture is scanned 25 times per second. An interlaced scanning is used in which the scanning beam completes 2 patterns of 202 $1/_2$ lines each, displaced by the width of half a line in order to cover a complete picture. This process reduces the overall flicker at the cost of high detail flicker to which the eye is relatively insensitive.

The bandwidth of the transmission is based on the following assumptions:

(1) The effect of line structure is ignored.

(2) The number of active picture elements per unit length is made equal in the vertical and horizontal direction.

(3) The system is designed to be capable of handling Black and White Chequerboard.

The Marconi - E.M.I. Specifications[8] allow for 4.94% vertical blanking time in the 405 - line system, so that the number of active picturepoints in the vertical direction can be calculated to be 385. The line duration is 98.8 μ sec of which 15% is used for blanking leaving an active line period of 84 μ sec. The aspect ratio of the picture is 4:3, hence, for the picture to have equal vertical and horizontal resolution, the active line must be capable of having $385 \times \frac{4}{3} = 513$ independent picture points.
To transmit 513 independent picture points in 84 μ sec., the minimum bandwidth necessary is $= \frac{513}{84 \times 2} \times 10^6$

$\simeq 3$ Mc/s.

1.1.1. Capability of the System.

With the advent of the statistical theory of communication [9,10], there has been a much better understanding of communication systems, their capacity and their efficiency. It has disclosed that our communication systems are used well below their capacity. The excess capacity is used up in transmitting "redundant" or repeated information. If some of this redundancy is removed and the signal is recoded, so as to present information to the channel at a constant rate, the channel will be used at much greater efficiency and hence bandwidth may be reduced. The redundancy associated with the signal, however, is not totally undesirable. It offers resistance to noise degradation in transmission and also serves as a protection against perceptual errors.

An alternative way to look at this is as follows: The present television system is capable of sending nearly 500 x 400 = 200,000 independent picture points in every

frame. For reasonable picture quality, each picture point can assume, say, one of sixty four of levels of intensity. Thus, the total number of possible pictures are $(64)^{200,000}$ A vast majority of these so-called pictures, which the present systems are perfectly capable of transmitting, will never occur in this age, because the average picture statistics virtually preclude their occurrence[11]. But the present communication system, based on an absolute independence of picture points, considers all these $64^{200,000}$ pictures to be possible and has to specify the particular picture that has occurred from this vast "set". If we reduce our "set" by throwing out of it those millions of pictures that are highly unlikely to occur, the amount of information that will have to be transmitted to specify a particular picture will then be smaller, which may appear as bandwidth reduction, if a suitable coding scheme is used.

1.2. Statistical Coding of Signals.

Shannon[12] has considered the problem of coding as roughly analogous to the matching of a generator and load by a suitable transformer. The encoder should match the information source to the channel in a statistical sense. For a highly efficient coding system, the statistical structure of the source as seen from the channel through the encoder should be such as to maximize the entropy in the channel. In a general source, "information" * is produced at different rates at different times. For maximum efficiency, the channel capacity should be equal to the average rate of the information source.

---

* Information in inverted commas is used here in a non-rigorous and intuitive way to denote newness in the message or in other words to denote significant changes which cannot be extrapolated from the past signal.

Thus an efficient statistical encoder, working on a message must reduce the redundancy, and with the help of variable delay, present a signal to the channel, (at a constant "information" rate), which has a minimum amount of residual correlation compatible with the fidelity requirements and noise conditions in the channel.

Statistical coding for bandwidth compression invariably entails delay or storage. For the maximum efficiency of the channel, the processed signal is fed to the channel at a uniform rate. This is achieved, by having a variable or elastic delay which stores 'information' when the source is generating it at maximum rate and feeds it to the channel when the source rate falls below the channel capacity.

1.3. Non-Statistical Coding of Signals.

An important development since the war has been the increasing interest in the integrated study of communication systems including the properties of the ultimate destination which is a human being in a large number of cases[13,14]. In the case of visual and acoustic signals, the primary function of a communication system is to provide psychological clues which help the viewer to draw on his past experience to form the gestalten of the scene or sound. The present television systems have only been made possible by exploiting the most elementary perceptual properties of the viewer viz. persistence of vision and visual acuity limits.

The objective of non-statistical coding is to exploit the characteristics of human vision to modify the visual signal so as to make it more amenable to efficient transmission either directly or after statistical coding.

1.4. Some Properties of Human Vision.

The study of visual perception has led to the determination of the information intake rate of the human viewers. The figures obtained are astounding and thought provoking. Measurements made by Sziklai[15], suggest that the human eye brain mechanism can perceive information at a rate of 40 to 50 bits / sec. Experiments performed by other workers suggest similar figures[16,17]. All these experiments have been performed treating the human being as a channel rather than information sink. Jacobson[18] has calculated the information capacity of the eye regarding it as an information sink and has arrived at a figure of 4.3 million bits / sec. Even this figure is at least one order below the TV bit rate of 56 million bits/sec. This author believes that the recognition rate may be somewhere between the two extreme figures quoted.

The large disparity between the information perception rate of the human viewer and the transmission rate of present systems points out that a vast amount of information that is sent on the present channels need not be sent if all the characteristics and properties of the human viewer are precisely known and utilised. It is interesting to note that the capacity of the human ear is practically the same as that of the eye.[15]

These facts have led to greater interest in the study and exploitation of the perceptual properties of the human receiver. Some of the elementary properties which are relevant to efficient television transmission are listed below:

1. The resolving power of the eye is limited. Thus, nothing is gained if the resolution is increased beyond this limit.

2. The eye is able to see fine detail only in a very small angle which is of the order of 2°. The fall of the resolving power outside this angle is quite rapid.
3. Persistence of vision makes it possible to produce the illusion of continuous motion by rapid superimposition of stationary pictures. It is well known that smooth continuity of motion is obtained if the number of still pictures projected is between 12 and 16 per second.
4. While small area flicker is not easily noticed by the eye, large area flicker is noticeably objectionable.
5. Without any loss in visibility, increased brightness can be bartered for the loss of contrast.(20)
6. The very small information input rates accepted by humans obtained by Sziklai have already been mentioned. His experiments further showed that the first things perceived in a changing scene are large area patterns. The eye fills in the detail in these patterns as more and more time is spent looking at the picture.
7. The eye is extremely sensitive to distortions in edge positions. However, it can tolerate a very large error in the specification of the ~~amplitudes~~ brightness of these edges. In other words, in the regions of transitions in the picture, the ability of the eye to see various gradations, is considerably diminished as compared to large areas.(21)
8. Another property of the human viewer of a quite different nature has been studied by Jesty(22). Some interesting experiments have been performed to determine the preferred viewing distance and its dependence on the number of lines and the bandwidth of the picture. An attempt has been made to take into account the line structure, which is inherent in television pictures. The ratio of the viewing

distance to picture height has been taken as a criterion of picture quality and it has been suggested that the preferred viewing distance increases linearly with the size of the picture. The set of experiments gave a very consistent value of $V/_H$ which was equal to 8.8.

1.5. The Scanned Information Source.

For a picture to have any "meaning", correlation is essential. Our limited knowledge of human perception suggests that the eye-brain mechanism breaks a picture into familiar patterns (Gestalten) and draws upon its past experience to fill in missing details. A perfectly random visual pattern, normally known as "Snow" does not make sense to the viewer. Thus, a certain amount of redundancy is essentially present in every picture of human interest.

This redundancy is further enhanced by the mapping procedure used in the present day television system. There are three main types of correlation present in the scanned television picture:

(1) A considerable degree of correlation is present between the adjacent picture - points in a line. In other words, the transition probabilities between successive picture-points are not equal.

(2) There is a large amount of line to line correlation in the picture.

(3) Unless there is a complete change of scene, the picture frames are nearly identical but for the small amount of change due to movements in part of the picture.

A very complete and elegant analysis of the scanning process has been made by Mertz and Gray[23]. The spectrum of a television picture is shown to consist of the harmonics of the line repetition frequency. Each harmonic is surrounded by sidebands at multiples of the frame frequency. For a

picture, the rate of decay of these sidebands is completely dependent on the complexity of the picture. If there is movement in the picture, the sidebands around each line harmonic get diffuse because movement corresponds to a complex modulation of the picture signal components. Measurement of the spectrum of pictures[24,25,26] confirm that the sidebands of the line frequency harmonics decrease to negligible values between the line harmonics and that these sidebands are modulated with very low frequencies due to motion in the picture. Also, the energy in the television signal is not uniformly distributed in each harmonic but in a typical picture, most of the energy is present in the first 25 to 30 harmonics.[27,28]

All the three types of correlation manifest themselves in the structure of the spectrum. The discrete nature of the spectrum with periodicities at line and frame frequencies are due to line-to-line and frame to frame correlation present in the picture while the non-uniform distribution of energy in the line harmonics is due to adjacent picture-point correlation.

An ideal statistical encoder, will minimize these correlations. The encoded signal will have a power spectrum approaching that of a band limited white noise and a near optimum statistical match with the channel will be achieved.

1.6. The Efficient Coding of TV Signals.

The theoretical limits on the rate of transmission of information have been studied by Shannon[10] and it has been shown that if perfect statistical matching between the transmitter and the channel is achieved, the maximum rate at which information can be sent through a channel, with an arbitrarily small frequency of error is given by

$$C = W \log_2 \frac{P + N}{N} \quad \text{bits/second,}$$

where W is channel bandwidth in c/s,
P the average transmitter power.,

and N the average power of perturbing white thermal noise which is additive.

This equation shows clearly that with suitable coding schemes, bandwidth and the ratio of average signal power to noise power may be exchanged. Thus, the increase in efficiency of transmission due to a coding scheme may result in either a bandwidth reduction or a signal power reduction or both. The specific coding schemes, suggested for more efficient transmission, include both bandwidth reduction and power reduction schemes.

The study of relative efficiency of different communication systems suggests that to encode a random signal with flat distribution, Binary Pulse Code Modulation is one of the most efficient systems though the bandwidth requirement of a P.C.M. system is large.(29) Because of easy and error-free regeneration under most conditions, the transmission requirements of a P.C.M. relay link are almost independent of the length of the link. Moreover, a P.C.M is very "rugged" i.e. its susceptibility to interference is very low. The importance of this property can hardly be overstated, especially when the redundancy in the signal is minimized. Further, the P.C.M. system lends itself easily to time multiplexing which may be advantageous in certain cases.

On the other hand, there is a very strong case for signal coding schemes which achieve bandwidth reduction. In case of systems which use cable transmission, the cost and complexity of the system goes up considerably with increasing bandwidth. In certain applications such as video recording

bandwidth reduction is much more profitable than power saving. Another important factor is the cost of terminal equipment. Though there may be exceptions, it may be said as a general rule that P.C.M. apparatus is more complex and expensive than that of other communication techniques. This is very important if the terminal equipment has to be produced in any large quantity such as in the case of broadcast receivers or facsimile equipment for use in offices.

1.6.1. The Variable Velocity Scanner.

One of the first encoders for television signal bandwidth compression was suggested by Cherry and Gouriet[1] and also by Bell[30]. In this scheme, a non-linear mapping of the picture space is achieved by variable-velocity scanning. The velocity of the transmitter and receiver scanning spot is made to vary inversely with the modulus differential of the video waveform viz. $\left|\frac{de}{dt}\right|$. (Fig.2). Areas of considerable "picture detail" are scanned slowly while those of zero or little "detail" are scanned fast thus changing the statistical structure of the signal. It may be pointed out that unlike the velocity modulation system of Bedford and Puckle[31], the Cherry-Gouriet scheme is a closed loop feedback system i.e. the scan velocity is a function of a parameter which itself depends on the velocity.

Picture Detail has been precisely defined[32] as

$$D_l = \int_{\ell} \left|\frac{de}{dx}\right| dx \qquad (1.1)$$

where e is the amplitude of the video as a function of the scanning distance x and the integral is taken over any scan length l. Picture Detail Factor, D_f, is defined in terms of the average value of $\left|\frac{de}{dx}\right|$ over one complete picture scan length L, thus

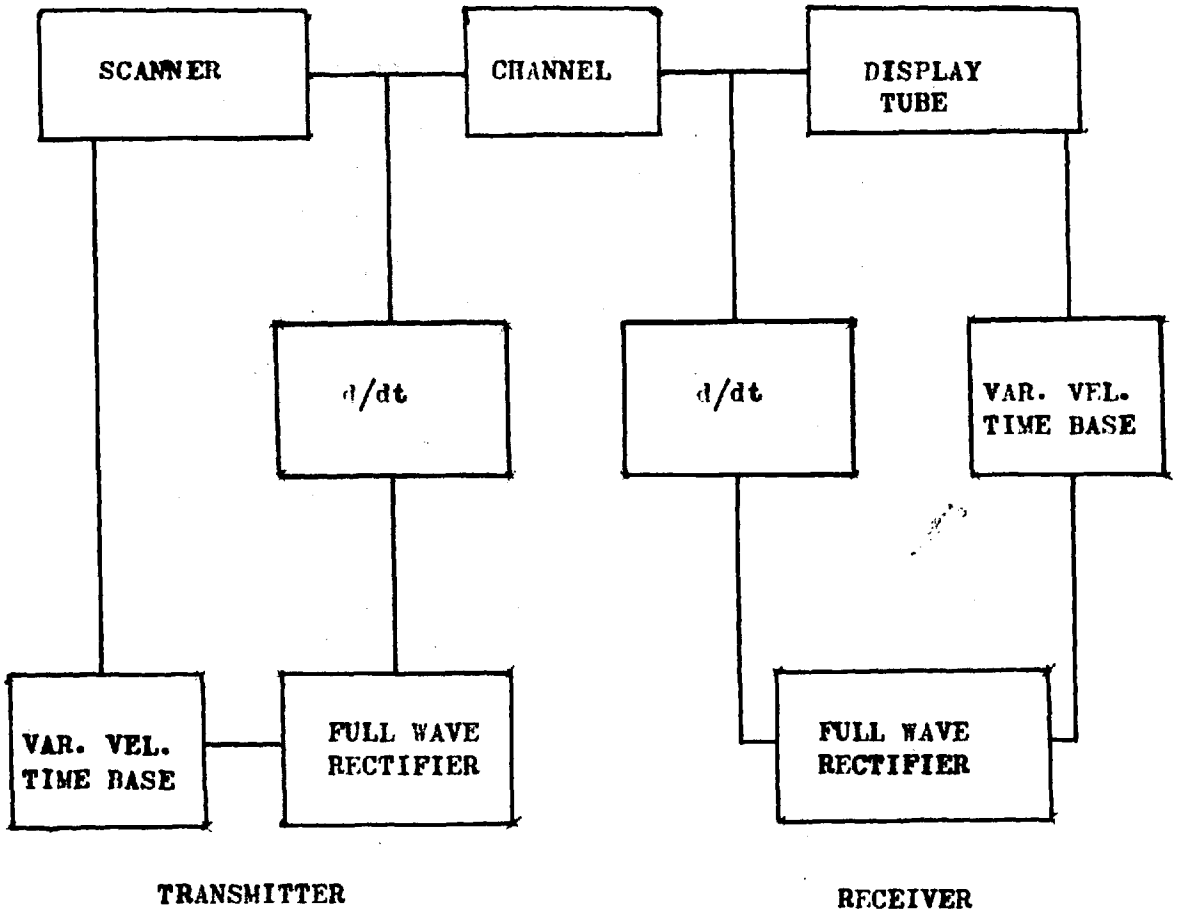
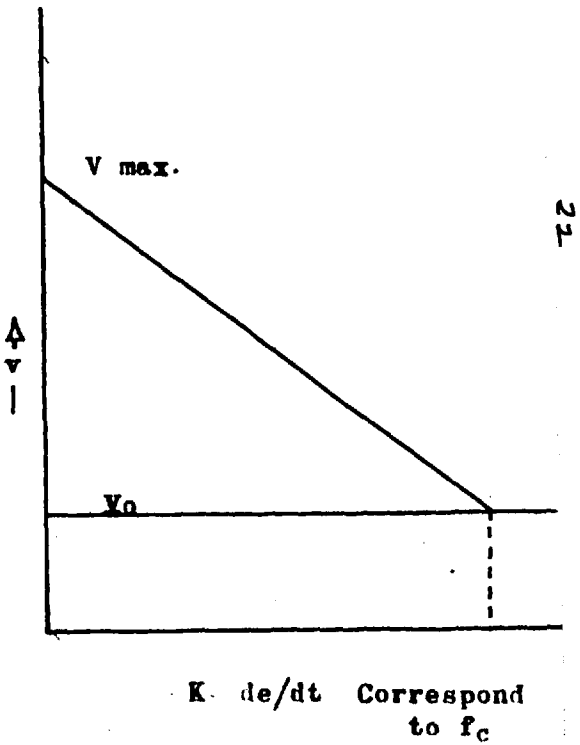


FIG. 2 a) CHERRY - GOURIET SYSTEM



b) SCANNING CHARACTERISTICS

$$D_F = \frac{1}{L} \int \left|\frac{de}{dx}\right| dx \qquad (1.2)$$

For constant velocity scanning, due to linear space-time transformation, this may be written as

$$D_F = \frac{1}{T_o} \int_{T_o} \left|\frac{de}{dt}\right| dt \qquad (1.3)$$

where T_o is the duration of one scan and e is the video output.

Expressions have been derived for bandwidth compression in the case of black and white pictures and also half tone pictures. For the sake of completeness, some of the important results are deduced below:

1.6.1. Velocity Modulation as a Function of Picture Detail

Referring to Fig.2, if v_o and v_{max} are the minimum and maximum scan velocities respectively, the instantaneous scanning velocity may be written as:

$$v = v_{max} - K \left|\frac{de}{dt}\right| \qquad (1.4)$$

where K is a constant with the dimension of length/time.

Since $\left|\frac{de}{dt}\right| = v \left|\frac{de}{dx}\right|$,

$$v = v_{max} - K v \left|\frac{de}{dx}\right|$$

Solving for v

$$v = v_{max} \frac{1}{1 + K\left|\frac{de}{dx}\right|} \qquad (1.5)$$

The ratio of the maximum to instantaneous velocity is

$$\frac{v_{max}}{v} = 1 + K \left|\frac{de}{dx}\right|$$

The average value of this ratio over one complete scan of length L will be

$$\left(\frac{v_{max}}{v}\right)_{av} = 1 + \frac{K}{L} \int_L \left|\frac{de}{dx}\right| dx$$

$$= 1 + K \quad D_F \qquad (1.6)$$

where D_F is the measured valueof the picture detail factor.

Let $v_{max} = n\, v_o$ and let $\left|\frac{de}{dx}\right|$ equal unity so that equation (1.5) becomes

$$\frac{n\, v_o}{1 + K} = v_o \qquad (1.7)$$

where $\overline{K}$ is the numerical value of K which results when the latter is multiplied by unit voltage per element.

Now $\overline{K} = n - 1$

hence $K = n - 1$ elements/volt.

Substituting this value of K and also putting $n = \frac{v_{max}}{v_o}$ in equation (1.6)

$$\left(\frac{n\, v_o}{v}\right)_{a_v} = 1 + (n-1)\, D_F$$

or $$\left(\frac{v_o}{v}\right)_{av} = \frac{1 + (n-1)\, D_F}{n} \qquad (1.8)$$

Since the time taken to complete a scan is inversely proportional to the velocity averaged

$$\frac{T}{T_o} = \frac{1 + (n-1)\, D_F}{n} \qquad (1.9)$$

where T and T_o are the times taken for one complete scan with and without velocity-modulation respectively.

Equation (1.9) gives the reduction in the time-bandwidth product in the case of a two level black and white picture. Obviously, if the v_{max} is so arranged (without changing n) that the time for the variable velocity scan, T, is made equal to normal frame period, the bandwidth will be compressed to a value f_c such that $f_c/f_o = \frac{T}{T_o}$ where f_o and f_c are the uncompressed and compressed bandwidths respectively.

Equation (1.9) is valid only for black and white pictures, because for the determination of K (Equation.1.7), the value of $\left|\frac{de}{dx}\right|$ was assumed to be unity. By definition, this occurs only when the finest detail is present at maximum contrast. Similar detail of lower contrast has a smaller value of $\left|\frac{de}{dx}\right|$ and therefore would result in a greater velocity of scan setting up frequencies outside the prescribed band. If low contrast detail occurs with an amplitude, which is a fraction 'a' of the maximum amplitude, it has been shown that Equation (1.9) is transformed into

$$\frac{T}{T_o} = \frac{1}{n}\left[1 + (n-1)\,\frac{D_F}{a}\right] \qquad (1.10)$$

If $n \gg 1$

$$\frac{T}{T_o} \simeq \frac{D_f}{a} \qquad (1.11)$$

Hence no reduction would be possible if $D_f = a$.

It has been pointed out by the authors that this particular scheme achieves bandwidth compression by sacrificing contrast range; however, under certain circumstances, it may be worthwhile to achieve bandwidth reduction at the cost of some finest detail at low contrast. The basic fault of the system is that it is a slope-compressing system and not a frequency compressing one.

Cherry and Gouriet have suggested another method in which velocity modulation may be used to achieve frequency compression. This is based on the assumption that the quantised video signal consists of two kinds of components:

(i) Transition regions which define all boundaries and edges.

(ii) Areas of uniform brightness in which the amplitude remains constant.

By differentiating the video signal and differentiating and shaping, a two level signal is obtained (Fig.3) which may be used to control the time base velocity. The velocity modulation can be made to achieve either.

(a) near equalisation of the time occupied by transition regions and non-transition regions over a suitable period, say, line duration.

or (b) near equalisation of all transition durations " t".

The instrumentation of this would be extremely complex as has been suggested by the authors.

Other suggestions in this paper include the possibility of compressions in the vertical direction. The picture is scanned twice, alternately in the horizontal and vertical directions.

In the Cherry-Gouriet variable-velocity system, the receiver is the mirror image of the transmitter (Fig.2). It is assumed that the time base velocity information is inherent in the compressed video waveform and can be extracted from it.

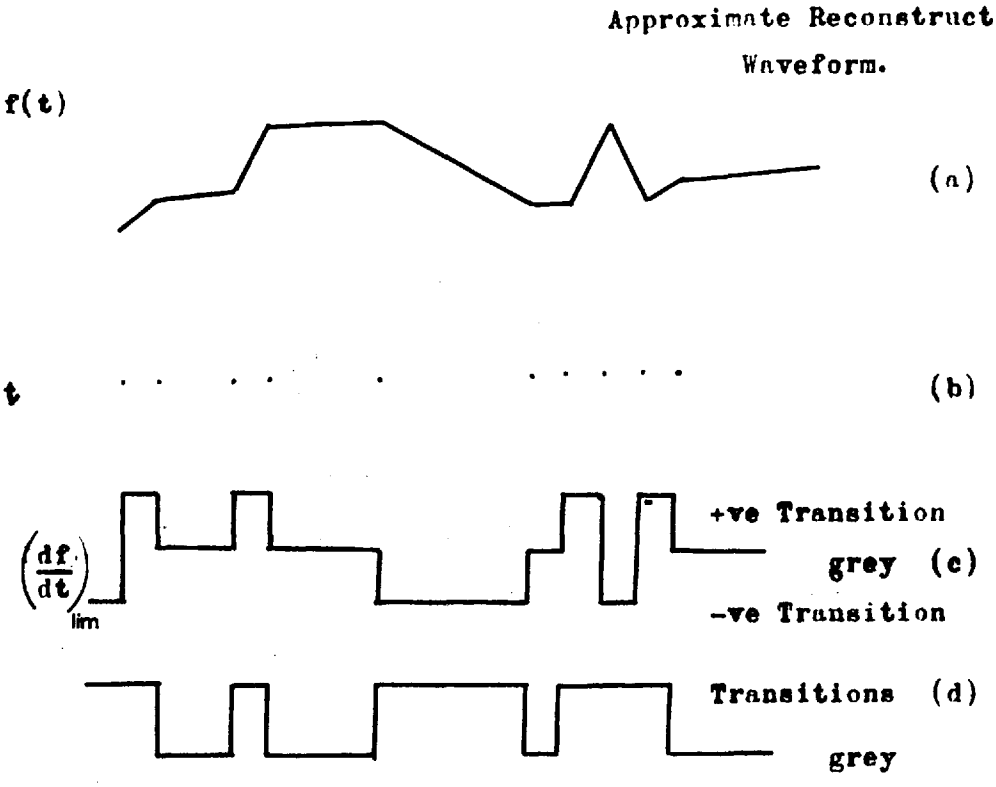
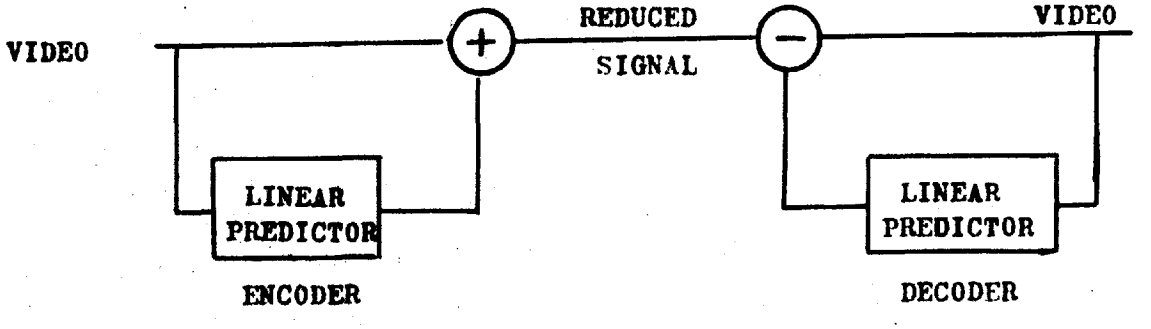


FIG. 3



A LINEAR PREDICTOR

FIG. 4

Experimental investigations[4] on the system have indicated that position errors integrate across the line and hence any sizable compression is accompanied by grave spatial distortions on one side of the picture.

This can be avoided and also greater compression may be achieved if the scanning spot position information is sent on a separate channel.[33]

1.6.2. Schroter's System.

Another television encoding scheme which uses velocity modulation for bandwidth reduction was proposed by Schroter.[34]

A picture is scanned by slow scanning and is stored both at the transmitter and the receiver. Corresponding points in successive frames of the stored signal are compared at the transmitter. If these signals differ, the scanning velocity is made low. If they are the same, the scanning velocity is increased and made high. The signal is transmitted to the receiver only in the case when it differs from the stored signal. The scanning produces bandwidth compression which is given by the expression

$$F = \frac{f}{f_c} = \frac{1 + (n-1)P}{n} \qquad (1.12)$$

where p : fraction of the scanned area in which adjacent frames differ.

$$n = \frac{v}{v_2} = \frac{\text{maximum velocity}}{\text{minimum velocity}}$$

This system resembles Cherry - Gouriet two velocity system and also Harrison's linear predictor.[35] Thus both signal power and bandwidth are reduced.

1.6.3. Linear Prediction.

In some interesting experiments, Harrison[35] and Kretzmer[11] have investigated the savings in channel capacity by linear prediction. Kretzmer has obtained histograms for the difference between a video signal and its delayed version. Harrison has investigated the possible savings in average power with different forms of linear predictors using the same scenes as Kretzmer.

In linear prediction, the prediction for the next picture point is a weighted sum of the previous ones. The nature of the weighting function and best value for its co-efficients are determined by the statistics of the signal. If the actual signal differs from the predicted value, then alone the difference is transmitted to the receiver (Fig.4).

The simplest form of linear prediction which is used is called the "Previous value Prediction". In this, the adjacent samples are assumed to be equal and error signals are transmitted when they are not. Some other forms of prediction used are: Slope Prediction which is equivalent to two previous value prediction in tandem.

Previous Line Prediction which is previous value prediction over two adjacent elements in the vertical direction.

Planar Prediction which is equivalent to previous value and previous line predictions in tandem.

The ratio of signal power to error power has been defined as "Power Reduction" and is used to evaluate the effectiveness of different predictions.

Power Reductions on three different pictures obtained by Harrison with different predictors are tabulated below:

TABLE 1.1.

POWER REDUCTION .

Type of Prediction	Picture With Low Detail. Close Up Of A Girl's Head	Picture With Medium. Detail The Sunflower Girl	Picture With High Detail. Packed Grandstand
Previous value	22 dbs	17 dbs	10.5 dbs
Slope	20 dbs	14.5 dbs	8.5 dbs
Previous Line	20 dbs	14.7 dbs	8 dbs
Planar	21 dbs	20 dbs	12.5 dbs

These results point out that "previous - value prediction" which exploits correlation between adjacent picture points only, yields a substantial power reduction while other more complicated prediction schemes seem to better it only by very small amounts. Kretzmer's measurements[11] of autocorrelation functions of these pictures suggest that they may be approximated by exponential curves. It has been theoretically proved by Wiener[36] that if the autocorrelation function is of exponential shape, the previous sample alone is needed for linear prediction.

1.6.4. Shannon - Fano Code.

The histogram for difference between video signal and its delayed version, obtained by Kretzmer, is a highly peaked curve. Thus, the difference signal from Harrison's predictor does not lend itself to efficient non-statistical codes like Binary P.C.M. A statistically - matched code has been devised independently by Shannon[10] and Fano[37] which can be used with advantage with peaked distributions. In

Shannon-Fano code, the amplitude levels are arranged in order of decreasing probability. This series is divided into two groups whose probabilities are made as nearly equal as possible. If an amplitude level falls in the first group, it is given zero as its first binary digit, otherwise 1. These groups are divided into sub-groups of nearly equal probability and the second digit is determined in a similar way as first. This process is continued till each subgroup contains only one amplitude level. Thus, a code is obtained in which different amplitude levels are represented by code-groups whose lengths vary, the most probable levels having the shortest code-groups and vice versa.

The great merit of the Shannon - Fano Code, unlike other codes of variable length, is that it does not require a punctuation code between code-groups.The decoder can be programmed to automatically distinguish between individual code-groups.

1.6.5. Run - Length Coding.

Another statistically matched code which is suitable for television signals is called Run - length Code[2,38]. This code exploits points to point correlation in the picture in the simplest case. Instead of describing a picture at every point, the amplitude level is stated and also the number of following picture points which have the same amplitude. The description of the picture becomes a set of number pairs and if the average run length is large (4 or more) a reasonable saving in channel capacity is obtained by transmitting the new description. Punctuation Code is necessary so that code groups representing amplitudes and run lengths may be separated at the receiver.

The increase of efficiency in transmission will depend on the mean value of run length. Measurements of run length

statistics (to be described later in this thesis) suggest that a mean value of run length of 4 picture - points is a realistic figure. Let us assume that the picture is quantised in 32 or 2^5 levels and that every line contains 600 picture points. By conventional means, the amount of information that must be transmitted = 600 x 5 = 3000 bits/line. Now it is further assumed that the total number of co-ordinates to be transmitted in run-length coding is

$$2 \times \frac{\text{No. of Picture points}}{\text{mean value of run lengths}} = 2 \times \frac{600}{4} = 300$$

Adding one extra bit for punctuation code: the information transmitted = 300 x 6 = 1800 bits/line which is a saving of 1.6:1

A coder based on the principle of run length coding has been suggested by Gouriet[39]. The action of the coder is best explained with the help of Fig.5.

The video waveform (Fig.5a) is sampled and quantised and passed through a hold circuit which produces the waveform in Fig.(5b). This waveform is differentiated by a circuit of a suitable time constant to give a series of pulses which denote the amplitude and position of all significant transitions in the waveform (Fig.5c). The length of the runs between the significant transitions is extracted from figure (5c) and so are the pulses carrying the amplitude information (Fig.5d and e). These are made equidistant in time with the help of elastic delay (Fig.5f and g). The brightness and position information can either be multiplexed or sent on separate channels.

The decoder is a variable-velocity receiver whose scan velocity is made proportional to the amplitude of the position pulses.

The position information is very inefficiently coded as is obvious from fig.5(f). The vast redundancy in it is

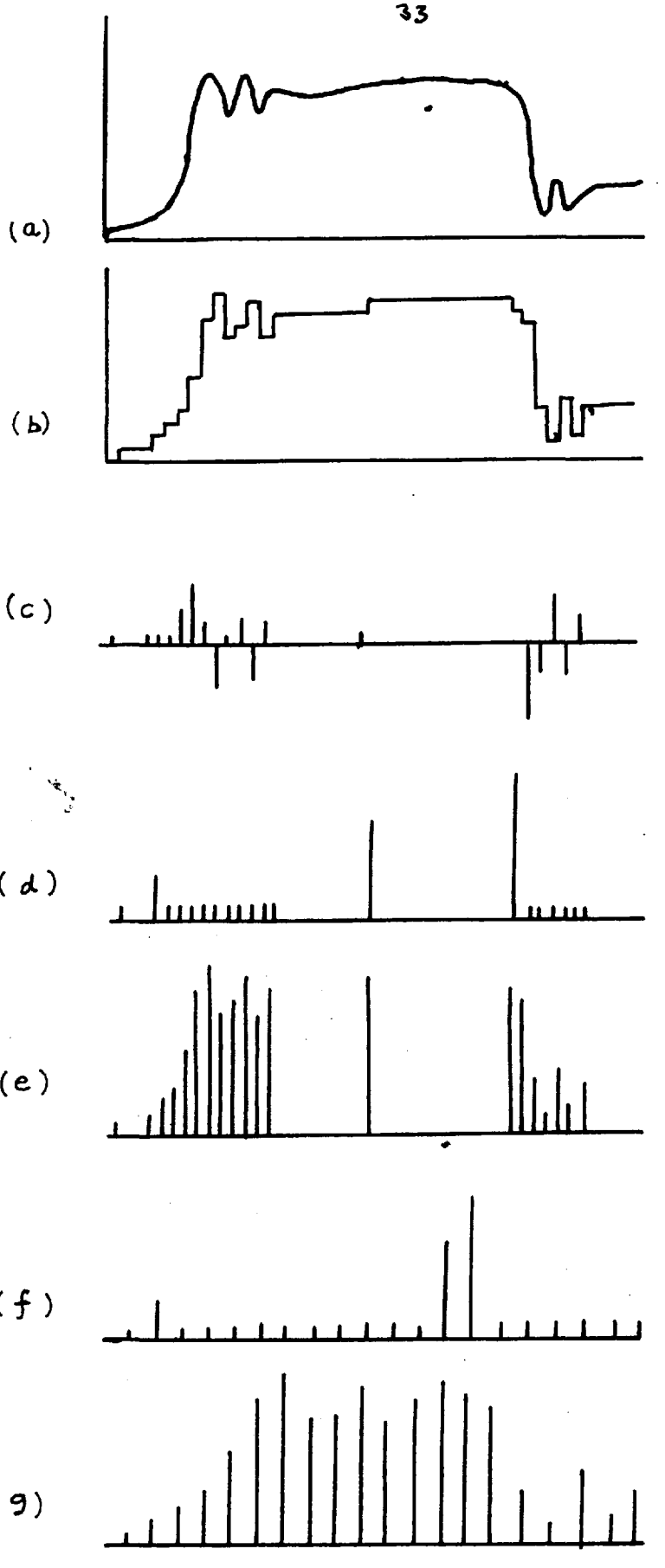


Fig 5

not being made use of. Errors along a line are cumulative and the code is so susceptible to noise that a $s/_N$ ratio of well above 60 dbs is required in the position channel to attain a frequency of error of 1 in 600.

There is an interesting suggestion in the appendix of the above mentioned paper. The number of transitions are counted in a line and the number of brightness quanta is varied inversely so that the product of quantum levels and number of samples is maintained constant. This can ensure that the channel is never overloaded. A similar suggestion has also been made by Seyler[40]. It is quite likely that this may be subjectively acceptable, because the eye can tolerate considerable amplitude errors in the specification of transitions.

1.6.6. Tapered Quantization of TV Signals.

In the first attempt to transmit television by P.C.M.[41], a linear amplitude quantisation was resorted to, for the conversion of the analogue signal into a digital one. It was found that unless the number of quantum levels were very large (100 or more requiring a 7 digit code), the quantisation noise produced spurious contours. These contours were visible and objectionable primarily in regions with very low details. Kretzmer[42] suggested that as the quantisation noise is objectionable in regions which are associated only with the lower end of the frequency spectrum, the transmission efficiency may be increased by progressively coarser quantisation with rising frequency.

In a practical case, the video signal spectrum may be split into several bands and the lowest frequency band may be allotted the largest number of quantum levels while the highest one may have the lowest number of quantum levels.

As a simple expedient, in the experimental set up shown in fig.6, the video signal spectrum is split into two

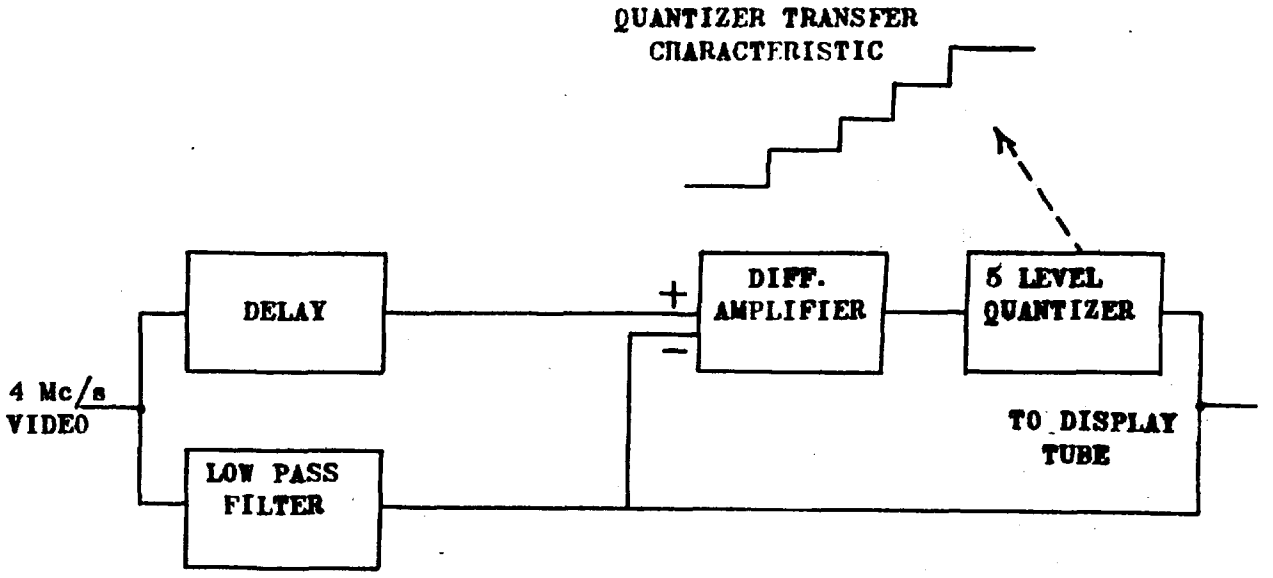


FIG. 6 KRETZMER'S REDUCED ALPHABET SYSTEM.

frequency bands:

i) "lows" extending from 0 to .5 Mc/s.
ii) "highs" extending from .5 Mc/s to 4 Mc/s.

The "highs" are quantised into five levels and recombined with the "lows" to reconstruct the picture for subjective assessment. The transfer characteristic of the quantizer has been tapered so that the quantizing error rises with higher quantum levels. Thus, small changes are produced more faithfully than larger ones. This is done ~~so~~ because the viewer is more sensitive to errors where small changes are concerned and also because experiment indicates that small changes are much more frequent than large ones.

In an actual transmission system the l.f. band will be quantised in 100 or more levels hence a 7 digit binary code would be needed for it. However the sampling rate for "lows" is only 1 Mc/s, hence the channel capacity needed to transmit the "lows" = 7×10^6 bits/sec. The "highs" can be coded in a 3 bit code (2^3 levels). The bandwidth of "highs" is 3.5 Mc/s hence the information capacity works out to be 21×10^6 bits/sec. Both these add up to 28×10^6 bits/sec. which is only half of 56×10^6 bits/sec. needed for a 7 digit conventional coding.

The experimental results suggest that the improvement in picture quality over a linear eight level quantisation is considerable. However, certain types of picture material such as human face show the presence of spurious ghost-like contours near the sharp edges.

It may be pointed out that this encoder obtains reduction in the information rate by achieving a better perceptual matching to the human receiver.

1.6.7. Predictive Quantisation

This problem of perceptual matching is approached in a different and rather novel way by Graham[43,44]. On the

basis of psychovisual observations and from experiments with circuit predictors, it is suggested that in situations where the predictor makes significant errors, i.e. is surprised, the perceptual discrimination of the human viewer is particularly low. In the case of the "previous value predictor" operating on a typical video waveforms large transient errors are produced at vertical edges in the picture. But the observer discrimination is low in these regions so that increased quantization noise in encoding these large prediction errors will not be noticeable. A strong link is suggested between prediction difficulty and viewer tolerance in reproduction of the amplitude. This leads to a concept of predictive quantisation as a means of perceptual coding where accurate prediction is demanded only when the viewer perception is high. This is ensured in practice by tapered quantization of the error signal employing fine quantum steps for the small prediction errors and coarse steps for the large errors of the predictor. This reduces the total number of quantum steps available to choose from, which in turn makes economical specification in digital form possible. It is emphasized that this principle of coding is non-statistical in nature and no consideration has been given to the effect that the quantizing process shall have on the statistical properties of the transmitted signal.

The simplest system using predictive quantization is called a Differential Quantizing System owing to its close resemblance to "delta-modulation"(45). A block diagram is shown in Fig.7(a). The predictor in this case consists of a delay equal to the sampling interval; so that the net effect of this process is that of tapered quantization of point-to-point difference signal.

A more sophisticated predictive quantizer employs a running selection from two simple prediction modes (Fig.7b). The error signals obtained by "previous value" prediction and "previous line" prediction are compared and the smaller

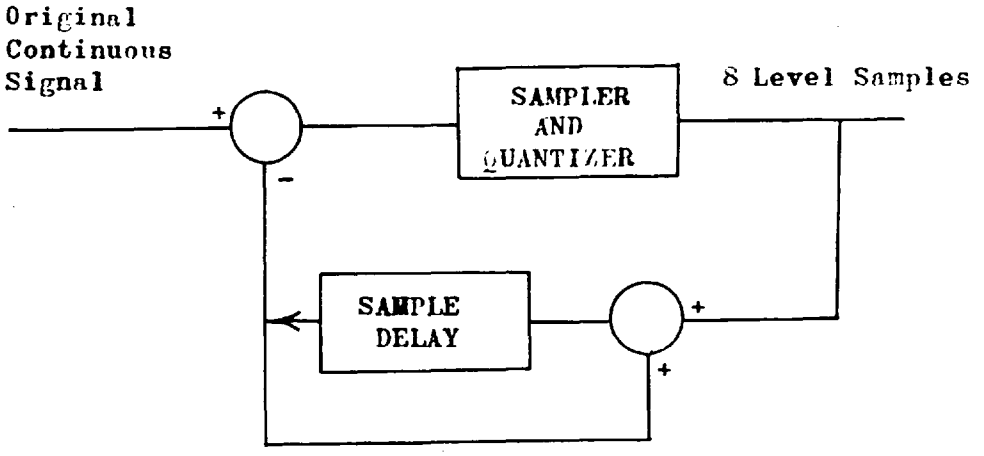
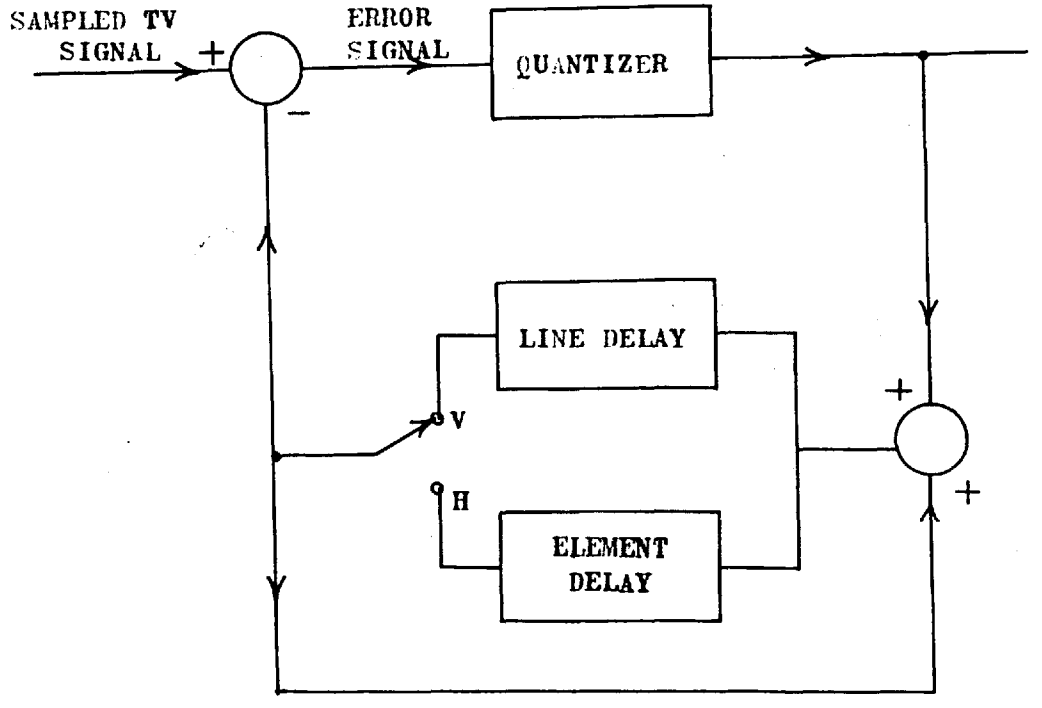

Original
Continuous
Signal
+
−
SAMPLER
AND
QUANTIZER
8 Level Samples
SAMPLE
DELAY
+
+

FIG. 7 A

FIG. 7 B


SAMPLED TV
SIGNAL
+
−
ERROR
SIGNAL
QUANTIZER
LINE DELAY
V
H
ELEMENT
DELAY
+
+

of the two is processed and transmitted to the receiver. Thus, the error signal will be zero whenever the contours are horizontal or vertical. This process has been called "Alternate-Mode Differential Quantization" (A.M.D.Q.).

The transfer characteristic of the quantiser used with both these predictive quantizers is shown in Figure 8. The eight quantum levels ($\pm$ 1, $\pm$ 3, $\pm$ 8 and $\pm$ 20 per cent) can be coded into a 3 bit/sample code instead of a 7 bit/sample code needed for linear quantisation. The vertical step at the origin in the transfer characteristic (Fig.8) will make the system hunt in the absence of an error signal.

Both the processes have been simulated on an I.B.M.-704 digital computer[46]. The differential quantizing system has also been built and tested.

The photographic results with the differential quantizing system are acceptable subjectively. There are slight defects near object outlines which may be discerned under critical viewing conditions. It is reported that the effect of random noise on the input signal is slightly aggravated by the system.

The pictures obtained by A.M.D.Q. leave very little to be desired as far as picture quality is concerned. This, however, entails line storage which is expensive in terms of money.

A virtually error-free transmission is desired because even a single error in the case of A.M.D.Q. may produce a constant brightness error over an extended rectangular area.

The amplitude probability distribution of the four test pictures after processing by A.M.D.Q. were computed by Graham. It is contended, on the basis of these statistics that a Shannon-Fano encoding of the signal will save only .9 bits/sample in the most favourable case and .36 bits per sample in the case of the most detailed picture. This saving is insignificant as compared to 4 bits/sample achieved by the non-statistical coding.

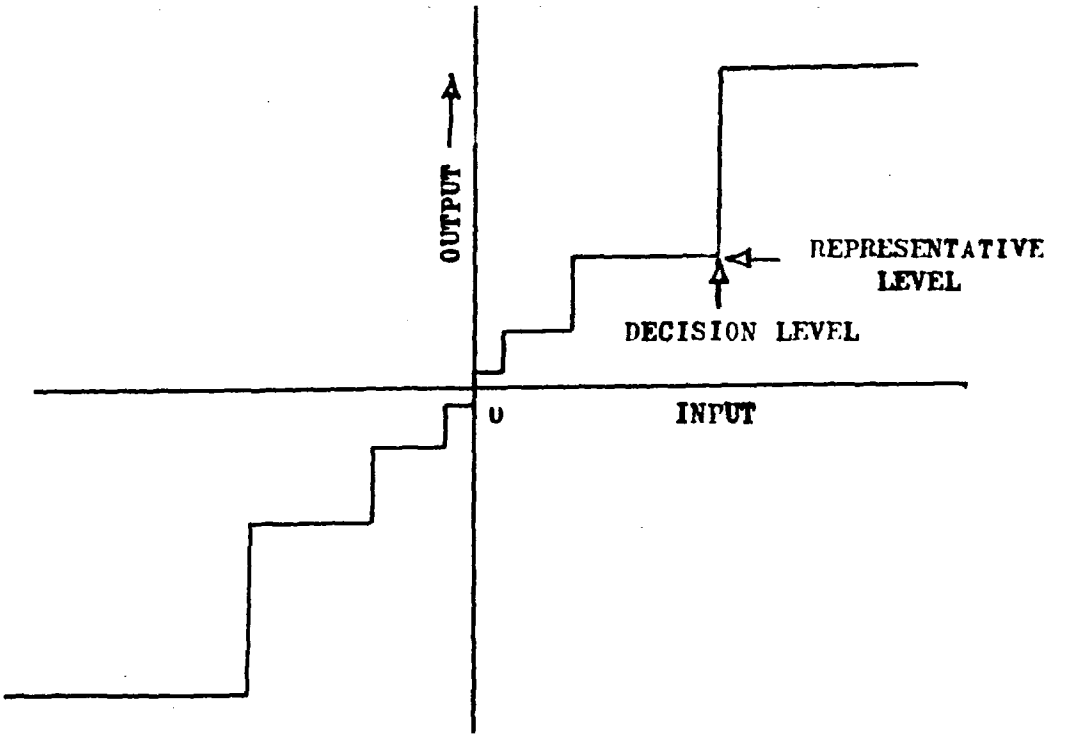
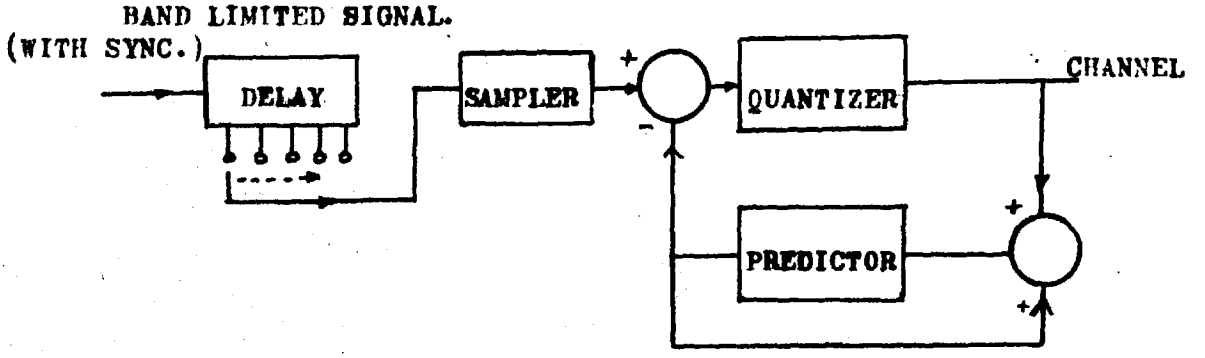
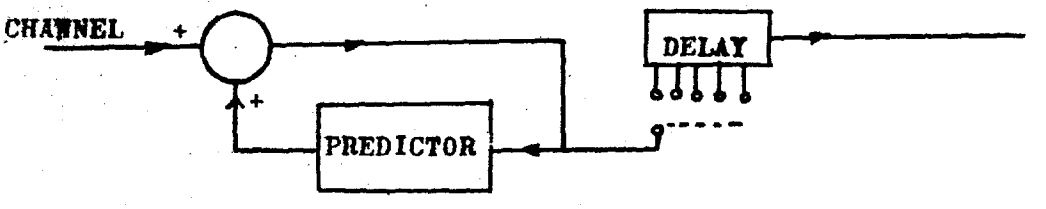


FIG. 8.



TRANSMITTER



RECEIVER

FIG. 9

An interesting suggestion has been made to utilise the blanking intervals which serve no useful purpose in digital transmission systems. It can be incorporated into predictive quantization systems to specify the samples occupying the extreme quantum levels with greater accuracy. One such system is shown in Figure 9. An elastic delay is added both at the transmitter and the receiver to the Predictive Quantizing system. Whenever the error signal occupies the outermost level, a delay of one picture point is introduced. Thus, the next sample which is also used to specify the same picture point is the error between the actual signal and the first predicted value. Thus the effect of coarse quantisation in the outermost level is reduced. The elastic delay is reset at the beginning of each line. It has been shown that by this technique with a 3 bit/sample code, a specification of 20 quantum levels are possible instead of 8.

1.6.8. Synthetic Highs.

A system called "Synthetic Highs", which exploits, both statistical correlations and the perceptual properties of the viewer is described by Schreiber et al[47]. A block diagram along with typical waveforms is shown in figure 10.

The low frequency component of the video signal is extracted by passing it through a low-pass filter of 350 kc/s bandwidth and is transmitted to the receiver. The edges in the picture are detected by point-to-point differencing and are subjected to a tapered quantization of eight levels excluding zero. These quantized edge pulses contain the edge amplitude and position information. With the help of these pulses, a signal is synthesized at the receiver. The "synthetic highs", as they are called, have the same amplitude as the edge pulse but their leading and trailing edges are shaped to be mirror images of the corresponding low frequency

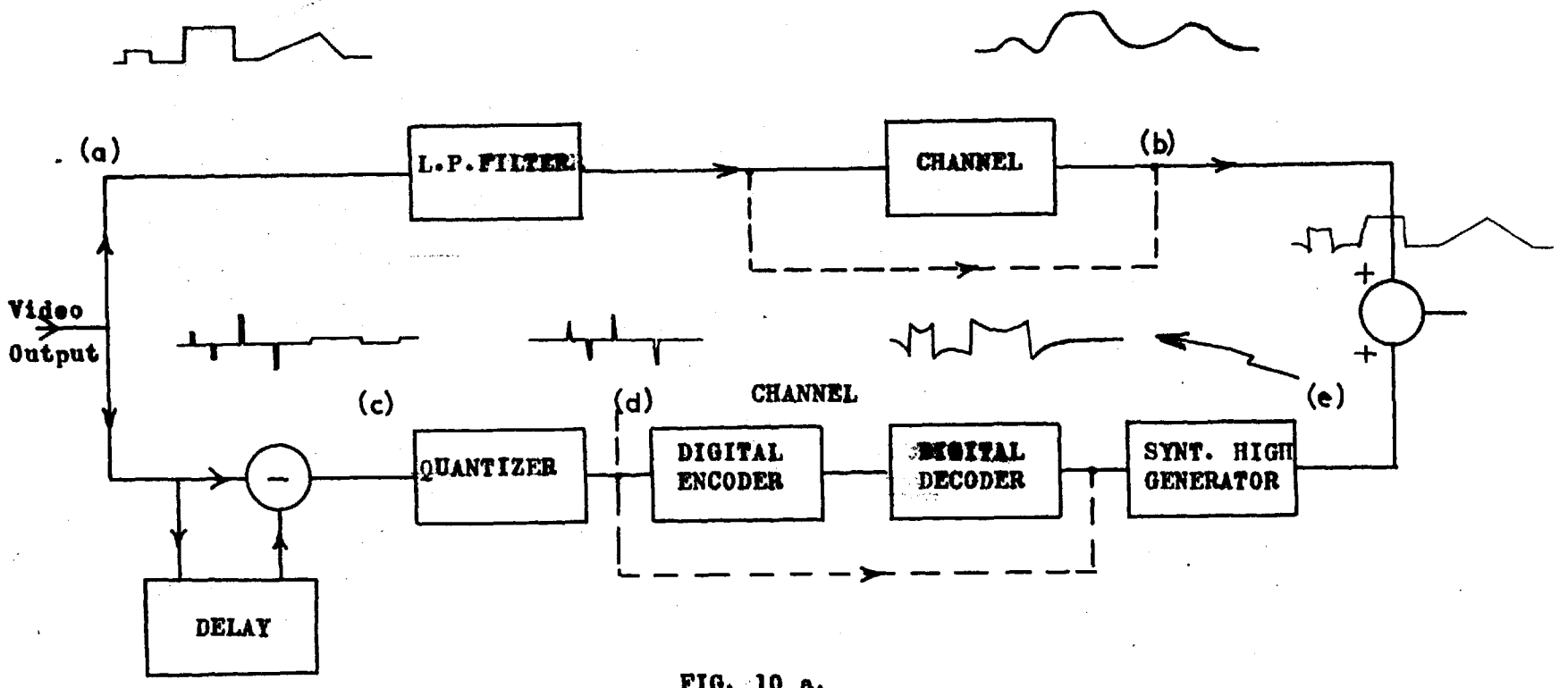


FIG. 10 a.

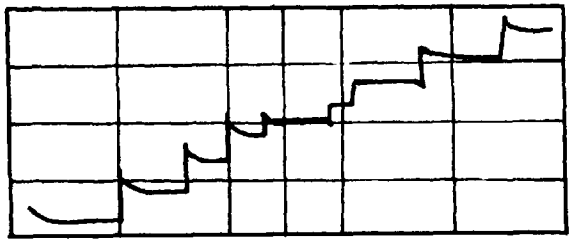


FIG. 10 b

signal. It is claimed that this prevents spurious edge effects which are visible in Kretzmer's Reduced Alphabet Code.[42]

The edge pulses are particularly amenable to statistical coding. An apparatus has been described[48] which performs run-length coding on edge pulses using 3 bits for the specification of amplitude and 5 bits for the position of the edge pulses. Thus each edge pulse is specified by 8 bits. Runs longer than 32 picture points are broken by the insertion of redundant edge pulses.

The encoded edge information is stored on eight Radechon storage tubes. Every time an edge pulse in encoded form arrives, it is written down on the storage tubes and the deflection system is so arranged that the writing beam moves by a fixed amount and waits till the next edge pulse arrives. The readout is performed at a uniform rate. The storage tubes are duplicated so that while one set up is being used for writing, the other is used for reading out. The receiver also uses 16 storage tubes for decoding.

In the experimental results produced, the statistical coding was by passed and the connection between the transmitter and the receiver was made as shown by dotted lines in figure 10. The saving obtainable by statistical coding was calculated from the average number of edges in pictures. It is reported that most pictures contain less than 30,000 edges/picture. Each edge is specified by 8 bits of information hence the information rate for the "highs" channel works out to be $30,000 \times 8 \times 30 = 7.2 \times 10^6$ bits/sec. The "lows" are quantized in 128 levels (7 digits), which gives a bit rate of $.7 \times 10^6 \times 7 = 4.9 \times 10^6$ bits/sec. Thus the total rate for the two signals is 12.1×10^6 bits/sec. This compares very favourably indeed with 56×10^6 bits/second which is the bit rate for conventional P.C.M. channel. In absence of statistical coding, the "highs" information rate shall be 24×10^6 bits/sec. This will mean a transmitter information rate of 28.9×10^6 bits/sec. which results in an economy of just below 2:1.

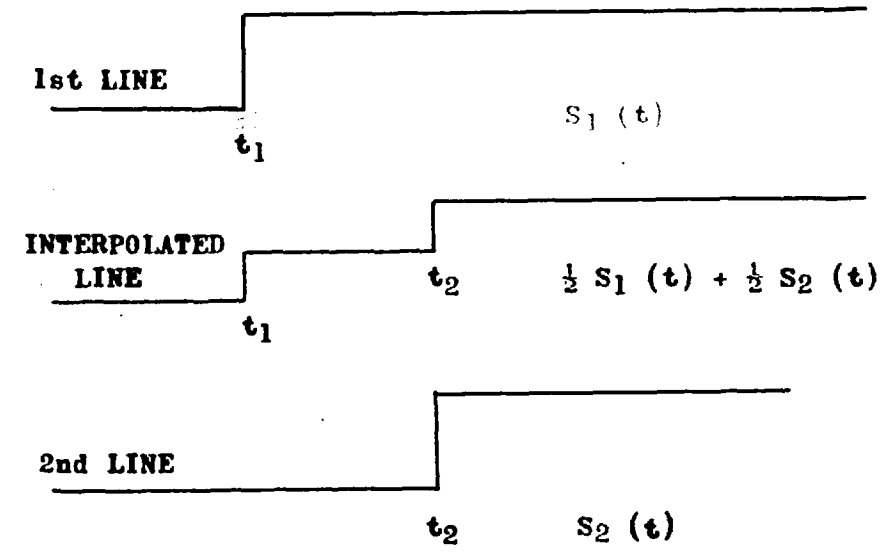
Like Kretzmer's and Graham's coders, an increase in the noise in the highly detailed areas is reported. The overall picture quality is acceptable. With the storage available at the receiver, the system is eminently suitable for standard conversion.

It is possible to achieve an actual bandwidth reduction, vis-a-vis present bandwidth of 4 Mc/s, for a non-digital channel. In this case, the amplitude of the point-to-point differencer is compared with the zero quantum step and if it exceeds this value, its analogue value is stored as a spot of charge in a continuous tone storage tube. This is read out at a constant rate generating a signal which requires a bandwidth of 450 Kc/s if the number of edges are assumed to be 30,000 per picture. With $S/_N$ ratio such that reliable recognition of 8 levels is possible, the 5 bits/edge or 4.5×10^6 bits/sec. position information can be coded by higher order A.M. code[49] to occupy a bandwidth of .75 Mc/s. This along with 350 Kc/s for "lows" and 450 Kc/s for "highs" adds up to 1.55 Mc/s which will result in a bandwidth reduction of over 2:1.

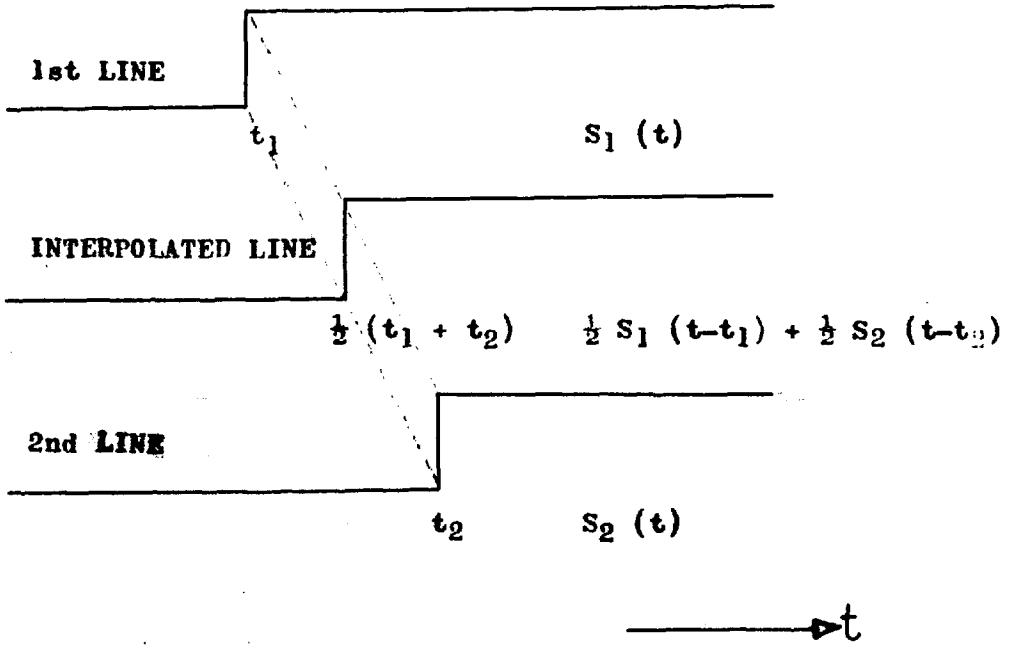
1.6.9. Contour Interpolation.

A system of bandwidth reduction which exploits line-to-line and frame-to-frame correlation is being investigated by Mr. P. Hill at Imperial College, London. It uses the principle of "Contour Interpolation" to interpolate lines and fields between the transmitted ones.[50] In linear interpolation or optical equalisation, the scheme gives good results only with stationary and vertical outlines. On the other hand, contour interpolation can reproduce without blurring a wide variety of slanting edges and also the outlines of a uniformly moving body.

The difference between linear interpolation and contour interpolation is illustrated in figure 11 which is self-explanatory. The 1st and 2nd lines in the figure may



(a) LINEAR INTERPOLATION



(b) GABOR'S "CONTOUR INTERPOLATION".

FIG. 11

represent next but one lines in the frame in which case the steps are caused by a slanting outline. If they represent corresponding lines in next but one frames, the displacement is due to motion.

In the experimental model for exploiting line-to-line correlation, two scanning spots are used. The picture itself provides storage for interpolation. The scanning spots move at the same velocity till one of them comes across an edge when velocity modulation along with the weighting of the two outputs provide the best interpolation. The experimental results are promising for a compression of 2:1.(57)

This scheme will run into difficulty in televising fast moving ball games like tennis, but for most pictures worthwhile compression without loss of quality is expected because the redundant information capacity in the conventional channel is provided by designing for flicker frequency rather than continuity of motion. It is expected that a saving of 8:1 may be possible - 2 from the saving of every alternate field and 4 from the saving of three frames in 4. The exploitation of frame-to-frame correlation entails large numbers of continuous tone storage tubes at the transmitter and the receiver besides very complex and exacting instrumentation.

1.6.10. Some Other Proposals.

A non-linear deflection system is suggested for bandwidth reduction of television signals.(2) This is based on the presumption that the entertainment value of the picture is mainly concentrated in the centre, hence a 2:1 degradation at the picture edges by constant angular deflection on a flat screen will be tolerated by the viewer.

Other proposals for economy include frequency interleaving(30), "Tete-Beche" system(52), higher order interlace and frame rate reduction with storage viewing

tubes[53,54].

In an application of variable-velocity principle[1,55] for coding of two-level signals, a reduction in the time-bandwidth product of 10:1 has been reported for "simple images" by Haynes and Hogers[56].

A study of the run-length statistics of two level printed material[57] indicates that the probability distribution is very highly peaked. In the case of a pica-type written letter of 300 words, the first ten runlengths (out of 850) have a probability of more than .7. A considerable amount of saving in the time-bandwidth product can be obtained by a statistically matched code like the Shannon-Fano Code, but the complexity of instrumentation will be prohibitive.

A compromise has been struck between instrumentation complexity and channel saving in "Coded Fax System"[58], in which variable length code groups are used for highly probable run-lengths, but code-groups of the same length are used for all the infrequently occurring run-lengths. The information storage requirements are greatly reduced by using the slide scanner itself as an elastic delay. The same line is scanned again and again at a constant rate. One run-length after the other is processed as the encoder is free to accept them. A certain amount of external memory is required to keep track of the point to which coding has proceeded in a line and to permit later resumption at the same point. The constant scanning rate is so adjusted that the processing machinery is never idle. Whenever one line is coded, a vertical timebase moves the scanning beam to the next line. For a given transmission facility, a time reduction of 3:1 is expected.

1.7. Discussion.

In the encoding of visual signals, unlike that of speech and music, there are two distinct operations involved. First is the mapping of a four dimensional signal space into

a single temporal dimension and the second is the encoding of the signal thus produced for efficient transmission through the channel.

Most of the proposals for encoding, discussed in the previous section, operate on the signals already produced by the conventional mapping technique. But in some systems, e.g. in Cherry-Gouriet system, mapping and encoding are not two separate operations but the mapping procedure itself is changed in such a way that the signal generated has a more uniform "information" rate.

In spite of the large multiplicity of proposals for efficient coding of television signals, experimental investigations have been very limited. Certain systems have been simulated on computers, others have been tested in parts and still others have been tested on scaled down models. An experimental investigation of ~~the~~ variable-velocity scanning for bandwidth reduction will be described in the later sectionsof this thesis.

1.7.1. Storage Requirements.

Encoding always entails some form of storage. The problem of wide-band storage devices with provision for very fast writing in and reading out is still the most important engineering challenge to be tackled. Almost invariably, the most expensive part of the proposed encoders is the video storage unit. Storage or delay devices are called upon to fulfill two different functions in different types of encoders:

(i) A constant delay used to store a picture point or a group of picture points for a predetermined period during which it is compared with another picture point or group of picture points and a decision is taken regarding the encoder programme on the basis of the outcome of the comparison. Examples of such delay in practical systems include Harrison's linear predictors and frame-to-frame differencing for power reduction. Both the non-statistical encoders of Schreiber

and Graham use point-to-point differencing to generate a difference signal suitable for tapered quantisation while in the more elaborate A.M.D.Q., both previous point and previous line predictors are used.

(ii) The other type of delay which is essential for any statistical encoder is called a variable or elastic delay. The elastic delay accepts the incoming "information" from a source at the rate at which it is generated and releases it to the channel at a constant rate. Storage tubes are often used for the purpose. The "information" is written on the tube at a variable rate and is read out by scanning at a constant rate. This usually involves use of two sets of storage tubes so that while one set is being used for writing the incoming "information", the other is used to read out "information" and vice-versa. The use of storage tubes[59] present many difficult engineering problems. When complete frames are stored, the problem of exact register of the read-out beam is very important. Moreover, in the continuous tone storage tubes, the $S/_N$ ratio of the output is poorer by about 10 dbs or more as compared to a typical input television signal of a $S/_N$ ratio of 35 dbs. If binary coded information is stored to get over the $S/_N$ ratio problem, the number of storage tubes increases considerably. The associated circuitry becomes more complicated and greater precision is demanded from the deflection system. All these add greatly to the cost and bulk of the equipment.

Other delay devices which are used for television work include lumped and distributed delay lines and acoustic delay line. These are suitable only for small delays of the order of 10 to 15 μsec. Acoustic delay lines may be used to provide delay up to 100 μsec. as an outside limit.

Some systems by-pass the need for a large elastic delay by using the scene itself as store[1,57,58]*. This necessitates the use of variable rate mapping of the picture which creates many problems at television frequencies.

* In the case of camera tubes, the mosaic acts as a store while in the f.s. scanner, the film or slide is used as a store.

1.7.2. Schemes in Tandem.

In Table 1.2. all the statistical encoding schemes discussed earlier are listed under the heading of the type of correlation they reduce in order to remove redundancy from the video signal.

TABLE 1.2.

Frame to Frame	Line to Line	Point to Point
Gabor	Gabor	Cherry & Gouriet
Schroter		Oliver
Seyler	Harrison	Harrison
		Jesty
		Schreiber et al
		Michel et al
		Haynes and Hogers
		Gouriet

An important reason for the preponderance of systems which exploit point-to-point correlations is the difficulty of storage.

The possibility of using more than one encoding scheme in tandem to achieve greater economy in transmission requirements has been considered. It is obvious that no two systems which exploit the same correlation can be usefully employed in tandem. Hence referring to Table II, no two schemes from the same column can be used together. Further, frequency interleaving can only be used with schemes which do not destroy line-to-line and frame-to-frame correlations.

The non-statistical proposals of Kretzmer, Graham and Schreiber et al, all exploit the same perceptual property of the viewer, hence they cannot be put in tandem. The perceptual property may, however, be exploited along with some form of statistical coding. In Schreiber's system, for example, both

statistical and non-statistical coding is used in tandem to achieve greater economy. It should be noted that tapered quantization of the edge signals produces a signal which may have a very different statistical structure from the incoming video. Whether the output signal is amenable to statistical coding is dependant on both the transfer characteristic of the non-statistical encoder and the statistics of the input signal.

1.7.3. Graham's And Schreiber's Coders.

There seems to be an apparent contradiction in the findings of Graham and Schreiber et al about the statistical properties of the output signal from the tapered quantizer. The differential quantizer of Graham is virtually identical to the edge signal encoder of the "synthetic highs" system. The picture material used in the two instances are similar in nature and yet while Graham concludes that statistical encoding of the processed signal will provide insignificant savings, Schreiber et al claim that statistical encoding of significant edge pulses will produce a worthwhile reduction of well over 2:1 in bandwidth. This apparent discrepancy may be explained on the basis of the transfer characteristic of the tapered quantizer used in the two systems.

The decision levels in Graham's quantizer are 0, $\pm$ 2, $\pm$ 5 and $\pm$ 15 per cent of the maximum amplitude and the representative levels are $\pm$ 1, $\pm$ 3, $\pm$ 8 and $\pm$ 20 per cent respectively (Fig.8). It is instructive to reproduce the relative level occupancy (i.e. probabilities) of the four pictures processed by A.M.D.Q. system.

TABLE 1.3

PICTURE	REPRESENTATIVE LEVELS ± 1	± 3	± 8	± 20
RMA Test Card	0.77	0.12	0.07	0.04
Close up of face I	0.64	0.24	0.10	0.02
Close up of face II	0.64	0.23	0.11	0.02
Man in bright check shirt	0.48	0.24	0.21	0.07

Assuming that there are 400 picture points in a line, the number of pulses occupying the different quantum levels can be calculated.

TABLE 1.4

PICTURE	No. of Pulses per line 0 ± 1	2 ± 3	5 ± 8	15 Decision level ± 20 Ref: levels
RMA Test Card	308	48	28	16
Close up of face I	256	96	40	8
" " " " II	256	92	44	8
Man in bright check shirt	192	96	84	28

The transfer characteristic of the quantizer used by Schreiber et al (Fig.10b) has a horizontal edge at the origin in contrast with Graham (Fig.8). Thus no pulse is produced at the output of the quantizer unless the input amplitude exceeds the first decision level. Unfortunately, the decision levels of the quantizer have not been quoted. It is stated, however, that "an overwhelming majority of pictures contain

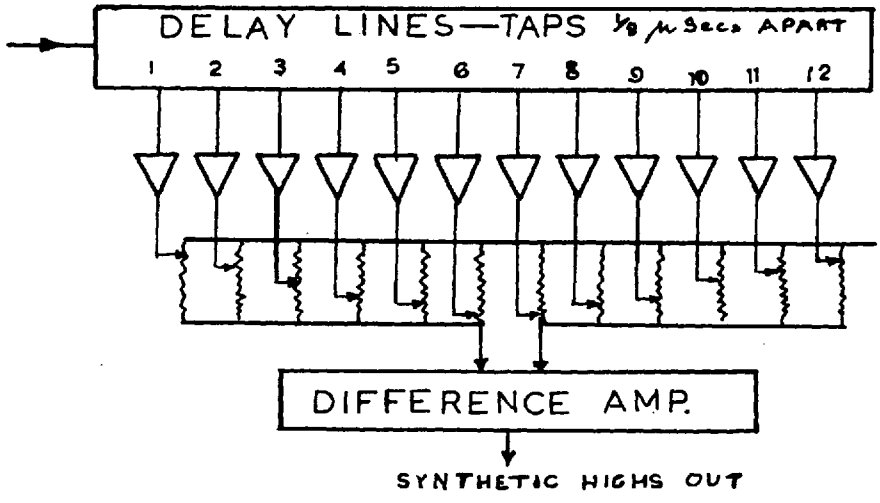
less than 900,000 edges/sec", i.e. about 75 edge pulses per line. If it is assumed that the statistical properties of the pictures investigated by Schreiber et al are similar to those of Graham, it is clear from Table IV that the first decision level in Schreiber's quantizer must be at least 5% of the maximum amplitude. If a scale is arbitrarily fitted to the transfer characteristic of the quantizer (Fig.10b) such that the first decision levels are ± 5%, the other decision levels work out to be approximately ± 9, ± 16 and ± 26% of the amplitude.

In the "synthetic highs" system, the 350 Kc/s "lows" channel quantized in 128 levels takes care of low frequency low contrast signal. But signal containing fine detail at low contrast i.e. less than 5%, is excluded from both the channels. Thus the price paid for the low number of edge pulses is the sacrifice of low contrast detail at high frequencies.

Due to the absence of a low frequency channel, it is imperative for the decision levels to be set lower in the D.Q. and A.M.D.Q. Systems which makes it less amenable to statistical coding.

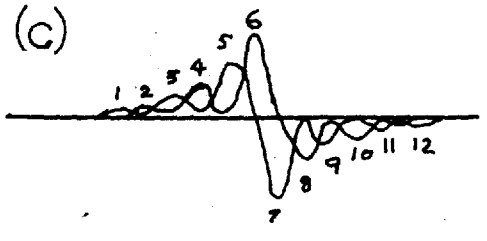
Another point that must be borne in mind is the fidelity standards set in the two systems. The prints in Schreiber's paper are, unfortunately, generally of a lower quality hence a direct and definite comparison is difficult.

In the system of Schreiber et al, a synthetic highs generator is used, at the receiver, to synthesize from the edge pulses, a signal which has the same amplitude but whose leading and trailing edges are shaped to be the mirror image of the corresponding low frequency signals (Fig.12). The generator consists of only linear elements, hence the law of superposition holds good. Some computations have been made to determine the output of the synthetic highs generator when the input consists of bursts of edge pulses very closely spaced. The results (Fig.13) show that when pulses separated


DELAY LINES—TAPS 1/8 μ Secs APART
1 2 3 4 5 6 7 8 9 10 11 12
DIFFERENCE AMP.
SYNTHETIC HIGHS OUT

(a)


(b)


(c)
1 2 3 4 5 6
7 8 9 10 11 12

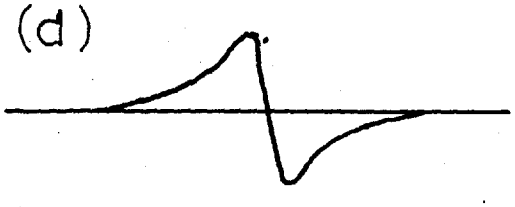
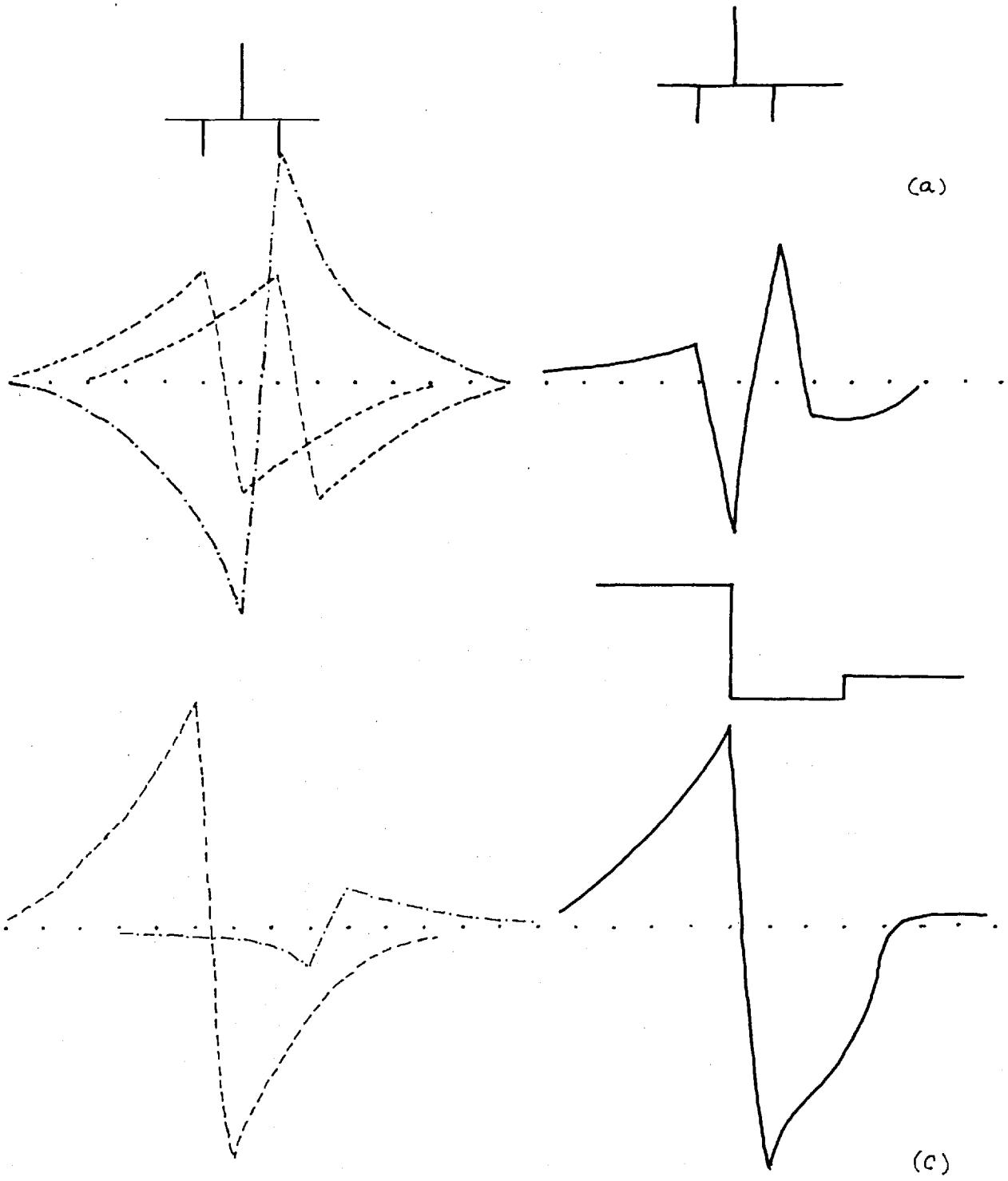
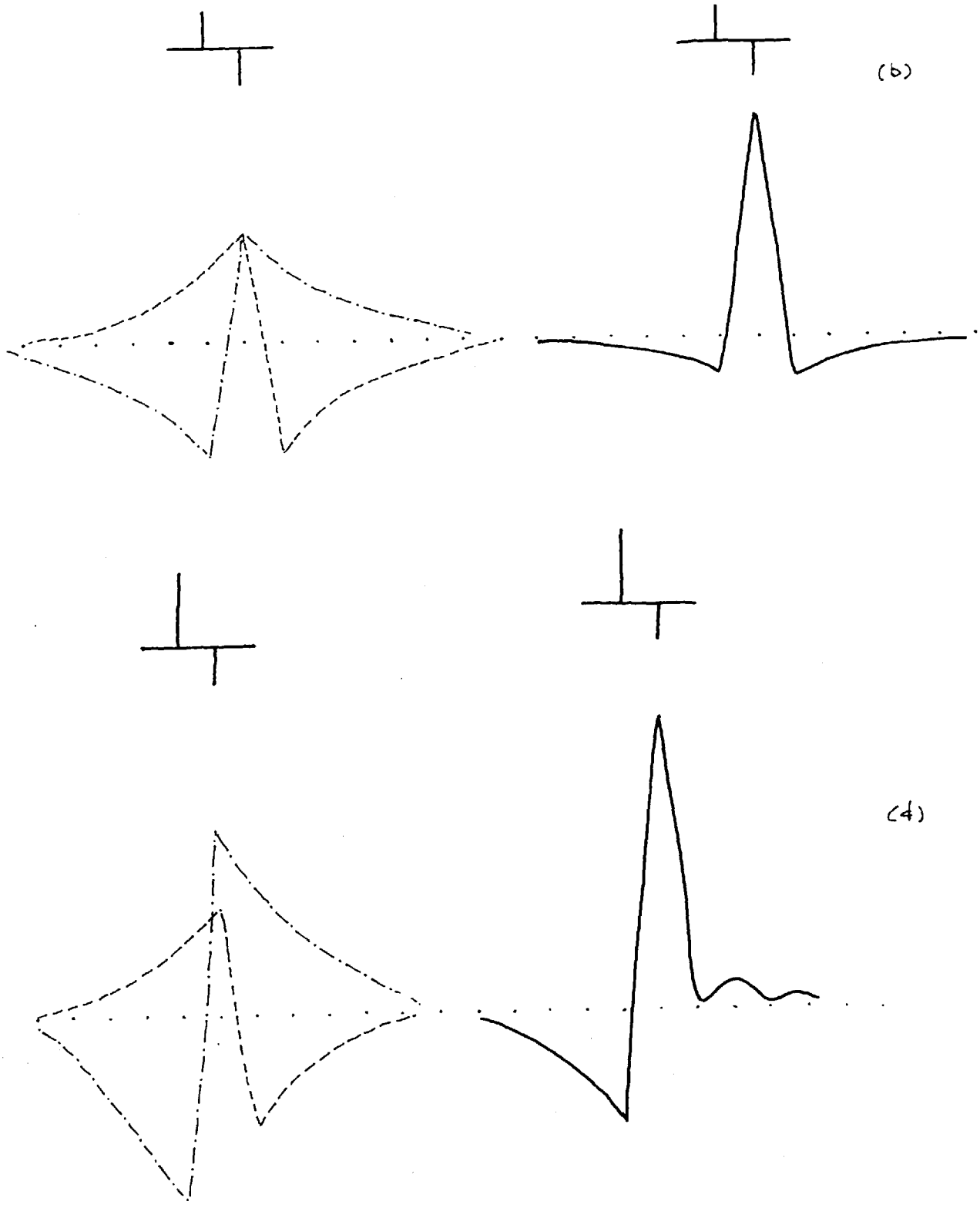

(d)

Fig. 12.



SYNTHETIC HIGHS COMPUTATION.

FIG. 13



SYNTHETIC HIGHS COMPUTATION.

FIG. 13

by only a few picture points arrive at the input, there can be substantial amplitude distortions in certain cases. The distortions are especially pronounced in figure 13a and 13c. which represent situations which can frequently arise. This type of distortion is additional to drastic quantization to which the edge pulses have been subjected. It must be emphasized, however, that the pictorial reproductions from this system seem to be of acceptable quality though the prints are not good enough to assess critically the effect of the above-mentioned distortions.

As mentioned earlier, the "synthetic highs" system requires 16 storage tubes at the transmitter and the same number at the receiver. The tubes are expensive and bulky. It seems that the brightness information which is quantized in only eight levels is eminently suitable for analogue storage on a continuous tone tube like Raytheon QK685. Thus the output of the tapered quantizer (Fig.10) can be stored on one tube and the position information on five Radechon tubes. The read out is performed at a constant rate and the output is then digitally coded. This set up cuts down the number of storage tubes by 4 at both the transmitter and the receiver. It also has the versatility that the brightness signal is available for transmission either as P.A.M. pulses or as binary P.C.M. at the same time.

1.8. Errors.

Errors in any system are caused due to noise or overload or both.

In the purely non-statistical encoders, the problem of overload does not arise but in any statistical encoding system with limited storage, there exists a finite probability of overload. It is imperative that an overload should not result in a complete breakdown but only in a temporary impairment of picture quality. This property is possessed by all the systems discussed. To prevent overload, special

constraints are introduced in certain systems, e.g. in Schroter's[34] system and Jesty's difference picture scheme[2], an abrupt change of scene can only be effected over several frames, hence abrupt cuts are to be avoided and changing scenes ought to be made to fuse into each other.

1.8.1. Channel Noise

The effect of noise on statistically encoded signal is very important. The decorrelated signal is vulnerable to interference hence a "rugged" code like P.C.M. is called for. In certain systems, the errors are cumulative so that one error is carried over large areas.

In the non-statistical A.M.D.Q. system, use of an error correcting code is recommended because a single error tends to produce a constant brightness error over an extended rectangular area.

1.8.2. Source Noise

The $S/_N$ ratio attainable with a camera or scanner is of the order of 30 to 40 dbs. This can have great effect on mapping as will be seen later in a detailed discussion of the variable velocity system. The increase of random noise in the fine detail reported by Kretzmer[21] is due to source noise. In Graham's system, in which the transfer characteristic of the quantizer has a vertical edge at the origin (Fig.8), the source noise will make the output hunt between the quantum levels ± 1 which will further enhance high frequency noise.

1.8.3. Quantization Noise

Another important source of noise in digital encoders is quantization noise. For linear quantization, very large number of quantum levels are needed to keep the quantization noise down. If the signal has a highly peaked distribution, a non-uniform quantization can be used with great advantage

TABLE 1.5

	System	Type of Coding	Type of Correlation	Storage Requirements	Bandwidth Reduction or Power Saving	Errors Brightness	Errors Position	Expected Saving	Remarks
1.	Cherry-Couriet	Statistical	Point to Point	Scene used as Store	Bandwidth Reduction	Non-Cumulative	Cumulative over line period	-	
2.	Cherry-Beddoes	" "	"	"	"	"	non-cumulative	4 : 1	Experiments performed on a 300 k/s 100 line system. Not suitable for subjective assessment.
3.	Schroter	"	Frame to Frame	Storage tube at the Transmitter. View-storage tube at the receiver.	Bandwidth Reduction and Power Reduction	Non-Cumulative		-	No experiments reported.
4.	Runlength Coding	"	Point to Point	Unspecified	Power Reduction	Non-Cumulative	Cumulative	-	No experiments performed.
5.	Linear Predictor	"	Point to point and line to line	Delay line	"	Cumulative	-	Power reduction 10-20 dbs.	10 dbs. - High detail 20 dbs. - low detail.
66.	Reduced Alphabet	Non-statistical	-	-	"			24 x 10^6 bits/ sec. out of 56 x 10^6 bits sec.	Ghost-like contours near sharp edges.
77.	Diff.Quantizer	"	-	Delay line	"	"	-	32 x 10^6 bits/ sec.out of 56 x 10^6 bits sec.	Computer simulation Results very good subjectively.
8.	Alternate-Mode Diff.Quantizer	"	-	"	"	"	-	"	"
9.	"Synthetic Highs"	Statistical & Non-statistical	Point to point	Storage tubes at transmitter and receiver.	Bandwidth Reduction & Power Reduction.	Non-Cumulative.	Cumulative	44 x 10^6 bits/ sec.out of 56 x 10^6 bits/sec.	Statistical part of encoder bypassed in experiments. Picture of acceptable quality
10.	Contour Interpolation.	Statistical	Line to line & Frame to frame	Storage Tubes	"	-	-	8 : 1	2:1 achieved on 1.f. model.
11.	Coded Fax System	"	Point to point	Scan used as store also Digital storage	Power Reduction.	Non-Cumulative.	Cumulative	Time reduction of 3:1 on a 3 kc/s. line.	For two level fassimile only.
12.	Stop-Go Scanner (Haynes & Hoger)	"	"	Scan used as store	Bandwidth Reduction	-	"	10:1 for simple patterns.	1.f. f.s. Scanner for two level facsmile only 3 kc/s bandwidth.

to minimize quantization noise[60].

1.9. Specialised Uses

With the exception of "The Coded Fax"[58] system and Hayne's and Hoger's Scanner[56], all the systems discussed have been suggested with a view to use for television transmissions. Most of these systems, however, can be modified for use in facsimile and visual data transmission. Certain requirements are different. If the receiver in a facsimile system uses photographic paper for recording, the problem of flicker does not arise. Furthermore, the $S/_N$ ratio attainable in the facsimile transmitter is much higher than in the case of television. This along with integration of random noise in photographs makes the effect of source noise much less acute.

On the other hand, research data obtained on topics like viewing distance, vs. picture height and non-linear deflection are not relevant to facsimile transmission.

1.10. Summary

In Table 1.5, the properties of different encoders have been summarised.

2. THE VARIABLE VELOCITY SCANNING SYSTEM.

2.1. Earlier Work.

The first experimental investigation of a system for facsimile transmission, based on the theoretical work of Cherry and Gouriet, was carried out by McCully[3]. A block diagram of the experimental set-up used by McCully is shown in figure 14. The transmitter consisted of a single line flying spot scanner with electrostatic deflection capable of coding black and white drawings. The experiments were performed on single edges which were generated by masking the beginning and the ending of the trace on the scanner tube.

The line deflection was provided by a modified Sanatron timebase. The timebase velocity was modulated by varying the voltage on the Miller resistance in the Sanatron. The timebase velocity was so adjusted that the output of the scanner needed a bandwidth of 20 Kc/s for undistorted transmission when the control loop was open. The differentiator and the full wave rectifier were so designed that the overall feedback loop bandwidth was about ten times larger than the uncompressed channel bandwidth. The $S/_N$ ratio of the transmitter output was 45 dbs.

The channel was made up of an adder and a lowpass filter. Two filters of bandwidths 20 Kc/s and 10 Kc/s were used to transmit uncompressed and compressed signals respectively.

The $\left|\frac{de}{dt}\right|$ circuitry and the variable velocity timebase at the receiver were identical to those at the transmitter. The output of the velocity modulated time base was applied to the x plate of a Cossor oscilloscope. The received signal was displayed as a waveform by applying it to the Y plate. Synchronization between the transmitter and the receiver was provided by a common synchronizing pulse generator for both the time bases.

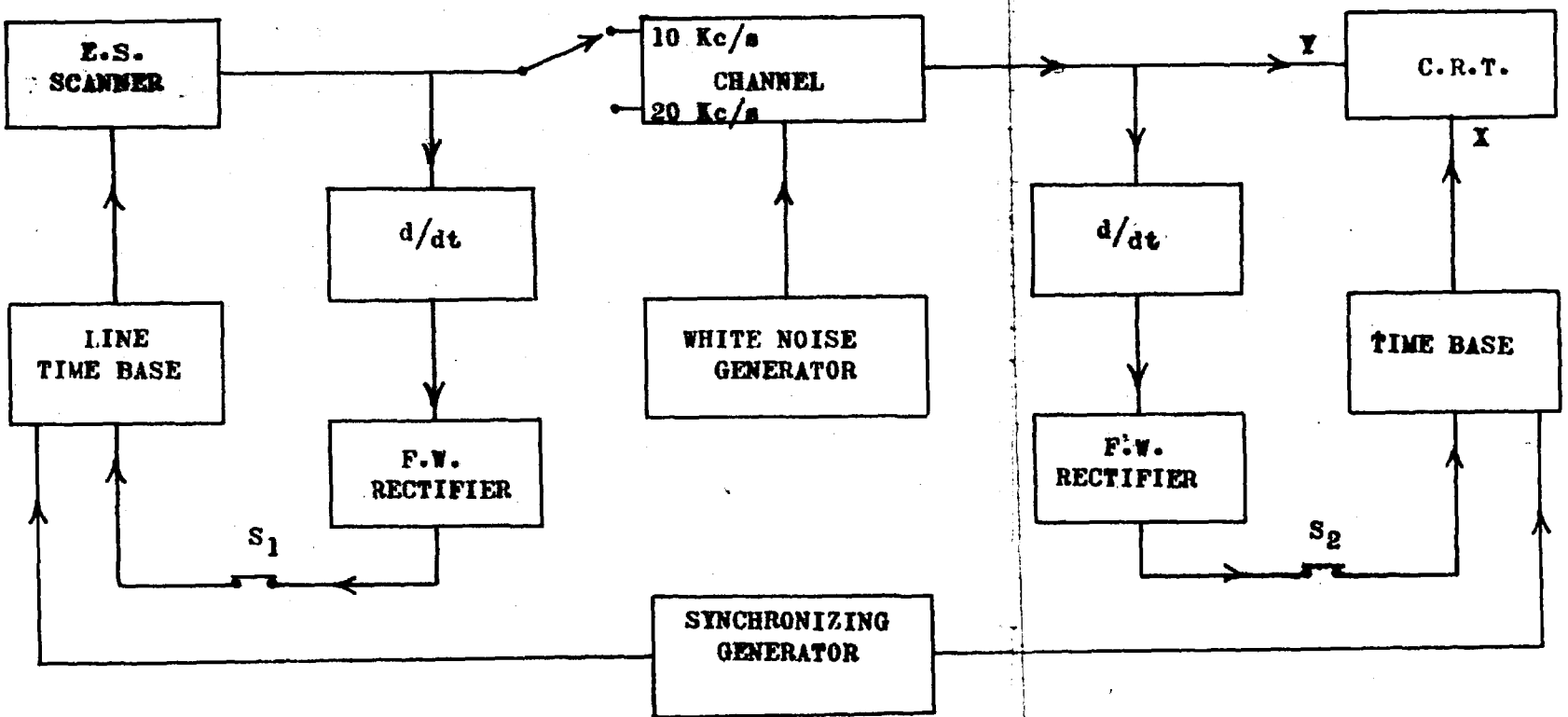


FIG.14. V.V. SYSTEM AS USED BY McCULLY.

The experimental results showed that for a 2:1 compression, the rise and fall timesof the edge at the receiver were virtually unaffected. It was observed, however, that low rates of change of amplitude were not completely decompressed at the receiver. This resulted in a long slow rise before the edge centre and rounding off near the top. In another experiment, noise was added to the signal in the channel. This caused a jitter on the displayed waveform at the receiver.

A more detailed investigation on Cherry-Gouriet system was carried by Beddoes[4]. A monoscope, with a test card 'C' target built in it was used as the video signal source.

To avoid expensive and time consuming circuit development, an experimental system was built with the following specifications:

Picture Repetition frequency	10 C/s
Frame Repetition frequency	20 C/s
Lines per picture	<100
Picture elements per line	600
Equivalent Uncompressed vision Channel bandwidth	300 Kc/s.

It may be noted that the line definition of the experimental system was made equal to that of the B.B.C. Electromagnetic scanning was used both at the transmitter and the receiver. The frame scanning process was conventional. A variable velocity line scanner for magnetic deflection was developed and analysed.[61] It was claimed that the bandwidth of the feedback loop at the transmitter was limited by the poor focus of the monoscope to 300 Kc/s. The $S/_N$ ratio of the output signal was reported to be 96 dbs.

The experimental results showed that bandwidth compression greater than 1.7:1 was accompanied by serious spatial distortion Decompression at the receiver, also reported by McCully,

proved serious for multi-level pictures. It was also found that the system became unstable for large feedback gain i.e. high compression.

Two major modifications were suggested to get larger compression without spatial distortion.

(1) A separate channel to transmit position information from the transmitter to the receiver.

(2) Use of "frequency feedback" (a high pass filter or a network with equivalent characteristic) instead of slope feedback.

The use of a high pass filter in the feedback loop produced results worse than those with the differentiator. The deterioration was attributed to inherent time delay in the high pass filter and to the poor focus of the monoscope. A "Difference Order" filter (Fig.15) was designed with which results slightly better than those with the differentiator were obtained.

A separate position channel made a great improvement in the performance of the system. The experimentally determined bandwidth for position channel was found to be "between 1/8 and 1/19 of normal channel bandwidth". Since errors in this set-up are not cummulative no spatial distortion resulted towards the end of the line.

The design of the receiver was greatly simplified in the modified system (Fig.16). It consisted of a video amplifier, a position signal amplifier with driving circuits and a conventional frame time base.

An overall bandwidth reduction of 3.75:1 was achieved on test card 'C'. The picture, however, suffered from the effect of jitter - especially visible in the band defining detail in the test card. Another defect in the picture was due to conventional frame scanning. In regions of the

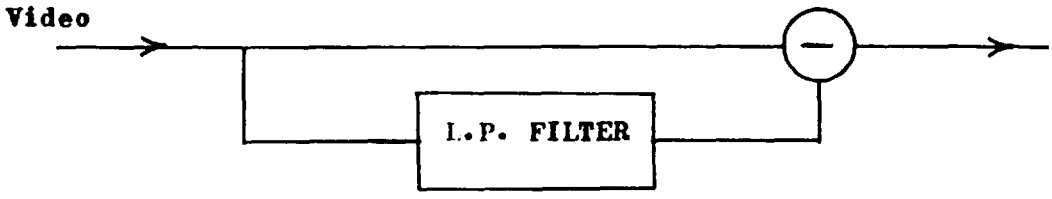


FIG.15 DIFFERENCE ORDER FILTER

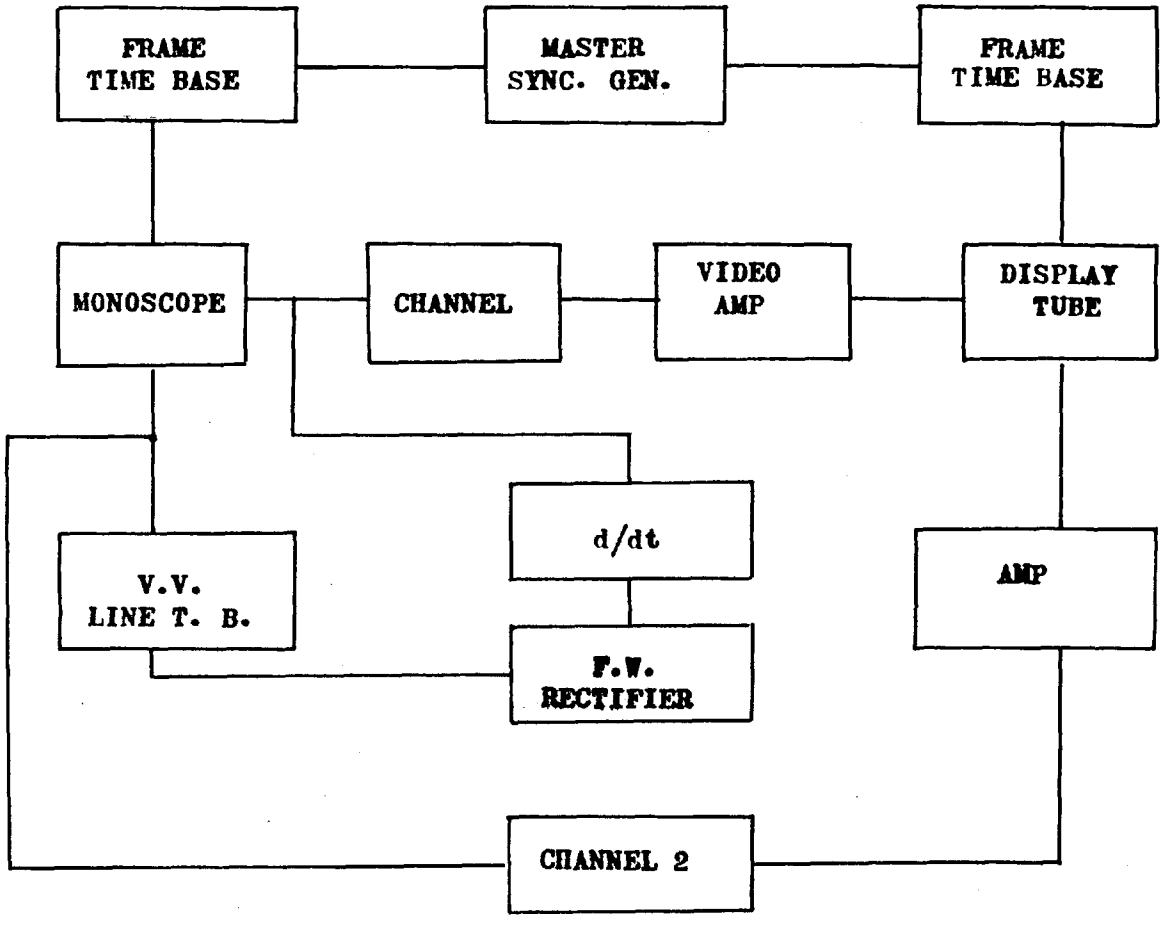


FIG.16. TWO CHANNEL SYSTEM AS USED BY BEDDOES

picture in which the lines contained a large amount of detail, the time spent in scanning each of these lines was larger while in the regions containing little or no detail, the line scan period was small. This brought about the crowding of the lines in the region of little detail at the cost of lines in the high detail region. The lines were, thus, no longer equidistant and the vertical resolution deteriorated in the regions in which horizontal fine detail was coded by the variable velocity scanner.

2.2. Some Limitations.

The results of McCully and Beddoes were encouraging and suggested the need of investigating some aspects in greater detail while considering others which had not been taken into account in the earlier work.

Someof the limitations of the experimental setup used by Beddoes are as follows:

(1) The monoscope had a fixed pattern built into it. This restricted the flexibility of the system. Experiments on different types of pictures or even on some small portion of interest in the built-in test card itself were not possible.

(2) The system standards were scaled down. While this helped the initial investigators very much in saving both money and time, it had three serious limitations:

Firstly, owing to the reduced number of lines and low flicker rate, a subjective evaluation of the picture was not possible.

Secondly the $S/_N$ ratio achieved was very high owing to slow scanning and reduced bandwidth. The effect on the encoder performance of lower $S/_N$ ratios, that are inevitable in a standard system was not studied. The importance of this point cannot be overemphasized. One of the cardinal weaknesses in many systems discussed in Section I is that

the signals have been assumed virtually noiseless at the source and only channel noise has been considered. The tacit assumption that a noise free signal is available from the source for processing is far from true.*

Lastly, the design problems for standard systems are different. To achieve a large bandwidth in the feedback loop in a variable velocity system built to B.B.C. standards, challenging circuit design and development problems have to be faced.

(3) The non-uniform vertical resolution due to conventional frame time base has already been mentioned.

2.3. A New Slide Scanner.

In order to remove the above-mentioned limitations, it was considered desirable to build a slide scanner to B.B.C. standards with provision for variable velocity scanning in the horizontal direction and a staircase type (Ratchet) deflection in the vertical direction. The interest in this problem was further enhanced by the fact that with the type of components available, viz. short decay time phosphors, photomultipliers etc., the investigation tended to be a feasibility study of the system rather than mere substitution of wider bandwidth in an already tried-out technique.

The claims of both the television camera tube and the flying spot scanner were considered and it was decided to build a scanner of the latter type. Because of almost noise-free multiplication[62] by the photomultiplier in the flying spot scanner, it is possible to obtain better quality pictures than those produced by camera tubes.

A very important factor in favour of the flying spot scanner is that no cumulative effect takes place in it. The signal at any instant is due solely to the illumination at that instant. In the case of the camera tube, on the other hand, the charge pattern builds up during the entire frame

* The noise, referred to, is the shot noise generated in the photo-electric device as distinct from the grain noise which may be treated as perceptually redundant detail.

period (1/25th of a second). For this reason, it will be essential to incorporate a velocity-modulation correction signal at the transmitter if a camera tube is used while this complication is eliminated in the case of the flying spot scanner.

Another disadvantage of camera tubes, e.g. the iconoscope, is that they produce spurious signals in the absence of illumination, which is superimposed on the picture signal when the tube is working.

In the flying spot scanner, an important factor, affecting the system performance, is the afterglow of the phosphor of the scanner tube light source. The effect of afterglow is similar to band limiting and methods have been suggested(64) to reduce it. Unfortunately, compensation for afterglow results in a diminished $S/_N$ ratio. However, with modern phosphors like P16, a decay time constant of 1/10 μsec. may be obtained. It was decided to use a phosphor with the shortest available decay time constant without any afterglow correction.

2.3.1. The Flying-Spot Scanner.

A flying - spot slide scanner built to B.B.C. standards with conventional scanning was kindly provided by Marconi Wireless and Telegraph Company Ltd. The block schematic diagram of this scanner is shown in figure 17. This equipment has been used to measure the spectra of pictures which shall be described later. The mechanical parts, viz., the housing for the scanner C.R.T. and the photomultiplier as well as part of the optical system have been used in the variable velocity flying spot scanner.

In the Marconi scanner, the scanner C.R.T. was housed in an enclosure built on a standard rack to prevent external illumination from affecting the scanning process. A photographic lens with an aperture f.3 was used to form a

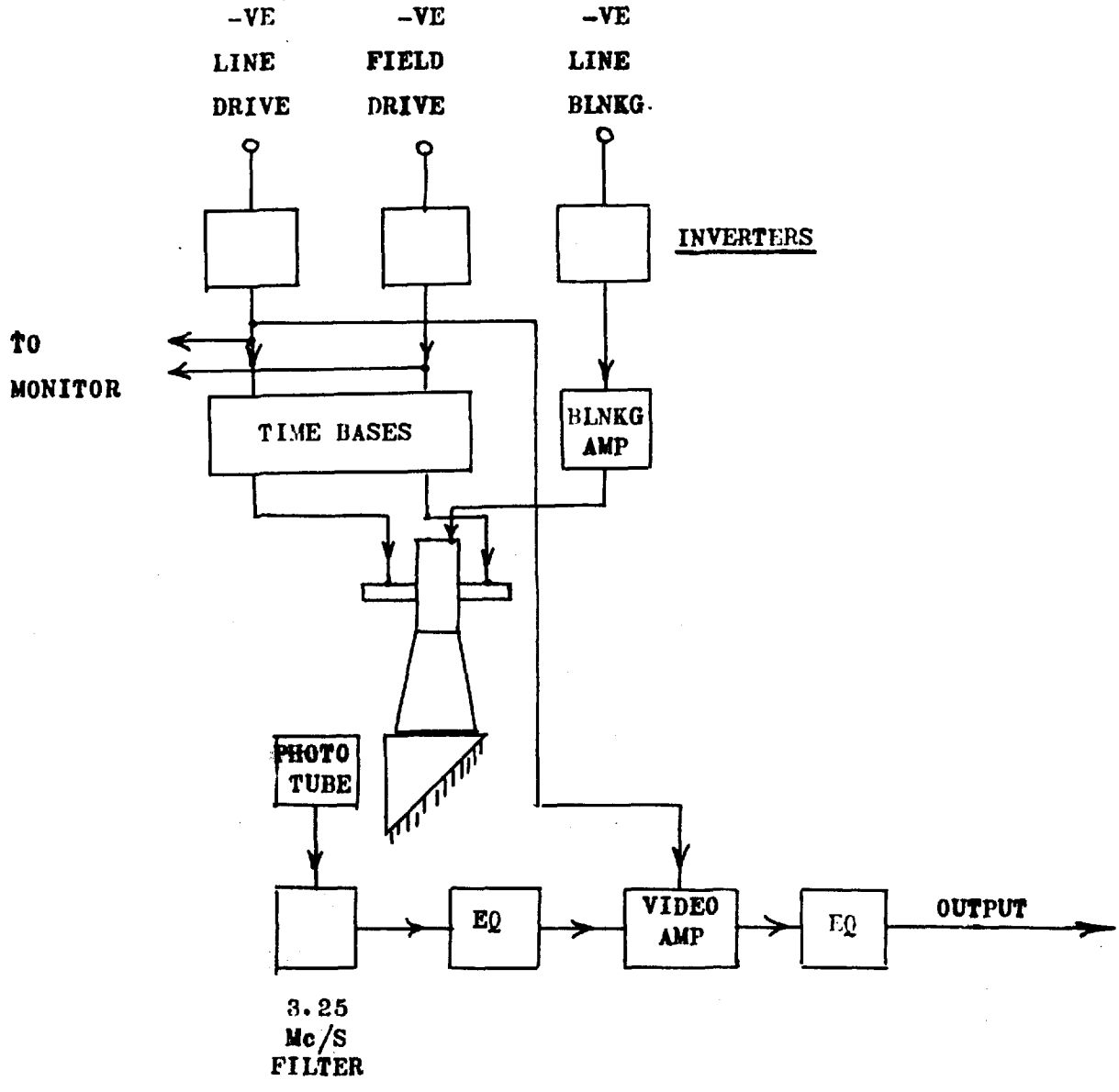


FIG. 17 FLYING-SPOT SLIDE SCANNER

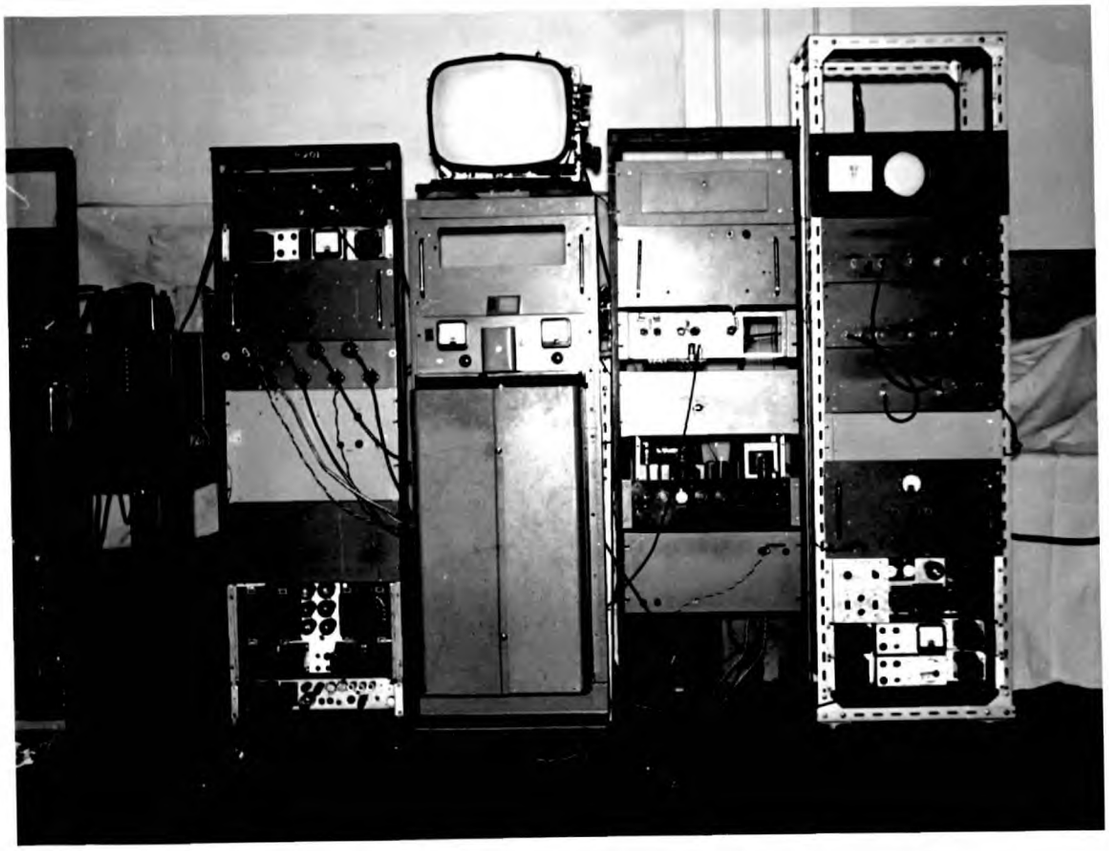
sharp undistorted image of the raster on the slide. A large condensing lens collected the transmitted light, which with the help of the mirror arrangement, was made to fall on the circular photocathode of a head-on photomultiplier type R.C.A. 5819 (Fig.18 b and c). The output of the photomultiplie was taken to a head amplifier (Fig.19) which produced a picture signal of 1 volt peak to peak across an output impedance of 75 ohms.

The video amplifier was a three stage conventional amplifier using series and shunt peaking and with a cathode follower as the output stage. A synchronous clamp was built-in which clamped to a fixed level the output of the video amplifier during the blanking period to establish the black level. The deflection system consisted of a line and frame time base of conventional design for electromagnetic deflection.

2.4. The Variable Velocity Flying Spot Scanning System.

One of the most important and exacting requirements of the variable - velocity system is the wide bandwidth in the internal feedback loop at the transmitter. This is especially difficult to achieve when experimenting with magnetic deflection systems. The research department of Marconi W.T. Co. undertook to provide a line output transformer and coil for the deflection system with a "bandwidth of 3 Mc/s. However, the supplied transformer and coil combination had a response as shown in figure 20. It was measured by putting the deflection system in operation with a sine wave input and by measuring the length of the scan at the cathode ray tube face. A separate examination showed that the main limitation was imposed by the transformer.

The scanning coils consisted of series connected saddle coils for line deflection and a toroidal winding for the frame deflection. The inductances of the two coils were 116 μH and 212 μH respectively. Because of the very low impedances, the deflection sensitivity of the coils was low but also the



The F.S. Scanning System and the Receiver



The Scanner tube



Close up of the mirror and
Photomultiplier Housing
(Lightproof cover removed)



Condensing lens and Mirror Assembly

FIG. 18

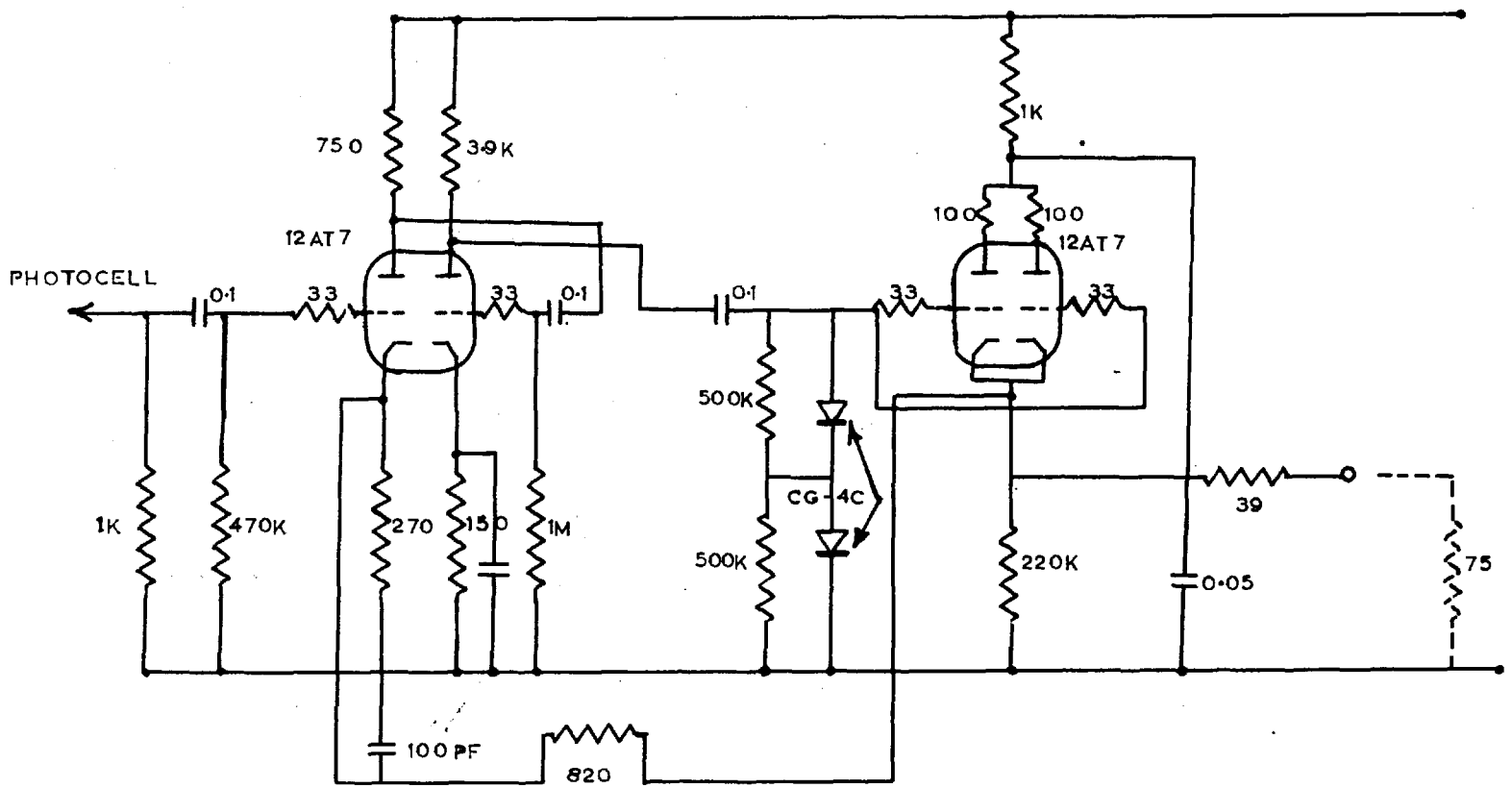


FIG.19. HEAD AMPLIFIER

first resonance was above 1 Mc/s. It was decided to retain the coil and to aim to design and build a transformer, which with the coil would give a deflection system "bandwidth" of 1 Mc/s and also a reasonable scan length.

A block schematic of the new variable velocity system is shown in figure 21. The frame time base at the transmitter has been omitted to save time and funds, but provision has been made to instal one later if the apparatus is deemed suitable for performing subjective tests on full pictures. By including a facility for frame deflection at the receiver, the effect of jitter on edges, reported by Beddoes, can be studied.

The specifications of a complete system may now be summarized as follows:

(a)	Picture Repetition Frequency	approx. 25 c/s
(b)	Lines per picture	405
(c)	Picture Elements per line	600
(d)	Line repetition frequency	10 Kc/s (mean)
(e)	Equivalent Uncompressed Vision Channel Bandwidth	3 Mc/s

The line repetition frequency and the frame repetition frequency are not fixed in this system. The time spent in scanning any line is dependent on the amount of picture complexity in that line. A line with no transitions will be scanned in a much shorter time than one with many transitions. Since the number of lines in a frame is kept constant, the time taken to scan the picture would be equal to the sum of all the line durations in the frame. Hence the flicker rate in the system is not constant but varies with the amount of complexity in the picture. If the system is overloaded, the flicker rate will fall below the minimum that is subjectively acceptable. In a well-designed system, designed on the basis of picture statistics, the probability of overload can be specified. A disadvantage in this

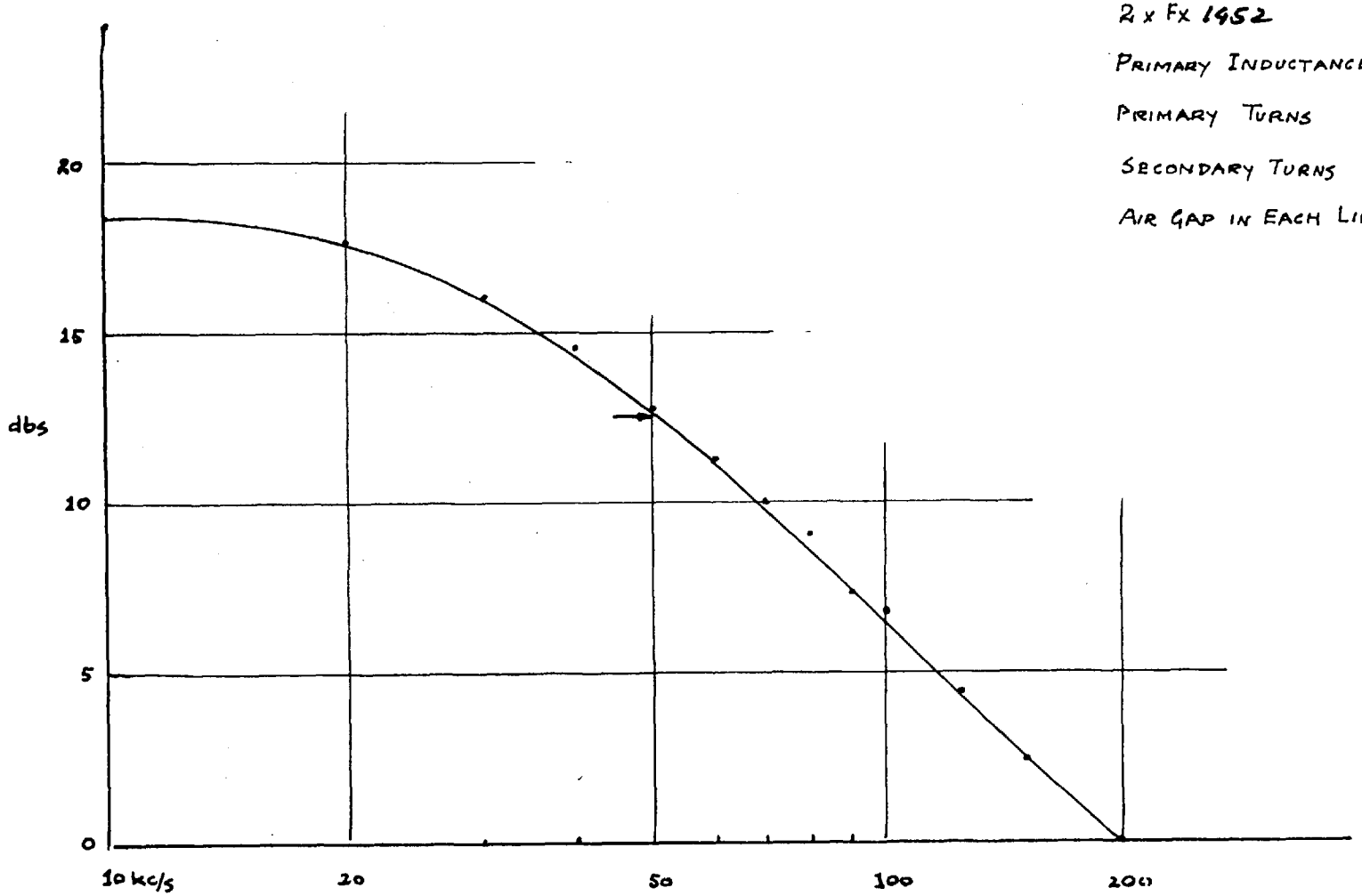


Fig. 20. Deflection System Response with Marconi Transformer.

arrangement is that the frame deflection circuit cannot be locked to the mains frequency. However, the hum modulation can be made very small by careful design of the system.

Two possible methods are available to keep the flicker rate constant. The first is to introduce waiting time at the end of each line, the second at the end of each frame. The first would be very wasteful and would show overload effect as incomplete lines in the picture. In the second, overload will result in a diminution of the number of lines in the frame with the resultant loss of the lower part of the picture. This may be more objectionable to the viewer than the falling off of the flicker rate, though experiments may have to be performed to test the validity of this suggestion. Further, if display tubes with longer persistence become available, the performance of the system adopted will improve automatically.

2.5. Components Of The System.

In this section, the component parts of the system are discussed. The important features of circuit design are described and the choice of certain components is explained.

2.5.1. C.R.T. for the Scanner.

The effect of the phosphor afterglow on the bandwidth of the scanner has already been mentioned in Section 2.3. Correction for the afterglow is accompanied by a reduction of the $S/_N$ ratio. The $S/_N$ ratio in a flying - spot scanner depends on the photocathode current in the multiplier and on the decay time-constant of the phosphor[65]. Hence the two most important properties specified for a scanner - tube phosphor are very short decay time-constant and large light output.

Two scanner tubes types 6/22 QM and C 219 - QIF were used in the experiments. The first, manufactured by Ferranti Ltd. had a decay time-constant of $1/_{10}$ µsec. The second was a cintel tube with a P16 phosphor which had a

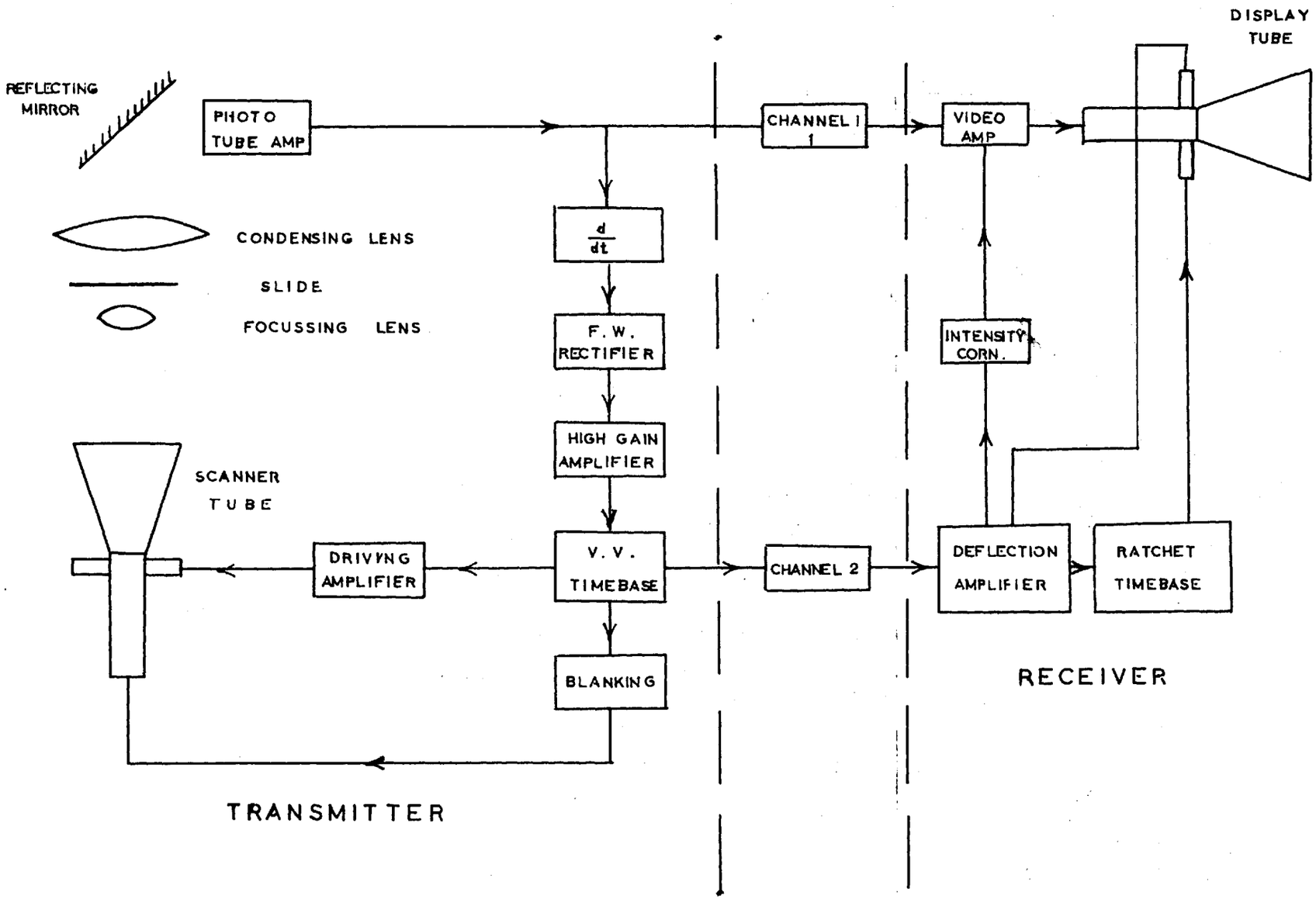


FIG.21. BLOCK DIAGRAM OF THE VARIABLE VELOCITY FLYING SPOT SCANNER AND THE VARIABLE VELOCITY RECEIVER

decay time-constant of less than 1 μsec. but had a finer grain structure.

2.5.2. The Optical System

The optical system, shown in figure 21, consists of a f.3.0 photographic lens on a helical mounting, a large condensing lens and surface silvered mirror. The photographic lens forms an undistorted image of the flying spot on the transparency. The transmitted light is collected by the condensing lens, turned through 90° by the mirror and falls on the circular photocathode of the photomultiplier tube. As the photomultiplier responds to the total light flux falling on the photocathode, an inexpensive condenser lens is adequate because aberrations and distortions are not important. A large aperture increases the optical efficiency and hence the performance of the scanner.

2.5.3. The Photomultiplier Tube

Photomultipliers with large area semi-transparent photocathodes have been specially developed by many firms for use with large aperture scanning equipment. For use in a flying-spot scanner, a photomultiplier should have high sensitivity, large photocathode area, small time spread and a good spectral match with the scanner tube light output spectrum. A study made by Hoover et al[66] shows that type S11 photocathode has a good spectral match with P16 phosphor.

An E.M.I. photomultiplier type 9536B is used in the present system. This tube has a Sb - Cs photocathode of S11 spectral response. The sensitive photocathode is formed as a semi-transparent film on the end window, a circular flat face with a diameter of two inches. A "venetian blind" type dynode structure is used and there are ten stages of multiplication in the tube. This type of dynode structure has certain advantages.[67] The photo-sensitive surfaces on the dynodes are protected from positive ion bombardment. The structure prevents radiative and optical feedback from anode to cathode. Ionic feedback is small. The time dispersion in this tube is

about 18 m μsec with a supply voltage of 1.9 KV. This is higher than in R.C.A. tubes because variation in the path lengths of electrons during multiplication is greater in tubes with unfocussed dynodes than in the focussed type.(68) The magnitude of the time dispersion is considered satisfactorily low for this particular application.

The overall gain of a photomultiplier varies as a high power of the operating voltage. In the case of a 10 stage multiplier with C_{s_3} S_b dynodes, the overall gain is proportional to v^7 where v is the inter-dynode voltage.(68) In order to keep the overall gain of the photomultiplier reasonably constant, a specially designed power supply, designed and built by Marconi W.T. Ltd. is used. The supply voltage can be varied between - 1.4 KV and - 1.8 KV which provides a very effective gain control. Fig.22 shows the supply circuit for the photomultiplier tube. The photomultiplier is used with a peak output current of 500 μamps. The output of $1/_2$ volt peak to peak across the 1 kilo-ohm load resistor is fed to the head amplifier.

2.5.4. The Head Amplifier.

The head amplifier (Fig.19) is part of the scanner designed and built by Marconi W.T.Co.Ltd. The amplifier provides an output signal of 1 volt, peak to peak, across an output impedance of 75 ohms.

2.5.5. The Differentiator.

It is well known that a lead can be used to differentiat an electrical input if the time-constant of the lead is small. Referring to figure 23(a), the transfer function may be written as:

$$\frac{\bar{e}_{out}}{\bar{e}_{in}} = \frac{p}{p + \frac{1}{RC}} = \frac{p \cdot RC}{1 + pRC} \qquad (2.1)$$

where $\bar{e}_{out}$ = Laplace transform of the output waveform
$\bar{e}_{in}$ = " " " input "

9536 B

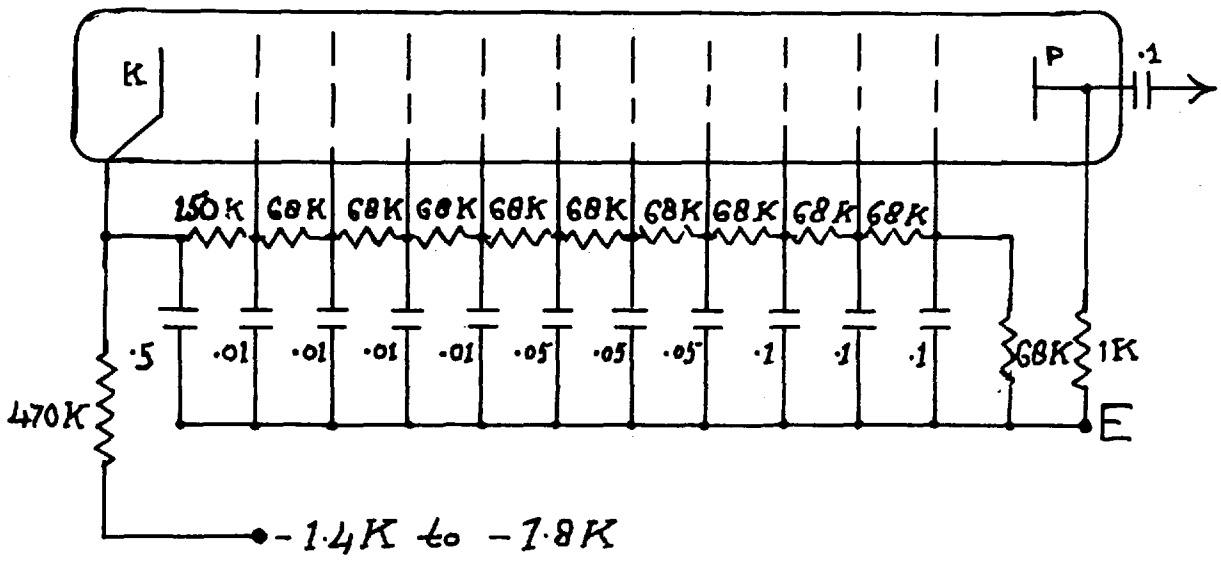


FIG. 22. SUPPLY CIRCUIT FOR THE PHOTO TUBE

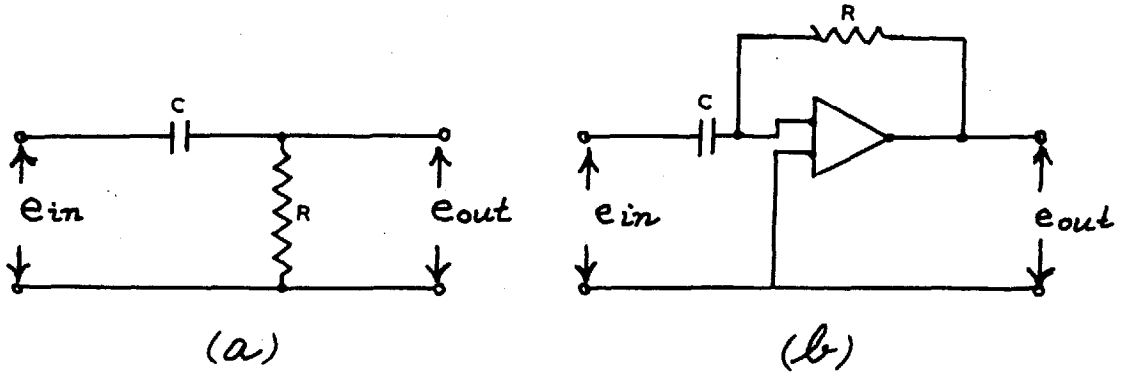


FIG. 23.

If pRC is very small as compared to 1, pRC can be neglected in the denominator giving $pRC \ll 1$

$$\frac{\bar{e}_{out}}{\bar{e}_{in}} = p \cdot RC \qquad (2.2)$$

This method, like most others, depends upon the current through a capacitor being proportional to the derivative of the voltage impressed across it.

The product RC cannot be reduced indefinitely. The smaller the time-constant, the higher is the attenuation. At high frequencies where pRC in the denominator of equation (2.1) cannot be neglected, the action of the lead may be visualised as that of a perfect differentiator cascaded with an integrating circuit.

The effects of this integrating circuit can be minimised and excessive attenuation prevented by using a feedback differentiator as shown in figure 23b. Negative feedback tends to keep the grid potential constant, thus creating a virtual earth. If the gain of the amplifier is assumed to be infinite and if its output impedance is assumed zero, it can be easily shown that perfect differentiation can be performed. If the gain of the amplifier in figure 23b is -A, the transfer function can be written as[69]

$$\frac{\bar{e}_{out}}{\bar{e}_{in}} = \frac{-A \cdot p}{p + \frac{A + 1}{RC}} \qquad (2.3)$$

A comparison of equation (2.3) and (2.1) shows that the time constant and the attenuation that would have resulted from a simple RC circuit is absent.

The feedback differentiator is more stable than an equivalent combination of an R-C circuit and an amplifier compensating for the attenuation. In the feedback differentiator, the transfer function is invariant to small

changes in valve characteristics or component drifts. A low impedance virtual earth at the grid minimises the effects of extraneous pick-up. Other attractive features of the feedback differentiator are freedom from distortion and a low output impedance.

In the system described, the most important specifications of the differentiator are that it should perform error-free differentiation in a wide range of frequencies, from a few Kc/s to at least 3 Mc/s, and that its transfer function should be invariant to small changes in valve characteristics or component drifts.

A feedback differentiator, shown in figure 24, was designed to obtain these characteristics. The input valve V_1 is a cathode follower used to drive the differentiating stage. Because of the virtual earth at the grid of V_2, the input impedance of the differentiating stage is equal to the input capacitance. The amplifier valve V_2 is a pentode with a very high trans-conductance (16.5 mamps/volt). The cathode current of V_2 is stabilised by using a 10 K ohm cathode resistor Cathode degeneration in the operating frequency range is prevented by bypassing the cathode resistor. The feedback resistor R with the input capacitance C forms the differentiati time-constant. The large gain and the low output impedance is provided by V_2 and V_3. The capacitor C_s is inserted to stabilise the feedback circuit. The cathode follower V_4 acts as a buffer stage and provides a low output impedance. This is introduced to prevent excessive capacitive loading at the cathode of V_3 which would have a deleterious effect on the performance of the differentiator.

The response of the circuit of figure 24 is plotted in figure 25 which shows near ideal response between 4 Kc/s and 4 Mc/s.

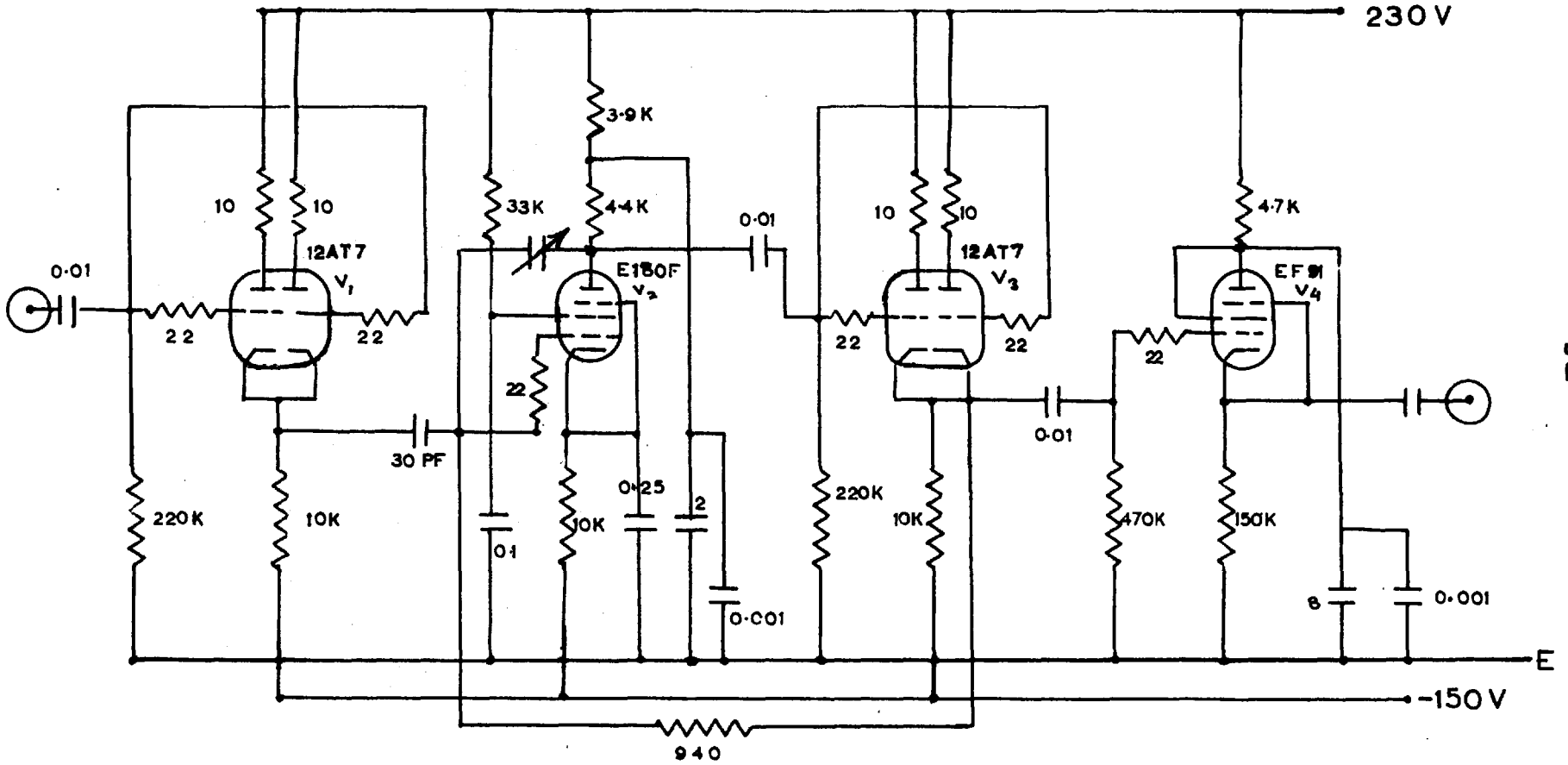


FIG.24. DIFFERENTIATOR

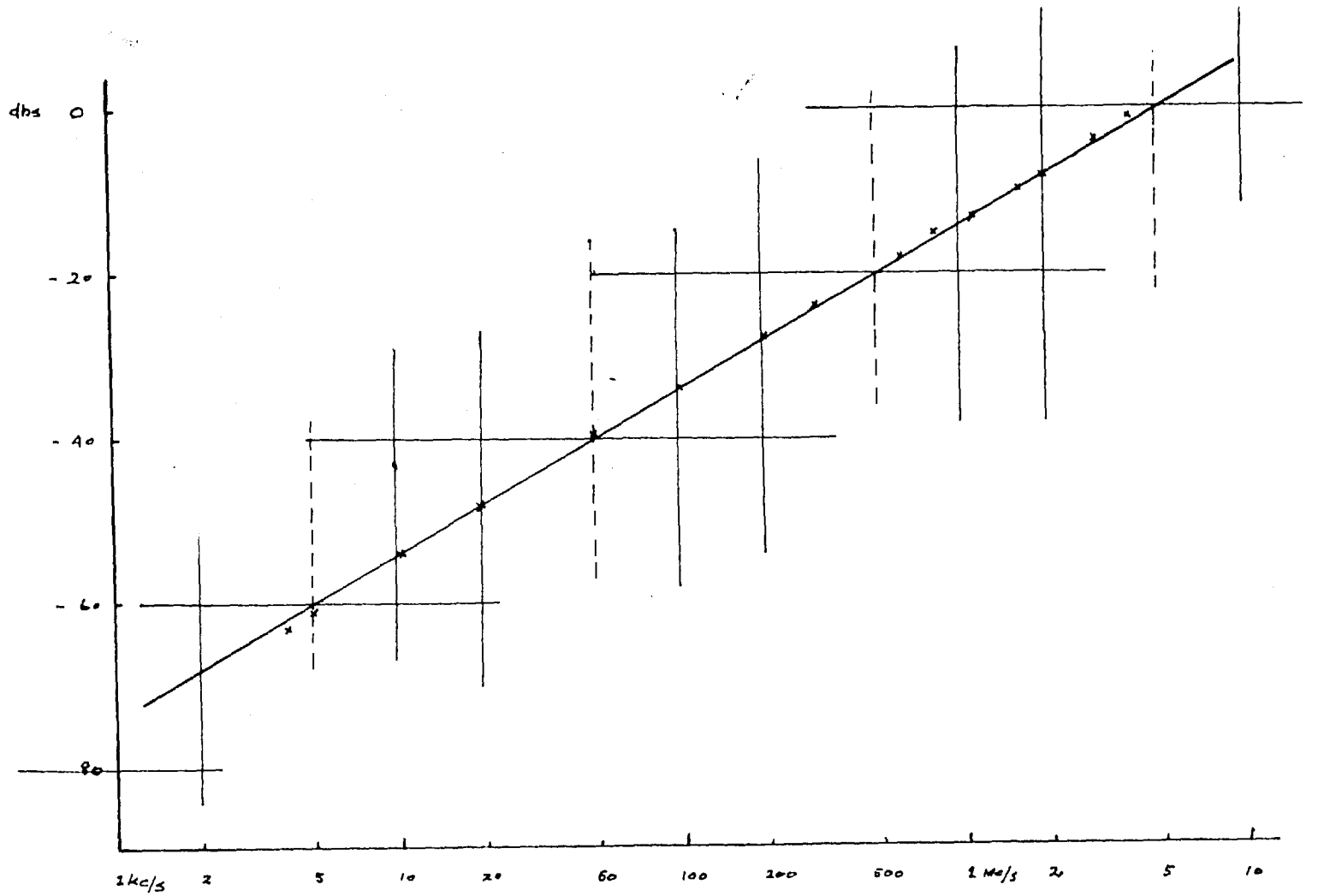


FIG: 25. RESPONSE OF THE DIFFERENTIATOR.

2.5.6. The Full Wave Rectifier.

Figure 26 shows the circuit diagram of the amplifier and the full-wave rectifier. V_1 and V_2 are two R-C coupled amplifying stages. The current in each valve is stabilised by large cathode resistors which are bypassed by capacitors to prevent cathode degeneration. V_3 is a cathode coupled phase-splitter providing paraphase outputs which are fed into the cathode followers, V_{4_a} and V_{4_b}, which drive a balanced bridge rectifier. The output stage, V_5, is a cathode follower and and has an output impedance of nearly 40 ohms. All the screen grids and anodes in the valve stages are appropriately decoupled.

With a sinusoidal input, the output of the circuit is constant up to 3 Mc/s and is reduced by less than 50% at 5 Mc/s.

At a later stage in the work, a diode base clipper was introduced to clip the lower part of the output waveform. The R-C coupling between points A and B as shown in figure 26 was removed, and a series diode clipper, shown in the inset in the figure, was installed.

2.5.7. The High Gain Amplifier.

The output of the full wave rectifier is used to control the scan velocity. However, the output signal has a peak amplitude of about 1.5 volts while a signal of the order of 100 volts is needed to change the velocity of the time base by a factor of 10.

This necessitated the design of an amplifier with a gain of 40 dbs, "bandwidth" of more than 3 Mc/s and an undistorted output of about 100 volts peak to peak. The circuit diagram of the amplifier is shown in figure 27. A cathode follower input stage V_1 is followed by an inverse-feedback pair V_2 and V_3. The current in V_2 is stabilised by a large cathode resistor bypassed to prevent cathode degeneration while the stability of the

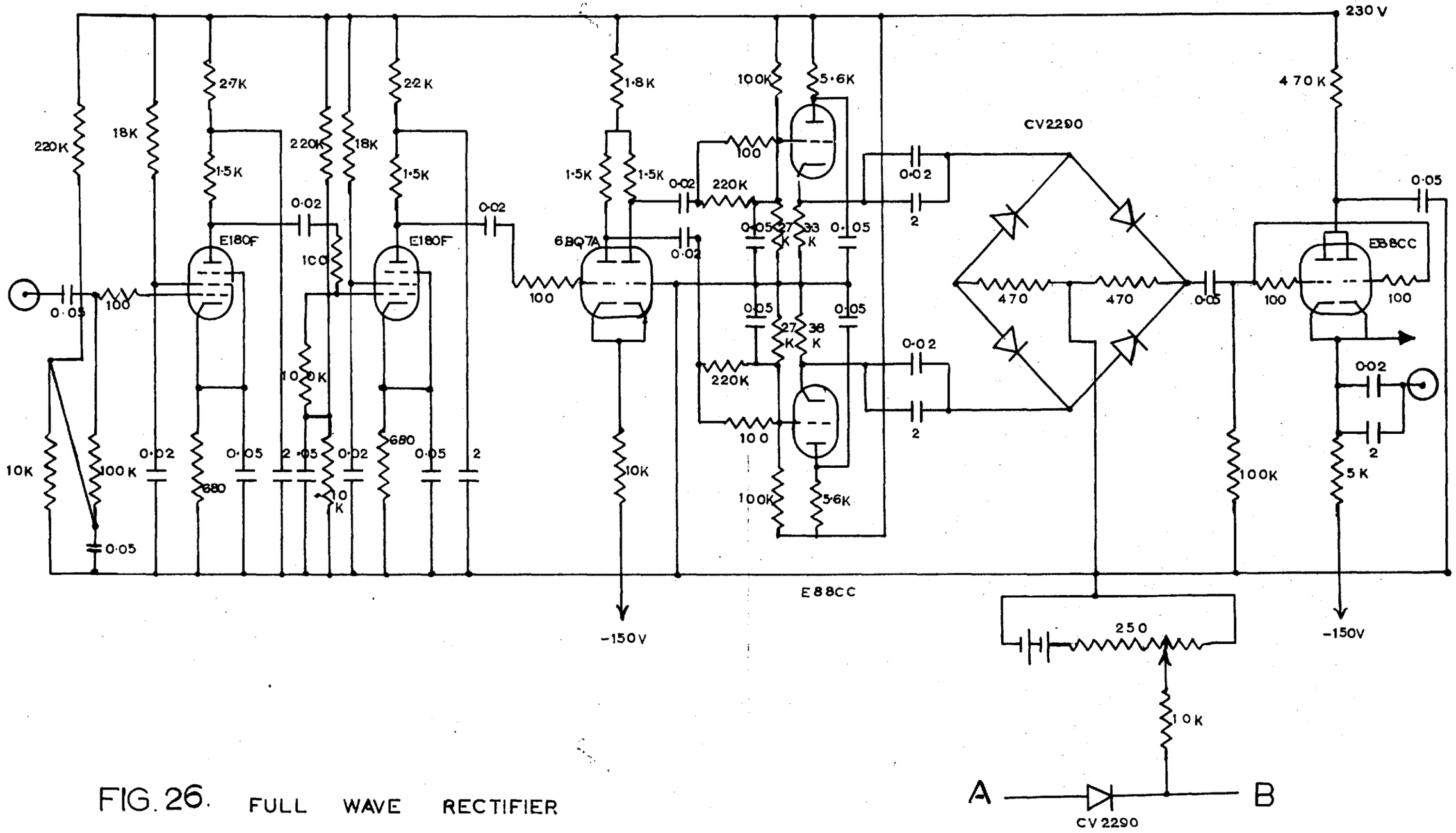


FIG. 26. FULL WAVE RECTIFIER

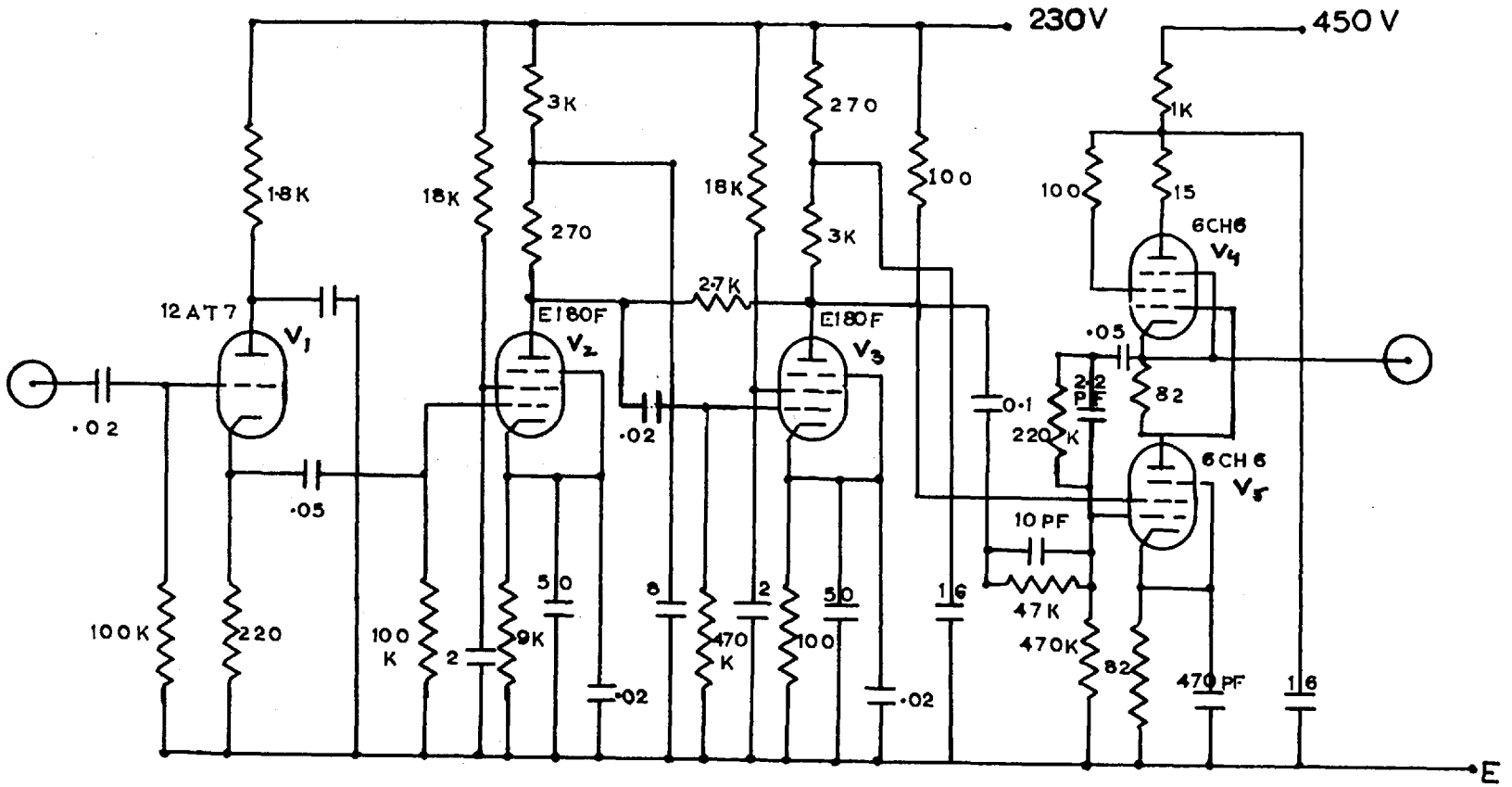


FIG27. HIGH GAIN AMPLIFIER

stage comprising V_3 is increased by the feedback. The signal output from V_3 drives the output stage which combines the features of an anode follower and a "totem-pole" amplifier.[72] The gain of the stage is approximately equal to the ratio of the feedback and feed-in resistors. A virtual earth is created at the grid of V_4 due to the feedback. This prevents overload at the grid. The amplifier can handle signals of peak amplitude of 100 volts without noticeable distortion. The output impedance is of the order of 1 kilohm.

An inverse-feedback pair has many interesting features.[70] The gain of V_3 is stabilised. The "bandwidth" of the pair is determined by the overall gain. This property is very useful in handling signals of large magnitudes. The gain of the first stage is made small, say unity, thus preventing overload at the grid of the second valve. This makes it possible to use valves which have high transconductance and short grid base without running the risk of grid conduction or cut-off.

2.5.8. The Variable - Velocity Time Base.

The variable - velocity time base comprises a linear sweep generator and an amplitude comparator which provides the resetting pulse for the sweep generator. The velocity modulation is obtained by using the same basic principle as that used by Beddoes.[61] The slope of a Miller sweep circuit is directly proportional to the voltage to which the grid resistor is returned. The slope is modulated by adding, to the d.c. voltage, the amplified control signal.

Figure 28 shows a circuit diagram of the variable-velocity time base. The Miller valve is gated on the suppressor grid. A G.E.C. valve, type Z759, is used in which the anode current can be completely cut off when the suppressor grid is made about 60 volts negative with respect to the cathode under normal operating condition. It was found that, in the case of two other video pentodes, types 6 CH6 and E180F, the suppressor has negligible control on the anode current.

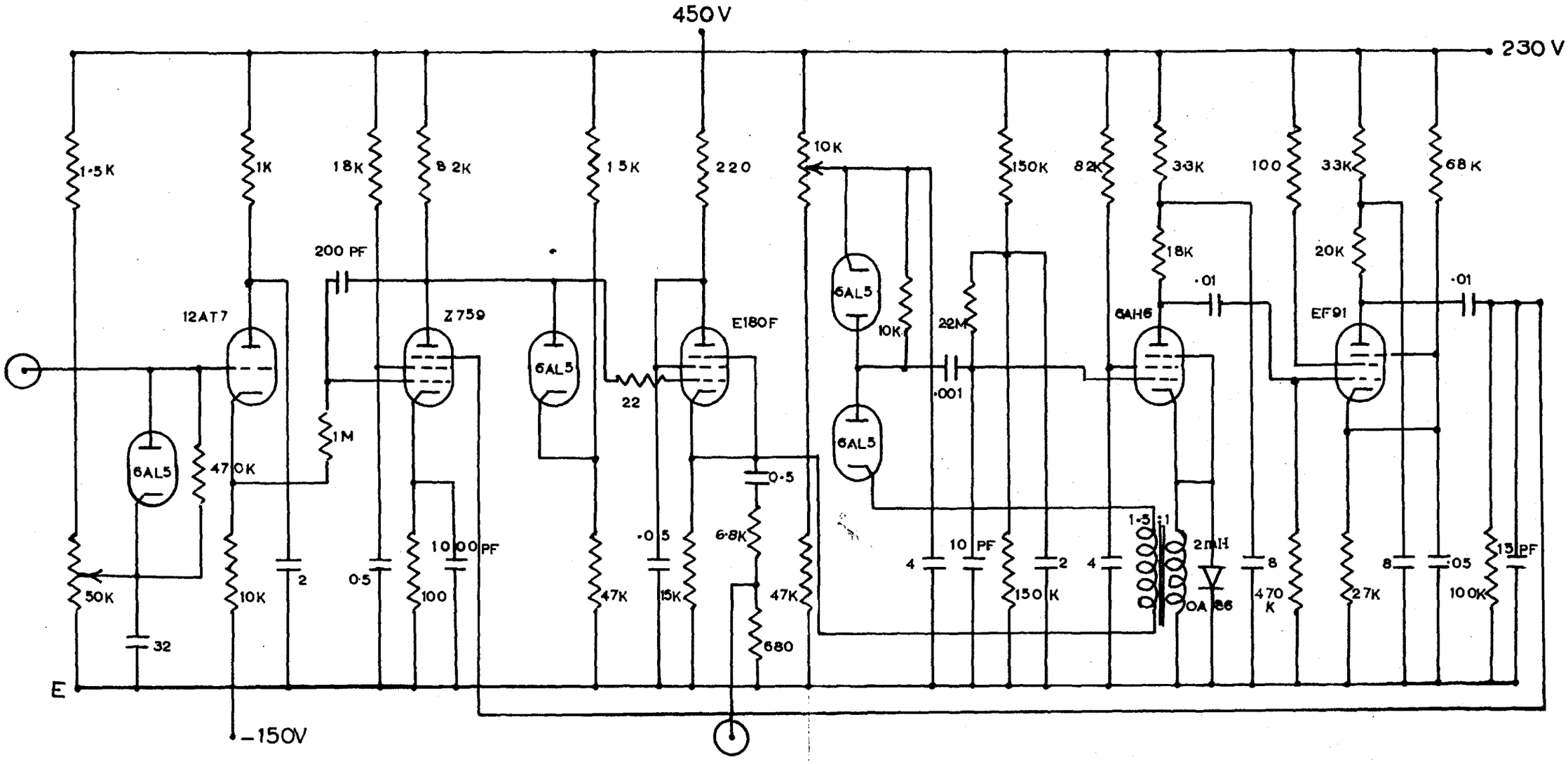


FIG.28. TIME BASE FOR VARIABLE VELOCITY SCANNING

The input control signal is d.c. restored by diode D_{1a} at the grid of the cathode follower V_1. The cathode of V_1 is the voltage source to which the grid resistor of the Miller valve is returned. If the potential at the grid of V_1 is E_1 in absence of any control signal, it would be $E_1 - e$ if a control signal is imposed whose instantaneous amplitude is e. The cathode of V_1 follows its grid thus varying the potential to which the grid of the Miller valve is returned.

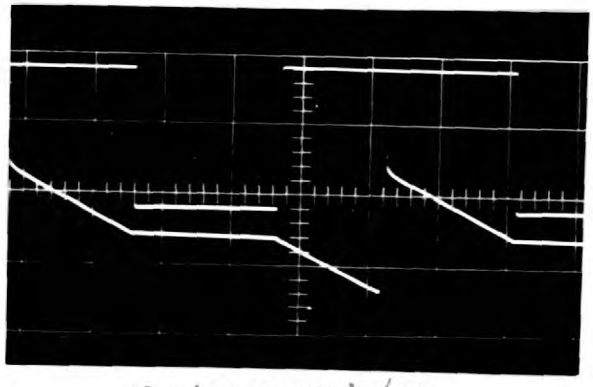
The cathode follower V_3 provides the output and also acts as a buffer stage between the Miller valve and the multiar comparator which generates the resetting pulses for the suppressor grid of V_2. The current in D_{1b} is adjusted to minimise the initial step inherent in suppressor - gated Miller sweep circuits.

The sweep is reset by a multiar when the spot reaches the end of a line. The multiar[71] is a very stable and accurate amplitude comparator. The stability of the regeneration point in a well-designed multiar is dependent only on the break characteristic of a diode.

In figure 28, D_{2a} is the comparator diode. A thermionic double diode, 6AL5, is used, the other section being connected to compensate for cathode drift.[69]. The heater supply for this valve is reduced to 4 volts to obtain a sharp break characteristic.

The pulse transformer is wound on a Ferroxcube core, type FX1239. To obtain a loopgain higher than unity, a step-up of 1.5 is derived from the cathode to the grid winding. The cathode winding inductance is 2 mH and care has been taken to minimise the interwinding capacitance.

In the quiescent condition, the diode D_{2a} does not conduct, the feedback loop through the transformer is open and the grid of V_4 is clamped to the cathode. When the sweep voltage at the output is just lower than the reference voltage, the diode D_{2a} conducts, at some point the loopgain exceeds unity and regenerative action drives the grid of V_4 negative cutting V_4

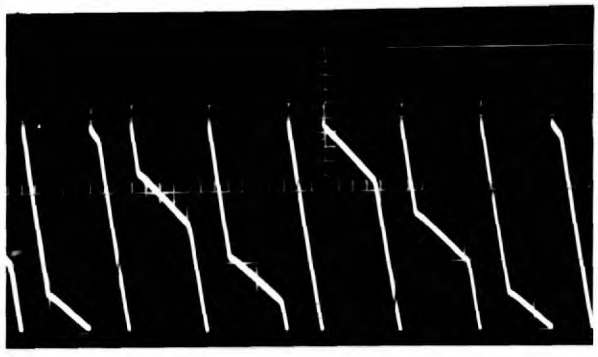


(i) Modulating Pulse
25 Volts/cm

ii Sweep Waveform
10 Volts/cm

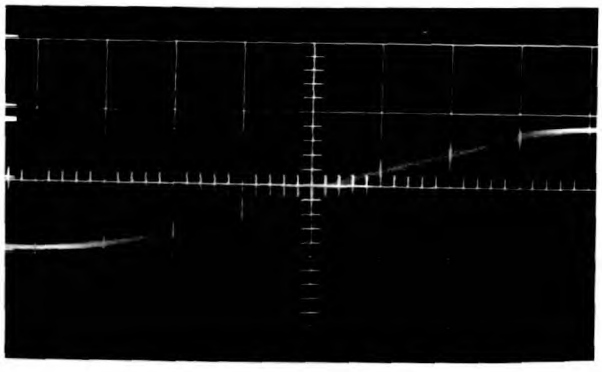
20 microseconds/cm

(a)



40 microseconds/cm

(c)



20 millimicroseconds/cm

(b)

FIG. 29. TESTS ON VARIABLE-VELOCITY TIME BASE.

PLOT OF SWEEP FREQ VS THE VOLTAGE TO WHICH THE MILLER RESISTANCE IS RETURNED IN THE V. V. TIME BASE.

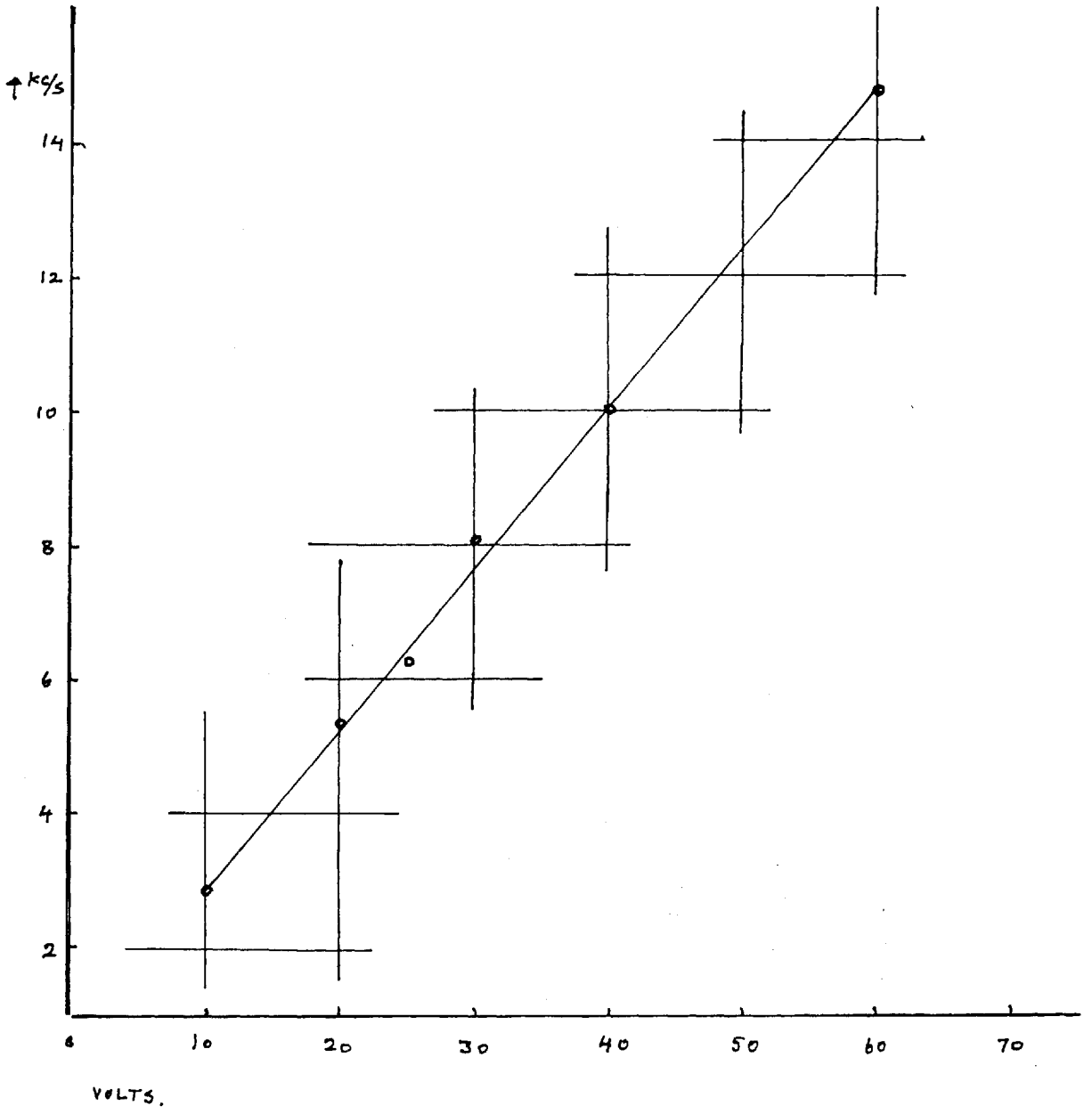


FIG. 30.

off. The primary of the transformer in the cathode of V_4 rings, but is damped by D_3. Thus a single negative pulse is obtained. During the trailing edge of the pulse, D_{2a} is backbiased due to the step-up ratio of the transformer. The grid of V_4 enters the conduction region and the anode of D_{2a} approaches the reference voltage. A positive pulse is generated on the anode of V_4. This is inverted and amplified by V_5 and is then applied to the suppressor grid of the Miller valve for resetting the sweep generator.

To prevent relaxation oscillation or "bouncing" in the multiar,[72] a short grid base pentode, type 6AH6 is used with low screen voltage.

Some results of the tests on the timebase are shown in figure 29. Figure 29(a) shows the change in the slope due to modulation by a rectangular pulse. Figure 29(c) shows a photograph of the flyback on a highly expanded time scale. The spread in time is less than 5 m μsec. which denotes the high degree of accuracy and stability obtained by the amplitude comparator. Fig.29(b) clearly shows that the time duration of a line depends on the control signal and that the resetting circuit of the timebase acts only when the sweep runs down to a predetermined voltage. Figure 30 shows the variation of the sweep period with the d.c. voltage to which the grid resistor of the Miller valve is returned.

2.5.9. The Deflection Amplifier.

In the deflection amplifier, a push-pull driving stage drives the line output transformer, the secondary of which provides the scan current for the line deflection coil.

A circuit diagram of the deflection amplifier is shown in figure 31. The output of the time base is fed into the cathode-coupled phase-splitter V_1. The paraphase outputs from the two anodes of V_1 are amplified by identical stages. The input capacitance of the line output valve, when it is hot, is of the order of 30 pf. Cathode followers V_4 and V_7 prevent

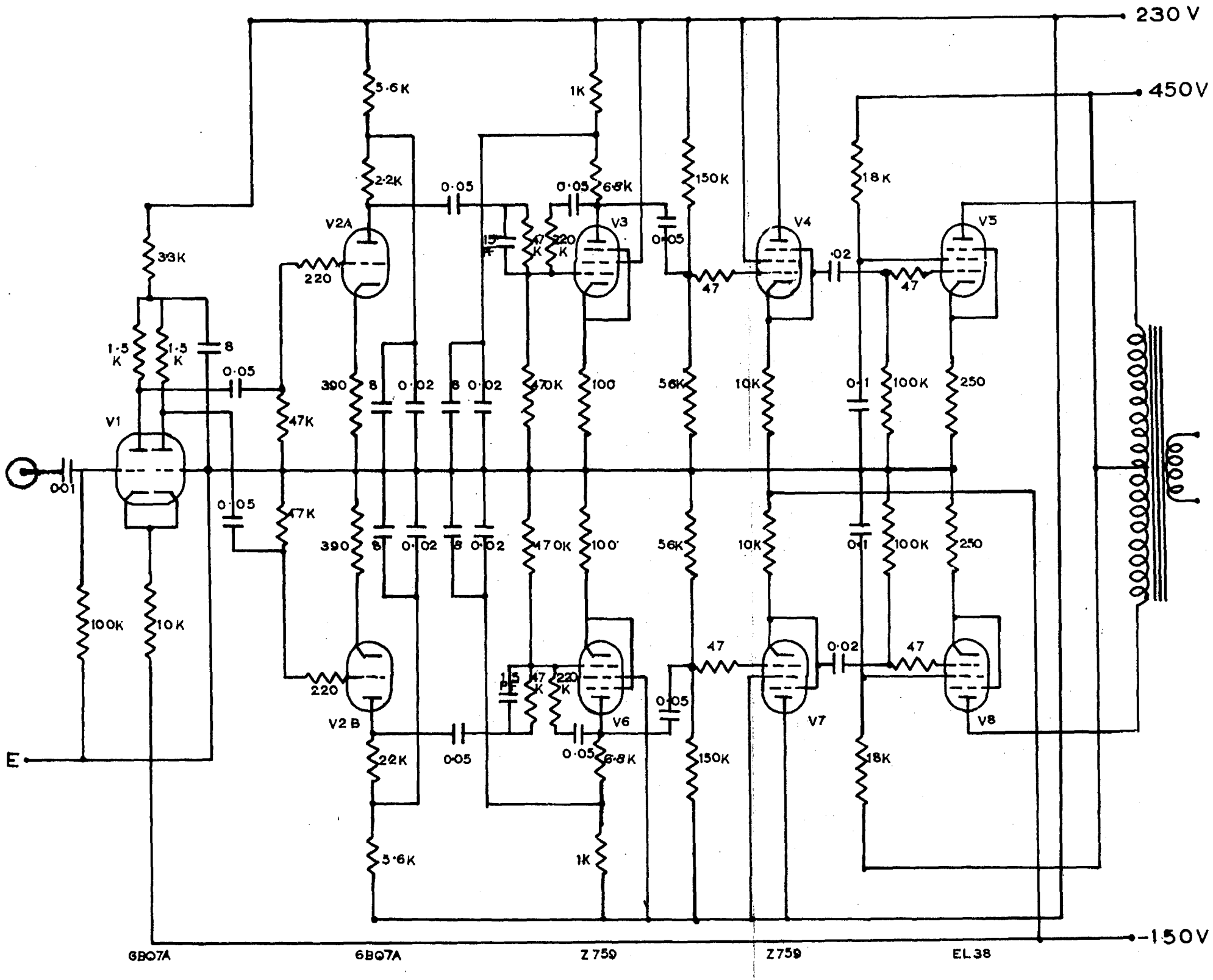


FIG.31. VARIABLE VELOCITY LINE OUTPUT AMPLIFIER.

undue capacitive loading of the anode follower stages V_3 and V_6. The frequency response of the entire driver stage, at the grid of V_5 or V_8, is level within $\pm$ 3 dbs up to 5 Mc/s. A pentode driven output stage has been used which tends to give a constant current output provided that the core losses in the transformer are small and the primary source has no loading.

Considerable time was spent in the design and development of a line output transformer. It has already been pointed out that the Marconi transformer was quite unsuitable because of its small "bandwidth". The low-impedance deflection coils supplied by Marconi W.T.Co.Ltd., was retained and it was aimed to design a deflection system of a "bandwidth" of nearly 1 Mc/s.

The specifications of the transformer include a constant deflection current response from 1 Kc/s to 1 Mc/s and a large step-down ratio to supply current to the low impedance coils for a reasonable scan length. Besides these steady-state conditions, the transformer must also possess the transient performance of a pulse transformer.

The most general equivalent circuit of a practical transformer is shown in figure 32(a), though even this circuit is only approximate. If there is a common a.c. earth between the primary and the secondary, figure 32(a) reduces to figure 32(b). In figure 32(b), R_2, the equivalent shunt eddy current loss resistor has been neglected because in a good design with Ferroxcube cores, which have high resistivity, the power dissipated in the core due to eddy currents can be made very small as compared with other losses. Noneof the equivalent circuits in figure 32 have taken the hysteresis losses into account. The copper losses can be made negligible in small transformers, hence r_p and r_s have been ignored in figure 32(b) In figure 32(c), the transformer has been replaced by its equivalent T-network and the secondary impedances have been transferred to the primary side by taking the conversion ratio into account. The proof of the equivalence of the circuits in figure 32 can be found in the standard textbooks.(72,73)

C_p: Equivalent capacitance at the primary terminals due to internal and source capacities.

C_s: Equivalent capacitance across the secondary terminals due to internal and load capacities.

C_w: Intervinding capacitance.

E: Source voltage.

L: Inductance at the primary terminal when the secondary is open circuited.

L_2: Inductance at the secondary terminal when the primary is open circuited.

L_p: Part of primary inductance that couples 100% with the secondary. $L_p = KL$.

L_s: Part of the secondary inductance that couples 100% with the primary $L_s = KL_2$.

C_e: Effective intervinding capacitance when transferred across the primary terminal.
$= C_n \left(\frac{N_p - N_s}{N_p} \right)^2$ across the primary.

C: $\frac{C_s}{n^2} + C_e$

n: Turns ratio $\frac{\text{secondary turns}}{\text{primary turns}} = \frac{N_s}{N_p}$

N_s: No. of Secondary turns.

N_p: No. of Primary turns.

: Leakage Inductance.

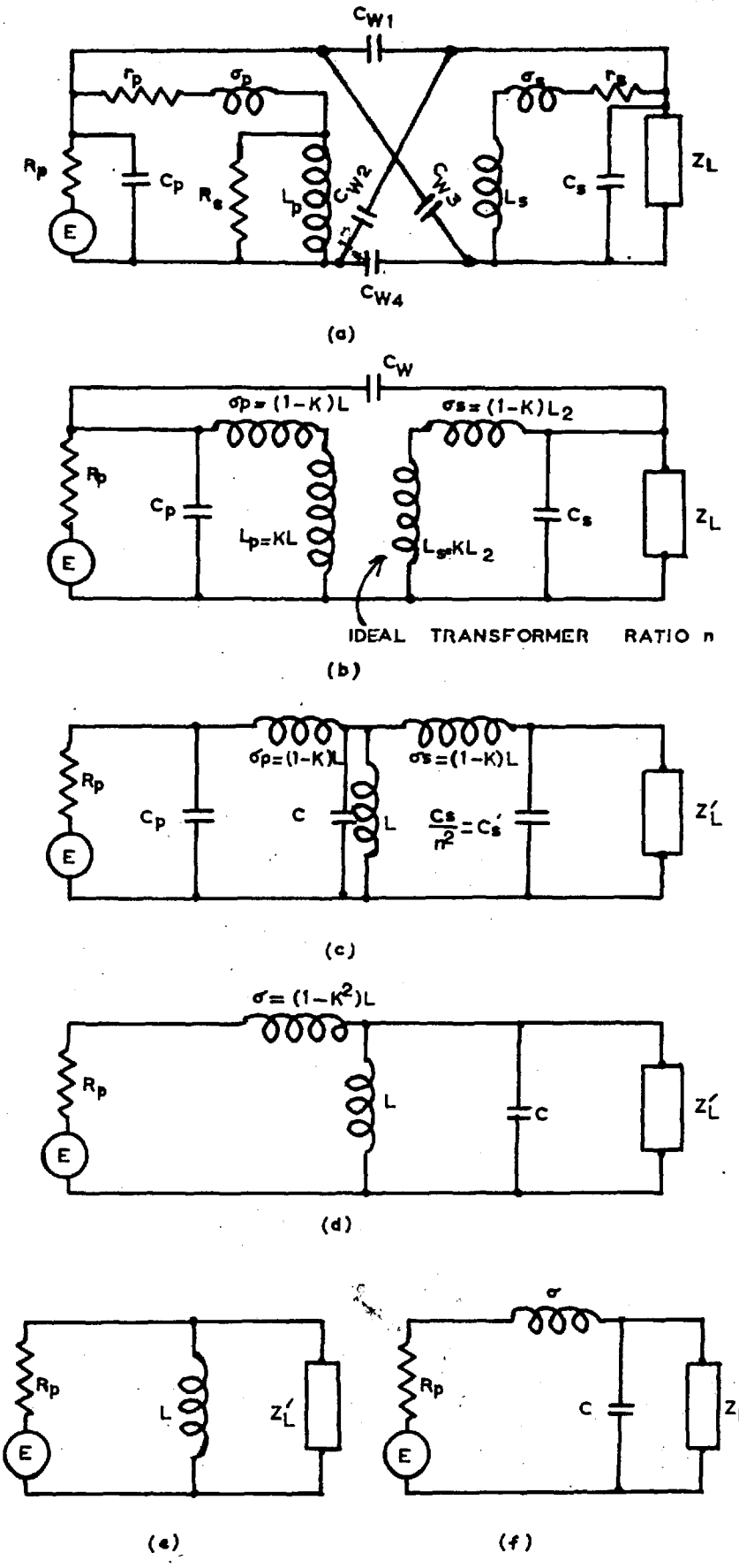


FIG.32. SOME EQUIVALENT CIRCUITS OF A TRANSFORMER.

In the case of a step-down transformer, the interwinding capacitance, C_w, may be represented as a capacitance, C_e, shunting the primary inductance since this winding will be mainly affected by the current from C_w [74]. The value of C_e can be shown to be equal to $C_w\ (N_p - N_s)/N_p^2$. By lumping the leakage inductances in figure 32(c), figure 32(d) may be obtained. The capacitance C is the sum of C_s' and C_e and the capacitance C_p has been omitted in figure 32(d). It has been shown by Moody[74] that the error introduced by ignoring C_p is negligible provided C_p is less than half the equivalent secondary capacitance across the primary terminal and provided the source impedance R_p does not exceed the value given by $R_p = 1/2\sqrt{\frac{\sigma}{C_p}}$.

Even after all these approximations, the equivalent circuit (d) is represented by a third order differential equation which is difficult to solve. Further simplification leads to two equivalent circuits, figure 32(e) for the low frequency response and figure 32(f) for the high frequency response. The h.f. response is almost entirely dependent on the leakage inductance and the shunt capacitance. Small value of leakage inductance must be obtained for good h.f. response. For good l.f. response, a high value of primary inductance is desired. The primary inductance as well as the leakage inductance are functions of the square of the number of turns in the primary winding. The designer, in this case, is confronted with conflicting requirements. Another example of conflicting requirement can be seen in the nature of winding, e.g. sectionalised interwinding reduces the leakage inductance but increases the interwinding capacitance. It will be seen that the leakage inductance and the self-capacitance in a transformer are greatly dependent on the geometry and the nature of the windings. The solution of the above-mentioned differential equation is, therefore not very useful in the design of a transformer.

It is generally recognised[75,76] that the art of transformer design, to a great extent, is emperical and lies in reconciling the various conflicting requirements by an orderly procedure of trial and error.

The parameters of the transformer, which determine the overall response, are briefly discussed below:

(a) Leakage Inductance: Leakage Inductance is one of the most important factors in the determination of the h.f. response of the transformer. It is greatly dependent on the geometry of the transformer and it can be varied over a range of 16 to 1 by variation in the structure[74]. Formulae for approximate determination of the leakage inductance from the coil geometry have been provided by Moody.

(b) Transformer Capacitances: The transformer capacitance, like the leakage inductance, introduces a delay in the transient responseof the transformer, hence the need to minimise it. The capacitances in a transformer are contributed by various sources, e.g., the capacitance inherent in the source, the inter-turn capacitance, the inter-layer and interwinding capacitances and the capacitance across the load. Some of these capacitances may be distributed but are lumped at certain places as approximations. In most transformers, the inter-turn capacitance may be ignored. The interwinding capacitance can be expressed as a shunt capacitance across the primary as mentioned earlier. The capacitances in a transformer depend greatly on the type of winding used. In a wave winding, the capacitance can be minimised but with a corresponding increase in the leakage inductance.

(c) Choice of the Core: The bandwidth of the transformer is proportional to the ratio of the magnetizing inductance to the leakage inductance. This ratio is virtually independent of the number of turns because both the magnetizing inductance and the leakage inductance are proportional to the square of the number of turns. The ratio is proportional to the

incremental permeability of the core, if the eddy current losses are negligible. Thus the use of a core material which has high incremental permeability provides both high primary inductance and low leakage inductance.

The size of the core is dependent on the window gap needed and on the insulation desired. A very large core may introduce problems of dimensional resonance while in a very small core, saturation or increased leakage inductance and self capacitance or both may adversely affect the performance.

The saturation of the core and the loss of initial permeability, caused by d.c. polarization, can be reduced, by using a push-pull drive and a suitable air gap. Methods exist to calculate the airgap.(77) As a result of the introduction of an airgap, the incremental permeability is decreased but the frequency of dimensional resonance of the transformer core is increased and there is reduction in distortions caused by saturation.

Practical design features: Several transformers were wound and tested. Two Ferroxcube E cores, type FX1527, with the windings round their centre leg, have been found to give the best results. Plain π - sectioned layer winding has been preferred because it helps to keep the leakage inductance low. The design equations provided in the Mullard Ferroxcube Handbook(77) have been used to calculate the spacer thickness and to check for the saturation of the core. A centre tapped transformer with a push-pull drive has been found to give better results than a single-ended one.

The specifications of three different transformers with their frequency response are shown in figure 33. Large step-down adversely affects the h.f. performance of the transformers but is essential to drive the low impedance deflection coils. Figure 33(c) shows the best frequency response but this has been achieved by reducing the step-down ratio. This results in a very small scan length of about 2 cms when the E.H.T. supply voltage for the scanner tube is 15 KV. The transformer,

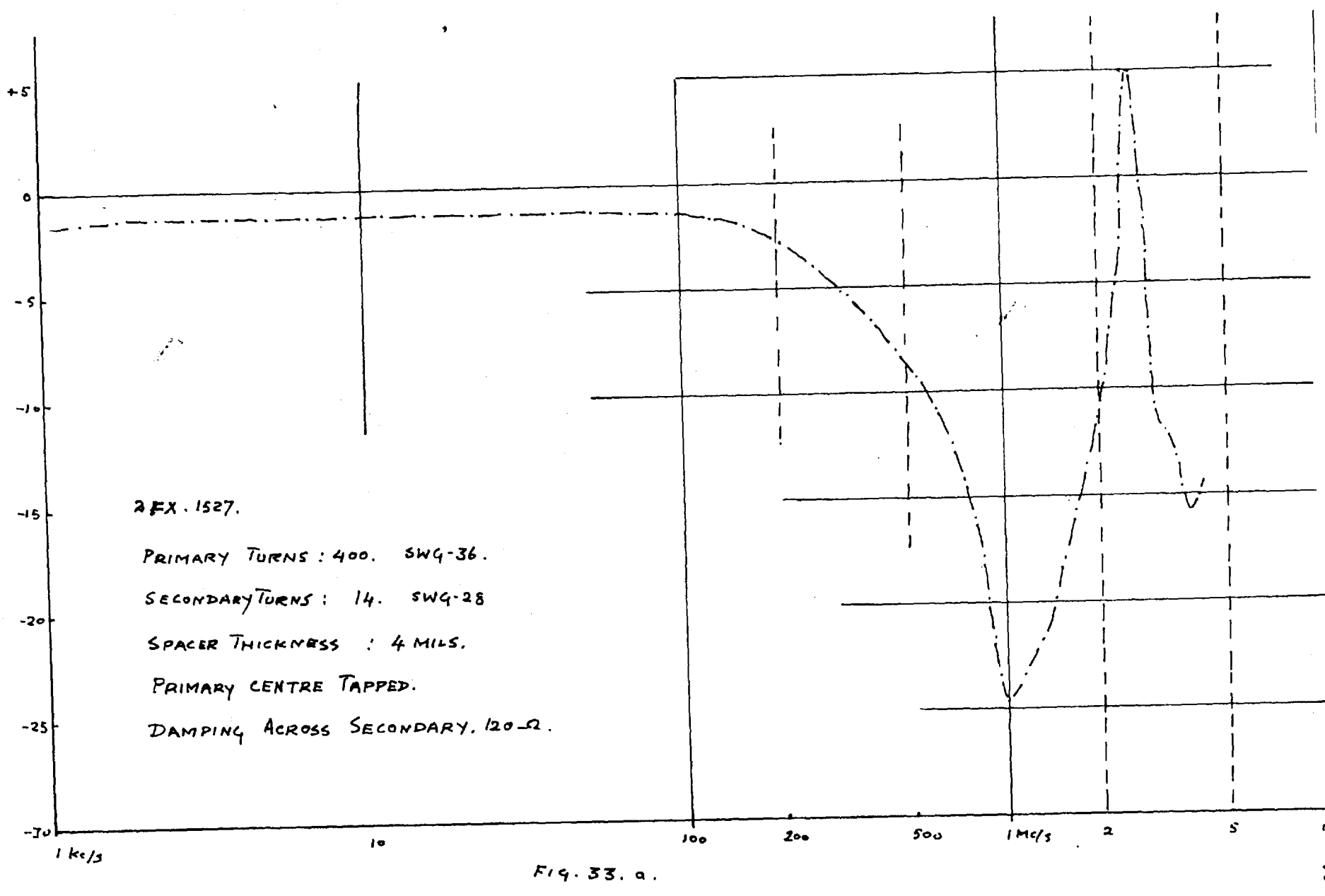

+5
0
-5
-10
-15
-20
-25
-30
1 kc/s
10
100
200
500
1 Mc/s
2
5
2FX. 1527.
PRIMARY TURNS : 400. SWG-36.
SECONDARY TURNS : 14. SWG-28
SPACER THICKNESS : 4 MILS.
PRIMARY CENTRE TAPPED.
DAMPING ACROSS SECONDARY. 120 Ω.

FIG. 33. a.

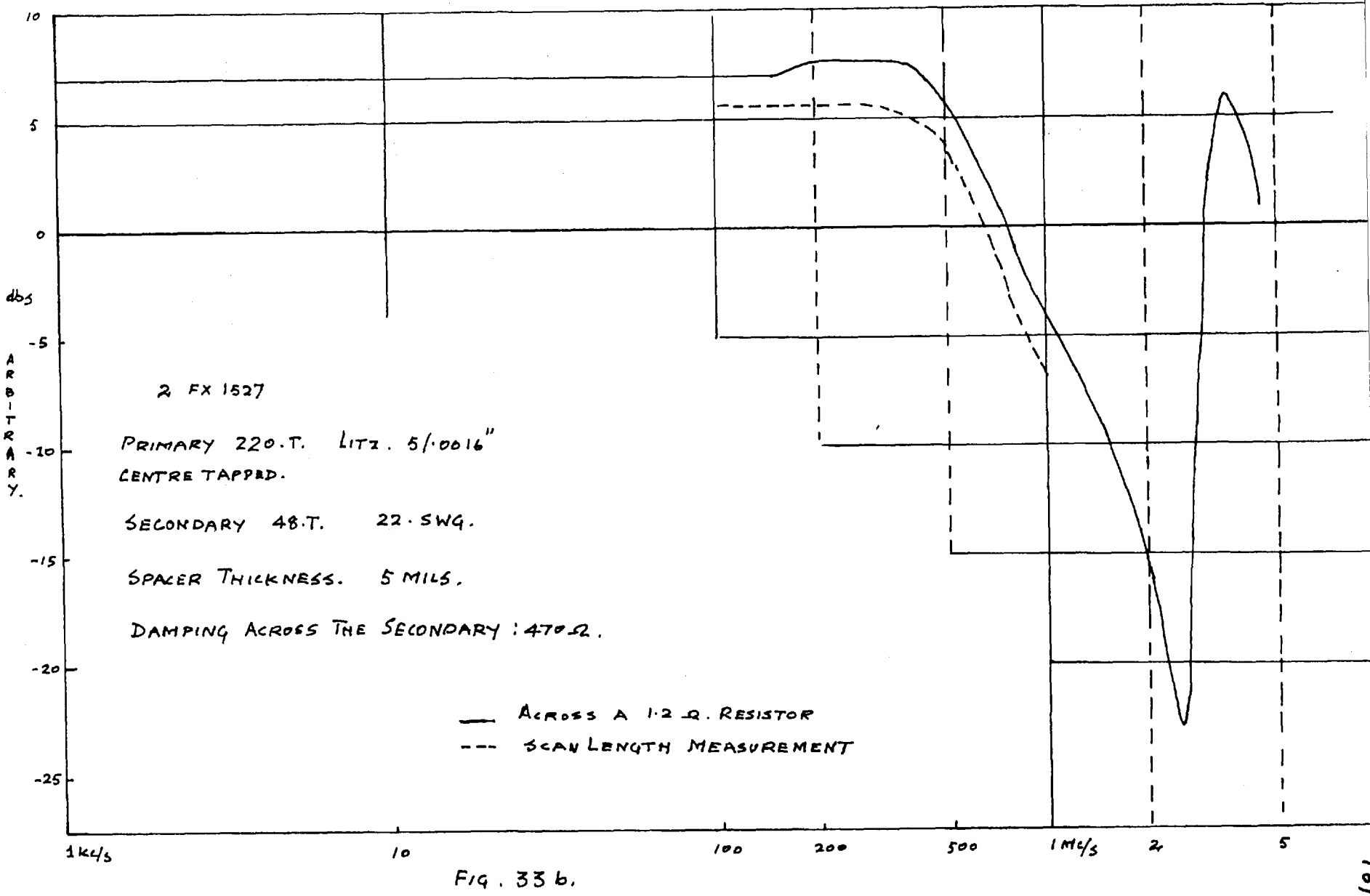

10
5
0
dbs
-5
-10
-15
-20
-25
ARBITRARY.
2 FX 1527
PRIMARY 220.T. LITZ. 5/.0016"
CENTRE TAPPED.
SECONDARY 48.T. 22.SWG.
SPACER THICKNESS. 5 MILS.
DAMPING ACROSS THE SECONDARY : 470Ω.
ACROSS A 1.2Ω. RESISTOR
SCAN LENGTH MEASUREMENT
1Kc/s
10
100
200
500
1Mc/s
2
5

FIG. 33b.

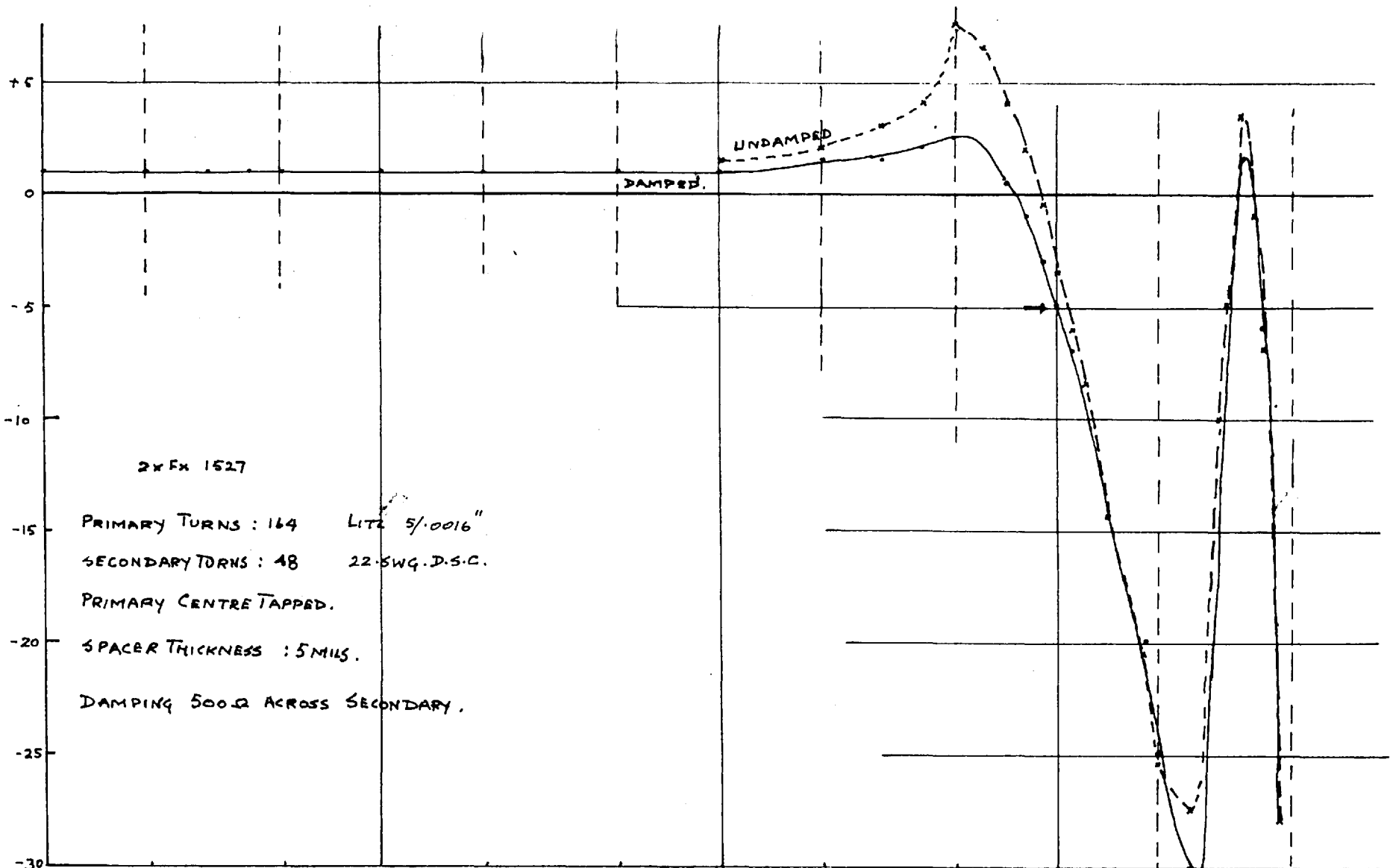

+5
0
-5
-10
-15
-20
-25
-30
1 Kc/s
2
5
10
20
50
100
200
500
1 Mc/s
2
5
UNDAMPED
DAMPED.
2 x Fx 1527
PRIMARY TURNS : 164 LITZ 5/.0016"
SECONDARY TURNS : 48 22 SWG. D.S.C.
PRIMARY CENTRE TAPPED.
SPACER THICKNESS : 5 MILS.
DAMPING 500Ω ACROSS SECONDARY.

FIG: 33C.

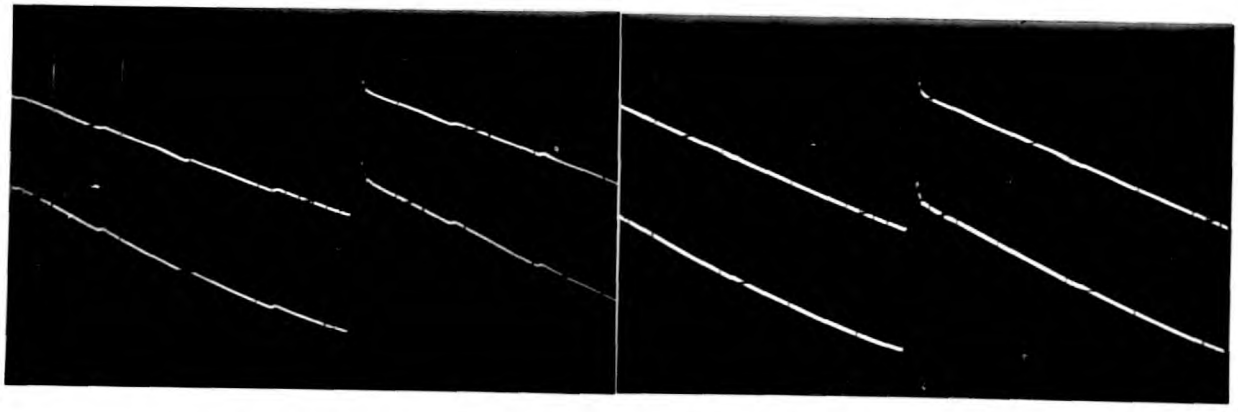
whose characteristics have been given in figure 33(b), has been used in all the experimental work. This transformer has a "bandwidth" of 675 Kc/s but it has a higher stepdown ratio, giving a scan-length of 4.5 cms. Damping of the deflection system has been obtained by connecting a 470 ohms resistor across the secondary winding. This value has been experimental found to give the best waveform response. All the frequency responses were obtained by measuring the voltage across a 1.2 ohm resistor connected in series with the deflection coil. A check has been made by measuring the length of the scan at the face of the scanner tube for sinusoidal drives of different frequencies and it is plotted in figure 3 (b). It is virtually identical to the response measured across the 1.2.ohm resistor.

Some photographic results, obtained with the deflection system using the selected transformer, are shown in figure 34. A pulse generator was used to provide the modulation signal for the variable velocity timebase. In figure 34(a) and (b), the upper trace shows the voltage waveform at the grid of one of the line output valves and the lower trace shows the current waveform measured across a 1.2 ohm resistor in series with the deflection coil when the width of the modulating pulse is equal to 80 µsec. The current waveform follows the voltage waveform faithfully and there are no deleterious transient effects visible at the points where the timebase slope is changed due to the modulation. Figure 34(c) shows the voltage and the current waveforms when the modulating pulse width is equal to 2 µsec. In figure 34(d), the pulse width has been reduced to 0.6 µsec. The difference signal, shown in figure 34(e), was obtained by the algebraic addition of the upper waveform and the lower waveform of figure 34(d). When the pulse width was reduced below 0.6 µsec., it was not possible to discern any modulation on the current waveform.



(a) 50 microseconds/cm (b) 100 microseconds/cm

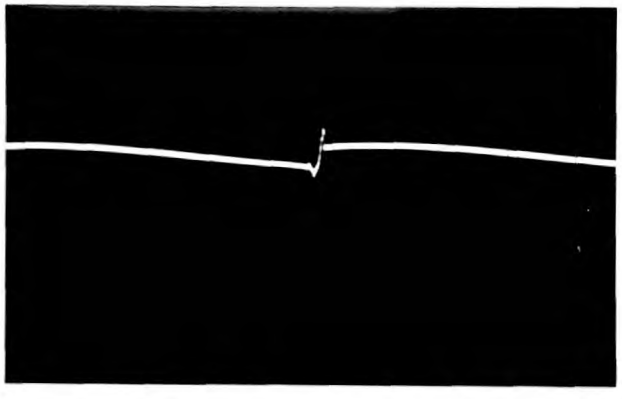
Modulation pulse width 80 microseconds



(c) 20 millimicroseconds/cm (d) 20 microseconds/cm

Modulation Pulse width 2 secs. Modulation Pulse width 0.6 secs

(i) voltage waveform (ii) current waveform



(e) (i) - (ii)

FIG. 34 TESTS ON THE SCANNER DEFLECTION SYSTEM

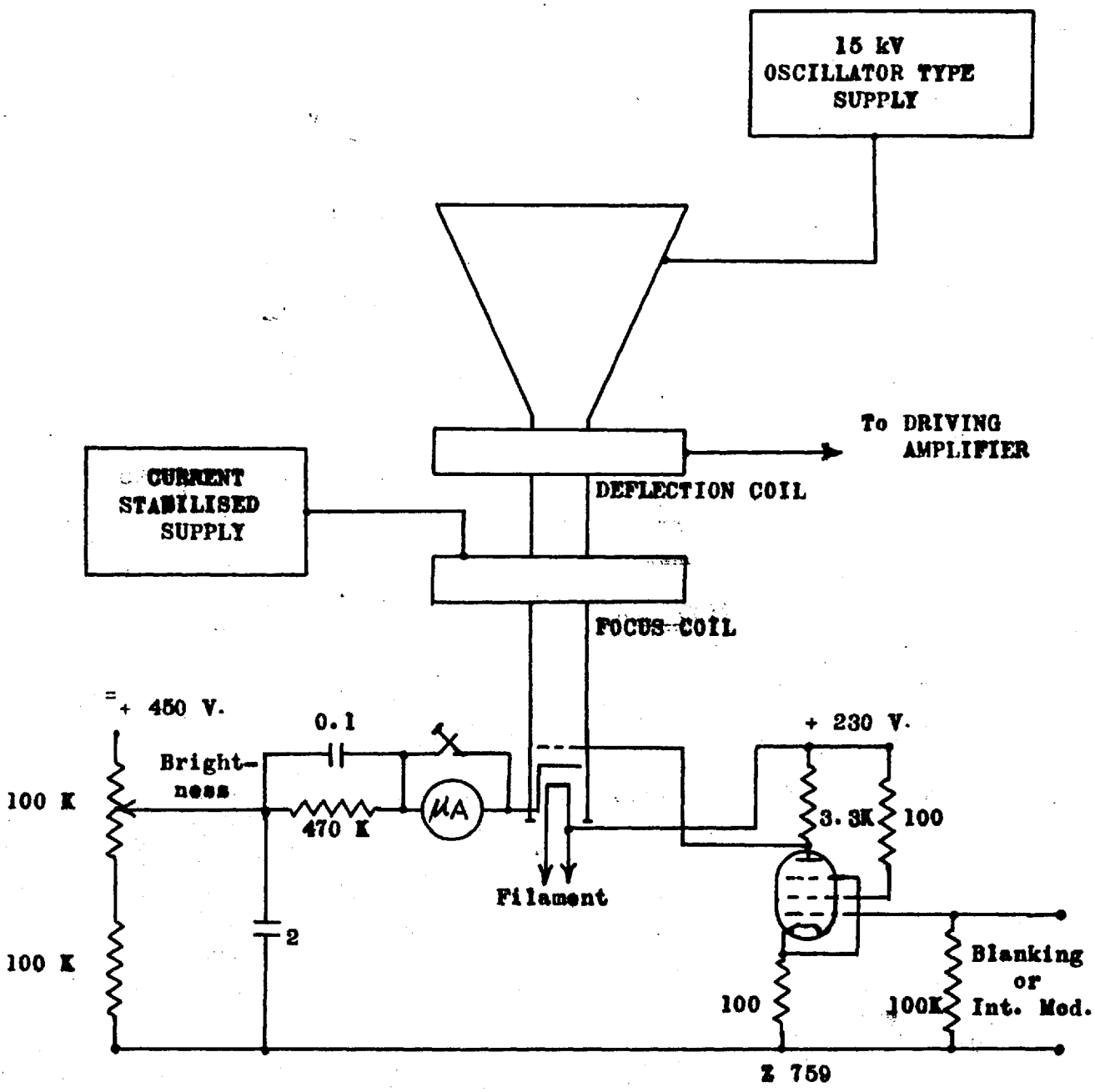


FIG. 35. SCANNER TUBE SUPPLIES.

2.5.10. Scanner - Tube Supplies.

The scanner - tube supply diagram is shown in figure 35 which is self-explanatory.

2.6. Design Of The Receiver.

The receiver consists of a video amplifier with provision for intensity - modulation correction, a line deflection amplifier, a ratchet (staircase) time base for vertical deflection and a display tube. A 5" oscilloscope tube, Mullard type DB13-2, with electrostatic deflection, was used as a display tube. This tube has a blue phosphor which is not suitable for subjective evaluation of pictures but it has a fine focus and good resolution. It can be easily replaced by a tube with white phosphor without any major modification. The display tube supply diagram is shown in figure 36. The other component parts of the receiver are briefly described below:

2.6.1. The Video Amplifier.

At the receiver, the variable-velocity scanning will superimpose an intensity modulation pattern on the video signal which will tend to brighten up all the regions of high detail. Correction of this unwanted intensity modulation is obtained in the first valve of the video amplifier (figure 37). V_1 is a double triode with a common anode and a common cathode resistor. The video input is fed in one grid and the differential of the line scan waveform in the other in the proper polarity. The corrected signal is amplified by an anode follower V_2 which is coupled to the grid of the display tube.

2.6.2. The Line Deflection Amplifier.

The line deflection amplifier is shown in figure 38. Two pentodes have been used as a cathode-coupled phase-splitter to provide pushpull drive to the "totem-pole" anode followers

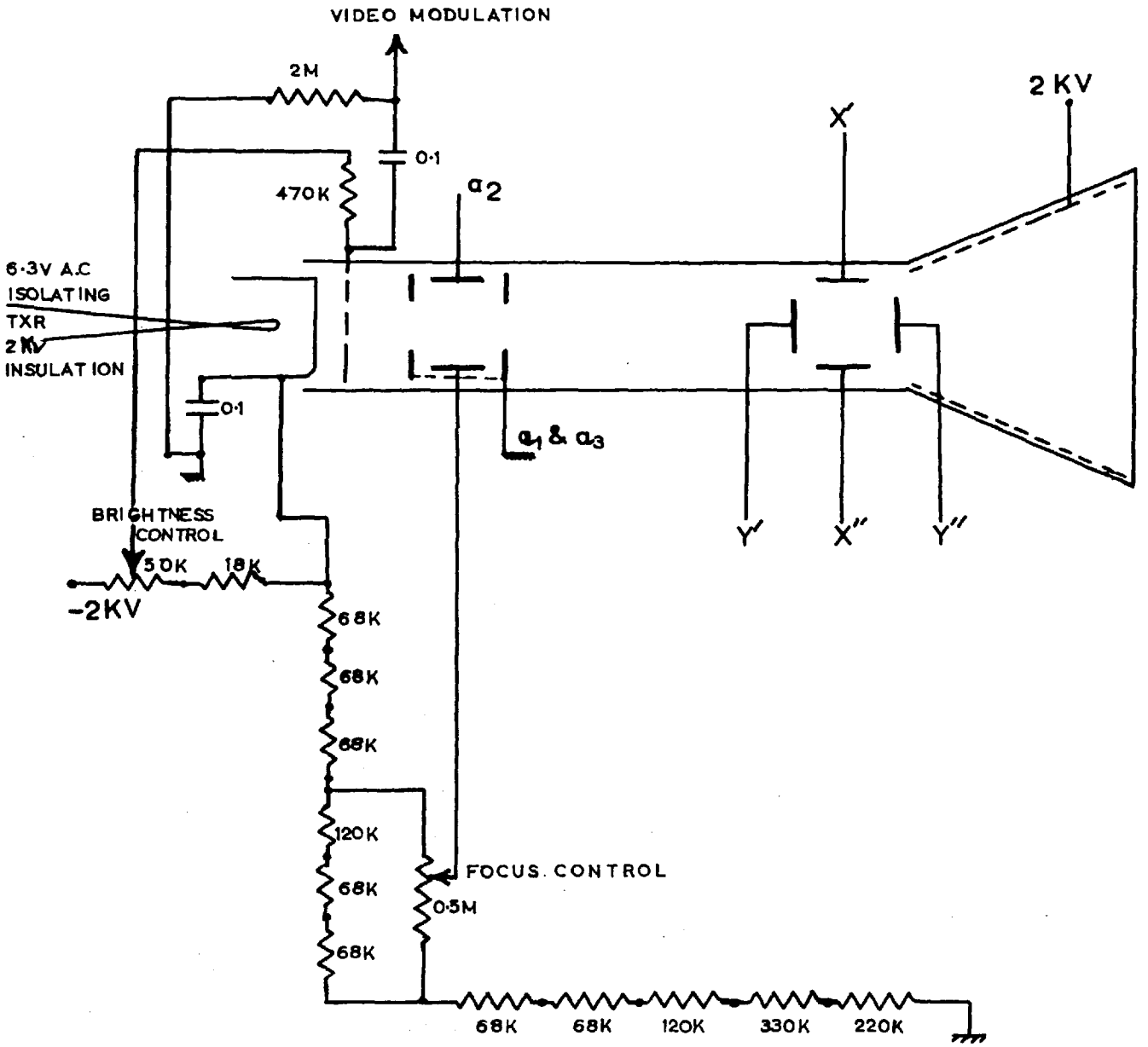


FIG. 36. DISPLAY TUBE SUPPLY DIAGRAM.

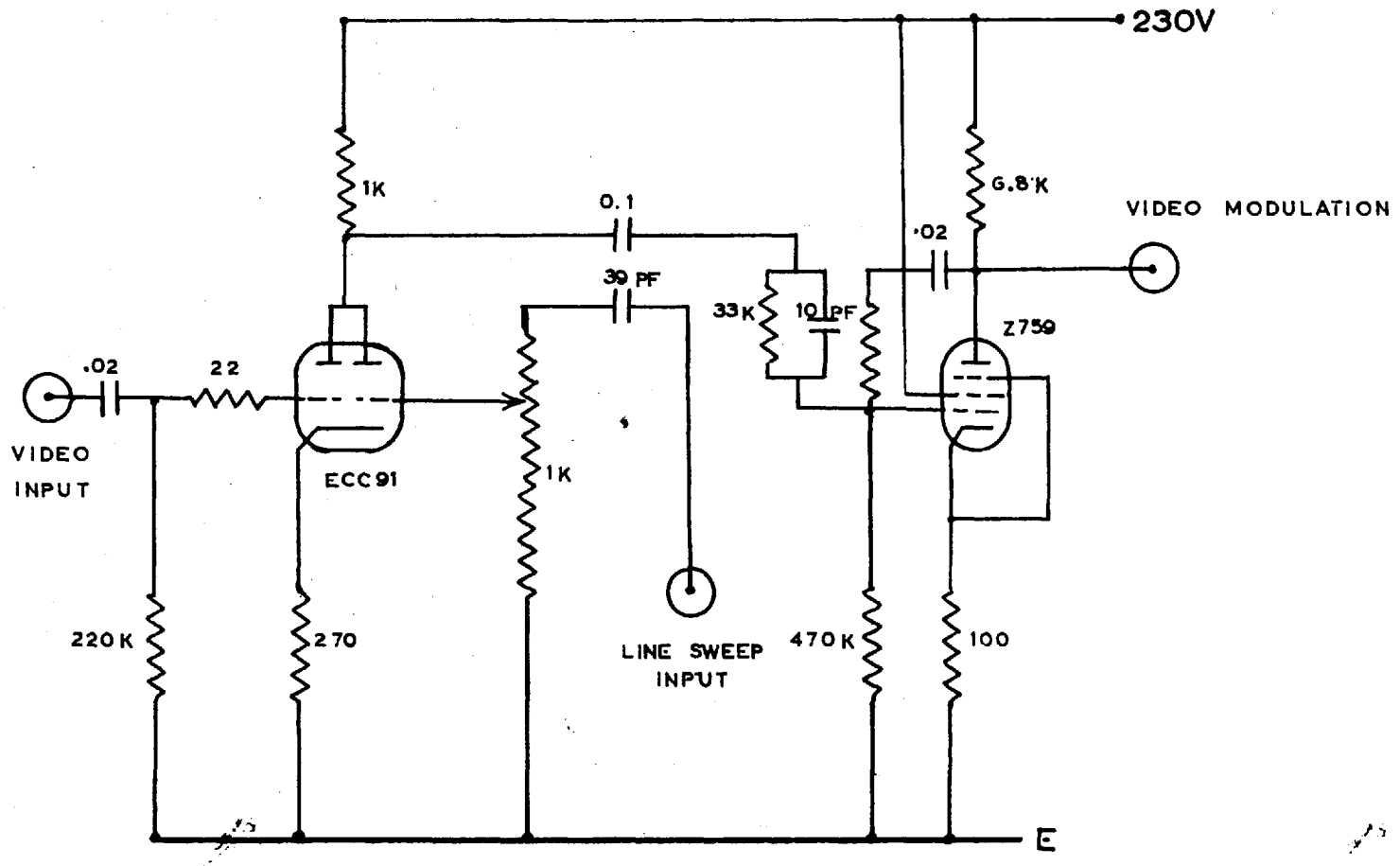


FIG 37. VIDEO AMPLIFIER — RECEIVER

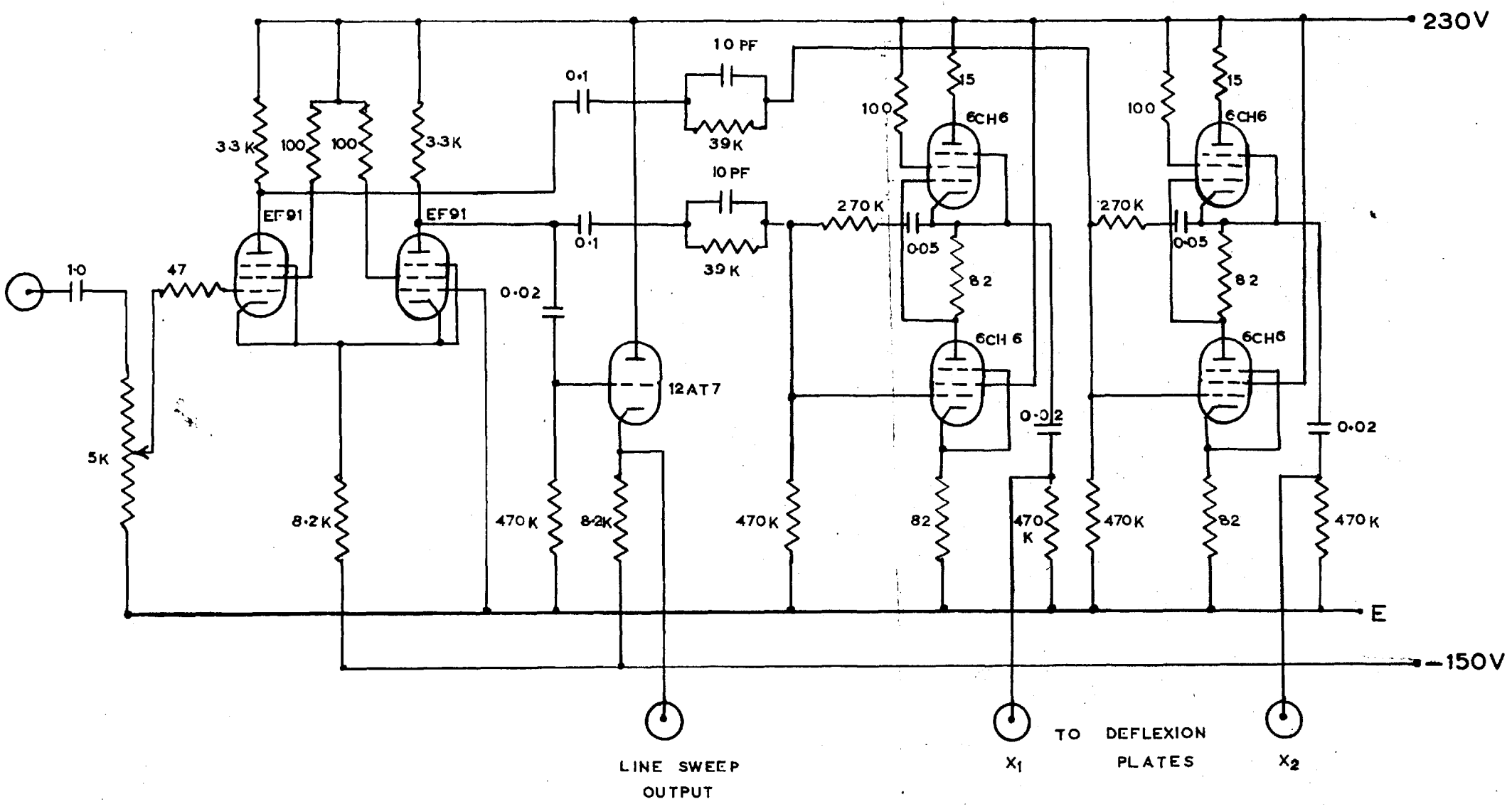


FIG. 38. LINE DEFLECTION AMPLIFIER

which in turn drive the X' and X" plates of the display tube. An output is taken from the anode of V_2 through the cathode follower V_3 for the intensity compensation circuit of the video amplifier.

2.6.3. Ratchet Time Base (Staircase Waveform Generator).

The need for a vertical ratchet time base arises owing to variable line periods as has already been explained.

A diode pump is used in energy storage counters to generate staircase - type waveforms (figure 39(a)). A capacitor, C_2, is used as the energy storage element. A good mica capacitor or a polysterene capacitor with gold plated electrode surfaces ensures energy storage for long periods without any significant loss due to leakage. It is obvious that in the circuit of figure 39(a), the voltage steps would not be equal but would progressively become smaller and smaller. The scope of this type of generator is, therefore, limited. Only a small number of steps can be generated with any degree of linearity. The input pulse amplitude has to be much larger than the totalstaircase waveform amplitude.

The range of a diode pump can be considerably increased by linearizing the envelope of the staircase waveform. The essential principle on which the linearization is based is the same as that used to linearize time base waveforms by bootstrap and Miller integration. A simplified diagram of a diode pump linearized by the bootstrap principle is shown in figure 39(b). If the gain of the cathode follower is assumed to be unity, the cathode potential of the cathode-follower drops by the same amount as the grid potential every time a pulse arrives. Let the grid voltage of the cathode follower be E, the cathode voltage E + k where k is of the order of a few volts. The point A in figure 39(b) is also at E + k due to the d.c. restorer action of D_2. Because of this d.c. restoration, the voltage drop across D_1 is made independent of the amount of charge on the capacitor C_2.

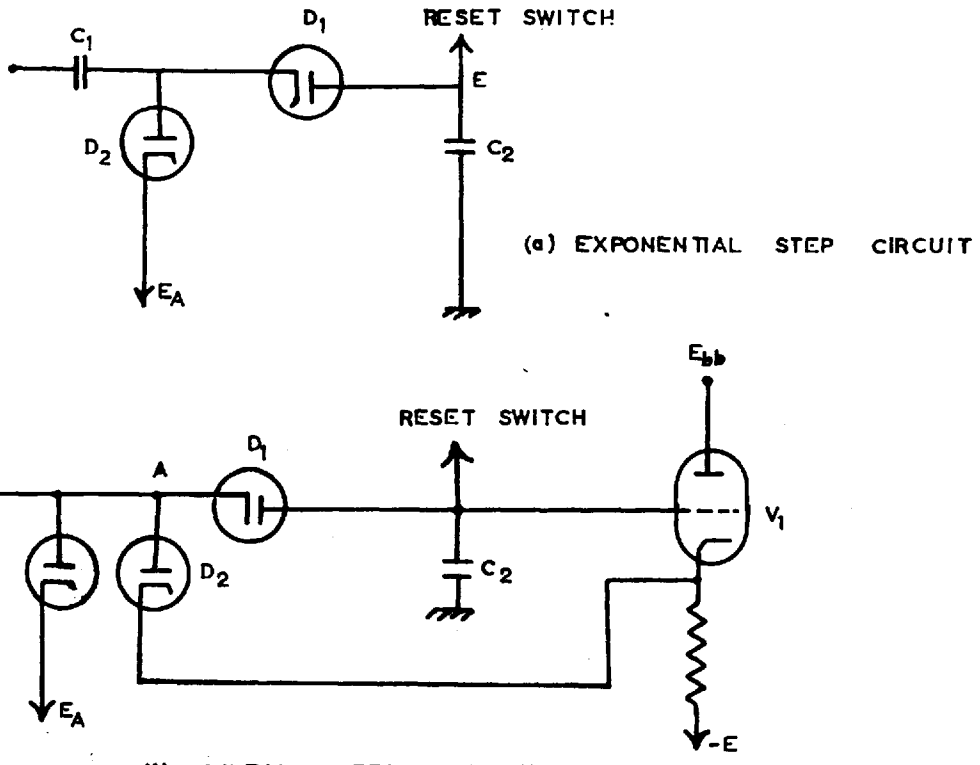

C1
D1
RESET SWITCH
E
D2
C2
EA
(a) EXPONENTIAL STEP CIRCUIT
Ebb
RESET SWITCH
C1
A
D1
V1
D2B
D2
C2
EA
-E
(b) LINEAR STEP CIRCUIT
LINE RESET PULSES
PRECISION PULSE GENERATOR
BOOTSTRAP DIODE PUMP
MULTIAR
DELAY MULTIVIBRATOR
BLOCKING OSCILLATOR
(c) BLOCK SCHEMATIC OF THE RATCHET TIME BASE

FIG. 39.

This ensures that each voltage step has the same magnitude and is given by

$$E_c \cdot \frac{C_1}{C_1 + C_2}$$

where E_c is the amplitude of the input pulse and C_1 the capacitance of the feed-in capacitor. In a linear step circuit, the need for a very large trigger is eliminated and the number of steps that can be generated with equal amplitude is greatly increased. E_A is the reset voltage level.

The circuit diagram of the ratchet time base is shown in figure 40 while the block schematic is shown in figure 39(c). The re-setting pulses of the line time base are used to initiate the steps. A cathode-coupled precision pulse generator comprising V_1 and V_2 provides a rectangular pulse whose amplitude and width is independent of variation in the line re-setting pulse.

A small value of feed-in capacitor is used to keep the time-constant, formed by the output impedance of the pulse generator and the series capacitance of the feed-in capacitor and the storage capacitor, small. D_{2b} has been introduced as a clamp to establish the initial value because the clamping action of D_{2a} is lost due to the bootstrap configuration.

The number of steps generated by the time base is about 400 with a total excursion of 130 volts. Good linearity over this wide range is obtained by using a constant current pentode as the cathode load of the cathode follower, V_3. The output is taken from the grid of V_3 through a cathode follower, V_5, which acts as a buffer stage and ensures minimum amount of loading of the storage capacitor.

A multiar amplitude comparator has been used to provide the re-setting pulse when the output amplitude reaches a certain reference voltage. The resetting pulse must completely charge the storage capacitor, to +230 volts in this case. Attempts to use the multi r pulse directly for the re-setting

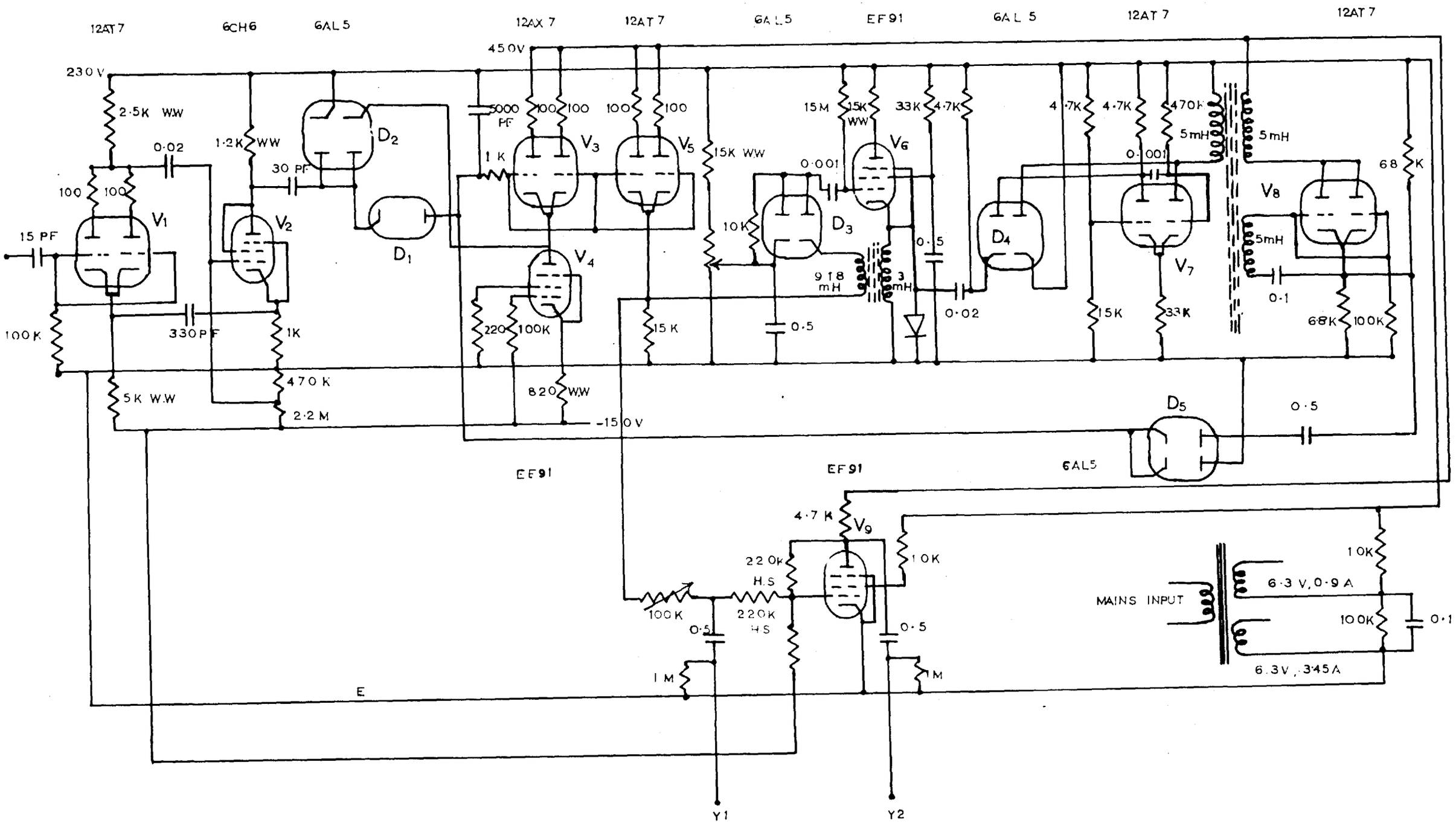
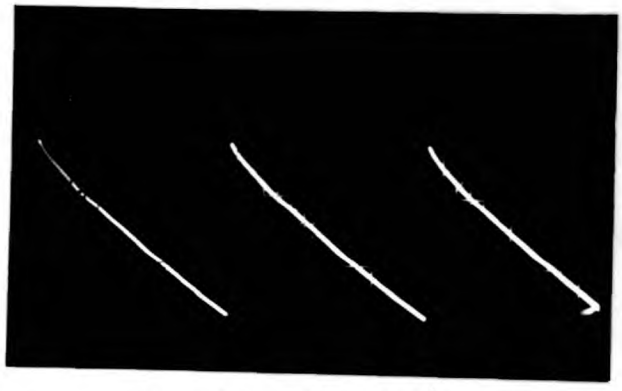
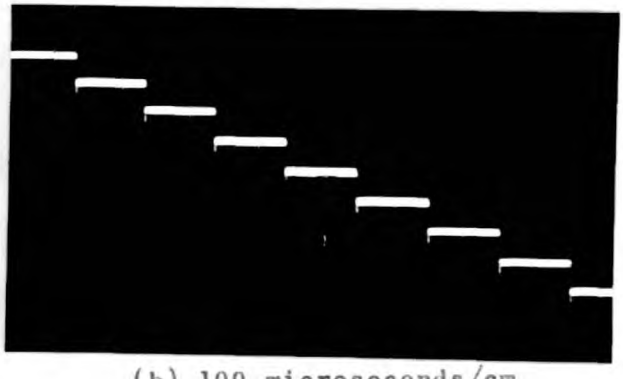


FIG. 40. RATCHET TIME BASE



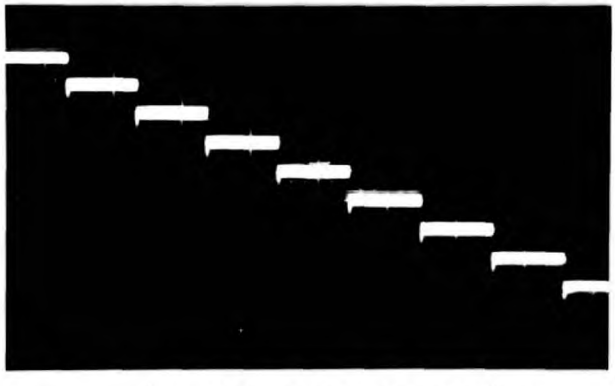
50 Volts/cm

(a) 10 millisecs/cm



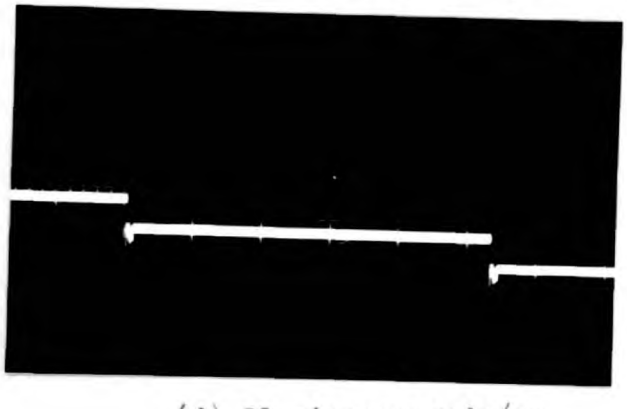
1 Volt/cm

(b) 100 microseconds/cm



1 Volt/cm

(c) 100 microseconds/cm



1 Volt/cm

(d) 20 microseconds/cm

FIG. 41. TESTS ON THE RATCHET TIME BASE.

were not successful. In absence of any delay, the pulse generated at the anode of the multiar pentode was instantaneously fed to the storage capacitor to charge it, which in turn terminated the multiar pulse prematurely, with the result that the storage capacitor was not fully charged. This has been overcome by the introduction of a delay multivibrator followed by a blocking oscillator in the re-setting pulse path. A large positive pulse of a predetermined width is generated across a low output impedance by the blocking oscillator. This pulse is used to recharge the storage capacitor fully. The pulse is connected to the storage capacitor through another diode pump, D_5. This arrangement achieves complete isolation of the storage capacitor from the resetting circuit during all times except when the resetting pulse comes in.

Some photographic results obtained from the ratchet time base are shown in figure 41. Extremely good linearity has been obtained for 400 lines. The time base can be made to work for 600 lines with good linearity. Figure 41(a) shows a scan of a duration of 30 m seconds with nearly 400 voltage steps in it. Figure 41(b) and (c) show steps which are separated by nearly 60 steps. Figure 41(d) shows a small part of the scan on an expanded time scale. The resetting time after each step can be seen to be less than 2 μseconds. The break characteristic of the multiar is sharper than the step voltage. This ensures jitter-free operation of the circuit.

The large magnitude of the output waveform makes it possible to drive the deflection plates without any further amplification.

Footnote: In this Section, Band width in inverted commas has been used to denote the frequency band extending to 50% voltage Response points. Band width normally has been used to denote the actual channel width required for Engineering use (extending to the order of 40-50 db points)

3. STUDY OF THE SYSTEM.

Some results obtained from the variable - velocity system are presented in this section. The receiver was not used in these experiments but waveforms were studied on a cathode ray oscilloscope. The experimental set-up for this investigation is shown in figure 42. A beam switching device, built into the oscilloscope, made it possible to display two waveforms together.

3.1. A Method Of Evaluation Of Bandwidth Reduction.

There are several ways in which the reduction in bandwidth may be estimated after variable - velocity recoding. In the earlier experiments, the results were assessed by measuring the width of the blocks of detail with and without variable - velocity scanning, but it is felt that this is not a very satisfactory method. In the following experiments, the bandwidth reduction has been evaluated from the time base scan waveform. Both the bandwidth reduction and the reduction in the time - bandwidth product have been calculated.

A typical scan waveform is shown in figure 43. Let θ_1 and θ_2 be the largest and the smallest angles respectively that the sweep waveform makes with the horizontal, i.e. with the time axis.

Since $\tan\theta$ varies as the velocity which in turn varies as the bandwidth W, the bandwidth reduction, C, is given by

$$C = \frac{\tan\theta_1}{\tan\theta_2} \qquad (3.1)$$

Referring again to figure 43, let T be the scan duration if a certain line in the picture was scanned by conventional scanning with velocity v_1 corresponding to the slope denoted by θ_1. Let the time taken by the variable - velocity scanner to scan the same line be $T + T_1$. Then the time - bandwidth product for the two cases can be written down. Time-bandwidth product for the constant - velocity

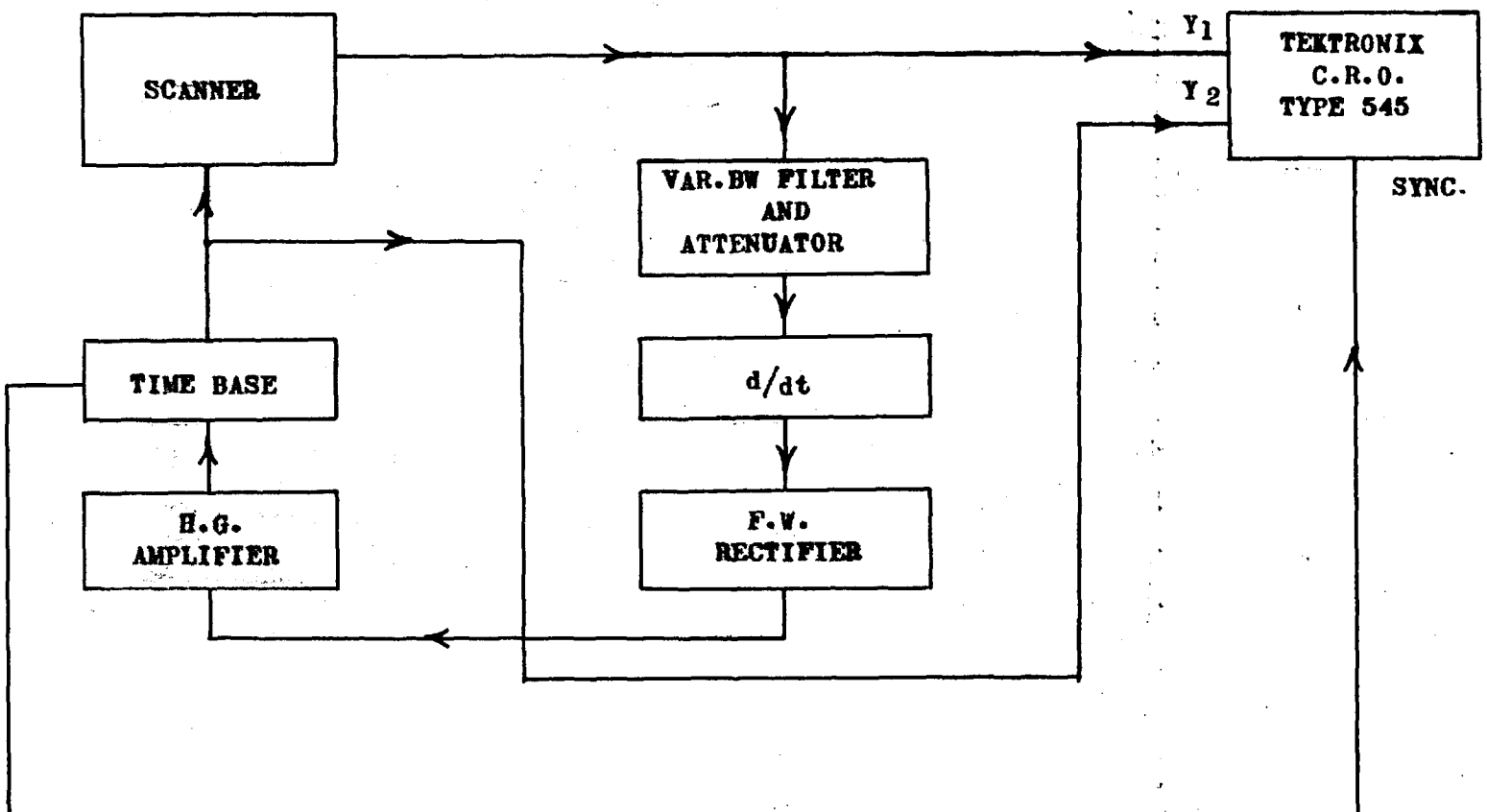

SCANNER
VAR.BW FILTER AND ATTENUATOR
TIME BASE
d/dt
H.G. AMPLIFIER
F.W. RECTIFIER
Y1
Y2
TEKTRONIX C.R.O. TYPE 545
SYNC.

FIG. 42

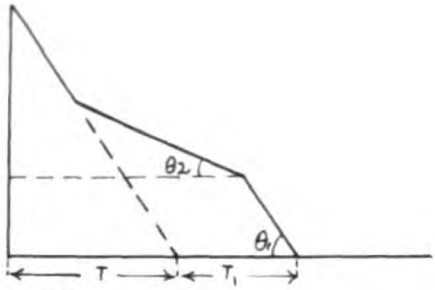
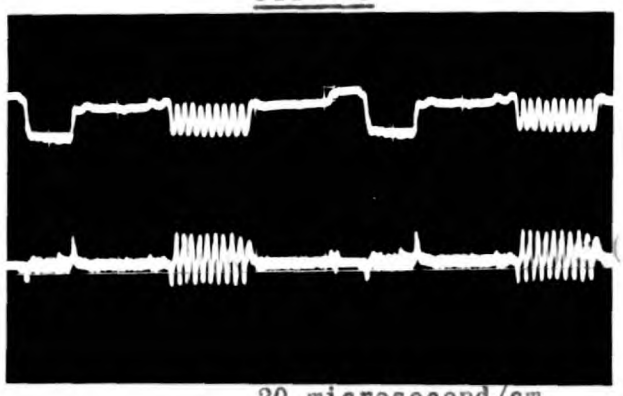


FIG. 43

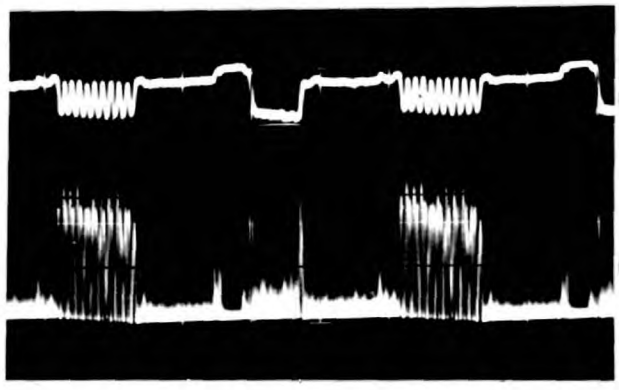


(i) Video 0.5 Volts/cm

(ii) d/dt 0.25 Volts/cm

20 microsecond/cm

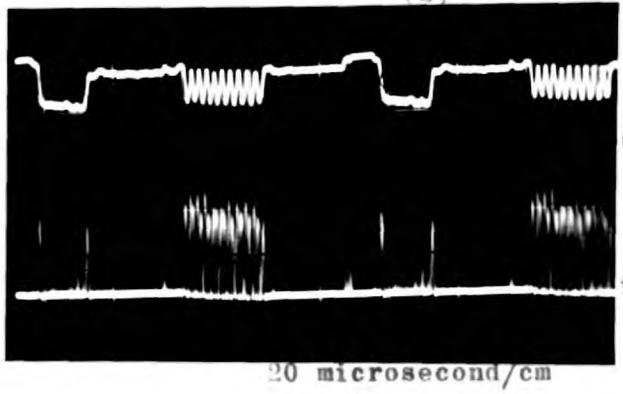
(a)



(i) Video 0.5 Volts/cm

(ii) $\left|d/dt\right|$ 1 Volt/cm

(b)



(i) Video 0.5 Volts/cm

ii) $\left|d/dt\right|$ after clipping 1 Volt/cm

20 microsecond/cm

(c)

FIG. 44

Scanning Case = $W\ T$

Time - bandwidth product for the variable - velocity Scanning Case = $\frac{W}{C}\ (T + T_1)$.

Hence the reduction in the time - bandwidth product may be expressed as

$$R = \frac{W.\ T}{\frac{W}{C}\ (T + T_1)} : 1$$

$$\text{or} \quad R = C\ \left(\frac{T}{T + T_1}\right) : 1 \qquad (3.2)$$

$$\text{where} \quad C = \frac{\tan \theta_1}{\tan \theta_2}$$

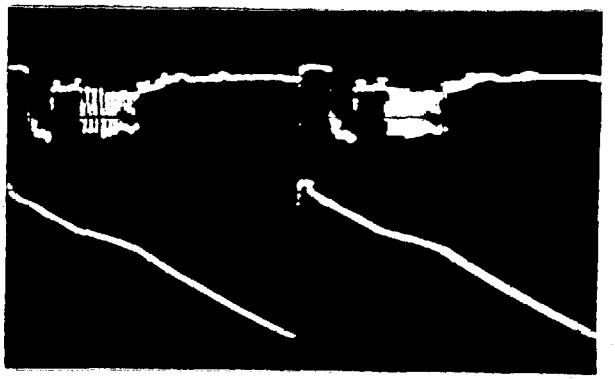
It is interesting to note that while C depends only on the ratio of the maximum and minimum scan velocities that may be achieved in the system, the factor $\left(\frac{T}{T + T_1}\right)$ is also dependent on the picture statistics. Thus R, the overall reduction depends on the amount of detail in the picture.

For the experimental evaluation of θ_1, θ_2, T and T_1, the negative transparencies of the scan waveform were projected by a microfilm reader which made accurate measurements possible.

3.2. Experimental Results.

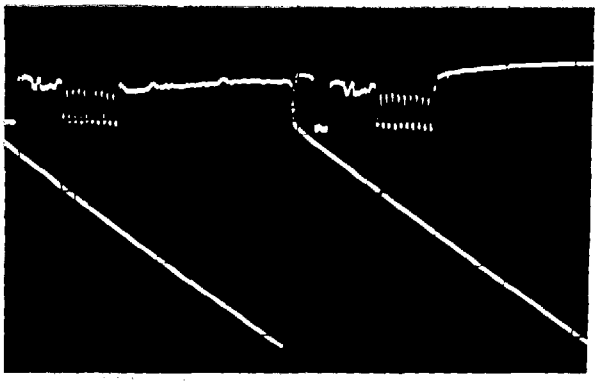
The results of the preliminary experiments were disappointing. Compression ratios of less than 1.8:1 were obtained when the jitter in the waveform became so excessive that synchronism was completely lost on the display device. It was felt that this failure of the compression system may be due to one or more of the following causes:

(1) The instability of the feedback loop: the transmitter is a closed loop non-linear feedback system and an analytical solution is difficult to obtain. The stability of the loop had, therefore, to be investigated experimentally.



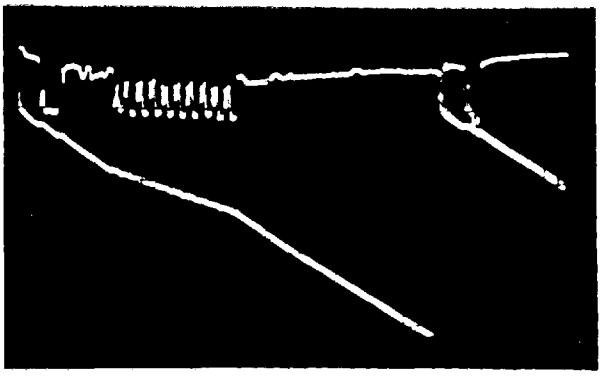
(a) 50 microseconds/cm

Closed Loop
(i) Video
(ii) Time Base
C 2.15:1
R 1.53:1



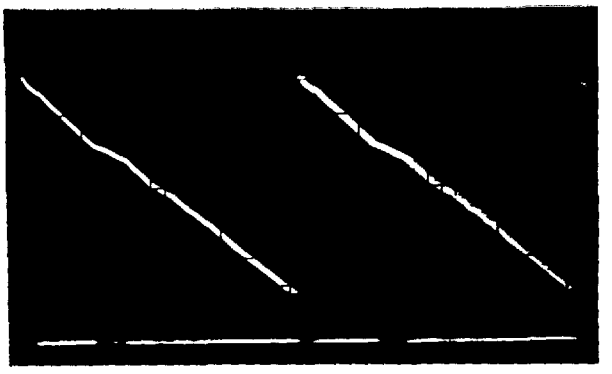
(b) 2o microseconds/cm

Open Loop
(i) Video
(ii) Time Base



(c) 20 microseconds/cm

Closed Loop
(i) Video
(ii) Time Base
C 2:1
R 1.6:1



(d)

Closed Loop
(i) Time Base
(ii) |d/dt|
C 2.33:1
R 1.99:1

FIG. 45 VARIABLE-VELOCITY SCANNING (WITH CLIPPING)

(2) The source noise: It is well known that noise and high frequency low contrast detail in a picture have comparable power and it is very difficult to separate them. It was observed by Beddoes[4a] that the addition of noise to a video signal increases the picture detail factor of the signal. The random nature of noise would prevent the superimposition of one scan over another, even though the signal is periodic, if the noise is allowed to control the feedback loop. Thus the jitter may be caused by a deterioration in the system performance due to the source noise.

A look at the output waveform (Fig.44) of the full wave rectifier, when the loop is open, suggests that during the process of detail detection, there has been a weighting in favour of the noise. In the absence of fine detail of high contrast, the feedback loop would be predominantly controlled by the noise. To reduce the effect of noise, it was decided to instal a clipper, with a variable threshold, after the full wave rectifier. This is accompanied by the reduction of contrast in fine detail. The inset in figure 26 shows the clipper that was used and figure 44(c) shows a clipped control signal. Comparison of figure 44(b) and (c) shows that the clipper was effective in reducing the noise in the feedback loop.

Figure 45 shows some results from the variable - velocity system using clipping. The values of C and R based on equations (3.1) and (3.2) are quoted in the figure. The jitter was considerably reduced owing to clipping and its effect was not serious for values of C up to 2.33 (Figure 45(d)).

3.2.1. An Experiment to Investigate Phosphor Loading And System Stability.

In the experimental set-up shown in figure 42, no vertical deflection was used. A single line was scanned all the time. It was considered desirable to ascertain whether phosphor saturation was taking place due to excessive loading

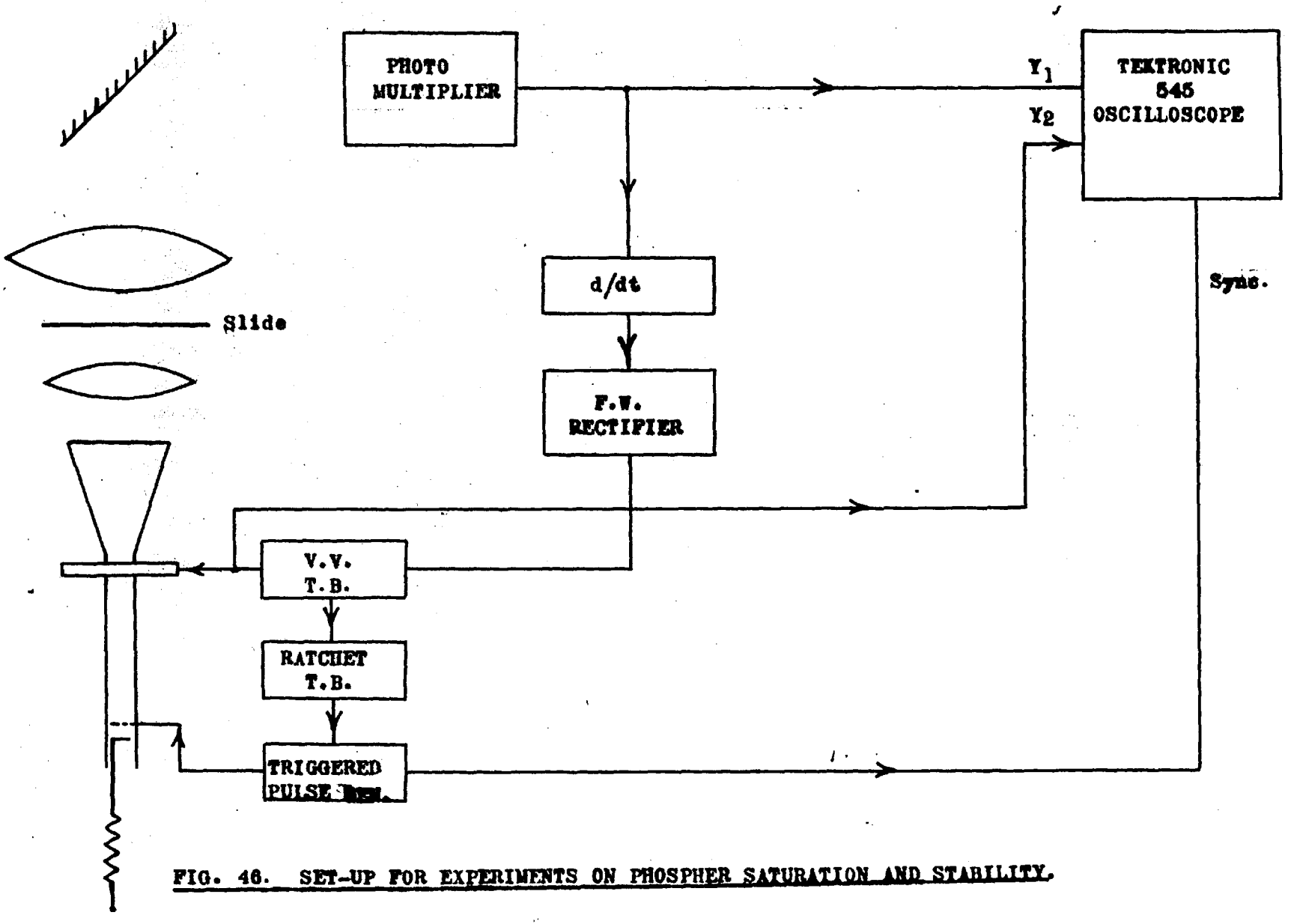


FIG. 46. SET-UP FOR EXPERIMENTS ON PHOSPHER SATURATION AND STABILITY.

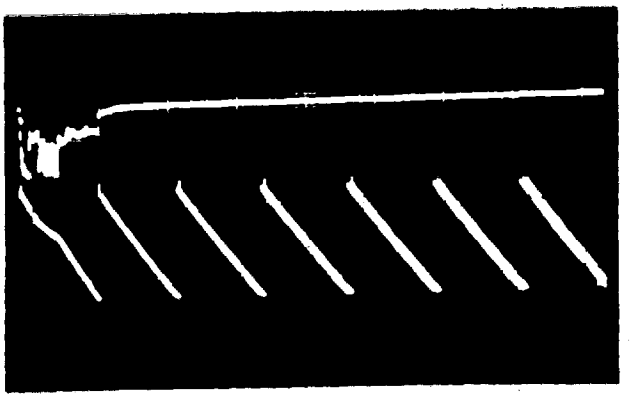
in a small area. An experiment was, accordingly, designed and performed. This also threw some light on the stability of the system.

A block diagram of the experimental set-up is shown in figure 46. The only alteration, from the previous set-up of figure 42, is that the brightness level in the scanner tube is so adjusted that the electron beam is normally cut-off and is switched on only when a positive pulse is applied to the grid. Synchronism between the intensity modulation pulse and the line time base is maintained by counting down the line reset pulses by using the ratchet time base as a counter. The ratchet time base re-set pulse is used to trigger a pulse generator whose output pulse width can be adjusted. This provides a control on the duty ratio of the phosphor.

Figure 47(a) shows the case when the width of the intensity modulation pulse is 125 μsec. Figure 47 (b) corresponds to an intensity modulation pulse width of 500 μsec. in which the effect of jitter is more pronounced. Values of R for (a) and (b) are 2.24 and 2.6 respectively. This slightly higher value is obtained, because in this configuration a brighter trace can be used without burning the phosphor in the scanner tube. This makes it possible to obtain a better $S/_N$ ratio in the video output. Figure 47(c) is taken with a white uplift i.e. without any slide. The effect of switching transient can be seen on the scan waveform. There is no instability produced due to these transients in any oneof the three pictures in figure 47.

3.2.2. Experiments With Special Signals.

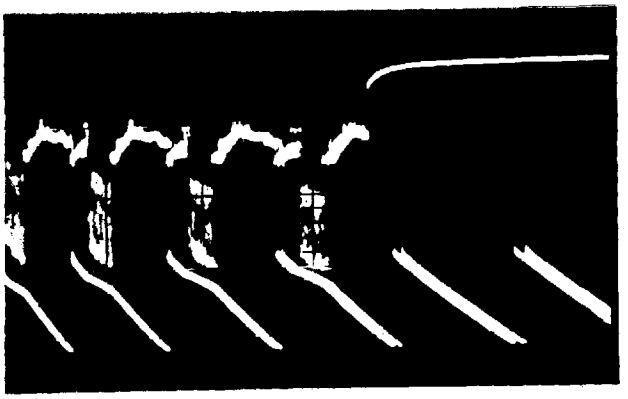
The experiment described above suggested that the system was stable but that the performance of the system deteriorated greatly with noise. The chief source of noise in a flying - spot scanner is shot noise in signal which is much larger than shot noise in dark current. As the multiplication noise in a photomultiplier is negligible, almost all the shot noise in-



(i) Video
(ii) Time Base

C 2.8:1
R 2.24:1

(a) 100 microseconds/cm
Intensity modulation Pulse width 125 microseconds



(i) Video
(ii) Time Base

C 3.4:1
R 2.63:1

(b) 100 microseconds/cm
Intensity modulati n Pulse width 500 microseconds



(i) Time Base
(ii) Video
(White Uplift)

(c) 100 microseconds/cm

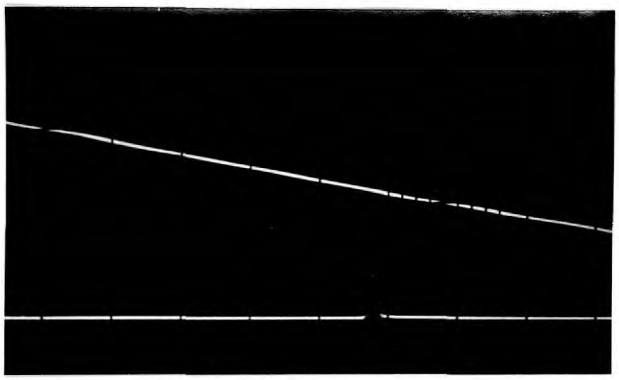
FIG. 47. TESTS FOR PHOSPHOR SATURATION AND STABILITY

the signal output is produced by the shot noise in signal component of the photocathode current.

The photographic results shown in figure 48 were obtained by the experimental set-up shown in figure 42. Instead of using a slide, a black paper with a narrow slit was used as a mask for the scanner tube face. Thus the signal was a single pulse and the shot noise in signal over the whole line wa considerably reduced. Values of R up to 3.63:1 were obtained. Figure 48 shows that even for this high value of R, there is no jitter at all in the signal. This experiment again points out that the lack of synchronism reported earlier was caused by source noise and not by any instability in the system itself.

Figure 49 was obtained with the experimental set-up shown in figure 46. The stationary pattern of the grain structure with the loop open, can be seen in figure 49(a) which was obtained with a white uplift. Figure 49(b) shows the white uplift when the loop is closed. A 350 µsec. intensity modulation gate was used in both cases; no clipping was used in the feedback loop. The sweep duration in figure 49(b) is increased by 35 µsec. which corresponds to an increase of 33% in the sweep duration. This increase is caused because the system treats noise as picture detail.

An attempt was made to reduce the thermionic emission from the photocathode by cooling the photomultiplier with solid CO_2. The scanner beam current was increased and the voltage between the cathode and the first dynode of the photomultiplier was increased to 250 volts. There was no provision in the apparatus to prevent condensation on the glass window of the photomultiplier tube. This, along with the fact that the brightness was turned above the safe level for the phosphor rendered it imperative that the experiment should be performed in a very short time. Single shot photographs were taken to separate the effects of jitter and of system instability, if any, In figure 50 (a) and (b), R of 3.95: 1 and 4.35:1 have been obtained on parts of test card 'C'. The oscilloscope was

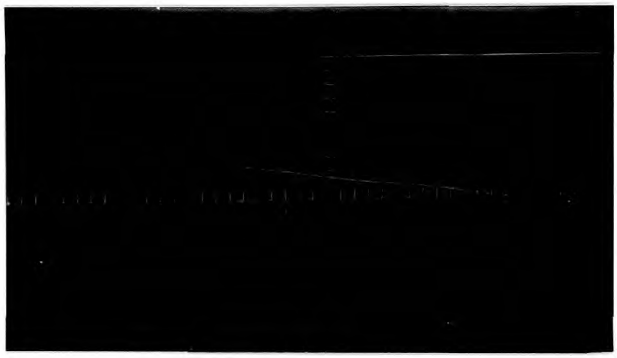


Open Loop

(i) Time Base

(ii) Video
0.25 Volts/cm

(a) 10 microseconds/cm



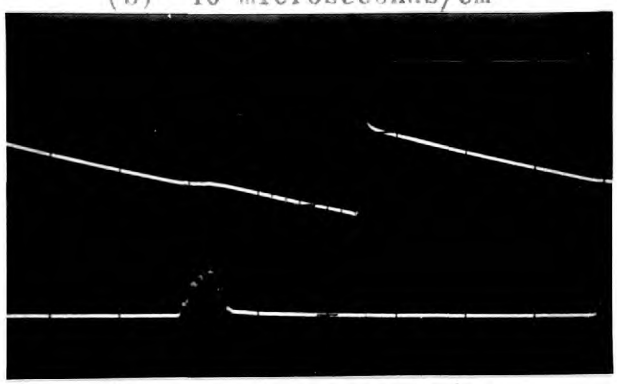
Closed Loop

(i) Time Base

(ii) Video

C 3.22

(b) 10 microseconds/cm



Closed Loop

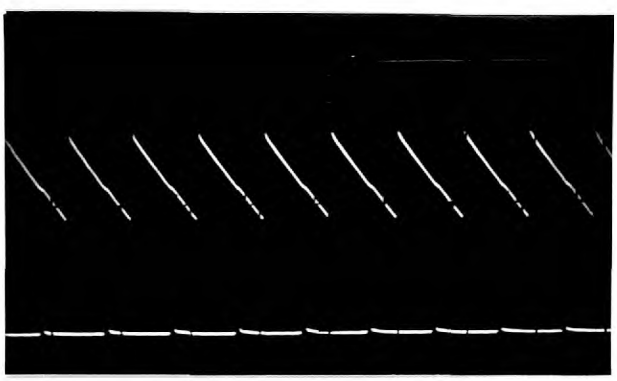
(i) Time Base

(ii) Video

C 3.8:1

R 3.4:1

(c) 20 microseconds/cm

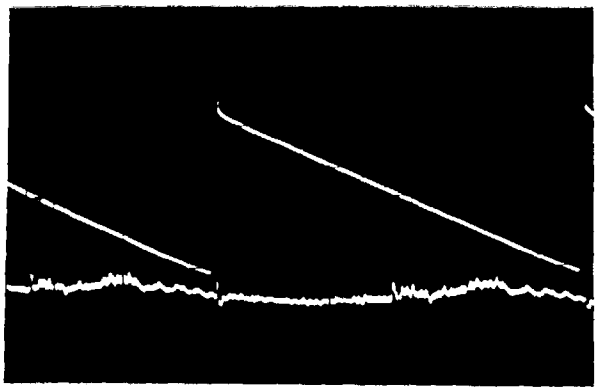


C 3.86:1

R 3.63:1

(d) 100 microseconds/cm

FIG. 48. EXPERIMENTS WITH SPECIAL PULSES



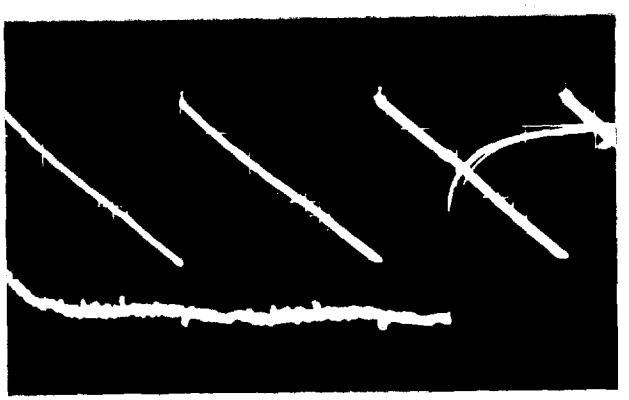
Open Loop

(i) Time Base

(ii) Head Amplifier Output
.5 Volts/cm.

Sweep Speed 20 microseconds/cm

(a)



Closed Loop

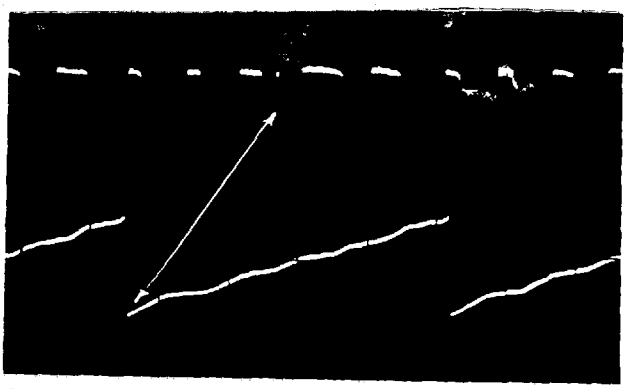
(i) Time Base

(ii) Head Amplifier Output
.5 Volts/cm

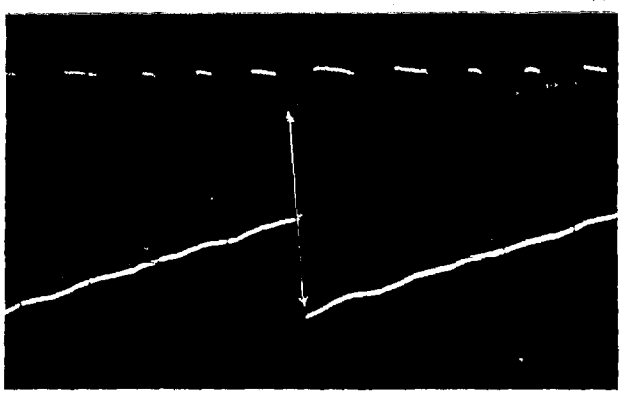
Sweep Speed 50 microseconds/cm

(b)

FIG. 49 GRAIN STRUCTURE



(i) Video
(ii) Time Base
R 3.95:1
(a)



(i) Video
(ii) Time Base
R 4.35:1
(b)

The Corresponding points on (i) and (ii) have been marked.

FIG. 50. SINGLE SHOT PHOTOGRAPHS

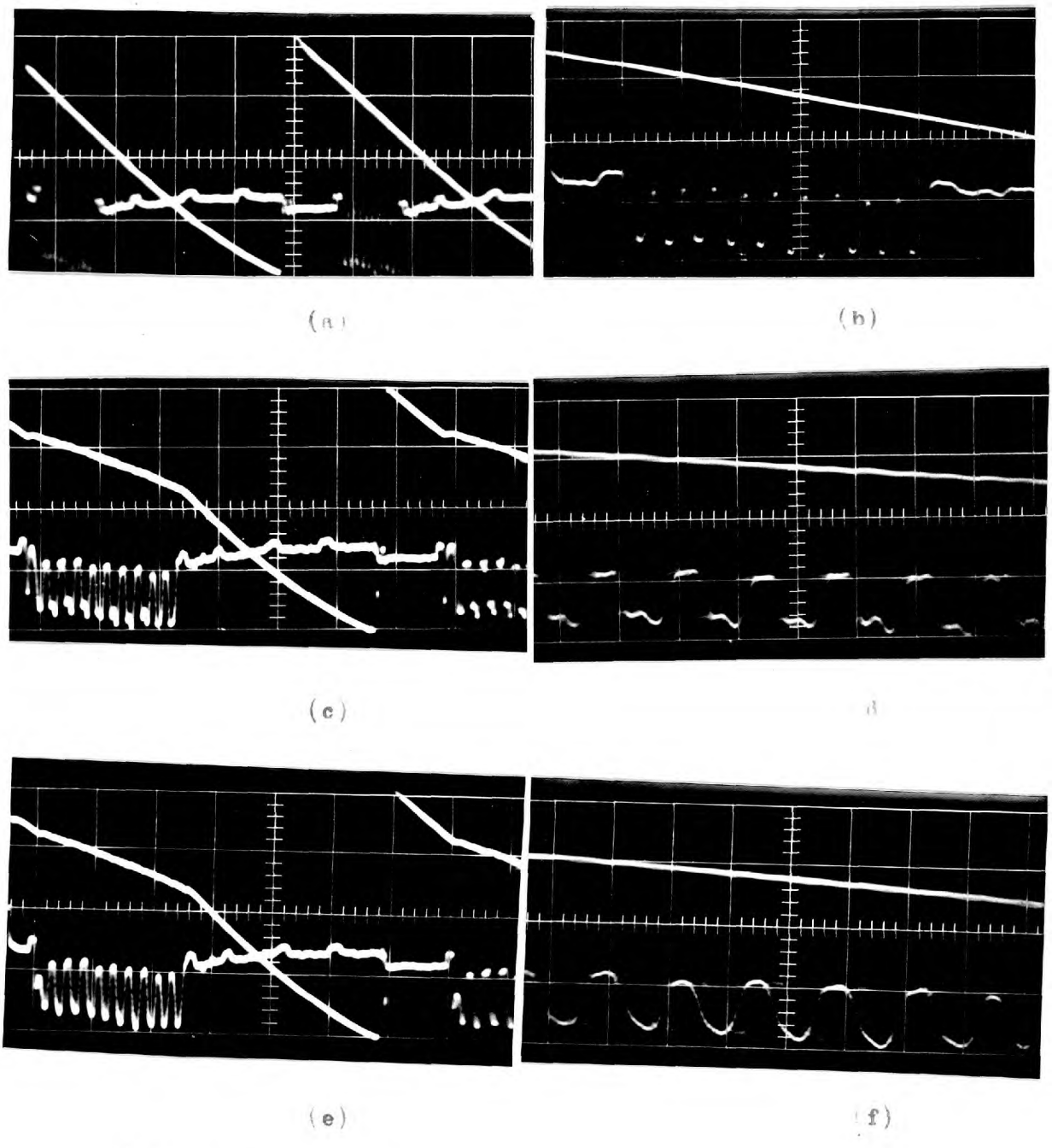
manually triggered for single shot operation hence there is no vertical correspondence in the photographs. The corresponding points have been marked in the figure.

3.2.3. The "Beat Effect" - Re-entrant Spot.

During variable - velocity operation, it was observed that some extra detail, which was not present in the slide, was introduced in the video output, especially noticeable in blocks of detail (Figure 51). This phenomenon was also observed by Beddoes[4a] and called "Beat Effect". Beddoes observed it while experimenting with a high-pass filter as the detail detector and attributed it solely to the characteristics of the high-pass filter. This explanation is not tenable for the case when a differentiator is used for detail detection.

An investigation has been carried which indicates that the only way, in which such a signal could be generated, would be by a re-entrant spot. Re-entrant spot can be caused by ringing in an underdamped deflection system or by excessive feedback with delay round the loop, or both. An illustration of a re-entrant spot is shown in figure 52(b). The spot was made re-entrant by modulating the time base with the output of a triggered pulse generator. The amplitude and the duration of the output pulse were made independent of the video output of the scanner. It may be remarked that the order of the pulses in figure 52(b) is reversed during negative slope of the time base waveform as expected. An example of re-entrant spot during variable - velocity operation is shown in figure 52(c). This was obtained, with the set up shown in figure 46, by increasing the loop gain excessively which also made the system unstable.

It was found that the re-entrance under investigation was caused because the deflection coil was slightly underdamped. By increasing the damping, the spot was prevented from re-entering the scanned part and the "Beat Effect" was eliminate as shown in figure 51 (e) and (f).



(a) (b)

(c) (d)

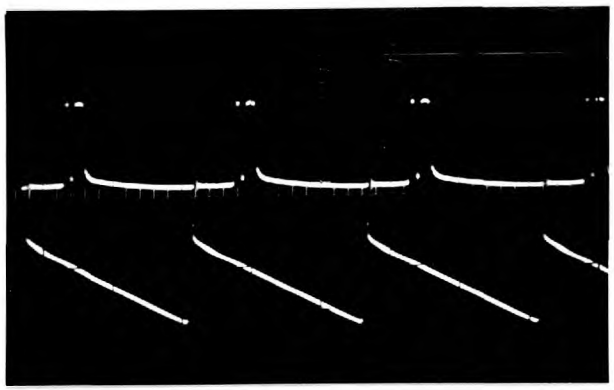
(e) (f)

(a) and (b) Open Loop

(c) and (d) Closed loop underdamped

(e) and (f) Closed loop optimally damped.

FIG. 51 The "BEAT EFFECT"

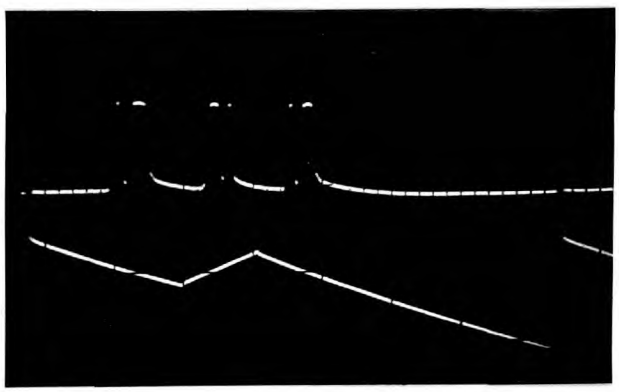


(i) Video

(ii) Time Base

Open loop

(a)

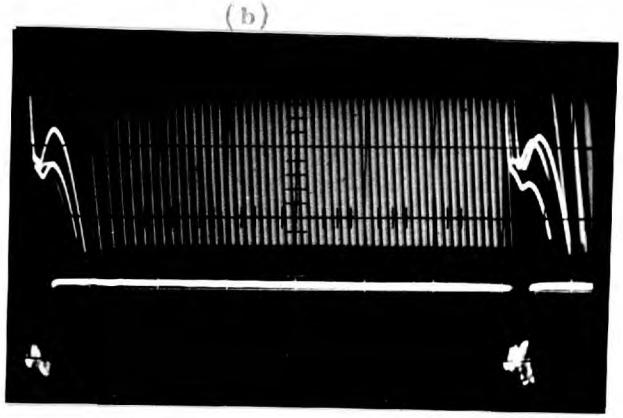


(i) Video

(ii) Time Base
Externally Controlled

Open loop

(b)



(i) Time Base

(ii) Head Amplifier
Output.

Closed Loop - Maximum Loop Gain

10 Milliseconds/cm

(c)

FIG. 52 RE-ENTRANT SPOT

3.3. The Bandwidth of the Feedback Loop.

In an analytical study of the variable - velocity scanner, it has been suggested by Beddoes[61] that for a displacement error of 1 in 500, the necessary bandwidth of the deflection coil varies between 700 Kc/s and 800 Kc/s as the ratio of maximum scanning velocity to minimum scanning velocity is varied from 10 to ∞ for a nominal line frequency of 10 Kc/s.

This figure is based on the assumption that the only bandwidth limitation is due to the self-capacitance of the deflection coil so that all other circuits have been assumed to have bandwidths which considerably exceed that of the deflection coil. This assumption is not realistic. The experiments described earlier have shown that the line output transformer introduces a serious bandwidth limitation which cannot be ignored. Further, this figure has been arrived at by considering a single transition of scan velocity. The displacement error will depend on the number of transitions in a line. Another assumption made in the analysis is that the transients, due to the previous transitions of velocity, are negligible at the time of a particular transition of velocity. This assumption implies that once a transition of scan velocity has taken place, the next transition should not take place for at least the next four picture points (if the deflection system bandwidth is assumed to be 750 Kc/s). It can be seen that this condition may not be fulfilled in practice without being wasteful.

Another factor which is relevant in the discussion of the bandwidth of the feedback loop, but which has been tacitly ignored in the above-mentioned analysis, is the actual transmission delay around the loop. The response time of the feedback loop is limited both by the loop transmission delay and the cut-off frequencies of the component circuits in the feedback loop.

Investigation carried by Gallaher[78] suggest that in a typical flying - spot scanner using a P16 phosphor, an e.h.t. supply of 10 KV and a ten - stage photomultiplier, transmission time delays of the order of 100 n μsec. are inevitable. Some of the figures quoted by Gallaher are given below.

Device	Transit time delay
Photomultiplier Tube	60 n μsec.
Scannar tube (P16 Phosphor)	11 n μsec.
Optical path	5 n μsec.
Connecting Cables	12 n μsec.

These add up to 88 n μsec. To Gallaher's figure must also be added the time spread in the photomultipliers, which, in the case of a typical E.M.I. tube is of the order of 18 n μsec.[68] The time spread is caused by differing path lengths during the multiplication stages and has to be taken into account. Thus a minimum figure of transmission delay of 100 n μsec. seems reasonable. In the case of the 3 Mc/s television standard, the fastest transition can take place in 167 n μsec. It is essential that the system response time should be less than 167 n μsec, otherwise single transitions of the shortest duration would not be recoded and would be lost. If the response time is made equal to 125 n μsec., i.e. 75% of the smallest transition time, ~~due~~ owing to the inherent delay of 100 n μs the bandwidth of the system should be such as to add only 25 n μsec. to the response time. Hence, the minimum desired system bandwidth

$$W = \frac{1}{2\,t_d}$$

$$= \frac{1}{2 \times 25 \times 10^{-9}} = 20 \text{ Mc/s}$$

If the specification is relaxed ~~such~~ so that the response time is made equal to 80% of the smallest transition time, the desired system bandwidth reduces to approximately 15 Mc/s.

3.4. Some Spectral Measurements.

In view of the important effect that the source noise has on the system performance, as suggested by the experimental results already presented, it was considered desirable to study the spectrum of the signal and the noise generated by the f.s. scanner. The weighting, of the signal and the noise frequency components, due to the differentiation made it important to ascertain, besides the overall $S/_N$ ratio, the signal to noise ratios in different frequency bands, especially towards the high frequency endof the spectrum.

3.4.1. The Experimental Set-Up.

The experimental set-up used for the spectral measurements is shown in figure 53(a). The Airnec wave analyser has a bandwidth of 3 Kc/s which can be swept over the frequency range 30 Kc/s to 30 Mc/s. It has a square law device and a meter incorporated in it. The signal energy is measured by tuning for the maxima at the multiples of the line repetition frequency, while sampling the noise in the minimum energy regions of the video spectrum provides the noise spectrum This method has been fully described by Weaver.(79) The R.F. sinewave generator is used to keep the gain of the wave analyser constant. The scanner was connected as a constant velocity scanner with the conventional line and frame deflection system mentioned in section 2.3.1. A converted television receiver was used as a picture monitor and a tele-equipment type WG/44 was used to provide synchronization pulses to synchronise the scanner and the monitor time bases.

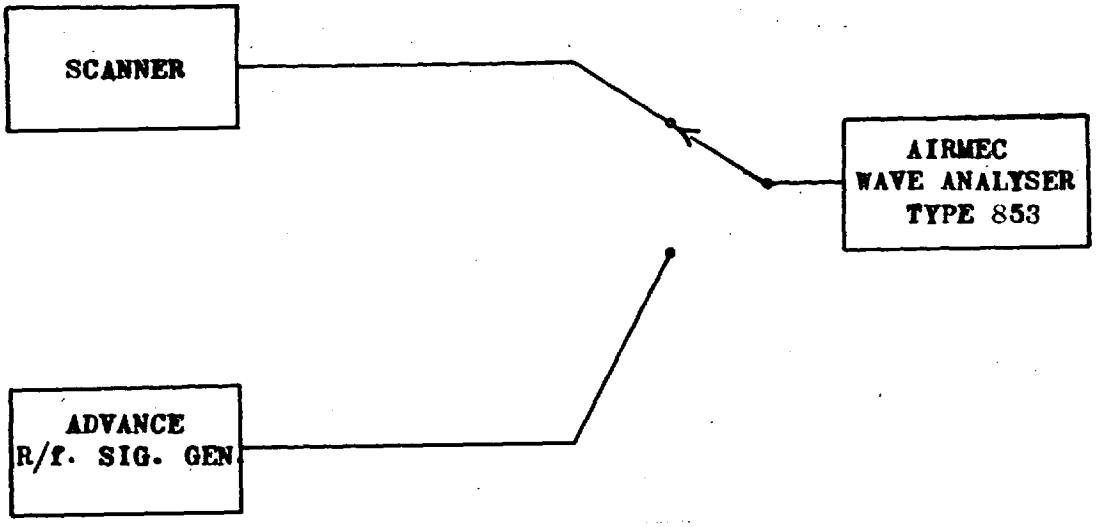


FIG. 53a

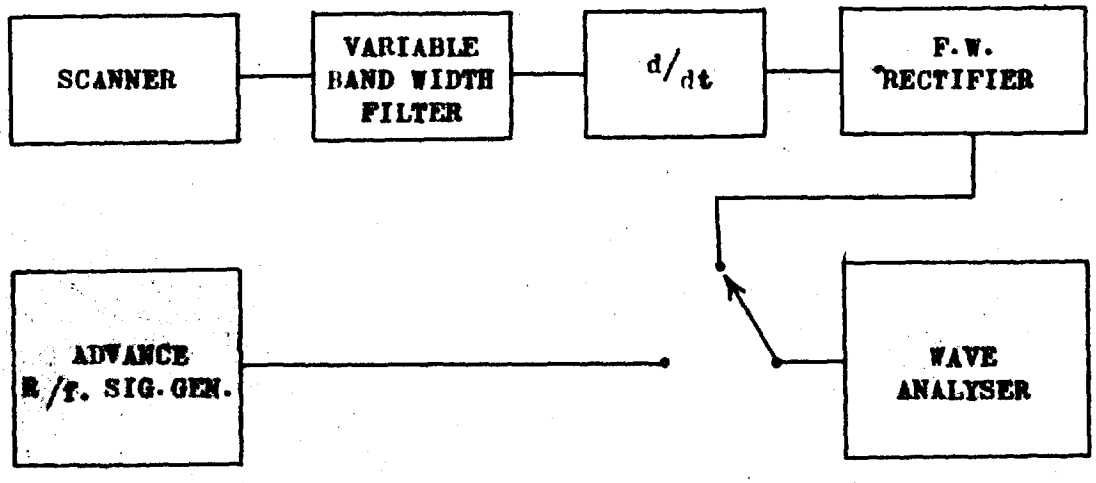
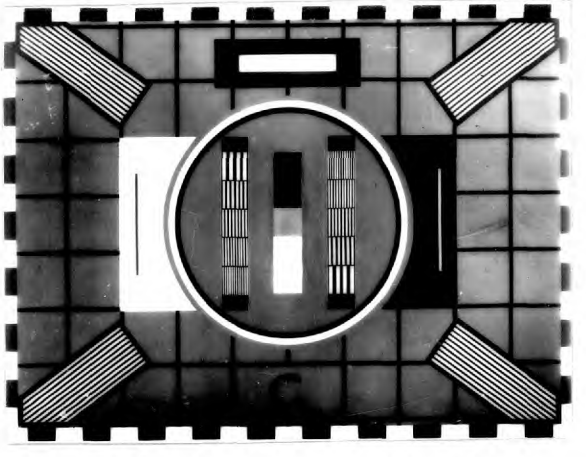


FIG. 53b



(a) Close-up of a girl.



(b) Test Card "C"

FIG. 54. PICTURES USED FOR SPECTRAL MEASUREMENT.

3.4.2. Some Results.

The method used in these measurements is based on the fact that the sidebands around each line harmonic decrease rapidly and that there is a frequency band between two adjacent line harmonics in which the energy present due to the signal is negligible. Therate at which the sidebands diminish depends on the complexity of the picture. The 3 Kc/s bandwidth of the wave analyser made it essential to choose simple pictures for the spectral measurements. A bright raster without any slide which is known as a "white uplift" was used along with two other pictures. The second picture was the close - up of a girl (Figure 54(a)) and the third picture was test card "C" (Figure 54(b)). No synchronizing or blanking pulses were added to the signal but the flyback was suppressed by clamping the video output to the black level during the flyback period.

The spectrum of the noise obtained in the presence of "white uplift" is shown in figure 55. A check was made with a white noise generator instead of a sine wave oscillator as the standard. The result obtained was considered significantly the same as that obtained with the sine wave oscillator, hence all the later measurements were made with the sine wave generator as shown in the block schematic (Figure 53a).

For the case when the raster is defocussed, the noise spectrum is flat within $\pm$ 1 dbs while when the raster is focussed, the effect of grain noise in certain frequencies can be seen. As the predominant source of noise is the shot noise generated by the photomultiplier, it is not surprising that the spectrum is flat.

Figure 56 shows the signal spectrum for test card "C" while figure 57 shows both the signal and the noise components measured for the close-up of the girl. It is instructive to note how the mean square signal to noise ratio varies at different frequencies. While the m-s signal to noise ratio is approximately 30 dbs at 100 Kc/s, it is less than 5 dbs at 3 Mc/s. This is particularly important because the l.f.

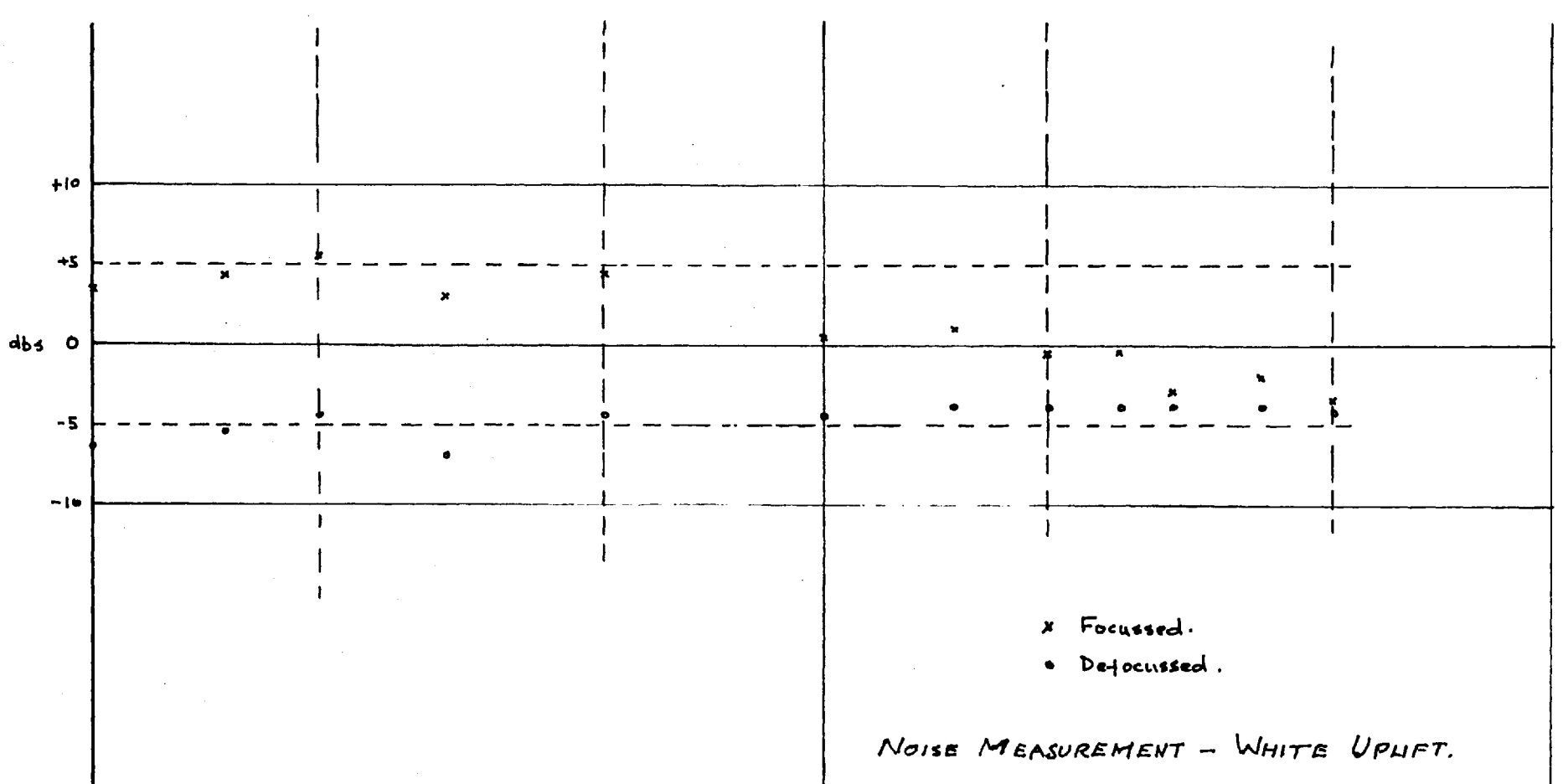

+10
+5
dbs 0
-5
-10
100 kc/s
200
500
1 Mc/s
2
5
10
x Focussed.
• Defocussed.
NOISE MEASUREMENT – WHITE UPLIFT.

FIG. 55.

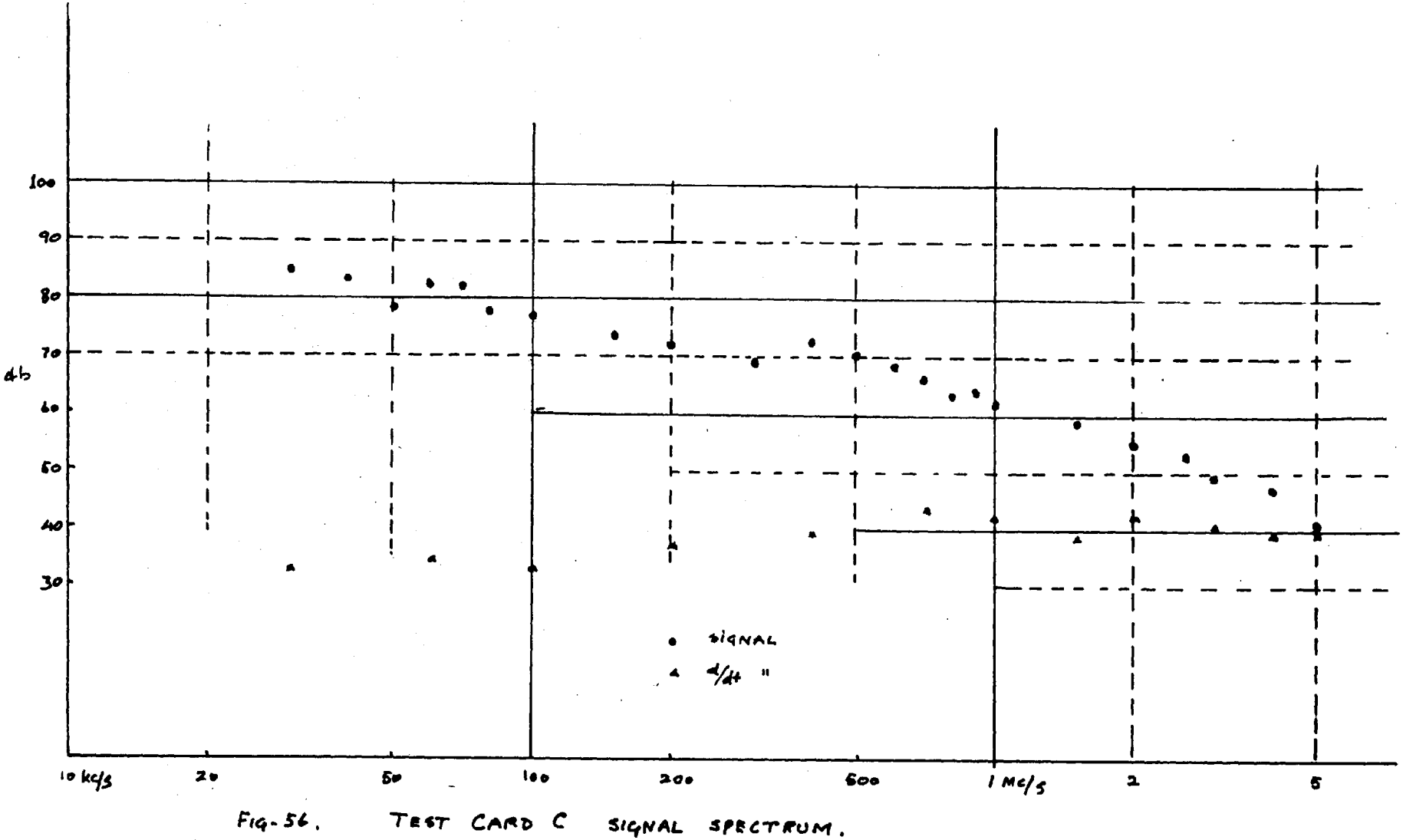


FIG-56. TEST CARD C SIGNAL SPECTRUM.

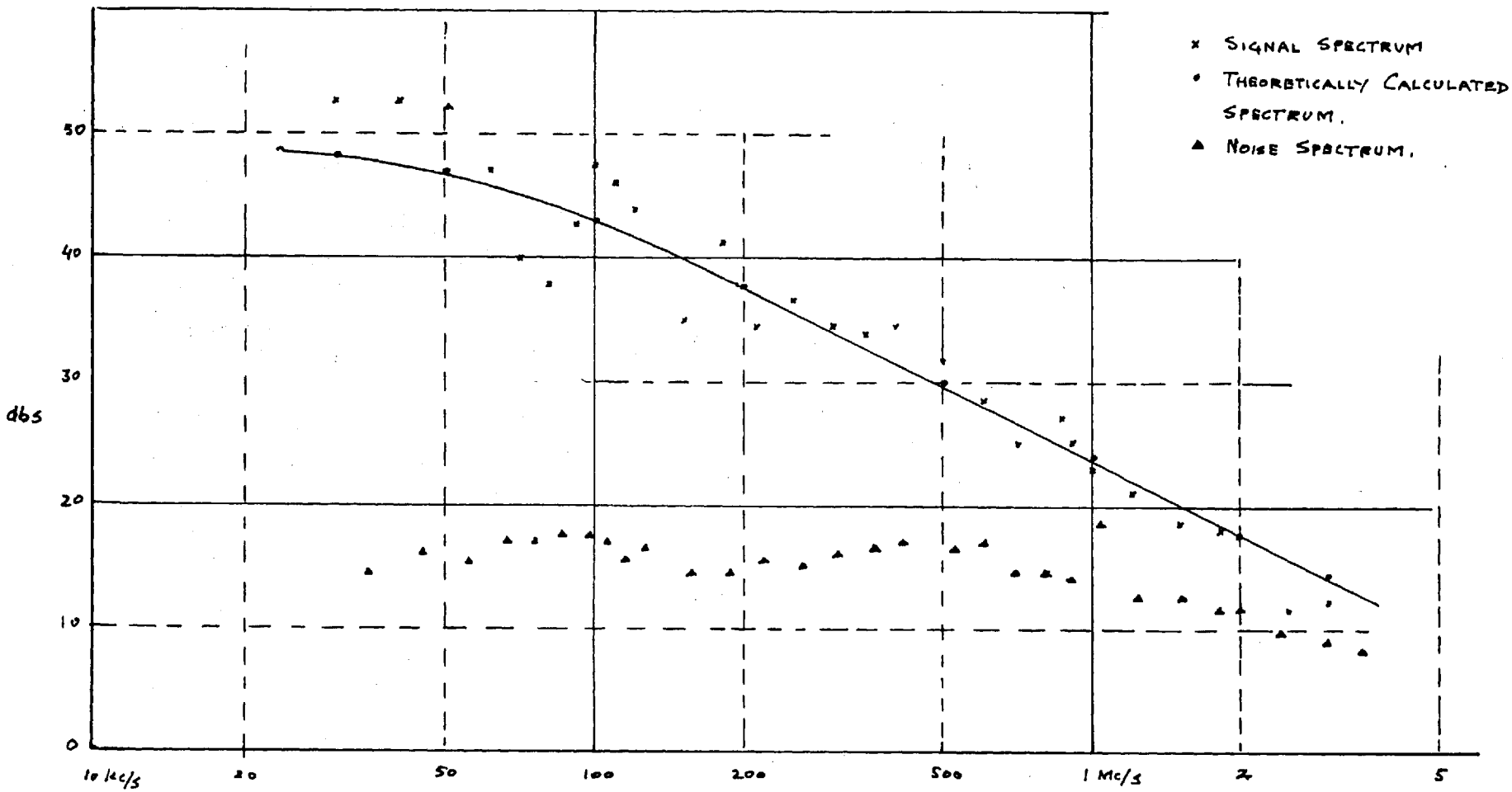


FIG. 57. SIGNAL AND NOISE SPECTRA OF "CLOSE UP OF A GIRL"

components of the signal and noise are weighted down by differentiation.

The signal spectrum shape appears to be of the form $\frac{1}{A^2 + B^2 f^2}$. Spectral measurements made by Seyler[28] on 18 pictures indicate that 80% of the power is concentrated below 250 Kc/s. A curve of the form $\frac{1}{A^2 + B^2 f^2}$ has been fitted to Seyler's data in Appendix I. The fitted curve, which has been plotted in figure 57, agrees with the experimental data obtained.

3.4.3. Measurements After Differentiation And Full Wave Rectification.

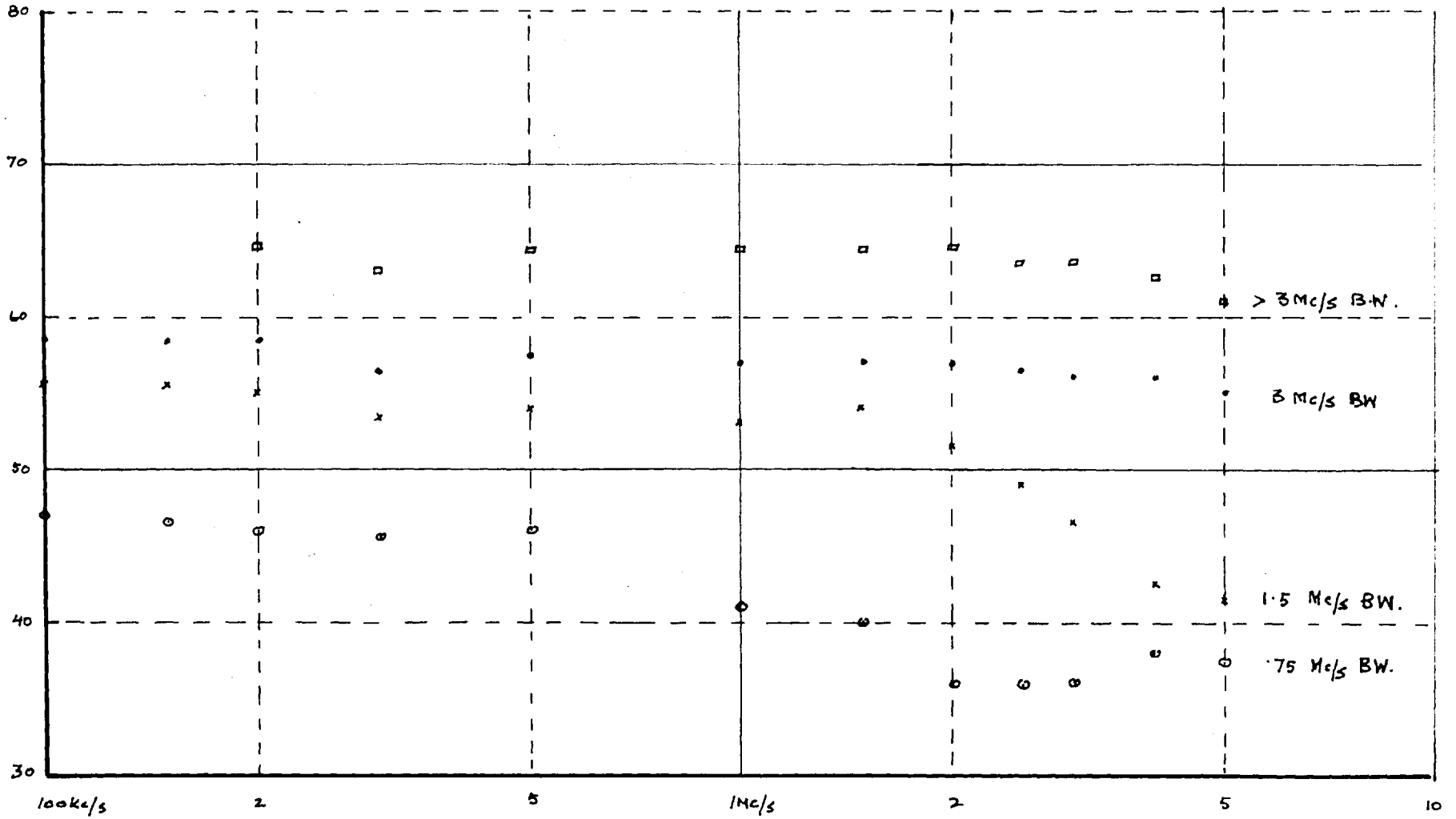
Measurements were also made of the signal and noise spectral components after differentiation and full wave rectification. The block schematic of the experimental set-up for these measurements is shown in figure 53(b).

The noise components after differentiation and full wave rectification, in presence of "white uplift", are plotted in figure 58. During these measurements, signal bandwidths of 750 Kc/s, 1.5 Mc/s and 3 Mc/s were used while one set of measurements was made without any filter. It is interesting to note that the output spectrum is nearly flat up to the cut-off frequency of the filter used.

The measurements on test card "C" are shown in figures 59, 60 and 61 for filter bandwidths of 750 Kc/s, 1.5 Mc/s and 3 Mc/s respectively. The spectrum for the "close up of a girl" is shown in figure 62.

3.4.4. Theoretical Analysis.

A theoretical analysis has been made to check the experimental results presented in Section 3.4.3. In the case of noise, the input to the differentiator has been assumed to be white Gaussian noise, band limited to an angular frequenc ω_c, and of power spectral density $\frac{K}{2\pi}$ in the pass band. It



WHITE UPLIFT. NOISE MEASUREMENT AFTER FULLWAVE RECTIFICATION.

FIG. 58

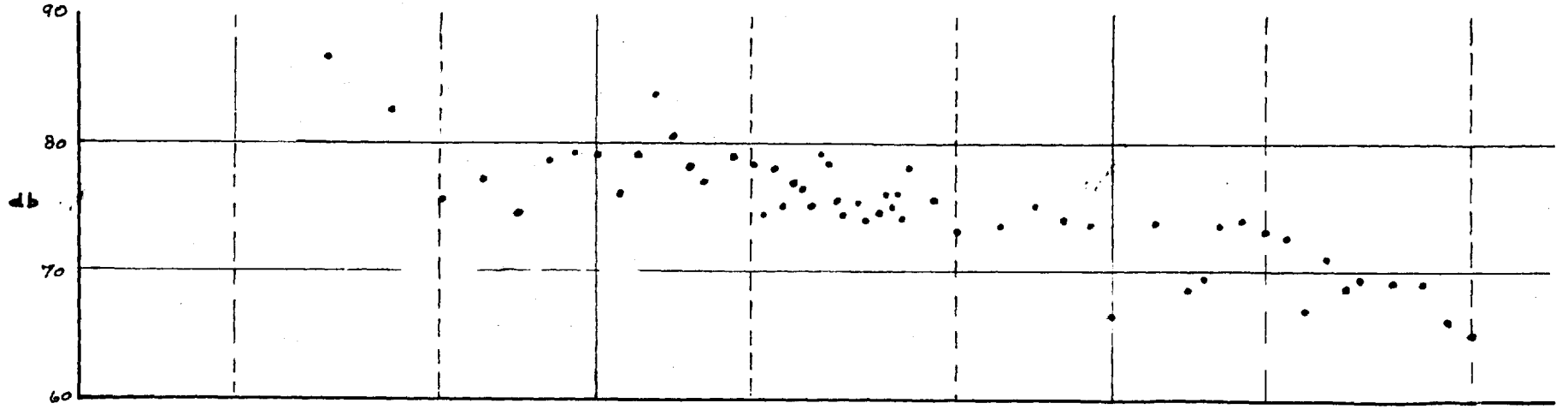


FIG. 59 $|\frac{df}{dt}|$ OF SIGNAL - BANDLIMITED TO 3 MC/S

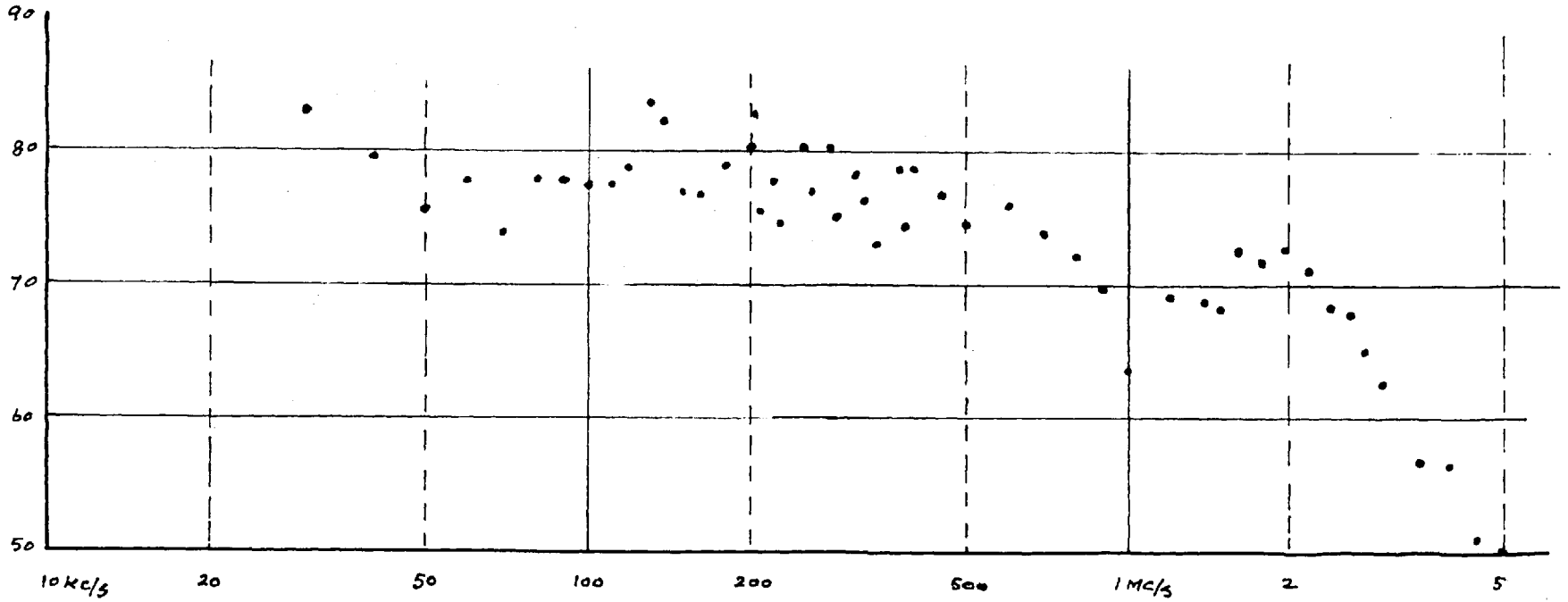


FIG. 60 $|d/dt|$ OF SIGNAL - BANDLIMITED TO 1·5 MC/S

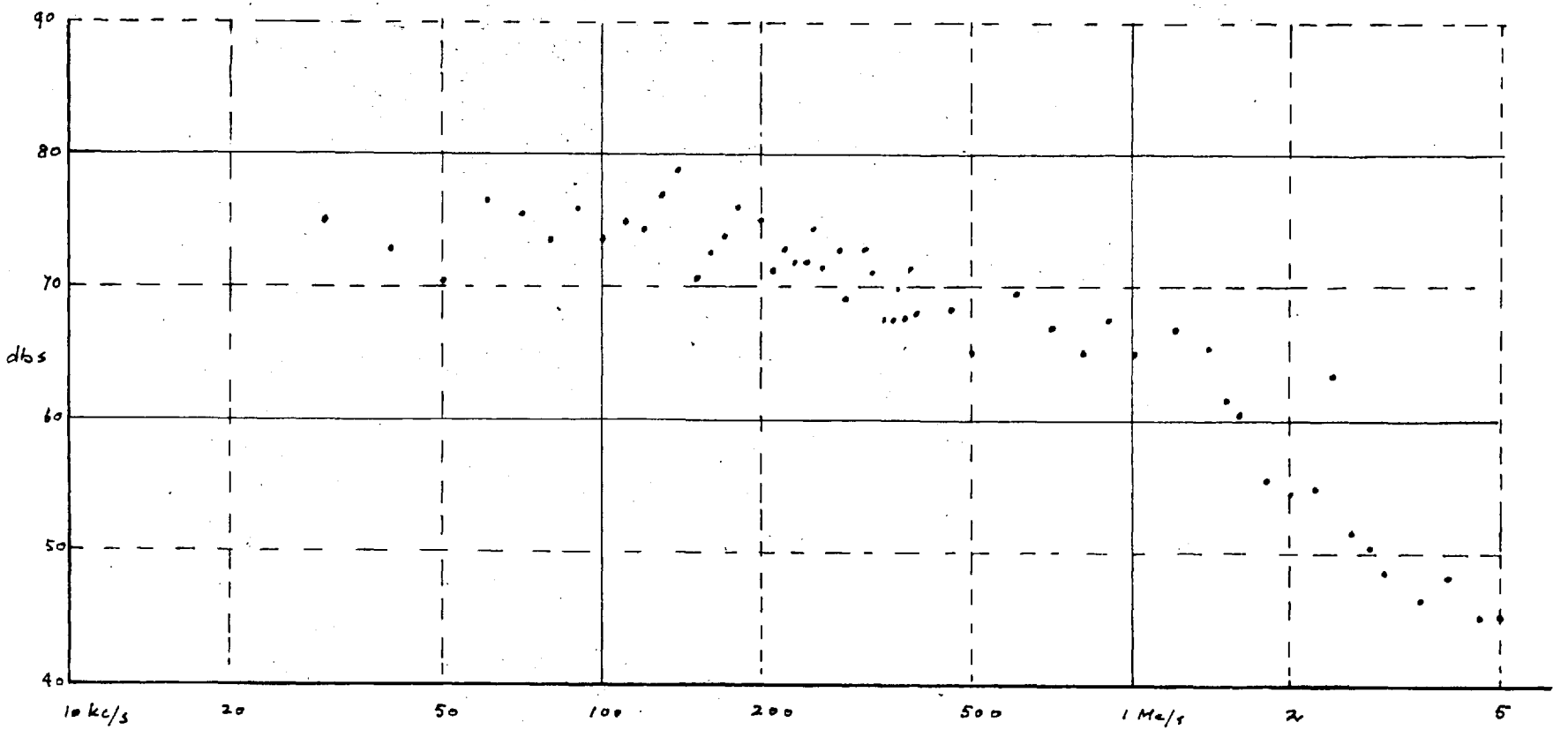


FIG. 61. TEST CARD C. $|d/dt|$ POWER SPECTRUM OF SIGNAL - BANDLIMITED TO .75 Mc/s.

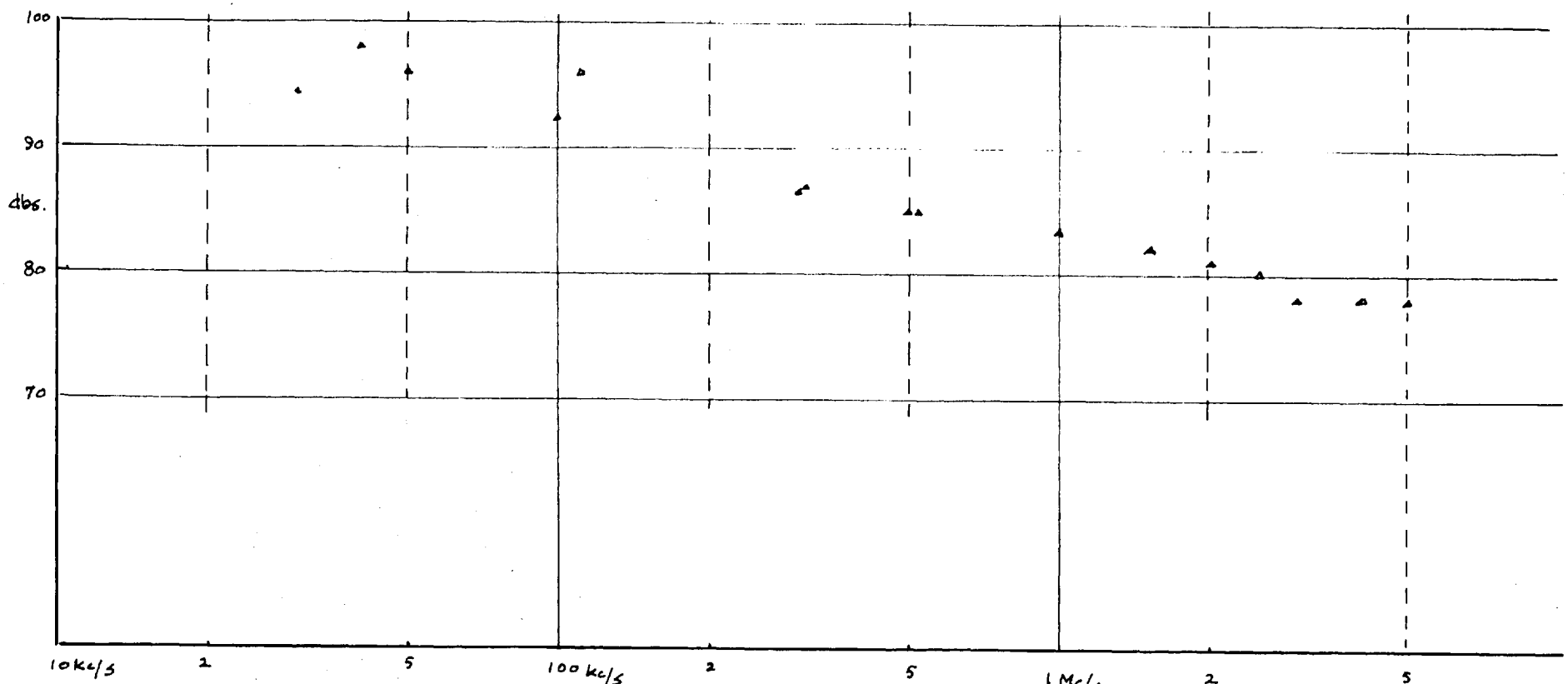


FIG. 62. $|d/dt|$ SIGNAL SPECTRUM. "CLOSE UP OF A GIRL"

is shown in Appendix II that the normalized autocorrelation function of the output of the differentiator is given by

$$\rho_n(\tau) = \frac{3}{\omega_c^3 \tau^3} \left[2 \omega_c \tau \cos \omega_c \tau + (\omega_c^2 \tau^2 - 2) \sin \omega_c \tau \right]$$

The output of the differentiator is then passed through the full wave rectifier. If $R_n(\tau)$ is the normalized autocorrelation function of the output of the full wave rectifier, it has been shown in Appendix II, based on a method due to Price[80], that

$$\frac{\partial^2 R_n(\tau)}{\partial \rho_n^2(\tau)} = \frac{2}{\pi \sqrt{(1 - \rho_n^2(\tau))}}$$

which yields upon the introduction of appropriate boundary conditions and integration, (Appendix II)

$$R_n(\tau) = \frac{2}{\pi} \rho_n(\tau) \sin^{-1} \rho(\tau) + \sqrt{1 - \rho_n^2(\tau)}$$

It is seen that

$$R_n(\infty) = \frac{2}{\pi}$$

which denotes that the output has a mean d.c. level.

In figure 63, $\rho_n(\tau)$ and $R_n(\tau)$ have been plotted along with the normalized autocorrelation function of the input to the differentiator which is equal to $\frac{\sin \omega_c \tau}{\omega_c \tau}$

By Wiener - Khinchin relation[81], the output noise spectrum i.e. the noise spectrum after differentiation and full-wave rectification is given by

$$G_n(\omega) = \frac{2}{\pi} \int_0^\infty R_n(\tau) \cos \omega \tau \, d\tau$$

Unfortunately, the cosine transform of $R_n(\tau)$ is not obtainable. $R_n(\tau)$ can be split into the sum of a d.c. term and a variable

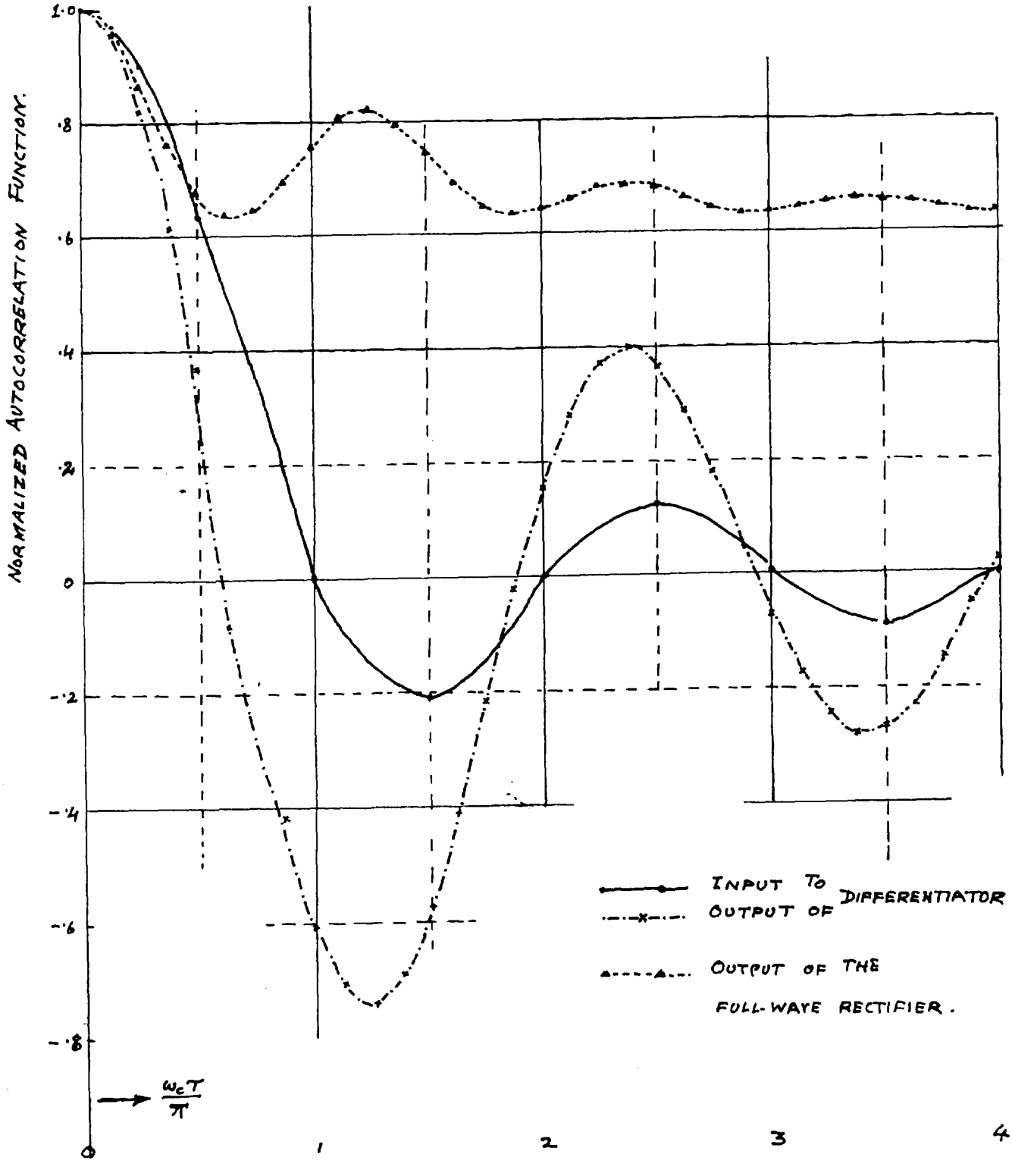

NORMALIZED AUTOCORRELATION FUNCTION.
1·0
·8
·6
·4
·2
0
-·2
-·4
-·6
-·8
$\frac{\omega_c T}{\pi}$
1
2
3
4
INPUT TO DIFFERENTIATOR
OUTPUT OF
OUTPUT OF THE
FULL-WAVE RECTIFIER.

FIG. 63.

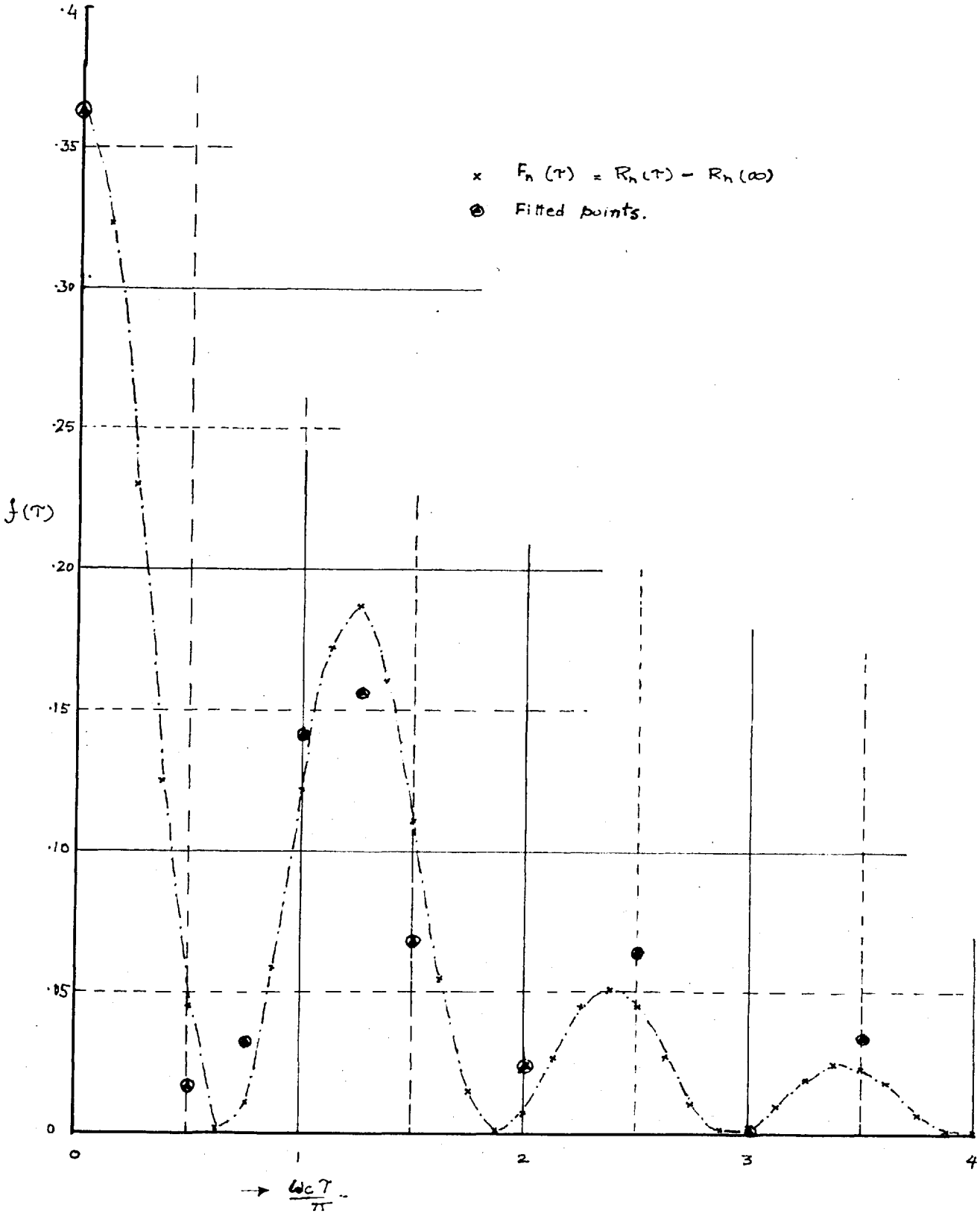


FIG. 64.

term. Let

$$F_n(\tau) = R_n(\tau) - R_n(\infty)$$
$$= R_n(\tau) - \frac{2}{\pi}$$

$F_n(\tau)$ is plotted in figure 64. The cosine transform of the d.c. term would give a dirac impulse at zero frequency which would not be of much interest in this investigation.

It is known[82] that if a process has a rational power spectral density function, then the associated autocorrelation function may be approximated by a set of exponential and exponential - cosine autocorrelation functions. $F_n(\tau)$ has been approximated by a function given by

$$F_n(\tau)_{\text{Fitted}} = .1821\ e^{-.66\frac{\omega_c \tau}{\pi}}\ (1+\cos 5.236\ \frac{\omega_c \tau}{\pi})$$

The cosine transform of this function has been obtained and is given by (Appendix III)

$$G_n\omega_{approx.} .244\ \frac{1}{\omega_c}\left[\frac{2(\omega/\omega c)^4 - 2.603(\omega/\omega c)^2 + 8.093}{(\omega/\omega c)^6 - 5.426(\omega/\omega c)^4 + 7.728(\frac{\omega}{\omega c})^2 + 351}\right]$$

A plot of $G_n(\omega)_{approx.}$ is shown in figure 65 on a normalized frequency scale and an arbitrary db. scale. Though complete agreement is lacking between $G_n(\omega)_{approx.}$ and the experimental result, the theoretical curve has the same overall trend as the experimental curve. Exact correspondence was not expected because of the very approximate fit that was obtained. It may be remarked that though the l.f. components of the signal are weighted down due to the differentiation, after the full-wave rectification, the energy is so distributed that a nearly flat spectrum emerges.

Similar analytical results have been obtained in Appendix IV for the signal. The spectrum of the input to the differentiator is assumed to be:

$$G(f) = \frac{1}{1.4352 \times 10^{6} + .5744 \times 10^{-3} f^{2}}$$

which is the fitted curve to Seylers data (Appendix I).

In figure 66, the normalized autocorrelation functions $\rho_s(\tau)$ and $R_s(\tau)$ are plotted. $R_s(\tau)$ and the results obtained from it are approximate in that Price's method,[80] which has been used to obtain $R_s(\tau)$, applies strictly only to functions having Gaussian amplitude probability distributions. It is well known that in the case of television pictures, the amplitude probability distribution is more correctly represented by a flat distribution.

$F_s(\tau)$, which is plotted in figure 67, has been obtained by subtracting $R_s(\infty)$ from $R_s(\tau)$. $F_s(\tau)$ has been approximated by (figure 68).

$$F_s(\tau) = .112\, e^{-1.652x}(1 - \cos 2\pi x) + .2075\, e^{-2.946x} \sin 2\pi x + .3634\, e^{-4.86x}$$

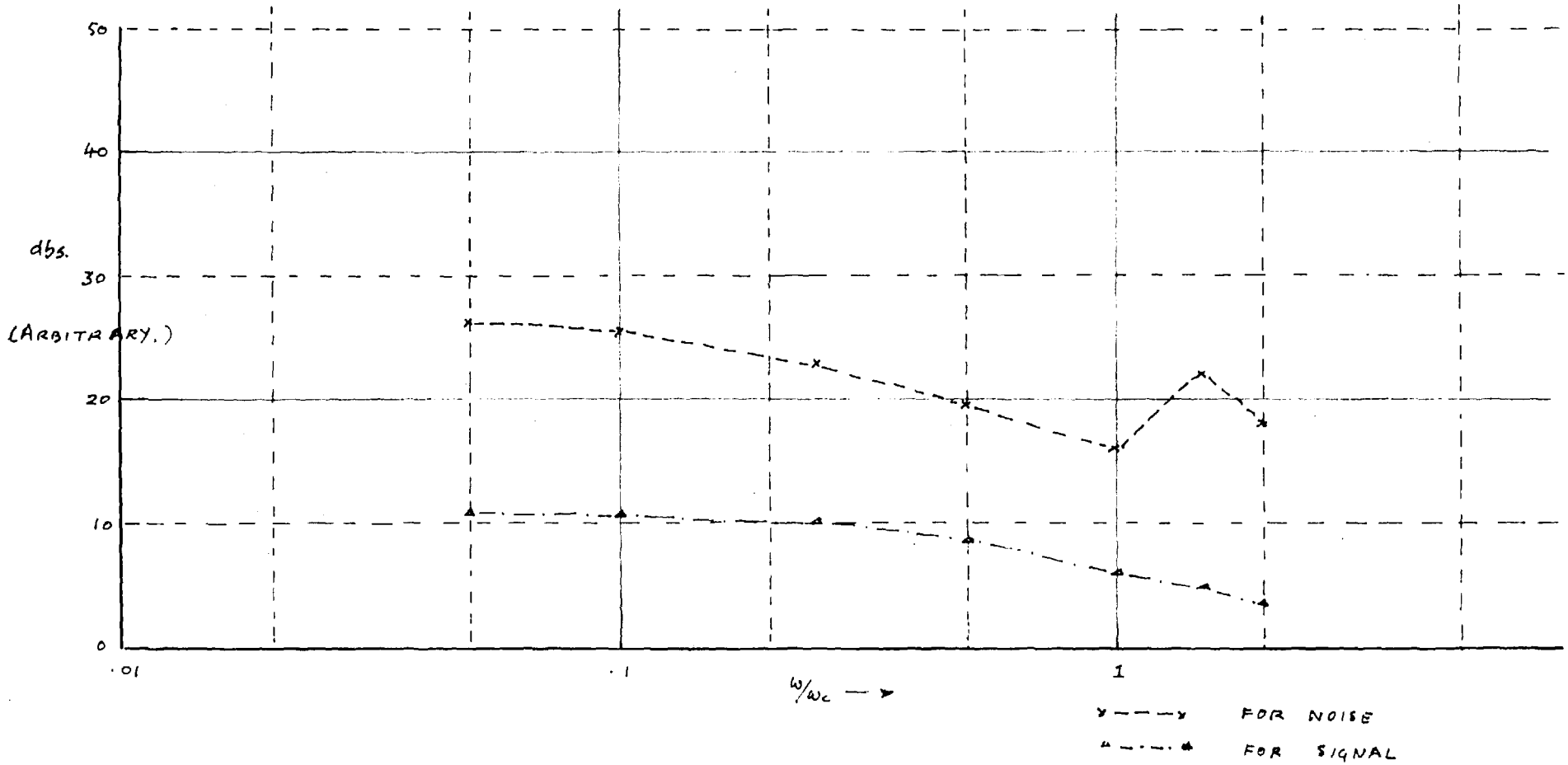
$$\text{where } x = \frac{\omega_c \tau}{\pi}$$

The cosine transform of $F_s(\tau)$ has been obtained in Appendix V and the spectrum thus obtained is shown in figure 65. The fitted calculated and the experimental curve have the same trend and seem to have a fair degree of agreement.

A computation has been made in Appendix VI for $R_{s+N}(\tau)$ when both signal and noise are present and the input $S/_N$ ratio is 36 dbs. The output of the differentiator has a normalized autocorrelation function

$$\rho_{s+N}(\tau) = \frac{\rho_s(\tau) + \frac{1}{K_1}\rho_n(\tau)}{1 + \frac{1}{K_1}}$$

$$\text{where } K_1 = \frac{\Phi_s(o)}{\Psi_n(o)} = \frac{\text{mean square signal power}}{\text{mean square noise power}}$$



SPECTRAL CHARACTERSTICS OF THE OUTPUT OF THE DIFFERENTIATOR AND THE FULLWAVE RECTIFIER CALCULATED FROM THE FITTED CURVE.

FIG. 65.

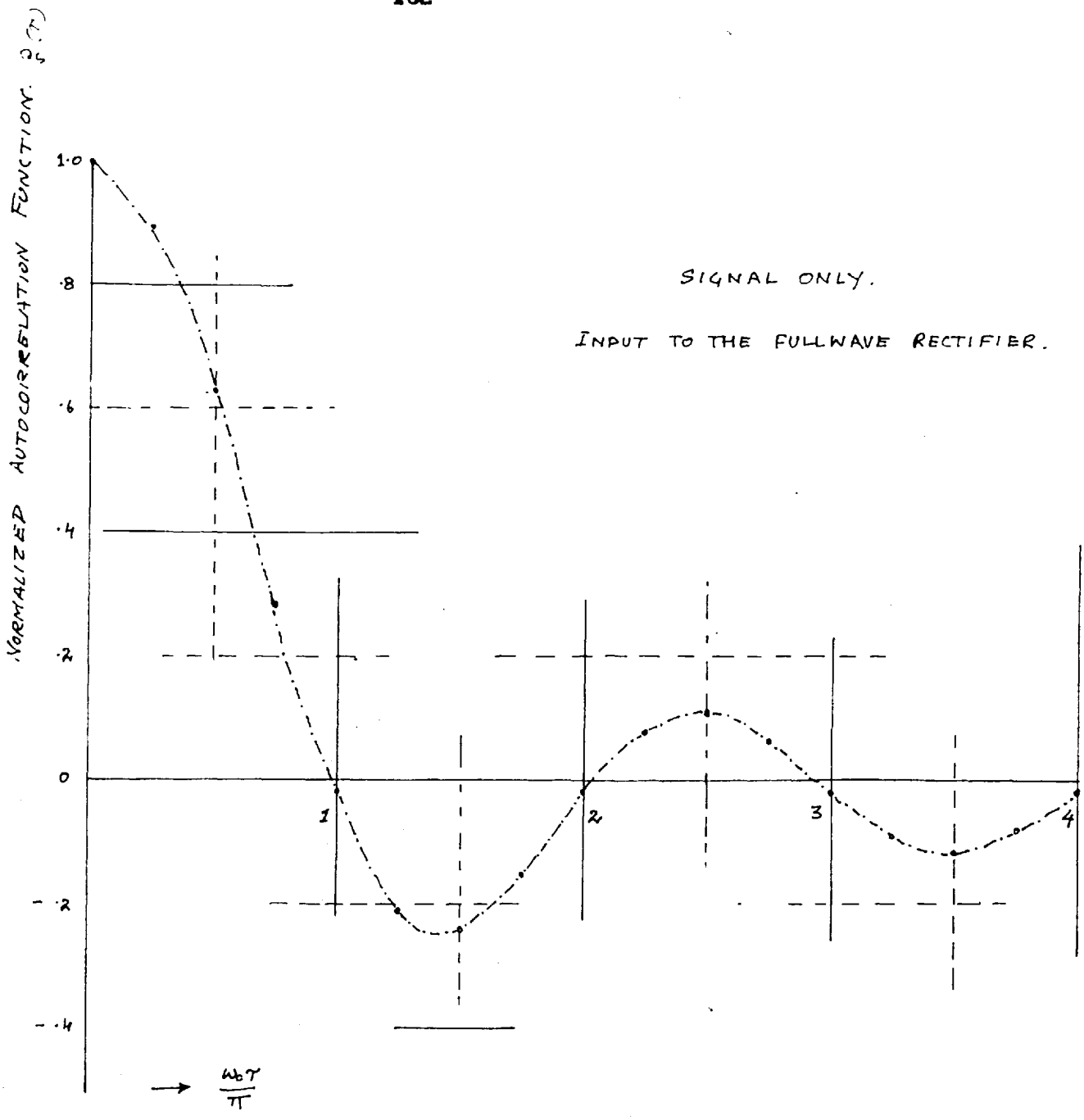

NORMALIZED AUTOCORRELATION FUNCTION. $\rho_s(\tau)$
1·0
·8
·6
·4
·2
0
-·2
-·4
1
2
3
4
$\frac{\omega_b \tau}{\pi}$
SIGNAL ONLY.
INPUT TO THE FULLWAVE RECTIFIER.

FIG. 66.

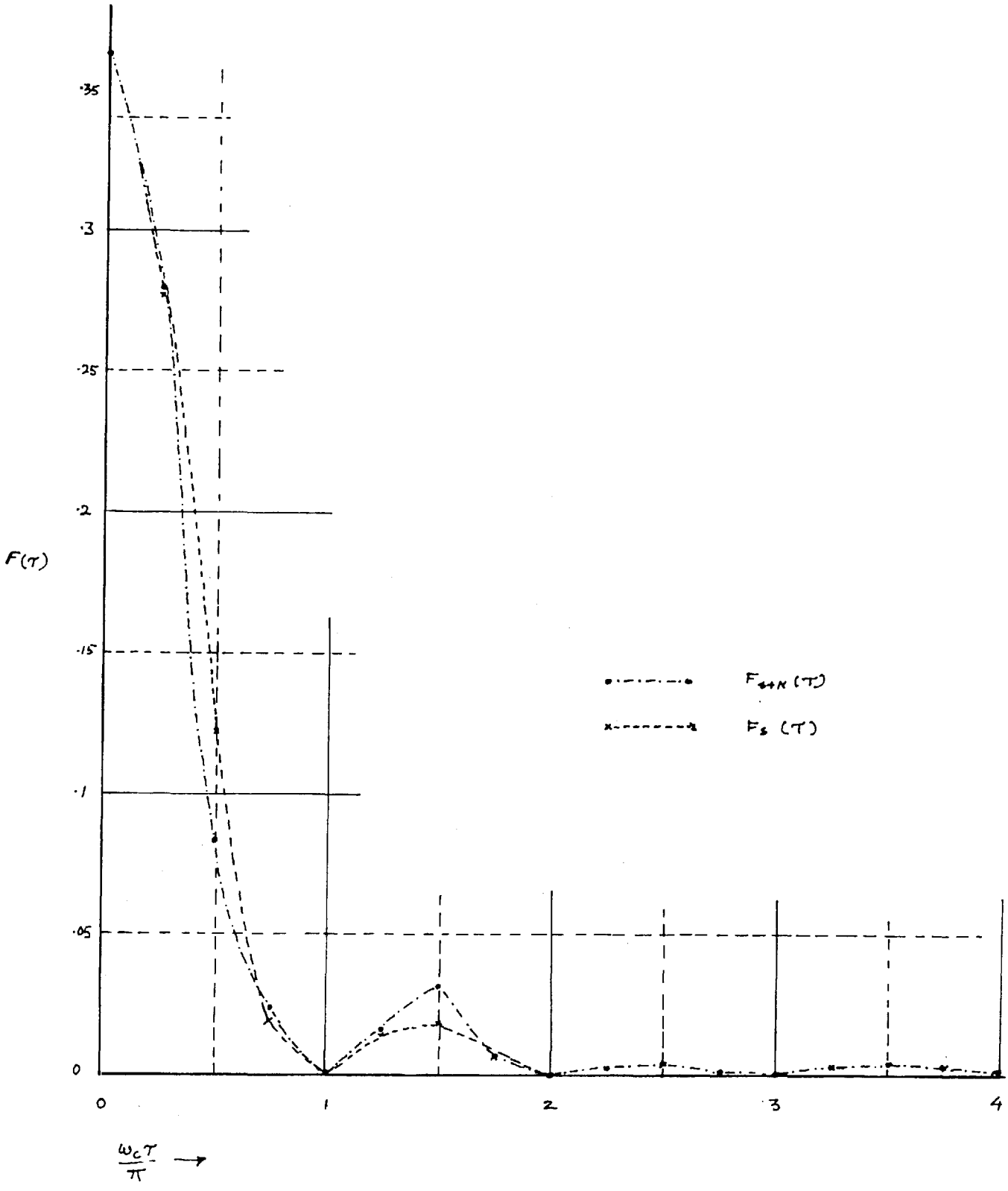
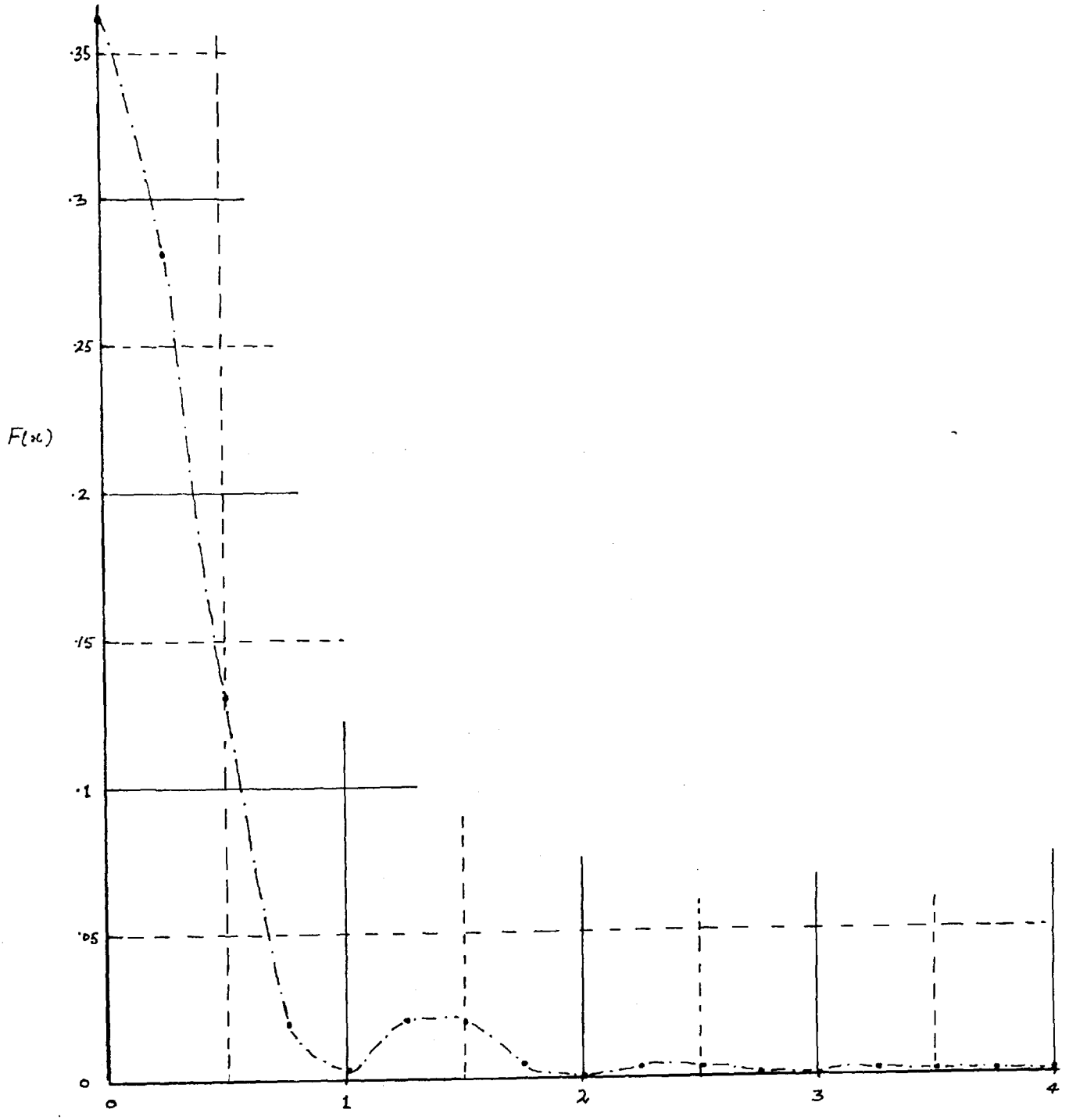


FIG. 67.



$$F(x) = \cdot 112\, e^{-1\cdot 652x} - \cdot 112\, e^{-1\cdot 652x} \cos 2\pi x + \cdot 2075\, e^{-2\cdot 946x} \sin 2\pi x + \cdot 3634\, e^{-4\cdot 86x}$$

FIG. 68. FITTED CURVE FOR $F_s(T)$

Now $F_{s+N}(\tau)$ is obtained by subtracting $R_{s+N}(\infty)$ from $R_{s+N}(\tau)$. A comparison of $F_{s+N}(\tau)$ and $F_s(\tau)$ in figure 67 shows that significant difference between the two curves exists only for small time delays. This suggests that the h.f. spectrum of the signal gets modified owing to the presence of noise.

The effect of frequency weighting of the signal and the noise due to differentiation is such as to enhance the importance of the noise. It has been quantitatively shown in Appendix VI that a $(S/N)_{T.V.}$ ratio (i.e. 20 log $\frac{\text{peak signal volts}}{\text{r.m.s. noise volts}}$ of 36 dbs corresponds to a $(S/N)_{m.s.}$ ratio (i.e. 10 log $\frac{\text{signal pow}}{\text{noise powe}}$ of 31.4 dbs. After differentiation the $(S/N)_{m.s.}$ ratio is reduced to 16.5 dbs.

3.5. Discussion.

The results presented in this section have emphasized the importance of source noise on the system performance. It can be seen from figure 57 that for a S/N ratio of 30 dbs, which is subjectively quite acceptable, the $(S/N)_{r.m.s.}$ ratio in the frequency band 2-3 Mc/s is only of the order of 6 dbs. An investigation carried out by Barstow and Christopher[83] suggests that if random noise is added to a video signal, the human viewer uses a weighting function such that l.f. noise is judged much more objectionable than h.f. noise of the same power. A weighting function obtained by Barstow and Christopher has the values 0 db at d.c., - 5 dbs at 600 Kc/s, - 12 dbs at 2 Mc/s and - 20 dbs at 3 Mc/s. While this tremendous subjective advantage in combating h.f. noise makes a picture with a S/N ratio of 30 dbs quite acceptable, in the case of the variable - velocity scanner, it is essential to achieve good h.f. S/N ratio for satisfactory system performance. The enhanced effect of noise* on the signal after differentiation and full wave rectification can be seen in figure 44.

* The noise referred to is the shot noise generated in the device.

The fundamental feature of the variable - velocity - scanner is that it reduces the signal energy in the h.f. band by recoding the signal. The closed loop feedback, when functioning properly, minimises the signal energy above 1 Mc/s (say) if a compression of 3:1 on the vision channel is sought. The generation of source noise, on the other hand, is quite independent of the feedback process and is predominantly the result of shot noise in the signal photocathode current. This again emphasizes the need for a large $S/_N$ ratio.

The analytical results obtained in this section broadly agrees with the experimental measurements. The effect of the clipper, which was incorporated in the apparatus at a later stage, has not been taken into account in the analytical study or the spectral measurements. The effect of the clipper can be seen in figure 44 (c). Though it reduces a considerable amount of noise from the control signal at the cost of contrast, the modulation of noise on the top of the h.f. detail is still visible and in absence of some form of slope quantization of the time base, may introduce jitter in the picture.

The experiments on the stability of the system suggest that the system remains stable for reasonable velocity ratios but can be made unstable by excessive loop gain accompanied with time delay.

The bandwidth requirement of the feedback loop is very high. There are some major limitations due to the component devices in the way of achieving a bandwidth of 20 Mc/s in the feedback loop. The first is the afterglow of the scanner tube phosphor. None of the phosphors used in the present day tubes are capable of providing a video signal with a bandwidth of 20 Mc/s. The use of afterglow correction would result in a diminished $S/_N$ ratio, which would adversely affect the system performance. The design of an electromagnetic deflection system with a pass-band extending from 1 Kc/s to 20 Mc/s does not seem to be practicable. However, it would be possible to

achieve the above-mentioned bandwidth in an electrostatic deflection system.

The finite size of the spot and the problem of aperture correction become serious limitations.

Increased bandwidth and higher $S/_N$ ratio are contradictory requirements to some extent, e.g. the afterglow correction, which has already been discussed, provides one at the cost of the other. Moreover, the noise power in the output depends on the system bandwidth.

To sum up, the results presented in this section suggest that with the present component devices available, it is not feasible to use the variable-velocity scanner for the recoding of multilevel television pictures. Important information has been obtained on the stability of the variable-velocity scanning system. The system is inherently stable under normal operating condition but can be made unstable by excessive loop gain accompanied with delay. The importance of the effect of source noise on system performance has been stressed.

This system seems to be ideally suited for facsimile transmission of two level and multi-level pictures. Very high $S/_N$ ratios may be obtained with low speed scanners.[4a,46] The devices are capable of giving large loop bandwidth as compared to the channel bandwidth. A low frequency variable - velocity scanning system is not only feasible but attractive because of the simplicity of the terminal equipment that obtains from the ingenious idea of using the picture itself as a store.

4. COMPRESSIBILITY OF PICTURES

The potential bandwidth compression which may be obtained by a statistical coding scheme, such as the Cherry-Gouriet system, is dependent on certain statistical properties of the picture. A complete statistical description of one single picture would entail the measurement of one conditional probability per picturepoint for each possible past. The approximate number of these distribution curves quoted by Kretzmer[11] is extremely large and is practically impossible to determine. The statistical properties which should be determined in order to assess the redundancy in a picture should be relevant to a particular type of coding scheme. If a run-length coding scheme has a storage capacity of one line duration (say) over which the rate of data flow is smoothed, then the measurement of frame-to-frame correlation in a scene is irrelevant, because this redundancy is not exploited by the particular scheme in question.

The "picture detail factor" may be measured to find the potential compressibility of a black and white picture. Howeve the inadequacy of the "picture detail factor", when applied to multi-level pictures has already been stated by Cherry and Gouriet.

4.1. Turning Points and Significant Intervals.

Cherry and Gouriet [1] have suggested the use of velocity modulation for equalising transition spectra bandwidth. This suggestion, which has been mentioned in section 1.6.1, can be called an analogue version of run-length coding. The probabil ity distribution of run-lengths could provide data for the assessme nt of potential bandwidth compression of pictures using run-length coding either by variable-velocity scanning or by some other method.

The concept of turning points and the derived concept of significant intervals (run-lengths) follows from the suggestion of Cherry and Gouriet and has been discussed by Beddoes.[4]

Consider a waveform e(t), derived from a spatial signal e(x) by conventional scanning. Let e(t) be band-limited to O-W c/s. Then e(t) may be represented by discrete samples at intervals of $\frac{1}{2W}$ seconds. Let the tips of these samples be joined by straight lines giving $e_d(t)$ by a number of constant slope elemental signals (Fig.69a). Now, the turning points are specified by $|D^2 e_d(t)| = \infty$. In between the turning points, $D^2 e_d(t) = 0$.

A significant interval is defined as the interval between two turning points.

It may be noted that the instrumentation suggested by Cherry and Gouriet to equalize transitions and plateaux is analogous to previous value prediction, while the one based on the significant interval is analogous to slope prediction.

A constant-slope ramp requires a bandwidth of at least $\frac{1}{2t}$, where t is the duration of the step. If t_{min} is the shortest duration between the turning points in $e_d(t)$, the minimum bandwidth required for the transmission of $e_d(t)$ is $\frac{1}{2\,t_{min}}$. If an encoder equalizes each significant interval and makes it equal to t_{mean}, then the bandwidth needed for its transmission is $\frac{1}{2}t_{mean}$. In general, $t_{mean} > t_{min}$, hence bandwidth compression may be achieved by equalizing the significant intervals.

4.2. Potential bandwidth Compression by Variable-Velocity Scanning.

Assume a variable-velocity scanner with provision for frequency feedback. Let the ratio of the maximum velocity of the timebase to the minimum velocity be n. Then with ideal frequency feedback, every element whose duration is less than n units long in the uncoded waveform would have a duration of n units.

Let P(i) be the normalized probability of the significant intervals which are 'i' units long, then the mean value of the significant intervals

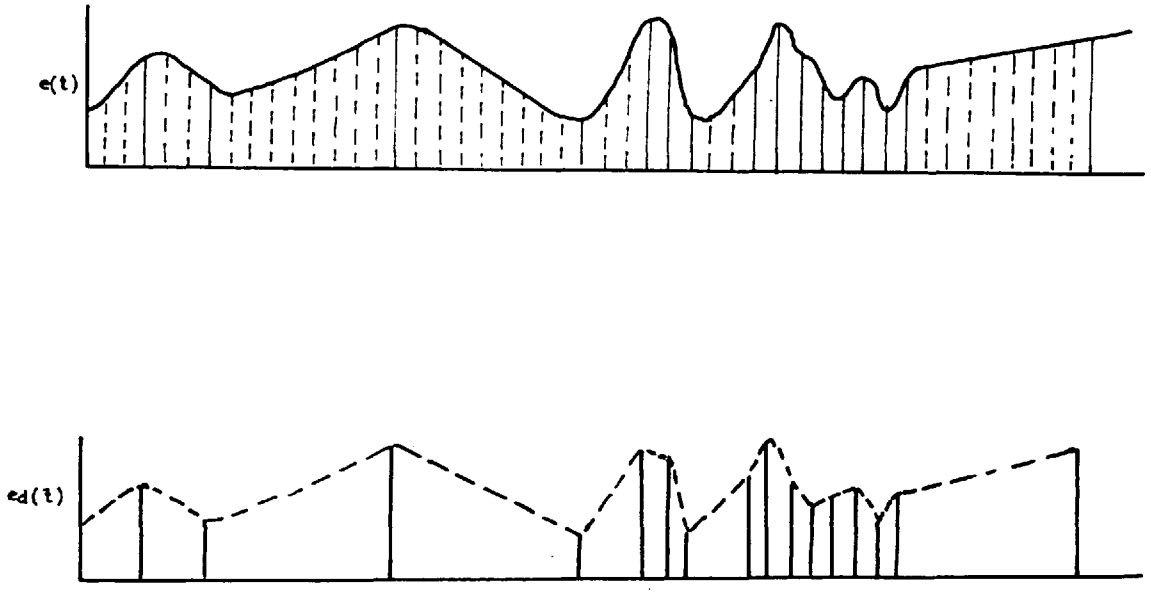


FIG. 69 (a)

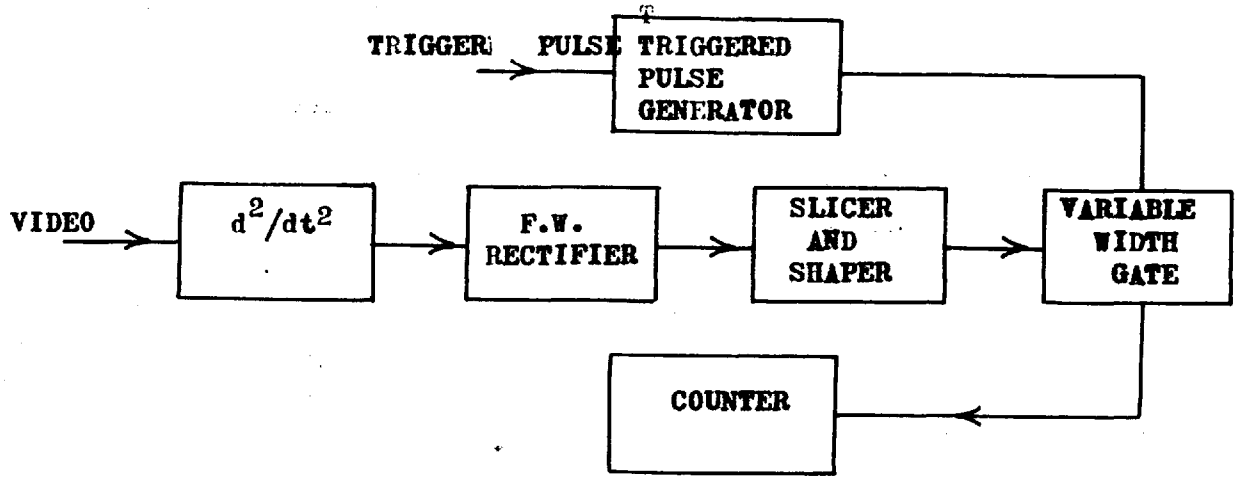


FIG. 69 (b)

$$t_m = \sum_{1}^{M} i\, p(i) \qquad - (4.1)$$

if the longest significant interval is M subdivisions. After the variable-velocity recoding, the mean of the new distribution of the significant intervals would be given by

$$t_{m_n} = \sum_{n}^{M} i\, p'(i) \qquad - (4.2)$$

The bandwidth reduction, C, as defined in equation (3.1) is given by

$$C = n \qquad - (4.3)$$

However $t_{m_n} \neq t_m$, while the total number of significant intervals in the two distributions remain equal. Hence, the actual reduction in the time-bandwidth product is given by

$$R = n \quad \frac{t_m}{t_{m_n}} : 1 \qquad - (4.4)$$

4.3. Measurements on Test Card 'C'

A straightforward but tedious method was employed to determine the distribution of significant intervals in test card 'C'. The monoscope set-up built by Beddoes (figure 16) was used for signal generation. The monoscope, with the test card 'C' target, was scanned by the constant velocity time bases and the generated picture was displayed on display tube. The number of lines per frame was low (about 100). A single line was separated by masking the rest of the display tube. The significant intervals in the line were measured visually with the help of a fine scale, calibrated to read up to 0.5 mm.

Though test card 'C' is quantized in five brightness levels, only three levels were easily distinguishable. However, due to the special structure of the test card, the errors introduced due to this would not be significant.

TABLE 4.1

Showing the distribution of significant intervals in a sample of 20 lines

Duration / line	1	2	3	4	5	6	7	8	9	10	11	12	13	14	15	16	17	18	19	20	21	22	23	24	25	26	27	28	29	30	>30	N	ΣΔ	ΣΔ/N
1	37	2	26	24																1			1							1	4	76	414	5.45
2	15	6	1			1				1																	1				6	31	415	13.4
3	51	4	12		2	1									1		1			1		1					1				4	79	396	5.00
4	60	22	6		1					2					1		1	1					1					1			4	100	413	4.13
5	97	13	2		2			1		1			1				1	1		1			1								4	125	395	3.16
6	64	25	4	1				1	1				1				2	1				1	1							2	2	106	384	3.62
7	58	6	12	2						1								1				3	1		1			1			2	88	360	4.09
8	26	8	1	1	2		1					1	1				3								1						4	49	321	6.55
9	51	12	30				1			1										2			1								4	102	408	4.00
10	27	5	10		2		2													2							2				3	53	335	6.32
11	28	8	4										4				6	4		3											57	342	6.00
12	58	9	38				3			1			1							1			2				1				1	115	344	3.00
13	27	7	3	1	1	1	3										2	1		1			1		1					1	3	53	363	6.85
14	57	7	11	1	3					1				1				1		1		1	2								4	89	389	4.37
15	58	21	1	1	3			2												1			1				1			2	3	94	405	4.32
16	57	21	3	2	1			1														1	1				1			2	2	93	390	4.20
17	95	9	3	3				1		1							1	1					1							1	4	121	404	3.34
18	15	3	2		2		1													1			1					1			4	30	349	11.6
19	57	10	12					1									1	1				3	1		1		1			2	2	91	320	3.52
20	31	2	16			1	2			2								1					1				1			1	3	61	404	6.63
Σ	969	200	177	37	19	3	14	7	1	11	-	1	8	1	2	-	20	12	-	15	-	10	17	-	4	-	9	3	-	12	63	1613	7551	4.68
P	.6007	.1239	.1097	.0229	.0117	.0018	.0087	.0043	.0006	.0068	-	.0006	.0048	.0006	.0012	-	.0124	.0074	-	.0093	-	.0061	.0105	-	.0024	-	.0056	.0018	-	.0074	.0378			

N ; denotes the total number of significant intervals

ΣΔ: denotes the duration of the line in terms of the Unit Significant interval.

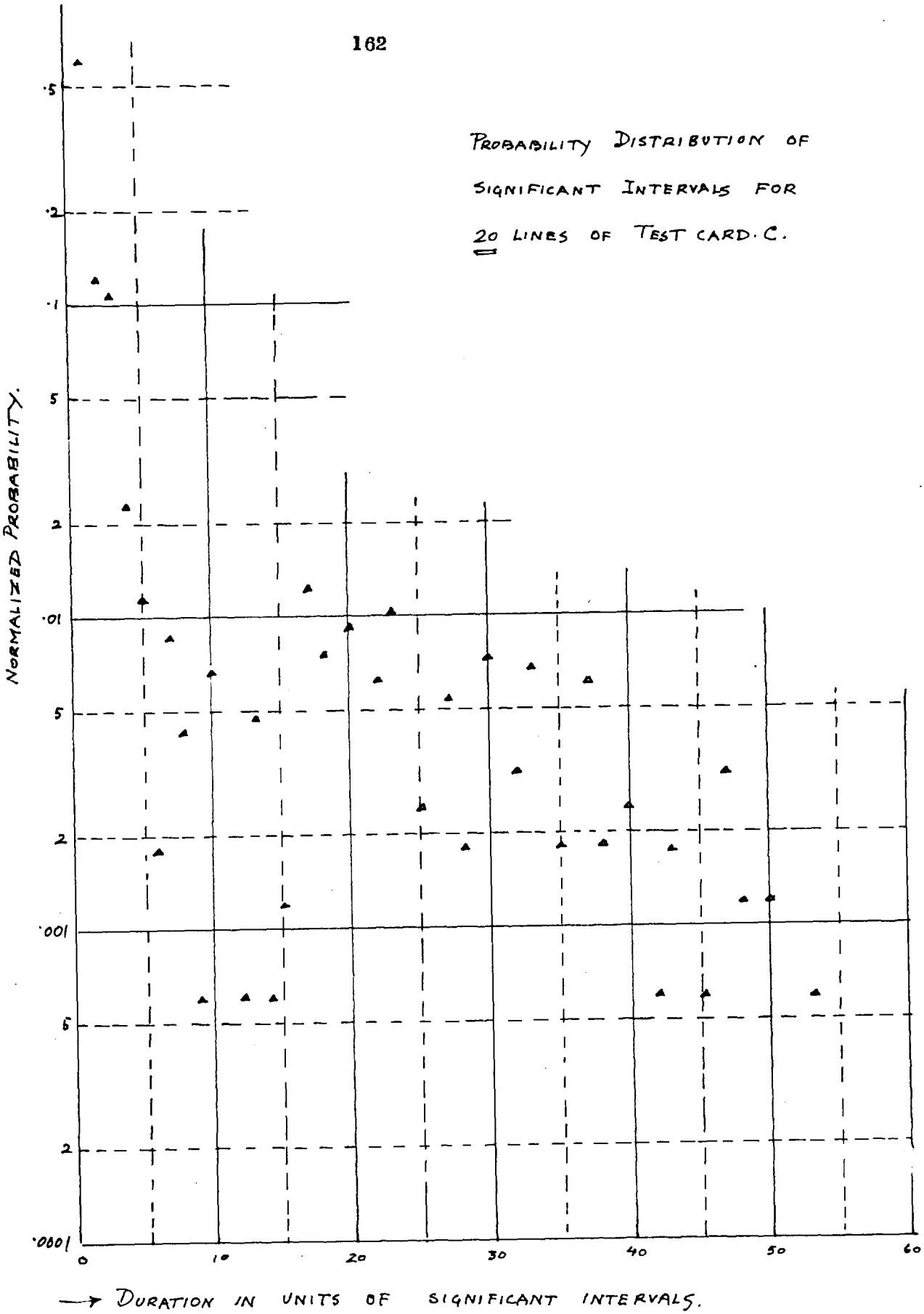

PROBABILITY DISTRIBUTION OF
SIGNIFICANT INTERVALS FOR
20 LINES OF TEST CARD·C.
NORMALIZED PROBABILITY.
·5
·2
·1
5
2
·01
5
2
·001
5
2
·0001
0
10
20
30
40
50
60
→ DURATION IN UNITS OF SIGNIFICANT INTERVALS.

FIG. 70.

The band defining blocks of detail in the test card consists of 4, 6, 8, 10, and 12 bars respectively. It was found experimentally that the waveforms due to the last two blocks of detail corresponded to sine waves. The unit significant interval was obtained by dividing the width of the block with the finest detail by the number of significant intervals it contained.

For the measurement, the picture was divided horizontally into four portions and five lines from each portion were picked. This ensured that there was no bias towards any particular region of the picture. Measurements on a set of twenty lines are contained in table 4.1 and the probabilities are plotted in figure 70.

In table 4.1, line No.5. has the largest number of significant intervals - N being equal to 125. The potential compressibility of this line would be minimum if the significant intervals are averaged over a line. The duration of this line is 395 units. Hence the average significant interval = $\frac{395}{125}$ = 3.15. In a similar manner, it can be shown that the average significant interval, averaged over the entire sample of 20 lines is given by

$$t_m = \frac{1}{N} \sum \Delta = 4.6$$

Using equation (4.4), the value of the reduction in the timebandwidth product, R has been calculated for different values of the scanning velocity ratio, n. In section 4.2, it was assumed that after variable velocity coding, all significant intervals, whose durations were less than n units long before coding, would have a duration of n units if the velocity ratio were equal to n, i.e.

$$t_{m_n} = \left[p(1) + p(2) + \ldots + p(n)\right] n + (n+1)\, p\,(n+1) + \ldots\ldots\ldots\ldots + Lp(M)$$

TABLE 4.3

Showing the distribution of significant intervals in another sample of 20 lines

Duration	1	2	3	4	5	6	7	8	9	10	11	12	13	14	15	16	17	18	19	20	21	22	23	24	25	26	27	28	29	30	>30	N	$\Sigma\Delta$	$\frac{\Sigma\Delta}{N}$
Line																																		
1	22	5	1	2	1	1	1	2				1		1		1						1		2						1	3	45	351	7.80
2	54	5	8	4		2		2		1		1				1		1						2							4	85	390	4.60
3	59	17	1	4				4		1						1		1		2								2			3	95	396	4.17
4	90	6		6				2		1		1				3		1						1		1		2			2	116	402	3.47
5	58	17		7				3		1						1		1		2				2		2					2	96	394	4.10
6	53	7	8	3		3						1		1		2										1					5	84	391	4.65
7	23	10	1	1		1		2		1						1								2				1		1	3	47	386	8.22
8	48	17	16	7		1						1								1				2							4	97	388	4.00
9	23	5	2	2								2		2		3		4		4												47	299	6.35
10	26	10		5		1		3														1		2				1		1	3	53	378	7.13
11	36	4	19	3				1		1		2								1				1				2			3	73	399	5.47
12	51	4	8	2		1		2		1						2				1				1		1		1			4	79	429	5.44
13	56	19		4		1		3		1						1				2		1				1		1			3	93	390	4.20
14	92	7		7				2		2						2		1		1				1		1				1	3	120	418	3.48
15	61	20		4		1		3		1						1				1		2		3						1	2	100	403	4.03
16	61	4	9	5		3		1				1		1				1		2				1						1	3	94	392	4.16
17	23	8		2		2		4										1						1		1		1			4	47	383	8.15
18	25	6	1	2		1		5												1		1		1							5	48	386	8.04
19	33	8	6	4		1		4				2				2		1		1				2							3	67	347	5.18
20	60	7	9	3		2		3		1						2				2				3						1	2	95	403	4.25
Σ	954	186	89	77	1	21	1	46	-	12	-	12	-	5	-	23	-	12	-	21	-	6	-	27	-	8	-	11	-	7	61	1580	7725	4.89
P	.6038	.1177	.0565	.0487	.0006	.0133	.0006	.0291	.	.0078		.0078		.0030		.0146		.0078		.0133		.0039		.0171		.0050		.0072		.0044	.0366			

N denotes the total number of significant intervals

$\Sigma\Delta$ denotes the duration of the line in terms of the unit significant interval.

For the distribution of table 4.1, the values of t_{m_n} for n = 1,2,3 ... 10 and the corresponding values of R_n are tabulated in Table 4.2.

TABLE 4.2.

Ratio of max. to min. velocity n	Mean of the distribution t_{m_n}	Ratio of the mean when n=1 to mean when n r. t_m/t_{m_n}	Reduction in time-bandwidth product $R=n(t_m/t_{r_n})$
1	4.63	1.00	1.00
2	5.23	0.88	1.76
3	5.96	0.78	2.34
4	6.79	0.68	2.72
5	7.65	0.60	3.00
6	8.52	0.54	3.24
7	9.39	0.49	3.43
8	10.27	0.45	3.60
9	11.15	0.42	3.78
10	12.04	0.39	3.90

Measurements were made on another set of twenty lines which are contained in Table 4.3. The 14th line has the greatest number of significant intervals. The average significant interval for this line

$$= \frac{418}{120} = 3.48$$

Averaged over the sample of twenty lines,

the mean $t_m = \frac{7725}{1580} = 4.7$

In table 4.4, the samples of tables (4.1) and (4.3) have been added and a distribution for 40 lines has been obtained which is plotted in figure 71.

TABLE 4.4

Showing the distribution of significant intervals in a sample of 40 lines obtained by adding samples of Tables 4.1 and 4.3.

Duration	1	2	3	4	5	6	7	8	9	10	11	12	13	14	15	16	17	18	19	20	21	22	23	24	25	26	27	28	29	30	>30	N	ΣΔ
Line																																	
I 20 lines	969	200	177	37	19	3	14	7	1	11	-	1	8	1	2	-	20	12	-	15	-	10	17	-	4	-	9	3	-	12	63	1613	7551
II 20 lines	954	186	89	77	1	21	1	46	-	12	-	12	-	5	-	23	-	12	-	21	-	6	-	27	-	8	-	11	-	7	61	1580	7725
Σ	1923	386	266	114	20	24	15	53	1	23	-	13	8	6	2	23	20	24	-	36	-	16	17	27	4	8	9	14	-	19	124	3193	15276
Normalized Probability	.6023	.1208	.0833	.0357	.0063	.0075	.0047	.0166	.0003	.0072	-	.0041	.0025	.0019	.0006	.0072	.0063	.0075	-	.0113	-	.0050	.0053	.0085	.0013	.0025	.0028	.0044	-	.0060	.0388		

Lines	1	2	3	i p(i) $\frac{1}{t_{mean}}$ x 100		6	7	8	99 and > 9
				4	5				
I 20 lines	12.8%	5.2%	7%	1.9%	1.3%	0.3%	1.3%	0.7%	69.5%
Line No. 5	24.5%	6.6%	1.5%	-	2.5%	-	-	2%	62.9%

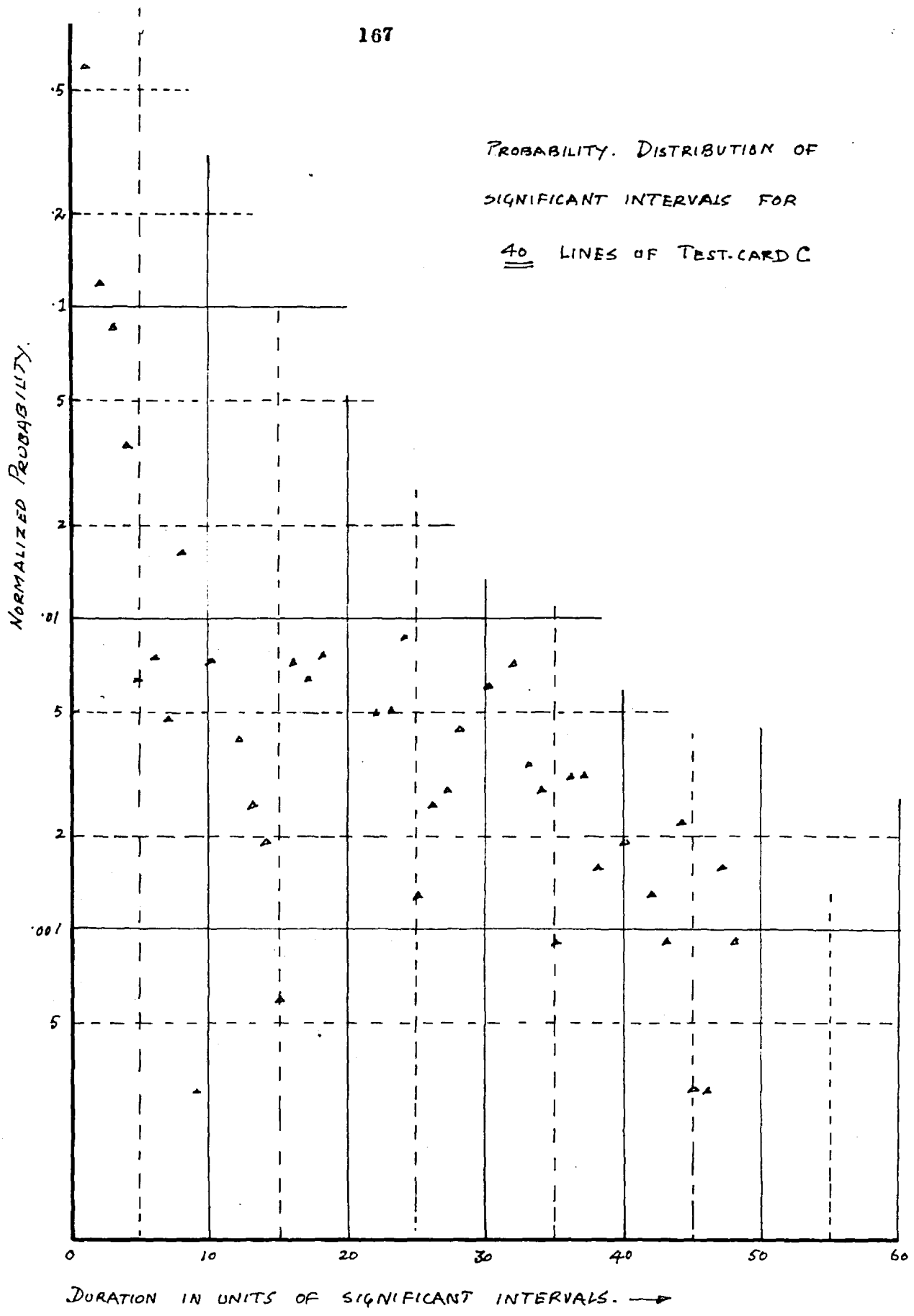

PROBABILITY. DISTRIBUTION OF
SIGNIFICANT INTERVALS FOR
40 LINES OF TEST-CARD C
NORMALIZED PROBABILITY.
·5
·2
·1
5
2
·01
5
2
·001
5
0
10
20
30
40
50
60
DURATION IN UNITS OF SIGNIFICANT INTERVALS. →

FIG. 71.

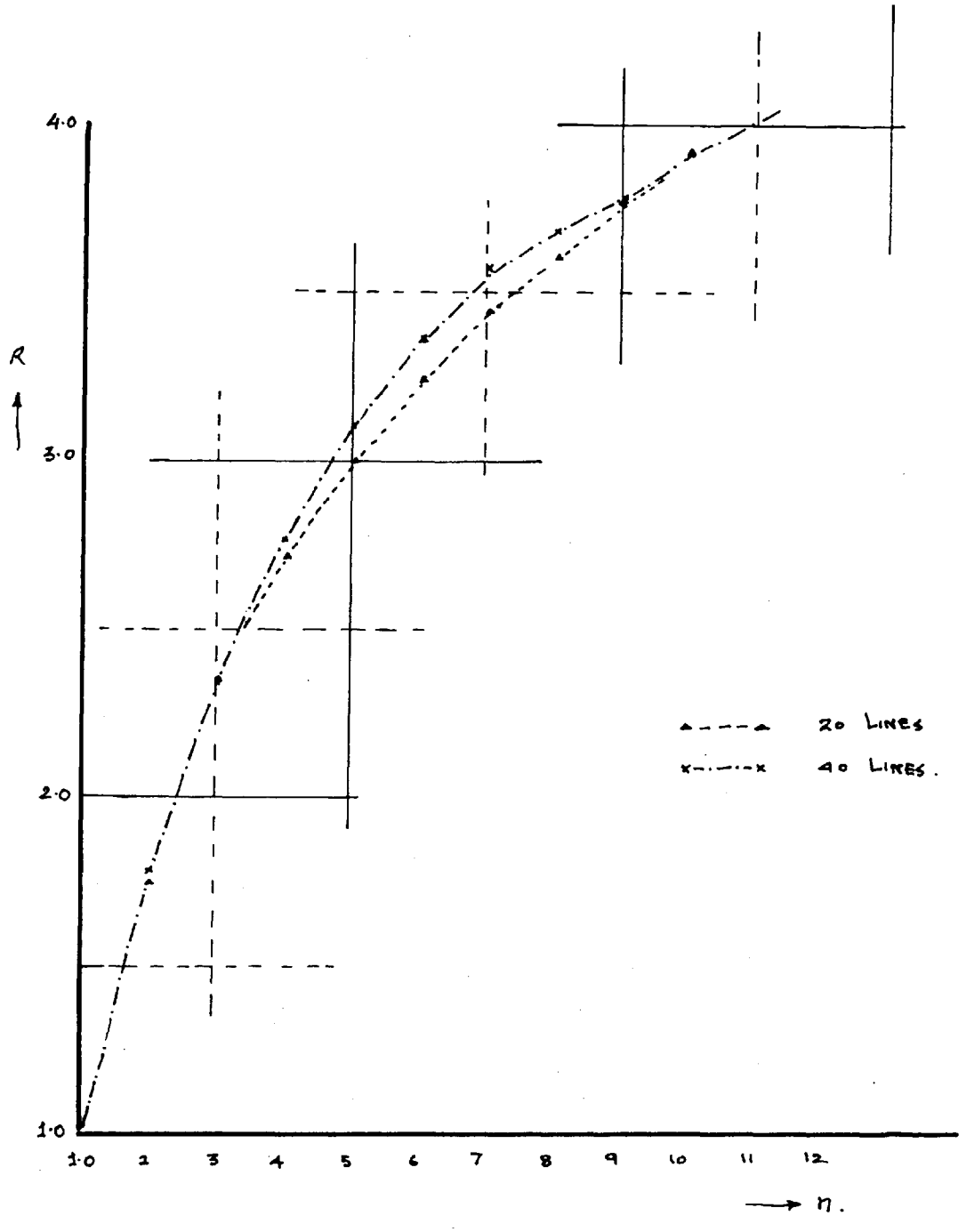


FIG. 72.

For the distribution of table 4.4. the values of t_{m_n} for n = 1,2,3, ... 10; and the corresponding values of R, are tabulated in table 4.5.

The values of R from tables 4.2. and 4.5. have been plotted in figure 72.

TABLE 4.5.

n	t_{m_n}	$t_{m/t_{m_n}}$	$R = nt_{m/t_{m_n}}$
1	4.79	1.00	1.00
2	5.39	0.89	1.78
3	6.12	0.78	2.34
4	6.92	0.69	2.76
5	7.76	0.62	3.10
6	8.61	0.56	3.36
7	9.47	0.51	3.57
8	10.33	0.46	3.68
9	11.21	0.42	3.78
10	12.08	0.40	4.00

4.4. Accuracy and Limitations.

The results obtained from the two sets of measurements are interesting and reasonably consistent. However, the method of measurement is very laborious, approximate and time consuming The smallest interval on the measuring scale was 0.5 mm. The unit significant interval was adjusted to be 0.33 mm and 0.25 mm for the measurements of tables 4.1 and 4.3. respectively. Fractional measurements were made by eye estimation. (Some empty columns in tables 4.1 and 4.3 might be explained on this basis.)

The effect of noise on the measurements was negligible because the terminations of the significant intervals were judged visually and also because of the geometrical nature of th picture. Hence the results obtained from these measurements

must be used with caution. Before reliable system design can be undertaken, the statistics of a number of representative pictures would have to be obtained. However, the statistics obtained may be used to determine the order of the parameters of systems. Since this measurement was made, other workers[84,85,86] have determined run-length statistics using normal pictures and have arrived at similar results. Though the criteria used for determining the run-length is different in all the three cases, the mean value as well as the general shape of the run-length distributions are comparable.

4.5. The Statistics Measuring Apparatus.

To facilitate the collection of statistics of different types of pictures, an apparatus has been designed and built. The block diagram of the apparatus is shown in figure 69(b). The video waveform is double differentiated which greatly emphasizes the turning points. The output of the double differentiator is full-wave rectified and sliced. The slicing level fixes an arbitrary amplitude level below which all the waveform is neglected. The sliced waveform contains peaks which may be shaped and used as markers. It has been presumed that the waveforms have constant slopes between the markers which correspond to the turning points and the distribution of the time intervals between the markers is desired.

This distribution may be obtained with a variable-width gate and a counter. The triggered pulse generator (fig.69b) provides a gating pulse whose width may be varied from .3 μ sec. to 10 μsec. in steps of .1 μsec. The width is set at the lowest value, the gate is opened for a large number of times and the count is recorded each time. The gate width is progressively increased and the experiment is repeated for each setting. The desired statistics can be easily obtained from these readings.

This apparatus may also be used to obtain the "detail burst" statistics of pictures. The "detail" in a picture is not evenly distributed in time and the study of "detail burst" is relevant to the storage requirements of a run-length encoder as will be seen in section 5.4.

The setting of the slicing level, to obtain the markers, is very important. A coarse setting would mean a small number of turning points and hence higher compressibility but at the cost of "detail" in the picture. A very fine setting, on the other hand, may reduce the compressibility considerably. This apparatus may be used, with modification, to study the relationship between picture quality and compressibility as the slicing level is changed.

4.6. Design and Testing of the Apparatus.

Basically, the double - differentiator consists of two differentiators, of the type shown in figure 24, in cascade. The full-wave rectifier and the slicer is the same unit which has been used in the investigation of the variable-velocity scanner and is shown in figure 26.

The circuit diagram of the variable-width gate is shown in figure 73. The circuit consists of a 6 BN 6 Gating valve (V_7), a precision pulse generator and inverter (V_3, V_4 and V_5) and provision for either manual or electrical triggering of the pulse generator. ~~In case~~ When the pulse generator is manually triggered, the pressing of the microswitch,s, fires the blocking oscillator (V_2), which in turn triggers the pulse generator. A negative pulse, whose duration can be controlled by the switched capacitor in the timing circuit of the pulse generator, is produced at the anode of V_4. This pulse is inverted by V_5 and is fed to the quadrature grid of 6 BN 6 through the cathode follower V_{6A}. The 6 BN 6 is a gated beam valve in which the cathode current is maintained constant and is independent of the plate current. The plate current only flows when both the control grid and the quadrature grid

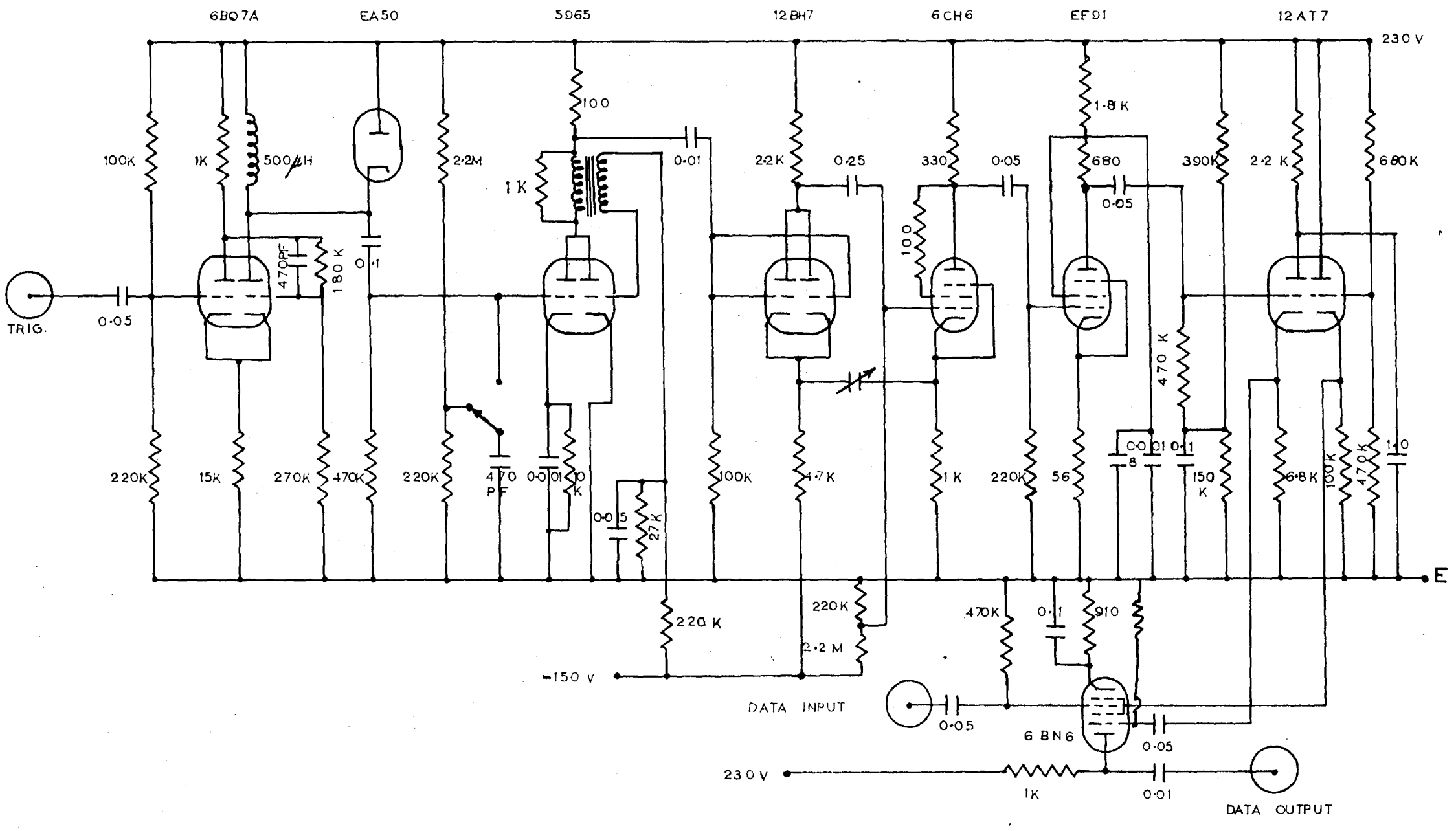
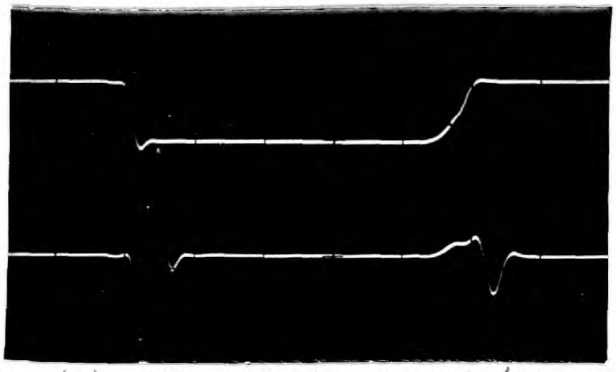


FIG. 73 VARIABLE WIDTH GATE AND TRIGGERED PULSE GENERATOR



(i) Input pulse
1 Volt/cm

(ii) d^2/dt^2
2 volts/cm

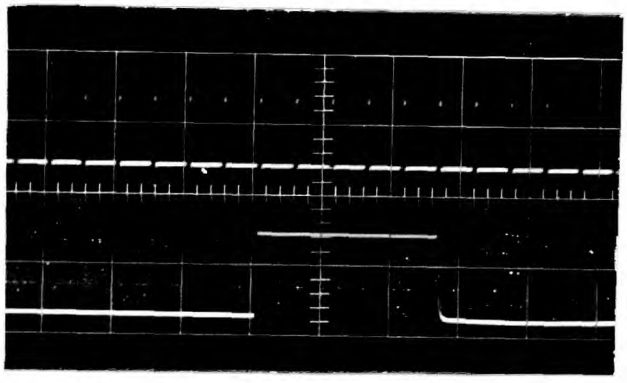
(a) 400 millimicroseconds/cm



(i) d^2/dt^2
1 Volt/cm

(ii) $|d^2/dt^2|$
2 volts/cm

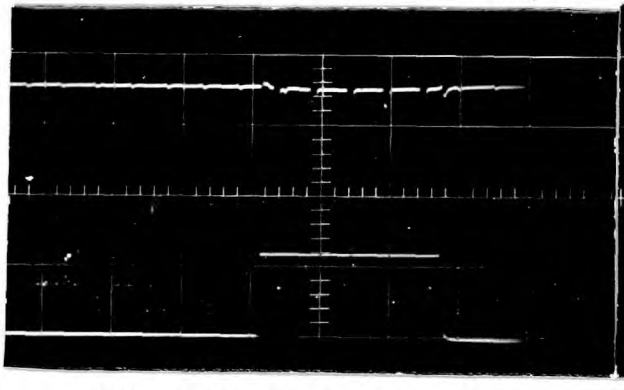
(b) 200 millimicroseconds/cm



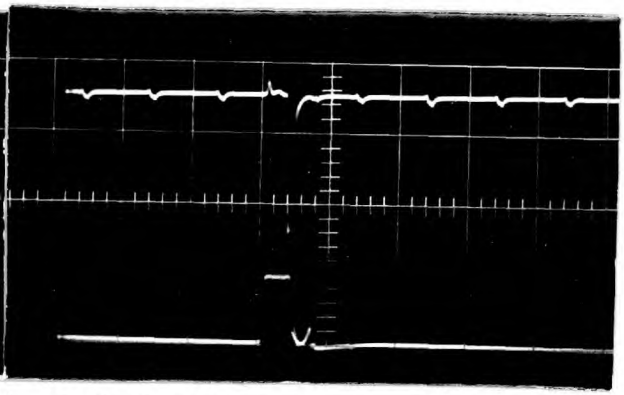
(i) 1 Mc/s Pulse Train
0.1 microseconds wide

(ii 5 Microseconds gate

(c) 2 microseconds/cm



(i) 6 BN 6 output
(ii) Gating waveform
2 microseconds/cm



(i) 6 BN 6 output
(ii) Gating waveform
1 microseconds/cm

FIG. 74 TESTS ON STATISTICAL APPARATUS.

have a marker pulse and a gating pulse on them simultaneously. The high frequency break-through is very small in this valve.

The facility for non-manual triggering has been provided by including the trigger circuit V_1. If band-limited white noise is fed into V_1, the Schmitt trigger circuit would generate rectangular waves in which the transitions or crossovers would be random. The inductor in the plate of V_{1b} differentiates the output and the diode D_1 clips the negative spikes. Hence a train of random pulses is obtained. These pulses are used to trigger the blocking oscillator which in turn triggers the pulse generator. The bandwidth of the noise is made very narrow i.e. of the order of 20 c/s or less. A mechanical counter may be connected to the output of V_2 to record the number of gating pulses.

The equipment has been tested and some photographic results have been obtained which are shown in figure 74. Figure 74(a) shows the input and output of the double-differentiator. The need for incorporating a regenerative device is obvious. Figure 74(b) shows the input and the output of the full wave rectifier. It clearly shows that the resolution time of the double differentiator and the full-wave rectifier is of the order of 100 m μsec. The variable width gate was tested with a pulse generator and a sinewave generator. A Cintel pulse generator provided a train of pulses, 0.1 μsec. wide, and with a repetition rate of 1 Mc/s. This was fed to the control grid of the 6 BN 6 to simulate the marker pulses. The circuit for the generation of the gating pulses was triggered periodically by the sine wave generator. (Figure 74(c) shows the waveform on the two grids of the 6 BN 6 gate. Figure 74(d) shows the plate waveform of the 6 BN 6 gate and the gating waveform. The breakthrough is very small compared to the transmitted pulse amplitude. Figure 74(e) shows the plate waveform of 6 BN 6 and the gating waveform when the width of the gating waveform is very low.

It is expected that this apparatus will be used in future work in the department.

5. THE OPEN LOOP SYSTEM.

In the variable velocity scanning system, the mapping and processing of the picture is one single operation so that conventional cameras cannot be used. Another drawback associated with the system is its method of "detail detection ". Sophisticated methods of detail detection are virtually ruled out because the decision about the scan velocity has to be made almost "instantaneously". The possibility of an open loop system of bandwidth compression, capable of processing waveforms produced by conventional cameras and in which more time can be made available for "detail detection", has been investigated because of its obvious potential advantages, especially in the case of point-to-point transmission.

5.1. Variable rate Sampling.

The concept of variable rate sampling is intimately connected with that of "short-term bandwidth".

Let e(t) be a video waveform (fig.69a) which is band-limited by a low-pass filter with the cut-off frequency, f_c.

Then by sampling theorem, the video waveform can be completely represented by giving its ordinates at a series of points spaced $\frac{1}{2f_c}$ seconds apart. Inspection of the sampled waveform (fig.69a) shows that the samples shown in dotted lines may be omitted from the transmission because they may be inserte at the receiver with a first order interpolator, if the samples shown by full lines are transmitted. Hence only the samples shown by full lines are necessary for the reconstruction of the

picture. These samples occur at time-intervals which are equal to or are multiples of $\frac{1}{2f_c}$ seconds. These selected samples may be considered to have been generated by associating different "short-term bandwidths" with different regions of e(t) and sampling each region with a pulse rate corresponding to the bandwidth associated with that region. Thus an experimental set-up may be imagined in which several sampling pulse generators working at pulse rates 2 f_c, $\frac{2f_c}{2}$, ... $\frac{2f_c}{n}$ pulses per second, and locked to each other, are available. The "detail detector" associates a "short-term bandwidth" with a part of the incoming video waveform and the corresponding pulse generator is switched on to generate the samples.

The run-length statistics for test card 'C', reported in section 4.3. are quantized in 30 time-intervals. With 30 sampling rates, the number of pulses would approach the number of turning points and the entire potential band compression may be realized. However, this would result in extreme complexity of instrumentation in the detail detector, sampling circuits and the elastic delay in the system with the added complexity of a very complicated first order interpolator at the receiver. Moreover, the decoding information, analogous to the position information in the closed loop system, would be high with the choice of so many sampling rates.

The run-length statistics of test card 'C' as well as other pictures[85,86] are highly peaked for small run-lengths. In Table 4.1, the total probability of occurrence of any run-length other than the first five is only 0.1311. This

suggests that the first few run-lengths occur very frequently while the other run-lengths occur rarely. From figure 70, it can be seen that the initial steep slope in the distribution ends at 5 run-lengths and the probability of occurrence of run-lengths of more than five units is more or less constant and is quite small.

This type of distribution suggests that if variable rate sampling is so employed that all run-lengths occurring with a small probability are sampled at one rate while the sampling rates are matched for the frequently occurring run-lengths, a considerable reduction in the number of sampling rates, and hence in instrumentation complexity, may be obtained for some sacrifice of the potential bandwidth compression.

5.2. A New System.

Various suggestions have been made jointly by Cherry, Holloway and the author[87] for the instrumentation of a system of bandwidth compression using variable-rate sampling. A simplified block diagram of one realization of the transmitter is shown in figure 75. For the purpose of explanation of the system, it is assumed that only three sampling rates are used which are $2\,f_c$, $\frac{2f_c}{3}$ and $\frac{2f_c}{9}$ pulses per second. These limitations are quite arbitrary, and in principle, more sampling rates or different sampling rates may be used, if desired.

The incoming video signal is passed through a delay unit which provides a delay of τ μsec., where τ μsec. is the time

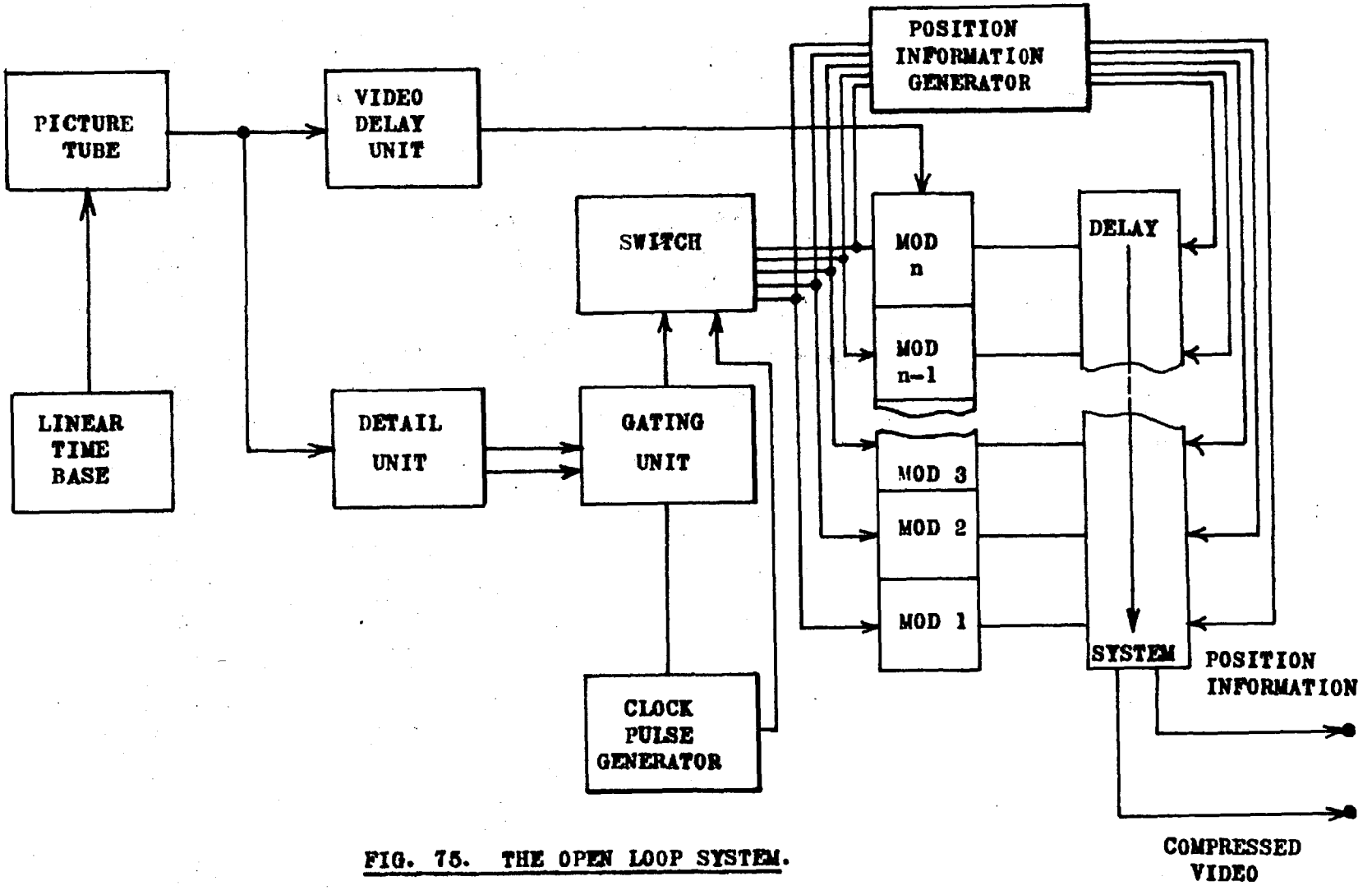


FIG. 75. THE OPEN LOOP SYSTEM.

duration necessary for the detail detection. The output of the detail detector is a three level signal signifying high detail, medium detail and low detail corresponding to the sampling rates of 2 f_c, $\frac{2f_c}{3}$ and $\frac{2f_c}{9}$ pulses/sec respectively. The clock pulse generator generates pulses of constant amplitude at the rate of 6 Mc/s (2 f_c). The gating unit, which is controlled by the output of the detail detector, passes all the clock pulses for a high detail signal, every third pulse for a medium detail signal and every ninth pulse for a low detail signal. The unit marked switch in figure 75 is a multiple position high speed electronic switch which is so arranged that, at any instant, only one of the modulators is connected to the gating unit. The switch is programmed so that if the output of the gating unit occupies every third clock pulse position, the switch keeps the modulator, through which the previous pulse has passed, connected. If every clock position is occupied, the switch moves up and if every ninth position is occupied, it moves down the bank of modulators. The video signal is fed to the bank of modulators so that the outputs of the modulators are amplitude modulated pulses. Each modulator is connected to a specified tap on the delay system. It is ensured that any signal introduced in the delay system travels only in the direction of the arrow in the figure. There is a constant delay difference of $\frac{1}{3}$ µsec. between any two consecutive inputs to the delay system. It can be seen now that the movement of the switch upwards would result in introduction of extra time delay, thereby expanding

the time difference between the signal pulses, while the movement of the switch down the bank would result in the reduction of delay and hence in the reduction of time difference between the signal pulses. In the absence of overload, the output of the delay system may be made into a train of equidistant pulses, $\frac{1}{2}$ μsec. apart. Thus a bandwidth reduction of 3 : 1 is sought.

The decoding information is generated by identifying each switch position by one level of a multi-level signal which is also elastically coded, either by time multiplexing with the video samples or by-passing it through an identical delay system.

The receiver can be either a mirror image of the transmitter or a variable-velocity receiver may be used.

The number of taps in the delay system would depend on the signal statistics. In the case of overload, the switch would get to the top of the bank of modulators and remain connected to the corresponding tap on the delay system. In the case of underload, the bottom switch would remain open. On the basis of run-length statistics, the storage capacity of the delay system can be made such that any predetermined probability of overload may be obtained.

An experimental system based on these lines is being investigated by Messrs. Pine and Kubba in Professor Cherry's laboratory. In the experimental set-up, sampling rates of $2\ f_c$, $\frac{2f_c}{3}$ and $\frac{2f_c}{9}$ pulses/sec. are used and distributed delay lines with buffers are used in the delay system.

5.3. Some Computations.

Computations have been made from the data of Table 4.1 to ascertain the relation between the number of sampling rates and the bandwidth compression. The percentage of total time which is occupied by all the run-lengths of duration i is given by

$$i\ p(i)\ \frac{1}{\bar{t}_{mean}}\ x\ 100$$

This function has been computed for the average of 20 lines and for line no.5. of Table 4.1. and is tabulated in Table 4.4. For two different upper bounds for the ratio of maximum to minimum sampling rates, the relation between the number of sampling rates and the desired channel bandwidth has been computed and is plotted in figure 76. It can be seen that for three sampling rates, the desired bandwidth is 1.1 Mc/s for the worst line and 0.8 Mc/s for the average of twenty lines. The three rates which gave the figure of 0.8 are 2 f_c, f_c and $\frac{f_c}{12}$.

For the sampling rates of 6 Mc/s, 2 Mc/s and 0.66 Mc/s, it can be seen from Table 4.4 that the sampling rates are employed in the following proportion:

6 Mc/s	18%
2 Mc/s	12.5%
0.66 Mc/s	69.5%

Let the line duration be 100 μsec. Then the total number of pulses per line can be found by adding the number of pulses for

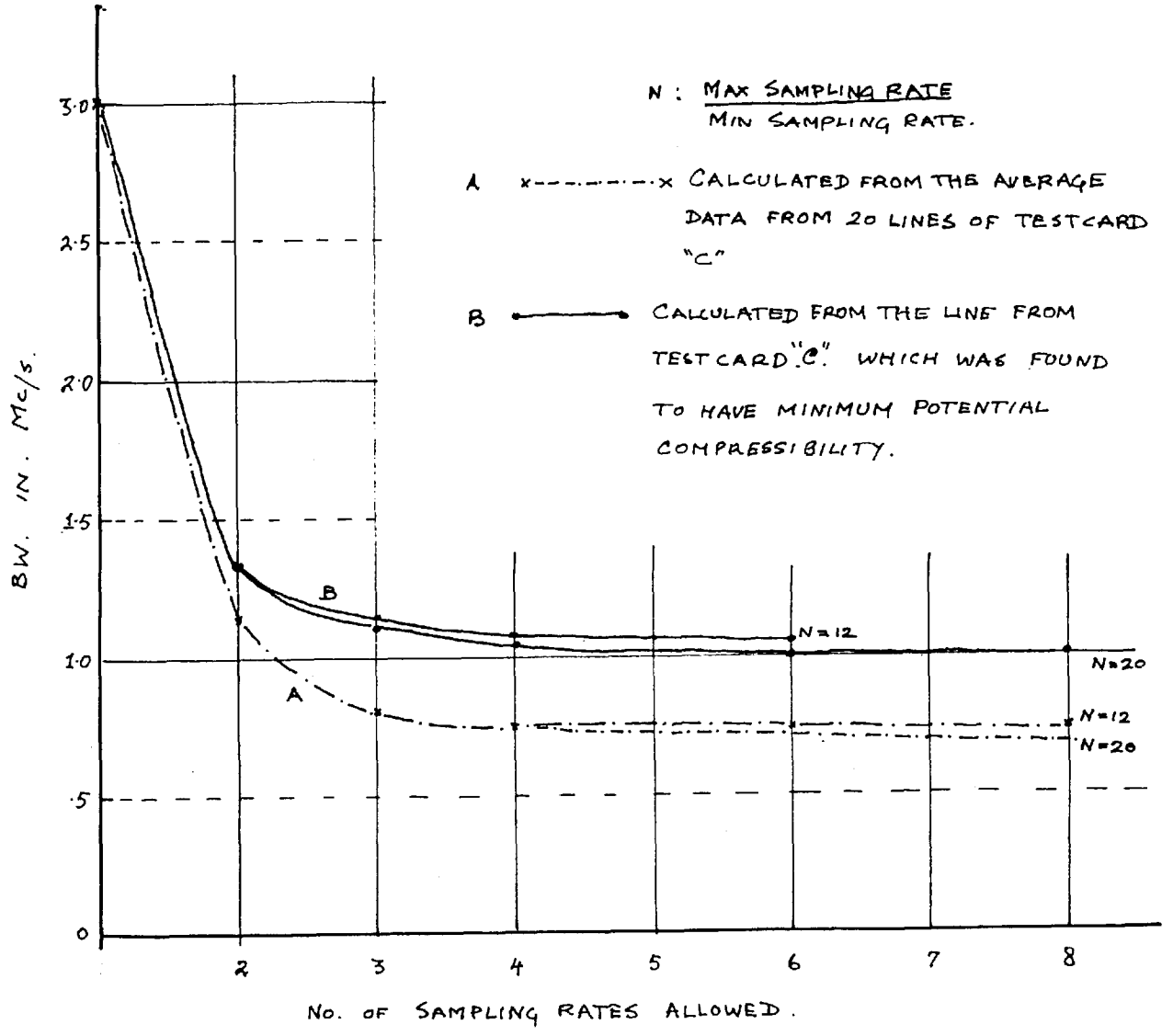

N : MAX SAMPLING RATE / MIN SAMPLING RATE.
A x----·-·-·-·-x CALCULATED FROM THE AVERAGE DATA FROM 20 LINES OF TESTCARD "C"
B ——•—— CALCULATED FROM THE LINE FROM TESTCARD "C" WHICH WAS FOUND TO HAVE MINIMUM POTENTIAL COMPRESSIBILITY.
BW. IN. Mc/s.
3·0
2·5
2·0
1·5
1·0
·5
0
2
3
4
5
6
7
8
B
A
N=12
N=20
N=12
N=20
No. OF SAMPLING RATES ALLOWED.

FIG. 76

each sampling rate, viz.

With the sampling rate of 6 Mc/s, no.of pulses in 18 μsec = 108

" " " " " 2 Mc/s, " " " " 12.5 " = 25

" " " " " 0.66 Mc/s " " " 69.5 " = 46

Hence the total number of pulses in 100 μsec. = 179.

The compression = $\frac{600}{179}$ = 3.4 : 1

Similarly for line no.5, Compression = 2.4:1.

All these computations give more optimistic results than is actually possible to obtain because in these calculations, it has been tacitly assumed that the run-lengths are either 1, 3, 9 units long or are their integral multiples. This implies that for its specification, it is not necessary to break a run into two or more runs. However, in practice a run of duration 7 units (say) would have to be broken into three runs, one of unit duration and two of three unit duration if only three sampling rates ($2f_c$, $\frac{2f_c}{3}$, $\frac{2f_c}{9}$) are used. Table 5.1 shows how run-lengths can be specified in terms of 1, 3 and 9 units.

TABLE 5.1.

Run length	1	3	9	Total No.of runs
1	1	-	-	1
2	2	-	-	2
3	-	1	-	1
4	1	1	-	2
5	2	1	-	3
6	-	2	-	2
7	1	2	-	3
8	2	2	-	4
9	-	-	1	1
10	1	-	1	2
11	2	-	1	3
12	-	1	1	2
13	1	1	1	3
14	2	1	1	4
15	-	2	1	3

etc.

On the basis of these, the computations show that, for the data of Table 4.1, the bandwidth compression is only 2.8:1 instead of 3.4:1 which was the figure obtained when the runs were assumed to be multiples of 1, 3, 9 units.

5.4. Storage Requirements.

The number of taps in the delay system and hence the total storage capacity in the elastic delay is dependent largely on the run-length statistics and the "detail burst" statistics of the picture. It also depends on the sampling rates because these can modify both the run-length statistics and the "detail burst" statistics.

The statistics of test card 'C' have been used to compute the number of taps for a system using 2 f_c, $\frac{2f_c}{3}$ and $\frac{2f_c}{9}$ pulses/second as the three sampling rates and with a time delay of $\frac{1}{f_c}$ seconds between the consecutive taps. As shown in Table 5.1, the runs are broken in terms of 1, 3, 9 units. In figure 77, the number of samples after break up is plotted across the x axis and the number of delay taps is plotted across the y axis. It has been assumed that for every run-length of unit duration, the tap is moved up by one, thus introducing two units of extra delay. For runs of three unit duration, the tap remains stationary and for runs of nine unit duration, the tap is moved down by three-switching out six units of delay. It is further assumed that whenever the system is underloaded, the transmitter breaks the run-lengths of 9 units into run-lengths of three units by introducing redundant pulses. This ensures that the same tap remains connected. The run-lengths of three units produced due to underload is shown by crosses as distinct from dots in the figure. Whenever a run is broken, the resultant runs are arbitrarily arranged in decreasing length, e.g. 14 = 9+3+1+1.

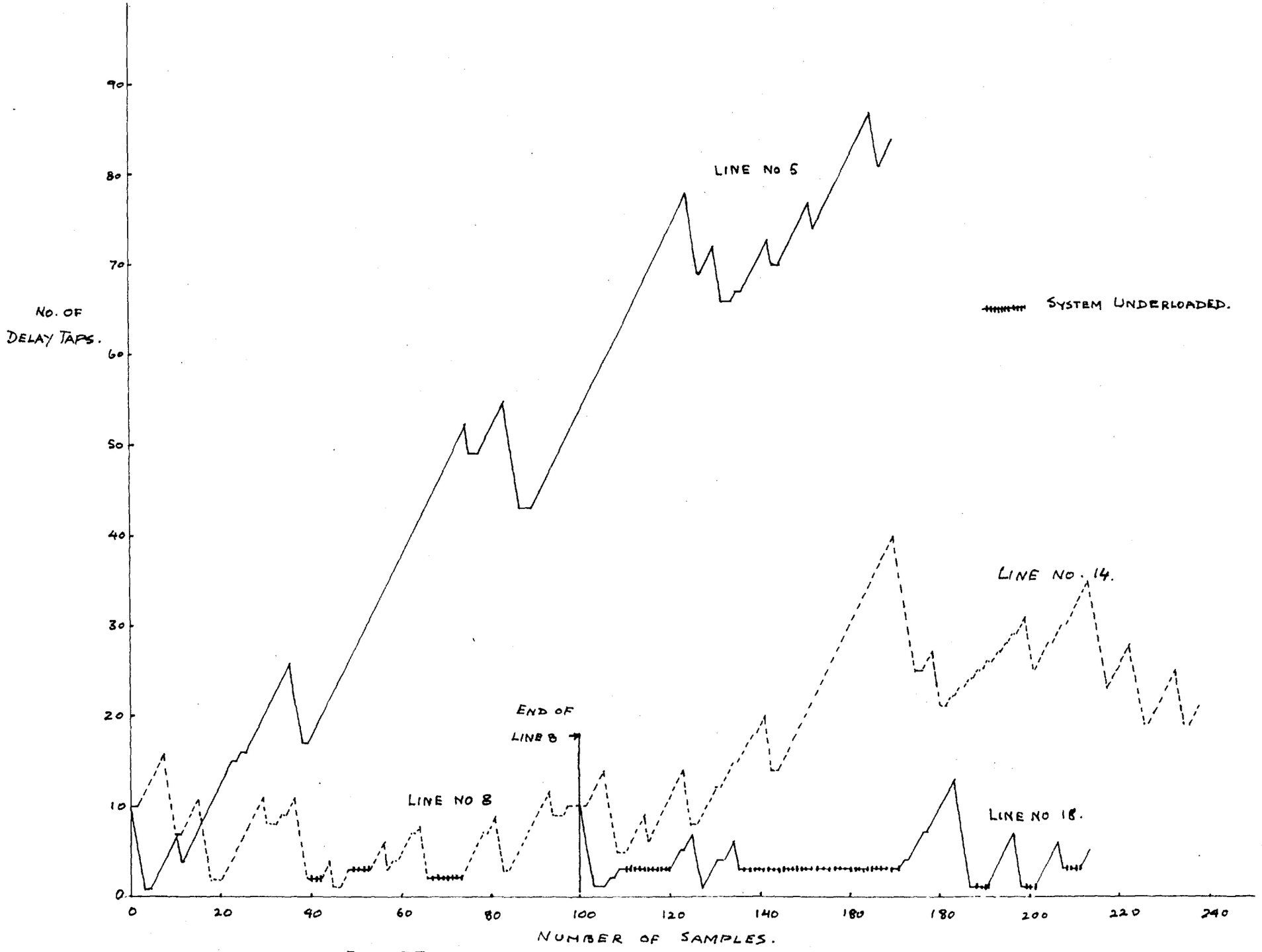

LINE No 5
LINE No. 14.
LINE No 8
LINE No 18.
END OF LINE 8
SYSTEM UNDERLOADED.
No. OF DELAY TAPS.
NUMBER OF SAMPLES.
0
10
20
30
40
50
60
70
80
90
0
20
40
60
80
100
120
140
160
180
200
220
240

FIG : 77.

The line length in the plot of figure 7 is a measure of the compressibility. Line No.5. which is the least compressible line in the entire data, denotes that if overload is to be avoided, 87 taps or a storage capacity of approximately 30 μseconds is desired in the elastic delay. Line No.18, which is one of the most compressible in the collected data has a smaller number of samples than line No.5, inspite of 57 redundant samples introduced due to underload. The number of taps used for this line is only 13. Line No.8 and line No.14 are more representative between the two extremes quoted.

Most of the lines of test card'C' can be elastically coded without any overload with 40 to 50 taps. It is stressed that test card '6' is a highly organised and regular pattern, hence the results obtained must be used with caution.

6. THE POSITION CHANNEL

All the figures for bandwidth - compression quoted in sections 3, 4 and 5 refer only to the reduction in the bandwidth requirement of the vision channel. These figures of bandwidth compression must be adjusted to account for the position channel bandwidth.

In the absence of any coding, the position information, in the arrangement of figure 75 or in the closed - loop variable- velocity system, would, in general, require the same bandwidth as the compressed vision channel.

In the case of the closed loop system, the time base velocity can assume any arbitrary value between the maximum and minimum velocities which are specified as system parameters. This fact makes the coding of the position channel extremely difficult. However, this property is not essential for the variable - velocity system and the velocities can be usefully quantized into a small number of quantum levels (of the order of four) without any substantial reduction in the compressibility. The quantization of the scan velocity would help in reducing the jitter introduced due to the noise in the feedback loop. It would also reduce the information in the position channel and make it amenable to certain types of coding.

By the reduction of choice to three or four in the position channel, a higher - order code may be used to reduce the bandwidth at the expense of the signal power. One such coder for halving the bandwidth of continuous signals of finite

bandwidth has been proposed by Billings.(88) The reduction of the position channel bandwidth to a third of the compressed vision bandwidth, using similar techniques, is within the realm of practical possibility. The position error can still be made non-cumulative. If the error in any sample of the decoded signal is $\pm$ 1 quantum, the position error could be arranged so as not to extend beyond two picture points. In the worst case when the error in a received sample is very large, the position error would remain limited to three picture-points.

This type of coding is purely non-statistical in which an exchange between the bandwidth and the signal power is effected. However, if a "rugged" code for the transmission of the position channel is used, as might well be the case when a digital open loop system is used, the changes of the sampling rates may be sent instead of the position information. This information, relating to the changes can be statistically coded with advantage. The differentiation of the curve in fig.77 gives the numbers of pulses that need be sent in the position channel and these are tabulated below:-

Line	No.5	33
Line	No.8	39
Line	No.14	56
Line	No.18	30

These are small numbers as compared with the number of samples in the vision channel. Furthermore, they can attain

one of only three or four values. Thus, the information transmitted by these pulses is much smaller than that transmitte by the vision samples and hence it is possible to use statistic methods to compress the position channel bandwidth. It may be noted that the statistical compressibility of the position channel is dependent on the number of sampling rates as well as their values. Hence the optimum sampling rates should be chose such that the expression

$$\left[\text{No. of samples in the vision channel} + (\text{No. of sampling rates}) \times (\text{No. of samples in the position channel})\right]$$

is minimized.

Quaternary phase-shift keying of the carrier has been suggested[89] as a possibility for the transmission of a four level or 2 bit position information with a "very small increase in bandwidth."

Thus, reduction of the position channel bandwidth is possible and obviously desirable. This preliminary work suggests the need for a thorough investigation of the possibilities.

7. PICTURE DETAIL DETECTION

Detail detection is the process of determining what constitutes a significant change in the picture.

It was seen in section 1 that differentiation or finite differencing has been suggested for detail detection in almost every system. The "picture-detail factor", as defined by Gouriet is the modulus of the time derivative of the signal and hence its relation to these detail detectors is obvious. The inadequacy of the picture detail factor as a measure of compressibility for multi-level pictures has been pointed out by Cherry and Gouriet[1] and other workers[4,90].

These detail detectors are deterministic in nature and have been suggested on the tacit assumption of a noise-free signal. In the presence of noise, they cannot discriminate in favour of the signal.

7.1. Statistical Approach.

To combat noise during detail detection, it is essential to treat the problem on a statistical basis. In this case, an understanding of the mechanism of picture generation is very helpful in the design of the detail detector. Various workers[35,91,92,93] have published results which throw light on the mechanism of picture generation. Schreiber has deduced from third-order probability measurements on television pictures that the process of picture generation is a "higher-than-second-order" process. The upper bound on the information content deduced from the third order statistics

is lower than the upper bound obtained from the second order measurements. The difference, though significant, is small and hence it has been suggested that the picture generation may be assumed to be a second-order process to avoid instrumentation complexities in the practical systems.

Stochastic models for the information source have been suggested by Voelcker[89]. The problem of run-length detection has been regarded as a problem in statistical inference and indications have been given for the practical realization of a run length detector based on this principle.

The conventional statistical approach has limitations in such problems. Testing for stationarity is not always possible therefore ergodicity becomes a convenient but quite arbitrary hypothesis. Some mathematical methods have been developed[94,95] which might make it meaningful to apply certain concepts of conventional random theory to small samples.

7.2. Short-term Bandwidth.

The concept of short-term bandwidth and methods of its measurement have obvious relevance to the problem of detail detection. The reciprocal relationship between the autocorrelation function and power spectra has been extended by Fano[96] to the case of short-term autocorrelation function and spectrum when these are properly defined. The short-term autocorrelation function is defined as

$$\varphi_t(\tau) = \int_0^T f(T-t)\, f(T-t-\tau)\, h(T)\, dt$$

where h(T) is the weighting function and is exponential in the case considered by Fano. It is stressed that the averaging time in the determination of the autocorrelation function is limited to a short time, not because of experimental limitations but because it is the variation of the autocorrelation function with time which is of primary interest.

The effect of the weighting functions on the short-term spectrum can be illustrated by assuming a window type of weighting function which is equal to one from $t = T$ to $t = T - T_1$ and is zero otherwise. Let $T - T_1 = T_N$. It is assumed that the first minimum in the autocorrelation function, τ_o, is a measure of the short-term bandwidth. Let f(t) be a signa band limited to f_c. When T_N is made very small ($\frac{1}{f_c}$ sec), then $\tau_o = \frac{1}{f_c}$, irrespective of the nature of the signal. This indicates that the bandwidth is maximum (f_c). If the conventional autocorrelation function ($T_N \to \omega$) is fourier transformed, the bandwidth requirement is again indicated as f_c. Thus for any waveform, there may be an optimum T_N which would denote the minimum short-term bandwidth. Theoptimum T_N may be obtained by a plot of $\Delta \tau_o / \Delta T_N$. The value of T_N may be dependent on short-term statistical structure of the signal.

"Instantaneous power spectrum" has been defined by Page[47] as a time dependent function . If the time parameter is considerably reduced, energy appears in high frequency bands which disappearswhen the averaging time is increased. This phenomenon is very similar to the effect of T_N described above. The concept of "instantaneous power

spectrum" has been further developed by Turner[98] who has established a relationship between the instantaneous power spectrum and the running autocorrelation function.

7.3. Effect of Visual Properties.

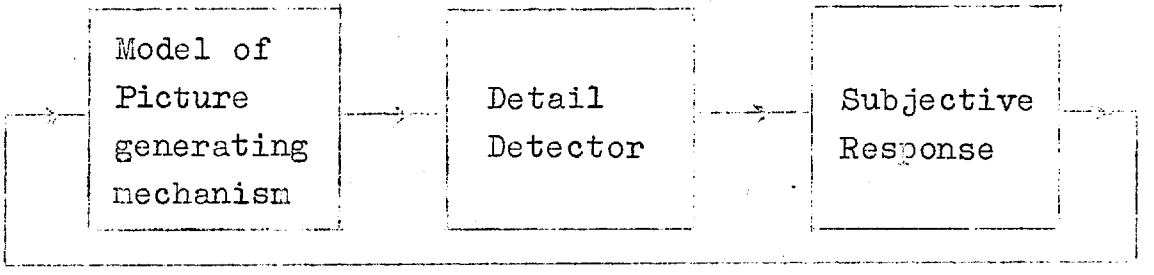
In the case of lossy or irreversible encoding, the perceptual properties of the viewer would greatly affect the design of the detail detector. The knowledge of the human fidelity criterion, which is essential for the design of an optimum communication system in which the human observer is the ultimate receiver, is incomplete. It has been seen in sect 1, that certain properties of the human viewers have already been usefully employed in system design. It has been pointed out by Graham[44] that, ideally, to exploit the perceptual redundancy fully, a complete map of the viewer discriminability for all points of picture space is desired.

7.4. Discussion.

The psycho-visual approach and the statistical approach are complementary in nature. The perceptual redundancy can be taken into account in the statistical models and detail detectors may be designed to remove them. The differentiator, as a detail detector, is based on the tacit assumption of a model which generates noise-free picture signal consisting of large plateaux followed by transitions - the transitions are weighted to carry most of the "information".

In absence of a complete mapping of viewer discriminability

at all points of picture space which is practically impossible to obtain, reasonable detail detectors may be intuitively built and the subjective response of viewers to a representative group of processed pictures tested. These responses may, sometimes, provide clues for the modification of the model which in turn would affect the detail detector. This process may be diagramatically shown as.



The work on pattern recognition[99-104] may lead to a better understanding of the human viewing process and may revolutionize detail detection and picture transmission.

8. SUMMARY OF CONCLUSIONS.

A survey of some relevant developments in the field of television bandwidth compression has been made in section 1. The comparative features of certain proposed systems have been tabulated in Table 1.5. In spite of multiplicity of proposals, efforts towards practical realization or feasibility study of statistical systems for bandwidth compression of television signals seem to be singularly lacking.

The design features of a flying - spot variable-velocity scanner are presented in section 2. The problems in the design of an electro-magnetic deflection system with wide bandwidth have been studied. A stepped (Ratchet) time base for the vertical deflection has been developed.

The performance of the system has been investigated under different conditions and the results are reported in section 3. These results stress the importance of source noise and the limitations it imposes on the system performance. The spectral components of the signal and noise at the output of the scanner and of the control signal have been measured when the loop is open. Analytical confirmation of some of the results has been obtained. The measurements show clearly the need for higher overall $S/_N$ ratio to obtain a reasonable mean square $S/_N$ ratio in the high frequency region.

The stability of the system has been experimentally investigated. The system is inherently stable but can be made unstable by excessive loop gain or delay or both.

It is submitted that the bandwidth in the internal feedback loop would have to be of the order of 20 Mc/s due to the inherent delay in the optical path, photomultiplier tube and the scanner tube phosphor.

Due to the limitations of the devices, it is considered that the variable-velocity-scanning system cannot be profitably used for the bandwidth compression of television signals. However, this system seems to be ideally suited for facsimile or low-bandwidth transmission of two level and multi-level signals.

In section 4, the significant interval statistics of test card 'c' is reported. The compressibility of the test card 'c' has been computed from these. An apparatus has been built and tested for the measurement of significant interval statistic automatically.

The results of section 4 as well as the general concepts of the variable-velocity scanning have led to the development of an open loop system in which variable-rate sampling is used. This has been described in section 5 and some computations have been made to ascertain various parameters of the system. With a set of three sampling rates, the storage requirement of the system has been assessed for four different lines of test card 'c'.

In section 6, Preliminary investigations on the position channel requirement of both the open loop system and the closed loop system have been reported. In absence of any subtle form of coding, the bandwidth requirement of the position channel

would be equal to that of the vision channel. However, the possibility of both non-statistical and statistical coding exists and reductions may be obtained by coding.

The problem of detail detection has been discussed in section 7. Almost each system discussed in section 1, uses a deterministic detail detector which fails to discriminate in favour of the signal in the presence of noise. The need for a statistical approach has been stressed. A complementary approach is by mapping the discriminability of viewers.

The problem of detail detection is fundamental to bandwidth compression. The need for more work is stressed and it is pointed out that the work on Pattern Recognition[99-104] may make substantial contribution towards a near optimum solution of the problem of detail detection and hence of picture transmission.

APPENDIX I

Let the power spectrum $G(f) = \frac{1}{A^2 + B^2 f^2}$ (I.1)

where A and B are constants
and f is the frequency in C/s

The angular frequency $\omega = 2\pi f$

Hence Power Spectrum $= \frac{1}{A^2 + \frac{B^2}{4^2}\omega^2} = \frac{1}{a^2 + b^2 \omega^2}$

where $a^2 = A^2$ and $b^2 = \frac{B^2}{4\pi^2}$

If the signal is band limited from d.c. to a frequency f_c, Power in watts in the spectrum

$$P = \int_0^{\omega_c} \frac{1}{a^2 + b^2 \omega^2} \, d\omega = \frac{1}{ab} \tan^{-1} \frac{b}{a} \cdot \omega_c \qquad (I.2)$$

putting $\omega_c = 2\pi \times 3 \times 10^6$

$$P = \frac{1}{ab} \tan^{-1} \frac{b}{a} \cdot 6\pi.10^6 \qquad (I.3)$$

It is given[28] that 90% of the signal power is concentrated below 250 Kc/s

Hence using (I.2)

$$\frac{1}{ab} \tan^{-1} \frac{b}{a} \cdot 2\pi \cdot 250 \times 10^3 = 0.9\ P \qquad (I.4)$$

Let $\frac{b}{a} \times 2\pi \times 250 \times 10^3 = y$

Then equation (I.3) and (I.4) may be re-written as

$$\frac{1}{ab} \tan^{-1} 12\ y = P \qquad (I.5)$$

$$\frac{1}{ab} \tan^{-1} y = 0.9\ P \qquad (I.6)$$

$$= \frac{A_m^2}{6} \frac{2N - 1}{N - 1}$$

It is assumed that the peak to peak signal voltage is 1 volt and that the signal has 25 quantum levels. Then

$$P = \frac{1}{6} \cdot \frac{49}{24} = .34 \text{ watts} \qquad (I.9)$$

Substituting for P in equations (I.5) and (I.6),

$$\frac{1}{ab} \tan^{-1} 12y = .34 \qquad (I.10)$$

$$\frac{1}{ab} \tan^{-1} y = .306 \qquad (I.11)$$

From eq.(I.10)

$$\tan .34\, ab = 12y = 60 \qquad (I.12)$$

Hence $.34\, ab = 1.554$

or $$ab = \frac{1.554}{.34} \qquad (I.13)$$

Multiplying equations (I.8) and (I.13)

$$b^2 = \frac{5 \times 1.554}{2\pi \times 25 \times 10^4 \times .34} = \frac{1.554}{\pi \times 34} \times 10^{-3}$$

$$= 14.55 \times 10^{-6}$$

Hence $b = 3.815 \times 10^{-3}$ (I.14)

From eq. (I.13)

$$a = \frac{1.554}{.34} \frac{1}{b} = \frac{1.554}{.34 \times 3.815} \times 10^3$$

$$= \frac{1554}{1.297} = 1.198 \times 10^3$$

$$a = 1.198 \times 10^3 \qquad (I.15)$$

Dividing (I.6) by (I.5) gives

$$\frac{\tan^{-1} y}{\tan^{-1} 12y} = 0.9 \qquad \text{(I.7)}$$

From the tables* , by inspection

$\tan^{-1} 5 = 1.3734$ Radians

$\tan^{-1} 60 = 1.5541$ Radians

which gives

$$\frac{\tan^{-1} 5}{\tan^{-1} 60} = \frac{1.3734}{1.5541} \simeq .9$$

$$\text{Hence } \frac{b}{a} = \frac{5}{2\pi \times 25 \times 10^4} \qquad \text{(I.8)}$$

To obtain the value of a and b separately, another condition is needed. To obtain this condition, it is assumed that (i) The signal amplitude is divided into N quantum levels. (ii) Each quantum level is equiprobable. and (iii) The maximum signal amplitude is Am volts.

If $p(A_x)$ is the probability of occurrence of the amplitude level A_x, then

$$\text{The mean power in watts} = \sum_{x=0}^{N-1} A_x^2 \, p(A_x)$$

$$= \frac{1}{N} \sum_{0}^{N-1} A_x^2$$

$$= \frac{1}{N}\left[\left(\frac{A_m}{N-1}\right)^2 + \left(\frac{2\,A_m}{N-1}\right)^2 + \ldots\ldots\left(\frac{N-1}{N-1}\,A_m\right)^2\right]$$

$$= \frac{1}{N}\left(\frac{A_m}{N-1}\right)^2\left[1^2 + 2^2 + 3^2 + \ldots\ldots(N-1)^2\right]$$

---

* Milne-Thomson and Comrie "Standard Four-Figure Mathematical Tables" Edition B. Macmillan andC Co.Ltd.,

Now $A^2 = 1.4352 \times 10^6$

$B^2 = 4\pi^2 b^2 = .5744 \times 10^{-3}$

Hence the Power Spectrum

$$G(f) = \frac{1}{1.4352 \times 10^6 + .5744 \times 10^{-3} f^2} \qquad (I.16)$$

The value of G(f) has been computed at seven different frequences which is tabulated below.

TABLE I.1.

frequency	G(f) in μ watts	arbitrary dbs
0	.6968	
30 Kc/s	.5122	88 dbs
50 Kc/s	.3483	87 dbs.
100 Kc/s	.1393	83 dbs.
500 Kc/s	.0069	70 dbs.
1 Mc/s	.0017	64 dbs.
3 Mc/s	.0002	54 dbs.

APPENDIX II

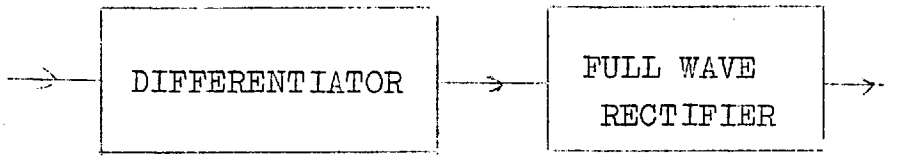


Figure II.1

It is assumed that the input to the differentiator is white noise whose

(i) Power Spectral Density $G_2(\omega) = \frac{k}{2\pi} \quad \omega \leq \omega_c$

$= 0 \quad \omega > \omega_c$

and (ii) Amplitude Probability distribution is given by

$$f(x) = \frac{1}{\sqrt{2\pi}\,\sigma_x} e^{-x^2/2\sigma_x^2} \qquad \text{(II.1)}$$

where $\sigma_x^2 = \int_0^{\omega_c} \frac{k}{2\pi} d\omega = \frac{k}{2\pi} \cdot \omega_c$ (II.2)

The autocorrelation function of the input,

$$\phi_x(\tau) = \int_0^{\omega_c} \frac{k}{2\pi} \cos \omega \tau \, d\omega$$

$$= \frac{k}{2\pi} \frac{\sin \omega_c \tau}{\tau} \qquad \text{(II.3)}$$

Hence the normalized autocorrelation function of the input,

$$\rho_x(\tau) = \frac{\phi_x(\tau)}{\sigma_x^2} = \frac{\sin \omega_c \tau}{\omega_c \tau} \qquad \text{(II.4)}$$

Let the transfer function of the differentiator be

$Y(j\omega) = j \omega T$ where T is a time constant

Then the spectral density at the output of the differentiator is given by

$$G_y(\omega) = \frac{k}{2\pi} |j \omega T|^2 = \frac{k}{2\pi} \omega^2 T^2 \quad \omega \leq \omega_c \qquad \text{(II.5)}$$

$= 0 \quad \omega > \omega_c.$

and the mean square value

$$\sigma_y^2 = \int_0^{\omega_c} \frac{k}{2\pi} \omega^2 T^2 = \frac{k}{6\pi} T^2 \omega_c^3 \qquad \text{(II.6)}$$

The autocorrelarion function of the output of the differentiato is given by

$$\phi_y(\tau) = \int_0^{\omega_c} G_y(\omega) \cos \omega \tau \, d\omega$$

$$= \int_0^{\omega_c} \frac{k}{2\pi} \omega^2 T^2 \cos \omega \tau \, d\omega$$

$$= \frac{k T^2}{2\pi\tau^3} \left[2 \omega_c \tau \cos \omega_c \tau + (\omega_c^2 \tau^2 - 2) \sin \omega_c \tau \right] \qquad \text{(II.7)}$$

From equations (II.6) and (II.7), the normalized autocorrelatio function,

$$P_n(\tau) = \frac{\phi_y(\tau)}{\sigma_y^2}$$

$$= \frac{k T^2}{2\pi\tau^3} \left[2 \omega_c \tau \cos \omega_c \tau + (\omega_c^2 \tau^2 - 2) \sin \omega_c \tau \right] \times \frac{6\pi}{k T^2 \omega_c^3}$$

$$= \frac{3}{\omega_c^3 \tau^3} \left[2 \omega_c \tau \cos \omega_c \tau + (\omega_c^2 \tau^2 - 2) \sin \omega_c \tau \right] - \text{(II.8)}$$

The amplitude probability distribution of the output of the differentiator would be Gaussian.(81)

Hence, $$f(y) = \frac{1}{\sqrt{2\pi}\,\sigma_y} e^{-y^2/2\sigma_y^2} \qquad \text{(II.9)}$$

The input to the full-wave rectifier is a Gaussian process whose properties are given by equations (II.5) to (II.9).

Let the input to the full-wave rectifier be represented by a stationary time series y(t)and let y_1 and y_2 be the values of y(t) at times t and t + τ respectively. If $R_n(\tau)$ is the cross-correlation function between the outputs of two zero - memory non-linear devices whose inputs are y(t) and y(t+τ) respectively and whose transfer functions are $f_1(y)$ and $f_2(y)$, it has been shown by Price(80) that

$$\frac{\partial^k R(\tau)}{\partial \rho^k(\tau)} = \overline{f_1{}^k[y_1(t)] f_2{}^k[y_2(t+\tau)]}$$

$$= \int_{-\infty}^{\infty}\int_{-\infty}^{\infty} \frac{f_1^{(k)}(y_1) f_2^{(k)}(y_2) \exp -\{[y_1^2+y_2^2-2\rho(\tau)y_1y_2]/2(1-\rho^2)\}}{2\pi\sqrt{1-\rho^2(\tau)}}$$

For the case of the full wave rectifier, Let

$$f_1(y) = f_2(y) = \begin{cases} y & y \geq 0 \\ -y & y < 0 \end{cases}$$

then $f_1^{(2)}(y)$ and $f_2^{(2)}(y)$ are first order δ functions of area 2 at $y = 0$.

Substituting in Price's equation and evaluating

$$\frac{\partial^2 R_n(\tau)}{\partial \rho_n{}^2(\tau)} = \frac{2}{\pi\sqrt{1-\rho_n{}^2(\tau)}} \qquad \text{(II.10)}$$

To solve this equation, the following two boundary conditions are used.

1. When $\tau = 0$ $\quad \rho_n(0) = R_n(0) = 1$

2. When $\rho_n(\tau) = 0$

$$\frac{\partial R_n(\tau)}{\partial \rho_n(\tau)} = \frac{1}{2\pi}\int_{-\infty}^{\infty}\int_{-\infty}^{\infty} f_1^{(1)}(y_1)\, f_2^{(1)}(y_2)\, e^{-\frac{y_1^2+y_2^2}{2}}\, dy_1\, dy_2$$

$$= \frac{1}{2\pi}\left[\int_{-\infty}^{\infty} f_1^{(1)}(y)\, e^{-y^2/2}\, dy\right]^2$$

$$= \frac{1}{2\pi}\left[\int_{-\infty}^{0} -1 \cdot e^{-y^2/2} dy + \int_{0}^{\infty} 1 \cdot e^{-y^2/2}\, dy\right]^2$$

$$= 0$$

because $e^{-y^2/2}$ is an even function.

Now, integrating equation (II.10)

$$\frac{\partial R_n(\tau)}{\partial \rho_n(\tau)} = \frac{2}{\pi} \sin^{-1} \rho_n(\tau) + k_1$$

Introducing the second boundary condition

$$k_1 = 0$$

Hence $$\frac{\partial R_n(\tau)}{\partial \rho_n(\tau)} = \frac{2}{\pi} \sin^{-1} \rho_n(\tau) \qquad \text{(II.11)}$$

Integrating equation (II.11)

$$R_n(\tau) = \frac{2}{\pi} \left[\rho_n(\tau) \sin^{-1} \rho_n(\tau) + \sqrt{1 - \rho_n^2(\tau)} \right] + k_2$$

Introducing the first boundary condition, $k_2 = 0$

Hence

$$R_n(\tau) = \frac{2}{\pi} \left[\rho_n(\tau) \sin^{-1} \rho_n(\tau) + \sqrt{1 - \rho_n^2(\tau)} \right] \qquad \text{(II.12)}$$

The value of $\rho_n(\tau)$ and $R_n(\tau)$ have been computed for different values of τ and are tabulated in Table (II.1). When $\omega_c \tau < \pi$, the calculation of $\rho_n(\tau)$ by direct substitution in equation (II.8) gives very misleading results because very small differences are involved in the expression. Even the use of a seven-figure table gives inaccurate results. An expansion of the right-hand side of equation (II.8) gives

$$\rho_n(\tau) = \frac{3}{x^3} \left[2x \left\{ 1 - \frac{x^2}{2!} + \frac{x^4}{4!} - \frac{x^6}{6!} + \frac{x^8}{8!} \quad \ldots\ldots\ldots\ldots \right\} + (x^2 - 2) \left\{ x - \frac{x^3}{3!} + \frac{x^5}{5!} - \frac{x^7}{7!} + \quad \ldots\ldots\ldots\ldots \right\} \right]$$

where $x = \omega_c \tau$

$$= \frac{3}{x^3}\left[2x - x^3 + \frac{2x^5}{4.!} - \frac{2x^7}{6.!} + \frac{2x^9}{8.!} - \cdots\cdots\cdots\cdots \right.$$

$$\left. + x^3 - \frac{x^5}{3.!} + \frac{x^7}{5.!} - \frac{x^9}{7.!} - 2x + \frac{2x^3}{3.!} - \frac{2x^5}{5.!} + \frac{2x^7}{7.!} \cdots\cdots \right]$$

$$= 1 - .3x^2 + .0179\, x^4 - .000446\, x^6$$

The higher powers may be neglected because this expansion is used only for values of $x < \pi$

If $x = \alpha\tau$

then $P_n(\tau) = 1 - 2.9609\,\alpha^2 + 1.7436\,\alpha^4 - 0.4292\,\alpha^6$

(II.13)

TABLE II.1.

$\frac{\omega_c \tau}{\pi}$	$\rho_n(\tau)$	$R_n(\tau)$	$\frac{\omega_c \tau}{\pi}$	$\rho_n(\tau)$	$R_n(\tau)$
0	1	1	2.125	+.2887	.6633
0.125	+.9541	.9601	2.250	+.3730	.6814
0.250	+.8217	.8672	2.375	+.3994	.6881
0.375	+.6169	.7621	2.500	+.3696	.6807
0.500	+.3754	.6820	2.625	+.2924	.6641
0.625	+.0839	.6389	2.750	+.1821	.6472
0.750	-.1901	.6480	2.875	+.0561	.6376
0.875	-.4265	.6954	3.000	-.0675	.6381
1.000	-.6079	.7583	3.125	-.1720	.6460
1.125	-.7166	.8085	3.250	-.2444	.6558
1.250	-.7453	.8234	3.375	-.2772	.6613
1.375	-.6959	.7969	3.500	-.2684	.6597
1.500	-.5793	.7467	3.625	-.2363	.6545
1.625	-.4132	.6918	3.750	-.1469	.6436
1.750	-.2199	.6521	3.875	-.0556	.6376
1.875	-.0239	.6368	4.000	+.0380	.6370
2.000	+.1522	.6440			

APPENDIX III

The curve fitted to $R_n(\tau) - R(\infty)$ is given by

$$F_n(\tau)_{Fitted} = .1821\, e^{-.66\frac{\omega_c\tau}{\pi}}\left(1+\cos 5.236\,\frac{\omega_c\tau}{\pi}\right) \qquad \text{(III.1)}$$

This function, for different values of $\omega_c\tau$, has been tabulated in Table III.1.

TABLE III.1

$\omega_c\tau/\pi$	$e^{-.66\frac{\omega_c\tau}{\pi}}$	$f.235\,\frac{\omega_c\tau}{\pi}$	$\cos.5.236\,\frac{\omega_c\tau}{\pi}$	$F_n(\tau)$
0.50	.719	2.618	-.866	0.017
0.75	.610	3.927	-.707	0.032
1.00	.517	5.236	+.500	0.141
1.25	.438	6.545	+.966	0.157
1.50	.372	7.854	0	0.068
2.00	.267	10.472	-.500	0.024
2.50	.192	13.090	+.866	0.065
3.00	.138	15.708	-1	0
3.50	.099	18.326	+.866	0.034

Equation (III.1) may be written as

$$F_n(\tau)_{Fitted} = K.\, e^{-\alpha\tau}\,(1 + \cos n\,\tau). \qquad \text{(III.2)}$$

where $K = .1821$

$\alpha = .21\,\omega_c$

and $n = 1.1667\,\omega_c$ (III.3)

The power spectral density function

$$G_n(\omega)_{approx.} = \frac{2}{\pi}\int_0^{\infty} F_n(\tau)_{Fitted} \cos \omega \tau \, d\tau$$

$$= \frac{2k}{\pi}\int_0^{\infty} e^{-\alpha\tau} \cos \omega \tau \, d\tau$$

$$+ \frac{2k}{\pi}\int_0^{\infty} e^{-\alpha\tau} \cos n\tau \cos \omega \tau \, d\tau \qquad \text{(III.4)}$$

The two integrals in the right hand side of equation (III.4) are tabulated*. From tables

$$G_n(\omega)_{approx} = \frac{2k\alpha}{\pi}\left[\frac{1}{\alpha^2+\omega^2} + \frac{\omega^2 + (\alpha^2 + n^2)}{\omega^4 + 2(\alpha^2-n^2)\omega^2 + (\alpha^2+n^2)^2}\right]$$

(III.5)

Substituting for k, α and n from equation (III.3),

$$G_n(\omega)_{approx.} = .0244\frac{1}{\omega_c}\left[\frac{2(\omega/\omega_c)^4 - 2.603(\omega/\omega_c)^2 + 8.093}{(\omega/\omega_c)^6 - 5.426(\omega/\omega_c)^4 + 7.728(\omega/\omega_c)^2 + .351}\right]$$

(III.6)

The expression in the square brackets in equation (III.6) has been tabulated for different values of ω/ω_c in Table III.2.

*(i) Pierce. Foster "A short table of Integrals" Ginn & Co.p.69
(ii) Ref.81. page 202.

TABLE III.2.

$\omega/\omega c$	$7.728\ x(\omega/\omega c)^2$	$2.603\ x(\omega/\omega c)^2$	$5.426\ x(\omega/\omega c)^4$	$(\omega/\omega c)^6$	[ ]	Arbitrary dbs
0.05	.0193	.0065	-	-	21.84	16
0.10	.0773	.0260	.0005	-	18.86	15
0.25	.4830	.1627	.0195	.0002	9.74	12
0.50	1.9320	.6507	.3391	.0156	4.19	9
1.00	7.728	2.603	5.426	1	2.05	6
1.50	17.388	5.8567	27.50	11.39	3.51	12
2.00	30.912	10.412	86.82	64	8.05	8

APPENDIX IV

Referring to figure II.1, it is assumed that the input to the differentiator has a spectrum denoted by

$$G_s(\omega) = \frac{1}{a^2+b^2\omega^2} \qquad \text{(IV.1)}$$

where (a) and (b) are given by equations (I.14) and (I.15).

Let the transfer function of the differentiator be $Y(j\omega) = j\omega T$ where T is a time constant.
Then the power spectral density at the output of the differentiator is given by

$$G(\omega) = \omega^2 T^2 \frac{1}{a^2 + b^2\omega^2} \qquad \text{(IV.2)}$$

The autocorrelation function of the output of the differentiator is given by

$$\phi(\tau) = T^2 \int_0^{\omega_c} \frac{\omega^2}{a^2+b^2\omega^2} \cos\omega\tau \, d\omega$$

$$= \frac{T^2}{b^2}\int_0^{\omega_c} \cos\omega\tau\, d\omega - \frac{T^2}{b^2}\int_0^{\omega_c} \frac{1}{1+\frac{b^2\omega^2}{a^2}} \cos\omega\tau\, d\omega \qquad \text{(IV.3)}$$

$$\simeq \frac{T^2}{b^2}\cdot\frac{1}{\tau}\sin\omega_c\tau - \frac{T^2}{b^2}\int_0^{\infty} \frac{1}{1+\frac{b^2\omega^2}{a^2}} \cos\omega\tau\, d\omega \qquad \text{(IV.4)}$$

The upper limit of the second integral in equation (IV.3) has been changed from ω_c to ∞ in equation (IV.4). This approximation has been made because the integral in equation (IV.4) is tabulated in the Table of Integrals while the one in (IV.3) is not easy to integrate. The energy in the h.f. spectrum decreases steeply with frequency, hence this approximation may be justified.

Now

$$\phi(\tau) = \frac{T^2}{b^2} \cdot \frac{1}{\tau} \sin \omega_c \tau - \frac{a}{b^3} \cdot \frac{\pi}{2} e^{-\tau \frac{a}{b}} T^2 \qquad \text{(IV.5)}$$

Substituting $\tau = 0$

$$\phi(0) = T^2 \frac{\omega_c}{b^2} - \frac{a}{b^3} \cdot \frac{\pi}{2} \cdot T^2 \qquad \text{(IV.6)}$$

Hence the normalized autocorrelation function

$$\rho_s(\tau) = \frac{\phi(\tau)}{\phi(0)} = \frac{\frac{1}{b^2} \cdot \frac{1}{\tau} \sin \omega_c \tau - \frac{a}{b^3} \cdot \frac{\pi}{2} e^{-\tau a/b}}{\frac{\omega_c}{b^2} - \frac{a}{b^3} \cdot \frac{\pi}{2}}$$

$$= \frac{\frac{1}{\tau} \sin \omega_c \tau - \frac{a}{b} \cdot \frac{\pi}{2} e^{-\tau \frac{a}{b}}}{\omega_c - \frac{a}{b} \frac{\pi}{2}} \qquad \text{(IV.7)}$$

where $\omega_c = 2\pi \times 3 \times 10^6$

and $\frac{a}{b} = \frac{2\pi \times 25 \times 10^4}{5}$ (from I.8)

$= .314 \times 10^6$

The normalized autocorrelation function of the output of the full-wave rectifier can be obtained by using equation (II.12). Hence,

$$R_s(\tau) = \frac{2}{\pi} \left[\rho_s(\tau) \sin^{-1} \rho_s(\tau) + \sqrt{1-\rho_s^2(\tau)} \right] \qquad \text{- (IV.8)}$$

$\rho_s(\tau)$ and $R_s(\tau)$ have been computed for different values of $\omega_c \tau$ and tabulated in Tables (IV.1) and (IV.2) respectively.

TABLE IV.1.

$$\left(\omega_c - \frac{a}{b}\,\frac{\pi}{2}\right) \times 10^{-6} = 18.356$$

$\frac{\omega_c \tau}{\pi}$	$\frac{a}{b}\cdot\frac{\pi}{2}\, e^{-\tau a/b} \times 10^{-6}$	$\frac{1}{\tau}\sin \omega_c \tau - \frac{a}{b}\cdot\frac{\pi}{2}\, e^{-\tau\frac{a}{b}} \times 10^{-6}$	$\rho_s(\tau)$
0.00	-	-	1.0000
0.25	.4868	16.4836	+.8980
0.50	.4804	11.5196	+.6276
0.75	.4743	+5.1825	+.2823
1.00	.4680	-0.4680	-.0255
1.25	.4620	-3.8561	-.2101
1.50	.4560	-4.4560	-.2427
1.75	.4500	-2.8746	-.1566
2.00	.4441	-0.4441	-.0242
2.25	.4384	+1.4473	+.0788
2.50	.4327	+1.9673	+.1072
2.75	.4271	+1.1156	+.0608
3.00	.4215	-0.4215	-.0230
3.25	.4161	-1.7215	-.0938
3.50	.4105	-2.1248	-.1158
3.75	.4053	-1.5367	-.0837
4.00	.4001	-0.4001	-.0218

TABLE IV.2.

$\frac{\omega_c \tau}{\pi}$	$\rho_s(\tau)$	$\rho_s(\tau).\mathrm{Sin}^{-1}\rho_s(\tau)$	$\sqrt{(1-\rho_s^2(\tau))}$	$R_s(\tau)$	$R_s(\tau)-R(\infty$
0	1	$\pi/2$	0	1	.3634
0.25	+.8980	1.0014	.4400	.9176	.2810
0.50	+.6276	.4258	.7785	.7667	.1301
0.75	+.2823	.0808	.9593	.6558	.0192
1.00	-.0255	.0007	.9997	.6368	.0002
1.25	-.2101	.0445	.9777	.6507	.0141
1.50	-.2427	.0595	.9701	.6554	.0188
1.75	-.1566	.0246	.9877	.6444	.0078
2.00	-.0242	.0006	.9997	.6368	.0002
2.25	+.0788	.0062	.9969	.6386	.0020
2.50	+.1072	.0115	.9942	.6402	.0036
2.75	+.0608	.0037	.9982	.6378	.0012
3.00	-.0230	.0005	.9998	.6368	.0002
3.25	-.0938	.0088	.9957	.6395	.0029
3.50	-.1158	.0134	.9933	.6409	.0043
3.75	-.0837	.0070	.9965	.6388	.0022
4.00	-.0218	.0005	.9998	.6368	.0002

APPENDIX V

The curve fitted to $R_s(\tau) - R(\infty)$ is given by

$$F_s(\tau)_{fitted} = .112\, e^{-1.652x}(1-\cos 2\pi x) + .2075\, e^{-2.946x}\sin 2\pi x + .3634\, e^{-4.86x} \qquad (V.1)$$

where $x = \frac{\omega_c \tau}{\pi}$

The function $F_s(\tau)_{fitted}$ has been tabulated, for different values of $\omega_c \tau$. in Table (V.1)

TABLE V.1.

$\frac{\omega_c \tau}{\pi} = x$	$.3634\, e^{-4.86x}$	$.112 e^{-1.652x}(1-\cos 2\pi x)$	$.2075\, e^{-2.946x} \sin 2\pi x$	$F_s(\tau)_{Fitted}$
0	.3634	0	0	.3634
0.25	.1078	.0741	.0991	.2810
0.50	.0320	.0981	0	.1301
0.75	.0095	.0324	-.0227	.0192
1.00	.0028	0	0	.0028
1.25	.0008	.0142	.0052	.0204
1.50	.0002	.0188	0	.0190
1.75	.0001	.0062	-.0012	.0051
2.00	-	0	0	0
2.25	-	.0032	.0003	.0035
2.50	-	.0036	0	.0036
2.75	-	.0012	-	.0012
3.00	-	0	-	0
3.25	-	.0005	-	.0005
3.50	-	.0007	-	.0007
3.75	-	.0002	-	.0002
4.00	-	0	-	0

The cosine transform of $F_s(\tau)$ fitted would give the approximate power spectral density function of $R_s(\tau)-R(\infty)$.
From Equation (V.1),

$$G_s(\omega) = \frac{.112x2}{\pi}\int_0^{\infty} e^{-1.652\ \frac{\omega_c}{\pi}\tau}\cos\omega\tau\, d\tau$$

$$+ \frac{.112x2}{\pi}\int_0^{\infty} e^{-1.652\ \frac{\omega_c\tau}{\pi}}\cos 2\omega_c\tau\cos\omega\tau\, d\tau$$

$$+ \frac{2\ x.2075}{\pi}\int_0^{\infty} e^{-2.946\ \frac{\omega_c}{\pi}\tau}\sin 2\omega_c\tau\cos\omega_\tau\, d\tau$$

$$+ \frac{2x.3634}{\pi}\int_0^{\infty} e^{-4.86\ \frac{\omega_c}{\pi}\tau}\cos\omega\tau\, d\tau \qquad (V.2)$$

The first expression on the right - hand side of equation (V.2)

$$= \frac{1}{\omega_c}\ \frac{.0375}{.2765+(\omega/\omega_c)^2} \equiv \frac{1}{\omega_c}\cdot I_1.$$

The second expression on the right hand side of equation (V.2)

$$= \frac{1}{\omega_c}\ x.0375\ x\ \frac{(\frac{\omega}{\omega c})^2+ 2.765 + 4}{(\frac{\omega}{\omega c})^4+ 2(.2765-4.0)(\omega/\omega c)^2+(.2765+4.0)^2}$$

$$\equiv \frac{1}{\omega_c}\ I_2$$

The third expression on the right hand side of equation (V.2)

$$= \frac{1}{\omega_c}\left[\frac{.0661(2+\omega/\omega c)}{.8794+(2+\omega/\omega_c)^2} + \frac{.0661(2-\omega/\omega c)}{.8794+(2-\omega/\omega_c)^2}\right] \equiv \frac{1}{\omega_c}\cdot I_3$$

and the fourth expression on the right hand sideof equation (V.2

$$= \frac{1}{\omega_c}\ x\ \frac{.3584}{2.396+(\omega/\omega_c)2} \equiv \frac{1}{\omega_c}\cdot I_4$$

Now

$$G_s(\omega) = \frac{1}{\omega_c}\left[I_1 + I_2 + I_3 + I_4 \right] = \frac{1}{\omega_c}\Sigma I$$

The value of $I_1 + I_2 + I_3 + I_4$ has been computed for different values of ω/ω_c and is tabulated in table (V.2).

TABLE V.2.

ω/ω_c	I_1	I_2	I_3	I_4	ΣI	Arbitray dbs
0.05	.1344	.0088	.0542	.1494	.3468	10.80
0.10	.1309	.0088	.0542	.1490	.3429	10.70
0.25	.1106	.0091	.0543	.1458	.3198	10.10
0.50	.0712	.0103	.0548	.1354	.2717	8.73
1.00	.0294	.0167	.0552	.1055	.2068	6.32
1.50	.0148	.0371	.0468	.0771	.1758	4.90
2.00	.0088	.0689	.0157	.0560	.1494	3.48

APPENDIX VI

Referring to figure (II.1), let $\phi_s(\tau)$ and $\phi_n(\tau)$ be the autocorrelation function of signal waveform and noise waveform respectively at the input of the full wave rectifier. Let $\phi(\tau)$ be the autocorrelation function of the input waveform at the input of the full wave rectifier. Then

$$\phi(\tau) = \phi_s(\tau) + \phi_n(\tau) \qquad - (VI.1)$$

By definition, the normalized autocorrelation function

$$\rho_s(\tau) = \frac{\phi_s(\tau)}{\phi_s(0)} \quad \text{and} \quad \rho_n(\tau) \frac{\phi_n(\tau)}{\phi_n(0)}$$

Hence $\phi(\tau) = \phi_s(0)\ \rho_s(\tau) + \phi_n(0)\ \rho_n(\tau)$

$$= \phi_s(0) \left[\rho_s(\tau) + \frac{\phi_n(0)}{\phi_s(0)}\ \rho_n(\tau) \right]$$

$$= \phi_s(0) \left[\rho_s(\tau) + \frac{1}{k_1}\ \rho_n(\tau) \right] \qquad - (VI.2)$$

where $k_1 = \dfrac{\text{Mean Square Signal Power}}{\text{Mean Square Noise Power}} = \dfrac{\phi_s(0)}{\phi_n(0)}$

From Equation (VI.2)

$$\phi(0) = \phi_s(0) \left[1 + \frac{1}{k_1} \right]$$

Hence

$$\rho(\tau) = \frac{\phi(\tau)}{\phi(0)} = \frac{\rho_s(\tau) + \frac{1}{k_1}\ \rho_n(\tau)}{1 + \frac{1}{k_1}} \qquad - (VI.3)$$

In figure (II.1), let the input to the differentiator have a $\frac{S}{N}$ ratio of 36 dbs and let the peak signal level be 1 volt. If each discernible amplitude level is equiprobable, the Mean Square Signal Power = .335 watts. (Appendix I).

Now $S/_N$ ratio in television is defined as

$$S/_N \text{ ratio} = 20 \log \frac{\text{Peak Signal Volts}}{\text{R.M.S.Noise Volts}}$$

Hence $36 = 20 \log \frac{1}{v_n}$ where v_n = r . m.s. noise volts

$$\frac{1}{v_n} = 64$$

So that $v_n = \frac{1}{64}$ volts $= .0156$ volts

Mean Square Noise Power $= (.0156)^2 = .000\,24$ watts - (Vl.4)

Referring to Equation (II.2)

$$\frac{K}{2\pi} \cdot \omega_c = .000\,24$$

Hence $K = \frac{240}{3 \times 10^6}$ μ watts/cycle/second.

$= 80$ $\mu\mu$ watts/cycle/second. - (VII.5)

It may be pointed out that the Mean Square Signal to noise ratio which is defined as

$$10 \log \frac{\text{m.s. Signal Power}}{\text{m.s. Noise Power}}$$

can be found at the input; of the differentiator

$$\left(\frac{S}{N}\right)_{\text{m.s.}} \text{ratio} = 10 \log \frac{.335}{.00024} = \underline{31.4 \text{ dbs.}} \qquad \text{(VI.6)}$$

For the differentiated Signal and Noise.
Using equation (IV.6) and (II.6)

$$K_1 = \frac{\phi_s(o)}{\phi_n(o)} = \frac{T^2 \left(\omega_c - \frac{10^5 \Pi^2}{2}\right) \frac{1}{14.55 \times 15^6}}{\frac{K}{6\pi} \cdot T^2 \omega_c^3}$$

Putting $\omega_c = 2\pi \times 3 \times 10^6$ and substituting for K from equation (VI.5)

$$K_1 = 44.405 \quad , \quad \frac{1}{K_1} = .0225 \qquad - (VI.7)$$

The signal to noise ratio at the output of the differentiato is given by

$$10 \log K_1 = \underline{16.5 \text{ dbs.}} \qquad - (VI.8)$$

Comparison of equations (VI.6) and (VI.8) shows the diminution in the Mean Square $S/_N$ ratio due to the differentiation.

Substitution of the value of $\frac{1}{k_1}$ from equation (VI.7) in equation (VI.3) gives

$$\rho(\tau) = \frac{\rho_s(\tau) + .0225\ \rho_n(\tau)}{1.0225} \qquad - (VI.9)$$

Corresponding to the input signal represented by eq.(VI.9) the normalized autocorrelation function of the output of the full-wave rectifier can be obtained by using equation (II.12). Hence

$$R_{S+N}(\tau) = \frac{2}{\pi}\left[\rho(\tau) \sin^{-1}\rho(\tau) + \sqrt{1 - \rho^2(\tau)}\right] \qquad - (VI.10)$$

$\rho(\tau)$ and $R_{S+N}(\tau)$ have been computed for different values of τ and tabulated in Table VI.1.

TABLE VI.1.

$\frac{\omega_c \tau}{\pi}$	$f_s(\tau)$	.0225 x $f_n(\tau)$	$f(\tau)$	$R(\tau)$	$R(\tau)-R(\infty)$
0	+1	+.0225	1	1	.3634
0.25	+.8980	+.0185	+.8963	.9164	.2798
0.50	+.6276	+.0084	+.6220	.7197	.0831
0.75	+.2823	-.0042	+.2720	.6603	.0237
1.00	-.0255	-.0137	-.0392	.6370	.0004
1.25	-.2101	-.0168	-.2219	.6524	.0158
1.50	-.2427	-.0130	-.2501	.6683	.0317
1.75	-.1566	-.0049	-.1579	.6445	.0079
2.00	-.0242	+.0034	-.0203	.6367	.0001
2.25	+.0788	+.0084	+.0853	.6389	.0023
2.50	+.1072	+.0083	+.1130	.6407	.0041
2.75	+.0608	+.0041	+.0635	.6379	.0013
3.00	-.0230	-.0015	-.0240	.6368	.0002
3.25	-.0938	-.0055	-.0971	.6396	.0030
3.50	-.1158	-.0060	-.1191	.6411	.0045
3.75	-.0837	-.0033	-.0851	.6389	.0023
4.00	-.0218	+.0009	-.0204	.6368	.0002

REFERENCES

1. Cherry,E.C. Gouriet,G.G.-"Some possibilities for the Compression of T.V.Signals by Recoding" Proc.I.E.E., 100, III. 1953, 9.

2. Jesty, L.C. - "TV. as a Communication Problem", Proc.I.E.E.99 IIIA, No.20, 1952, 761.

3. McCully, G.R.- M.Sc. Thesis, University of London, 1954.

4. Beddoes, M.P.- (a) D.I.C. Thesis, Imperial College, 1956. (b) Ph.D.Thesis, University of London,1958.

5. Zworykin, V.K. and Morton, G.A. "Television" John Wiley & Sons, Inc. N.Y. II Ed. 1954.

6. Cherry, E.C. - "On Human Communication" John Wiley & Sons Inc.N.Y. Chapman & Hall,London, 1957, p.47.

7. Garrat and Mumford - "A History of TV" Proc. I.E.E. 99 IIIA, No.20, 1952.

8. Blumlein A.D. et al - "The Marconi, E.M.I. TV System" Proc.I.E.E. Vol.14, No.40, March 1939, 65.

9. Gabor, D. "Theory of Communication" J.I.E.E. 93, Part III, 1946, p.429

10. Shannon, C.E. and Weaver, W. "The Mathematical Theory of Communication" University of Illinois Press, Urbana,1949; published earlier in B.S.T.J. 27, 1948, pp.379 and 623.

11. Kretzmer, E.R. "Statistics of TV Signals" Bell System Tech.Journal 31, Jul.1952, p.751.

12. Ref (10) page 31.

13. Tustin. A. Lecture, Imperial College, 1956.

14. Cherry, E.C. "Informal Lecture on Communication Theory". J.I.E.E. 99, 1952. p.404.

15. Sziklai, G.C. "Some Studies in the Speed of Visual Perception". I.R.E.Trans.on Inf.Theory, Vol.IT-2 *3 Sept.1956.p.125.

16. Pierce, J.R. and Karlin "Reading Rates and the information Rate of a Human Channel." B.S.T.J.March, 1957.

17. Newman "Men and ~~Machines~~ Information" - A Psychologist's Viewpoint. Supplemento al Nuovo Cimento 13 1959. P.539 Serie X

18. Jacobson, H."The Informational Capacity of the Human Eye", Science, 113, March 16, 1951. pp.292-293.

19. Haantjes "Physical Aspects of Coding Systems used in Colour TV". Acta Electronica Vol.2. 1957-58 (Nos.1 and 2).

20. Jesty and Phelp "Evaluation of Picture Quality with Special Reference to TV Systems". J. Brit.I.R.E. 12 1952.

21. Kretzmer, E.R. "Reduced Alphabet Representation of TV Signals". I.R.E. Convention Record, Part IV.1956.

22. Jesty, L.C. "The Relationship Between Picture Size, Viewing Distance and Picture Quality". J.I.E.E. Part B. 1958. p. 425.

23. Mertz, P and Gray - "A Theory of Scanning and its Relation to the Transmitted Signal in Telegraphy and Television". Bell System Tech.Journal 13, 1934. p. 464.

24. Bell.D.A. "Discussion on General System Aspects". Proc.I.E.E. 99 IIIA. 1952. P.860.

25. Bell, D.A. and Swann, G.E.D. "Spectrum of Television Signals". Wireless Engineer, 33, 11 Nov.1956,p.253.

26. Mertz, P. "The Scanning Process". Proc. I.R.E. 29, Oct. 1941, p.259.

27. Chatten, J.B. et al "The Composite Video Signal - Waveforms and Spectra". I.R.E. Trans. on Broadcast and TV Receivers. Vol.B.I.R-1, No.3. July 1955.p.31.

28. Seyler, A.J. "On the Application of Information Theory to Television". Unpublished Report, Australian Post Office, 1957.

29. Oliver, Pierce & Shannon, "Philosophy of Pulse Code Modulation". Proc.I.R.E., 36, 1948. pp.1324-1331.

30. Bell, D.A. "Economy of Bandwidth in Television". Journal Brit.I.R.E. 13 Sept.1953, p.447.

31. Bedford, L.H. and Puckle, O.S. "A Velocity-Modulation T.V. System". Journ.I.E.E. 1934, 75, p.63.

32. Gouriet, G.G. "A Method of Measuring Television Picture Detail". Electronic Engineering, 24, 1952. p.306.

33. Cherry and Beddoes, British Patent No.35,465/56.

34. Schroter, F."Speitherempfang Und Differenzbild Fernsehen". Archiv. der Elektrischen Übertragung 7, 1953.p.63.

35. Harrison, C.W. "Experiments with Linear Prediction in Television". Bell System. Tech.Journal. July 1952.

36. Wiener, N. "Extrapolation, Interpolation and Smoothing of Stationary Time Series". John Wiley, 1950.

37. Fano, R.M. "The Transmission of Information". M.I.T. Research Lab. of Electronics.Tech.Rept.65, 1949.

38. Oliver, B.M. "Efficient Coding" Bell Systm.Tech.Journal, July 1952.

39. Gouriet, G.G. "Bandwidth Compression of a Television Signal". Proc.I.E.E. Part B, May 1957, p.265.

40. Seyler, A.J. "Investigations of Potential Channel Capacity Reduction of TV Relay Links". Unpublished Report, Australian P.O. Feb.1957.

41. Goodall, W.M. "Television by P.C.M." Bell Syst. Tech. Journal, 30, 1951. p.33.

42. Kretzmer, E.R. "Reduced-Alphabet Representation of Television Signals". I.R.E.Convention Record 1956, Part IV.

43. Graham, R.E. "Communication Theory Applied to Television Coding". Acta Electronica, Vol.2. 1957-58.

44. Grahan, R.E. "Predictive Quantizing of Television Signals" I.R.E. Wescon Convention Record on Information Theory, August 1958.

45. de Jager. "Delta-Modulation" - A Method of PCM Transmissio Using the One-Unit Code". Symposium on "Communicatio Theory", Edited by Willis Jackson, Butterworth Scientific Publication, 1953, P.119.

46. Graham, R.E. and Kelly,Jr.J.L. "A Computer Simulation Chain for Research on Picture Coding". I.R.E. Wescon. August 1958, Computer Applications.

47. Schreiber, W.F., Knapp, C.F. and Kay, N.D. "Synthetic Highs - An Experimental Bandwidth Reduction System". 84th, S.M.P.T.E. Convention, October,1958.

48. Schreiber, W.F. and Knapp, C.F. "Television Bandwidth Reduction by Digital Coding". I.R.E.Convention Record, 1958. part 4, p.88.

49. Black, H.S. "Modulation Theory". D. Van Nostrand, Inc. N.Y. 1953.

50. Gabor, D. 1958 Lecture Course on Information Theory. "Television Compression by Contour Interpolation".

51. Hill.P. Ph.D. Thesis, University of London, (Under preparation).

52. Delbord, Y. "La television et la transmission des informations". Ann. des Telecomm., 6, 1951 p.11.

53. Schroter, F. "Picture Storage Problems". Bull, Assoc. Suisse Electr. Vol.40. 1949. p.564.

54. Seyler, A.J. "Bandwidth Reduction in Television Relaying" Part I and II. Proc.I.R.E.(Australia),16, July and August 1955.

55. Loeb, J. "Communication Theory of Transmission of Simple Drawings". - Symposium on Communication Theory, Ed. Willis Jackson, Butterworths, 1953, p.317.

56. Haynes and Hogers "Stop-Go Scanning Saves Spectrum Space". Electronics, Sept.26, 1958.

57. Michel, W.S. "Statistical Encoding for Text and Picture Communication". A.I.E.E.Trans.Part I.Comm. & Electronics. March 1958. p.33.

58. Michel et al "A Coded Facsimile System". I.R.E.Wescon Convention Record, 1957, Part II.P.84.

59. Knoll and Kazan "Storage Tubes". John Wiley & Sons, Inc. New York. 1952.

60. Garmash, V.A. "The Quantization of Signals in Non-Uniform Steps". Telecommunications No.10. 1957, p.10.

61. Beddoes, M.P. - "A Variable-Velocity Scanner for Magnetic Deflection of a Scanning Spot". I.E.E.Monograph No.241 R. June 1957.

62. Pierce J.R. and Schockley W. "A Theory of Noise for Electron Multipliers" Proc.I.R.E. 26.No.3. March 1938, p.321.

63. Schagen.P. et al "The Image Iconoscope, a Camera for TV" Philips Tech. Rev. 13, 1951. p.119-133.

64. Van der Poel, F.H.J. andValeton, J.J.P. "The Flying Spot Scanner". Philips Technical Review 15 1954. pp.221-232.

65. Brill and Klassens."New Phosphors for Flying-Spot Cathode-Ray Tubes"Philips Research Reports, 7, 421, 1952.

66. Hoover et al "Fundamental Concepts in the Design of the Flying Spot Store". B.S.T.J. 37 September 1958. p.1161.

67. Rodda, S. "Photo-Electric Multipliers". Macdonald & Co., Ltd. London, 1953.

68 Sharpe, J. "Photomultiplier Tubes". British Communications and Electronics, August, 1957.

69. Chance et al - "Waveforms". McGraw-Hill Book Company Inc., 1949.

70. Valley and Wallman - "Vacuum Tube Amplifiers" Radiation Laboratory Series 18. McGraw-Hill Book Co.Inc.,

71. Williams, F.C. & N.F.Moody: "Ranging Circuits Linear Time-Base Generators & Associated Circuits". J.I.E.E. Vol.93, Pt.IIIA, pp.1188-1198.1946.

72. Millman, J and H. Taub.-"Pulse and Digital Circuits". McGraw Hill Book Company Inc.1956.

73. Starr,A.T. "Electric Circuits and Wave Filters". Pitman & Sons. London, 1948.

74. Moody, N.F.-"The Design of Pulse Transformers for Handling Small Powers". Radar Research Establishment Journal, April 1946.

75. Moody, N.F. "Low Power Pulse Transformers" J.I.E.E. 1946, 93 Part IIIA. pp.311-12.

76. Melville - "Theory and Design of High Power Transforms". J.I.E.E. 1946, 93 Part IIIA pp.1063-80.

77. Mullard Ferroxcube Handbook. Components Division, Mullard Ltd., May 1955.

78. Gallaher, L.E."Beam Positioning Servo System for Flying Spot". Bell System Technical Journal, March 1959. p.425.

79. Weaver, L.E. "The Measurement of Random Noise in the Presence of a Television Signal". B.B.C. Engineering Division Monograph No.27.March 1959.

80. Price. R. "A Useful Theorem for Non-Linear Devices Having Gaussian Inputs". I.R.E. Transactions on Information Theory June, 1958. pp.69-72.

81. Bendat, J.S. "Principles and Applications of Random Noise Theory". John Wiley & Son Inc.1958.

82. Laning, Jr. J.H. and Battin, R.H. "Random Processes in Automatic Control". McGraw Hill Book Co.In.1956.

83. Barstow, J.M. and Christopher, H.N. "The Measurement of Random Monochrome Video Interference". Trans. A.I.E.E. 73 Part I. Communication & Electronics p.735. Jan.1954.

84. Youngblood, W.A. "Picture Processing". Quarterly Progress Report, Research Lab. of Electronics, M.I.T. Jan.15, 1958.

85. Youngblood, W.A. "Estimation of Channel Capacity Required for Picture Transmission". Sc.D. Thesis, Dept. of Elec. Engg. M.I.T. May. 1958.

86. Julesz. B. "A Method of Coding Television Signals Based on Edge Detection". Bell System Tech.Journal 38 July 1959. p.1001.

87. British Patent Application No.32,376/58, Cherry, Holloway and Prasada.

88. Billings, A.R. "A Coder for Halving the Bandwidth of Signals". Proc.I.E.E. 105 B, 1958. p.182.

89. Voelcker, H.B. "Notes on a Class of Compression Scheme". Unpublished Report, Imperial College,March,1959.

90. Powers, K.H. and Staras, H. "Some Relations Between Television Picture Redundancy and Bandwidth Requirements". Communication and Electronics. A.I.E.E. Sept.1957. p.492.

91. Stoddard, J.C. "Measurement of Second-Order Probability Distribution of Pictures by Digital Means". Technical Report 302, M.I.T. Research Lab. of Electronics. July 1955.

92. Capon J. "Bounds to the Entropy of TV Signals". Technical Report 296, M.I.T. Research Lab. of Electronics May 1955.

93. Schreiber, W.F. "The Measurement of Third Order Probability Distributions of TV Signals".

94. Brennan, D.G. "A New Approach to Certain Types of Random Fluctuations". Read at Physical Society Symposium on Fluctuation Phenomena and Stochastic Processes.Birkbeck College.March 19-20. 1959.

95. Furduyev, V.V. "Some Basic Concepts of Signal Theory". Radio tekhnika, 12, No.4, 32-38, 1957. (Translated from Russian).

96. Fano, R.M. "Short-Term Autocorrelation functions and Power Spectra" J. Acoustical Society of America 22, 546, 1950.

97. Page. C.H. "Instantaneous Power Spectra". Journal of Applied Physics, 23, No.1. Jan. 1952, P.103.

98. Turner, C.H.M. "On the Concept of an Instantaneous Power Spectrum andits Relationship to the Autocorrelation Function." Journal of Applied Physics 25, No.11. Nov.1954, p.1347.

99. Selfridge, O.G. "Pattern Recognition and Learning". Third London Symposium on Information Theory Ed. Colin Cherry,Butterworth Scientific Publication 1956.

100. Taylor,W.K. "Electrical Simulation of Some Nervous System Functional Activities". Third London Symposium on Information Theory. Ed. Colin Cherry, Butterworth Publications 1956.

101. Taylor, W.K. "Pattern Recognition by Means of Automatic Analogue Apparatus". Proc.I.E.E. Part B. March 1959. p.198.

102. Glovazky, A. "Determination of Redundancies in a Set of Patterns.".I.R.E. Transaction on Information Theory, Dec. 1956.

103. Gill. A. "Minimum - Scan Pattern Recognition". I.R.E. Transaction on Information Theory June, 1959.

104. Grimsdale, R.L. et al. "A System for the Automatic Recognition of Patterns". Proc. I.E.E. Part B. March, 1959. P.210.